GENETIC AND BIOCHEMICAL ANALYSES OF HSP70-HSP40 INTERACTIONS IN SACCHAROMYCES CEREVISIAE PROVIDES INSIGHTS INTO SPECIFICITY AND MECHANISMS OF REGULATION

by

Shruthi Sridhar Vembar

M.Sc. (Hons.) Biological Sciences, Birla Institute of Technology and Science, Pilani, India

Submitted to the Graduate Faculty of

Arts and Sciences in partial fulfillment

of the requirements for the degree of

Doctor of Philosophy

University of Pittsburgh

2009

UNIVERSITY OF PITTSBURGH

FACULTY OF ARTS AND SCIENCES

This dissertation was presented

by

Shruthi Sridhar Vembar

It was defended on

May 7, 2009

and approved by

Karen M. Arndt, Professor, Biological Sciences

Paula Grabowski, Professor, Biological Sciences

Anthony M. Schwacha, Assistant Professor, Biological Sciences

John L. Woolford, Professor, Biological Sciences, Carnegie Mellon University

Dissertation Advisor: Jeffrey L. Brodsky, Professor, Biological Sciences

GENETIC AND BIOCHEMICAL ANALYSES OF HSP70-HSP40 INTERACTIONS IN SACCHAROMYCES CEREVISIAE PROVIDE INSIGHTS INTO SPECIFICITY AND MECHANISMS OF REGULATION

Shruthi Sridhar Vembar, Ph.D.

University of Pittsburgh, 2009

Heat shock proteins of 70kDa (Hsp70s) and their J domain-containing Hsp40 cofactors are conserved chaperone pairs that facilitate diverse cellular processes. One essential Hsp70 in the endoplasmic reticulum (ER) lumen, BiP (Kar2p in yeast), participates in polypeptide translocation into the ER, protein folding, and ER-associated degradation (ERAD). Like other Hsp70s, BiP contains an N-terminal ATPase domain, followed by a substrate binding domain and a C-terminal lid domain. To better define how substrate affinity and Hsp40 interaction affect BiP function, I constructed and characterized a mutation, R217A, in the putative J domain-interacting surface of yeast BiP. The mutation compromises ATPase stimulation by Sec63p, an Hsp40 required for translocation, but stimulation by Jem1p, an Hsp40 required for ERAD, is robust. In accordance with these data, yeast expressing R217A BiP exhibit translocation defects, but no ERAD defects, and a genetic interaction study using this mutant yielded data consistent with defects in translocation. In contrast, mutations in the substrate binding domain that either disrupt an ionic contact with the lid or remove this domain are deficient for peptide-stimulated ATPase activity. Expression of these mutants in yeast results in varying translocation and ERAD defects. Taken together, these data indicate that BiP can distinguish between its ER-resident cochaperones, and that optimal substrate binding is a key determinant of BiP function.

Next, I tested the hypothesis that the functional specificity of Hsp70s is regulated by cognate Hsp40s. If this is true, one might expect divergent Hsp70-Hsp40 pairs to be unable to

function *in vivo*. However, I discovered that a mammalian ER-lumenal Hsp40, ERdj3, when directed to the yeast cytosol, was able to rescue the temperature-sensitive growth phenotype of yeast containing mutant alleles in two cytosolic Hsp40s, *HLJ1* and *YDJ1*. Moreover, ERdj3 activated the ATPase activity of Ssa1p, the yeast cytosolic Hsp70 that partners with Hlj1p and Ydj1p. Intriguingly, ERdj3 mutants that were compromised for substrate binding were unable to rescue the *hlj1ydj1* growth defect, even though they stimulated Ssa1p ATPase activity. These data suggest that the substrate binding properties of certain Hsp40s—not simply the formation of unique Hsp70-Hsp40 pairs—is critical to specify *in vivo* function.

TABLE OF CONTENTS

PREFACE ..... **XV**

1.0 INTRODUCTION **1**

1.1 HEAT SHOCK PROTEINS **3**

1.2 BIP IS AN ER LUMENAL HSP70 ..... **5**

1.2.1 Insights from Hsp70 structural studies **6**

1.2.2 Yeast BiP's Hsp40 cochaperones **17**

1.2.2.1 The human Hsp40, ERdj3 ..... **20**

1.2.3 Nucleotide Exchange Factors for yeast BiP and other BiP-interacting proteins **21**

1.2.4 BiP is required for co- and post-translational protein translocation across the ER membrane **23**

1.2.5 BiP participates in nascent protein folding in the ER **27**

1.2.6 BiP-mediated recognition and targeting of misfolded proteins for ER-associated degradation **31**

1.2.7 BiP is required for the induction of the unfolded protein response **38**

1.2.8 Other BiP functions **42**

1.2.9 BiP and human disease **44**

1.3 A PREVIEW OF CHAPTERS 2 AND 3 ..... **47**

2.0 THE TRANSLOCATION-SPECIFIC BIP MUTANT, R217A, GENETICALLY INTERACTS WITH ILM1, A NOVEL PLAYER IN CO-TRANSLOCATIONAL PROTEIN TRANSLOCATION ACROSS THE ER MEMBRANE 49

2.1 MATERIALS AND METHODS 52

2.1.1 Yeast strains and plasmids 52

2.1.2 Protein purification 56

2.1.3 ATP hydrolysis and limited proteolysis assays 57

2.1.4 Serial dilutions 58

2.1.5 Preparation of yeast cell extracts and immunoblotting 59

2.1.6 Pulse-labeling of cells and immunoprecipitation 59

2.1.7 β-galactosidase assays to measure the induction of the UPR 61

2.1.8 *In vitro* translocation and ERAD assays 62

2.1.9 Purification of the Sec63 complex 63

2.1.10 UPR-based genetic analysis 64

2.1.11 Native immunoprecipitations of FLAG-tagged Ilm1p 65

2.1.12 Cycloheximide-chase ERAD assays 65

2.1.13 Data analysis 66

2.2 RESULTS 66

2.2.1 Generation of the yeast BiP mutants, R217A, K584X and S493F 66

2.2.2 R217A BiP exhibits defective interaction with Sec63p and Scj1p 70

2.2.3 High level expression of BiP mutants results in yeast strains displaying varied sensitivity to elevated temperature and ER stress 73

2.2.4 Lower level expression of the K584X and S493F BiP mutants results in yeast strains exhibiting sensitivity to elevated temperature and ER stress 78

2.2.5 The *TEF1-R217A* strain exhibits a defect in protein translocation across the ER membrane, but is proficient for ERAD and ER protein folding 84

2.2.6 Sec63 complex formation is reduced for R217A BiP..... 91

2.2.7 Scj1p and Jem1p function redundantly in *TEF1-R217A* yeast 93

2.2.8 Identification of genetic interactions specific for the *R217A* BiP allele 97

2.2.9 Ilm1p is a novel player during protein translocation across the ER membrane 100

2.2.10 Deletion of *ilm1* does not result in ERAD defects..... 105

2.3 DISCUSSION..... 106

2.3.1 Identification of a translocation-specific BiP mutant, R217A..... 109

2.3.2 Substrate binding mutants of BiP affect ER homeostasis and multiple BiP functions..... 111

2.3.3 Characterization of the genetic interactions of R217A BiP..... 112

2.3.4 Ilm1p, a previously uncharacterized protein, plays a role in the translocation of BiP..... 114

2.3.5 Perspective..... 115

3.0 COMPLEMENTATION OF HSP40-DEPENDENT YEAST PHENOTYPES DIFFER IN THEIR REQUIREMENTS FOR THE J DOMAIN AND SUBSTRATE BINDING ACTIVITIES OF A MAMMALIAN HOMOLOG..... 117

3.1 MATERIALS AND METHODS..... 122

3.1.1 Preparation of Ydj1 and ERdj3 constructs..... 122

3.1.2 Expression and detection of Ydj1 in mammalian cells 124

3.1.3 Protein expression, purification and ATPase assays 125

3.1.4 Rescue of the slow growth phenotype of mutant yeast strains 125

3.1.5 Detection of ERdj3 in yeast 126

3.1.6 Assays for ER-Associated Degradation (ERAD) 126

3.2 RESULTS 128

3.2.1 Ydj1 expressed in the mammalian ER functions as an Hsp70 cofactor . 128

3.2.2 Overexpression of cytosolically localized ERdj3 rescues the temperature-sensitive growth defect of *hlj1Δydj1-151* yeast 131

3.2.3 The substrate binding domain of ERdj3 is required to rescue the slow growth phenotype of *hlj1Δydj1-151* yeast 138

binding properties of CaaX-ERdj3 are required to complement the growth defect of the *hlj1Δydj1-151* strain, and that this does not simply depend on (or even require) the functional interaction of JDPs with a cognate Hsp70 144

3.2.4 Cytosolically expressed ERdj3 compensates for cell wall defects in the *hlj1Δydj1-151* strain 144

3.2.5 CaaX-ERdj3 expression restores ERAD in *hlj1Δydj1-151* yeast 147

3.3 DISCUSSION 149

4.0 CONCLUSIONS AND PERSPECTIVES 153

APPENDIX A 168

APPENDIX B 172

APPENDIX C 264

BIBLIOGRAPHY 283

LIST OF TABLES

Table 1: Hsp90s, Hsp70s, Hsp70-like proteins and select Hsp70 co-factors found in the ER and cytosol 4

Table 2: Select human diseases related to BiP malfunction. 45

Table 3: Quantification of the genetic interactions between individual deletion strains (columns) and the indicated query strain (rows). 101

Table 4: Strains used in this study 162

Table 5: Plasmids used in this study 165

Table 6: A list of the genes that were analyzed in the UPR-based screen 199

Table 7: The $\log_2$ (GFP/RFP) reporter values obtained in the double mutant strains when *KAR2::NAT* or *kar2-R217A::NAT* were crossed against the genes listed in table 6 222

Table 8: The $\log_2$ (GFP/RFP) reporter values obtained in the double mutant strains when *KAR2* or *kar2-P515L* were crossed against the genes listed in table 6 232

Table 9: The $\log_2$ (GFP/RFP) reporter values obtained in the double mutant strains when *KAR2::NAT* or *kar2-P515L-DamP::NAT* were crossed against the genes listed in table 6 242

Table 10: The $\log_2$ (GFP/RFP) reporter values obtained in the double mutant strains when *KAR2::NAT* or *kar2-DamP::NAT* were crossed against the genes listed in table 6 252

Table 11: A list of the gene deletions that exhibited the highest correlation coefficients for (A) *kar2-R217A::NAT*, (B) *sec71Δ*, and (C) *sec72Δ*, and their corresponding genetic interaction values. 262

LIST OF FIGURES

Figure 1: A schematic depiction of the folding energy landscape of a polypeptide chain. 2

Figure 2: Hsp70 ATP hydrolysis cycle 7

Figure 3: Crystal structures of isolated Hsp70 domains. 10

Figure 4: Crystal structures of select truncated Hsp70 isolates and Hsp70-like proteins. 15

Figure 5: Protein translocation across the endoplasmic reticulum membrane. 25

Figure 6: N-linked glycosylation and the degradation of glycosylated proteins in the mammalian ER. 29

Figure 7: A step-by-step illustration of endoplasmic reticulum-associated degradation. 33

Figure 8: The ubiquitin-proteasome system. 37

Figure 9: Induction of the unfolded protein response (UPR) in yeast. 41

Figure 10: Three yeast BiP mutants: R217A, S493F and K584X. 69

Figure 11: R217A is compromised for stimulation of ATPase activity by the J domain of Sec63p and full-length Scj1p, but not by the J domain of Jem1p. 72

Figure 12: K584X and S493F are defective for peptide stimulation of ATPase activity. 74

Figure 13: Expression of BiP mutants from the galactose-inducible P_{GAL1} promoter results in yeast strains exhibiting varied sensitivities to elevated temperature and ER stress. 77

Figure 14: Expression of K584X and S493F BiP from the constitutive P_{TEF1} promoter results in yeast strains exhibiting sensitivity to elevated temperature and ER stress. 82

Figure 15: Yeast expressing R217A BiP exhibit translocation, but not ERAD or ER folding defects. 87

Figure 16: The translocation defect in *TEF1-R217A* yeast is due to reduced complex formation between Sec63p and R217A. 92

Figure 17: Jem1p and Scj1p function redundantly to support ERAD in the *TEF1-R217A* strain. 95

Figure 18: Genetic interaction profile of *kar2-R217A::NAT* with 350 gene deletions that induce the UPR. 99

Figure 19: Ilm1p is required for the efficient translocation of BiP and interacts with components of the translocation machinery. 104

Figure 20: Deletion of *ilm1* has no effect on ERAD. 108

Figure 21: An alignment of the J domains of Sec63p, Jem1p and Scj1p. 110

Figure 22: A schematic representation of select JDPs. 119

Figure 23: Sequence comparison of DnaJ, Ydj1, Scj1, ERdj3, Hlj1 and the J domain of Jem1. 121

Figure 24: Ydj1 interacts with both BiP and κLC in the mammalian ER. 130

Figure 25: ER expressed ERdj3 is unable to rescue the growth phenotype of the *scj1Δjem1Δ* strain. 134

Figure 26: Cytosolic expression of ERdj3 rescues the temperature-sensitive growth phenotype of the *hlj1Δydj1-151* strain. 137

Figure 27: Detection of the various wild-type and mutant ERdj3 proteins in yeast by indirect immunofluorescence. 140

Figure 28: ERdj3 substrate binding mutants fail to enhance the growth of *hlj1Δydj1-151* yeast. 143

Figure 29: CaaX-ERdj3 complements the cell wall phenotype of the *hlj1Δydj1-151* strain. 145

Figure 30: CaaX-ERdj3 substitutes for Hlj1 and Ydj1 during ERAD..... 148

Figure 31: Complementation of the N-glycan trimming defect of *sbh1Δsbh2Δ* yeast by either Sbh1p or Sbh2p..... 171

Figure 32: PCR amplification of wild-type and mutant *kar2* alleles from genomic DNA..... 177

Figure 33: Characterization of the growth patterns and BiP expression levels in the wild-type and mutant *kar2* strains generated for the UPR-based genetic screen..... 180

Figure 34: Characterization of the ERAD efficiencies of the wild-type and mutant strains generated for the UPR-based genetic screen. 182

Figure 35: Characterization of the translocation efficiencies of the wild-type and mutant *kar2* strains generated for the UPR-based genetic screen. 184

Figure 36: Genetic interaction profiles of the indicated mutant *kar2* strains. 187

Figure 37: Characterization of the translocation and ERAD efficiencies of *sur4Δ* and *erd1Δ* yeast..... 192

Figure 38: Characterization of the translocation and ERAD efficiencies of *ylr104wΔ* yeast. ... 195

Figure 39: An example of the step-wise purification of G247D-K584X BiP. 273

Figure 40: A comparison of the endogenous ATPase activities of wild-type and mutant BiP proteins..... 275

Figure 41: Characterization of the multimeric states of G247D-D559X and G247D-K584X BiP. 278

Figure 42: Optimization of the conditions under which G247D-K584X BiP separates as a single oligomeric species..... 281

PREFACE

Before getting into the nitty-gritty of my dissertation, I would like to acknowledge the people who have helped me to get to this point.

First and foremost, the person who has been instrumental in my training as a scientist, Jeff Brodsky. I don't know where to begin to express my heartfelt gratitude for your time and patience. Through the years you have always been supportive of my ideas and thoughts and never let me feel that I was lacking in anything. My development has been largely influenced by your outlook, both as a mentor and a researcher, and I hope that I can pass on all the knowledge that I have gained from interacting with you. Thank you for all the opportunities that you have created for me to improve not only my research skills, but also my oratory, writing, and mentoring skills. At this key juncture of my career, I stand on my own two feet, and the future is bright, thanks to your guidance.

The Brodsky lab, where I have spent a good chunk of the past six years, is truly a wonderful experience for any aspiring scientist. I have met some of the smartest people within the four walls of 274, Crawford Hall and each of them has influenced my life in unique ways. A special shout-out to:

Jennifer Goeckeler, the lab manager, who runs the lab like clockwork, who knows everything, and who never hesitates to speak her mind. Thanks, Jen, for putting up with my idiosyncracies and for all the fun times inside and outside the lab.

A phenomenal ex-post-doc, Kunio Nakatsukasa, who is now in Japan running his own lab. Kunio, your keen mind and admirable dedication to everything you do is something to behold, and I have learnt a LOT from you. Thanks and my best wishes are always with you!

My neighbor in the lab during my formative years, Nancy Kaufman. I still miss you, Nancy, and I can't thank you enough for all the insightful discussions, critical analyses of data and of course, the conversations over chai.

A big 'hey' to past graduate students, Stacy Hrizo and Christine Wright, the first people I connected with in the Brodsky lab. If I needed someone to speak to, you guys were always there- thanks!

Last, but definitely not the least, a person I admire and who I know will go places, Karen Hecht. Hang in there, Karen, and just enjoy your PhD; there is nothing like it.

And other past and current members of the Brodsky lab: Sarah Herrle, Annette Chiang, Sheara Fewell, Teresa Buck, Alex Kolb, Sandlin Seguin, Joe Tran, Annette Ahner, Craig Scott, Bob Youker, Chris Guirierro, Cristy Gelling and Patrick Needham.

The presence of undergraduate researchers in the Brodsky lab has also taught me the challenges and necessities of mentoring young minds. Not only have the undergraduates supplied me with the necessary reagents to perform my research smoothly, their attitudes and opinions have made for an interesting work environment. I would especially like to thank Brigid Jensen and Corinne Schneider. I trained Brigid on one aspect of my project and it has been very fulfilling to follow her progress. I wish her the very best for graduate school. Corinne was always there with a joke and a smile and I am rooting for her success in science. Other undergraduates who I would like to acknowledge are Mike (the most cheerful person I know), Lindsay (*2), Doug, Sarah, Sam, Jake, Bill, Alex and Raj.

The ambience of the Department of Biological Sciences has been great, educationally and socially. I have a great set of colleagues and I would like to thank all of them for truly wonderful times. My classmates, Julia van Kessel, Matt Bochman, Megan Dietz, Christy Reedy and Qian Wu have been supportive at different points of my career, and each of them holds a singular place in my heart. I especially cherish the times I have spent with Amrita Balachandran. Amrita, no one can fill your shoes. I also want to thank Cathy Barr and Natalie Marinzel for their help and conversations over the years, and of course, the candy.

I would like to acknowledge the members of my thesis committee. Karen, Paula, Tony, and John, thank you for your advice and suggestions at committee meetings. I have enjoyed our scientific discussions and hope that I do not put you to sleep with my dissertation. Today's science scenario is collaborative and I am lucky to have worked with very talented scientists: Yi Jin and Linda Hendershot at St. Jude Children's Hospital, Martin Jonikas and Jonathan Weissman at the University of San Francisco, Shuh-ichi Nishikawa at Nagoya University, Japan, and Andy van Demark at the University of Pittsburgh. Because of your contributions, I can definitely state that WE have discovered something new and exciting.

To maintain my sanity over the past six years, I have socially interacted with many people in Pittsburgh and I would like to thank them all for the happy times. Sangita Suresh and Vaishnavi Panchapakesa, my ex-housemates, were the only people I knew when I arrived in Pittsburgh. Thanks to them, I did not miss my family and friends back in India as much as I might have. A special thank-you to my friends Aarti Sahasranaman, Amrita Balachandran and Priya Kannan, to the members of AID-Pittsburgh who have helped me become a socially responsible human being, and to the members of my Samskritam class who have shared the joy of learning Samskritam with me.

Finally, I would not have been able to complete my thesis without the support of my wonderful parents and sister. I am so glad, mom and dad, that you are mine, and that you did not bully me into something I was never ready for, *i.e.,* marriage, especially arranged! And my dear sis, what would I do without you? I come from a large family, scattered all around the world. This has given me plenty of opportunities to travel within the U.S. and I thank my aunts, uncles and cousins, especially Radha and Pushpa, for always making me feel at home when I visited them. And, of course, my friends through thick and thin- Stuti, Supraja, Pallavi, Aparna, Shailaja and Edwin-thank you.

1.0 INTRODUCTION

The environment within a cell is chemically complex and crowded, with macromolecular structures occupying 20-40% of the total volume[16, 17]. It is in such an environment that proteins have to fold into their functional three-dimensional conformations. While small single domain proteins (<100 amino acids) fold *de novo* on a sub-second time scale, larger multidomain proteins require protracted folding periods[8]. This is due to the observation that the folding energy landscape of a longer polypeptide chain contains several off-pathway non-native intermediate states in addition to the lowest energy state corresponding to the native conformation[8] (Figure 1). Therefore, a larger protein might 'sample' several states before it reaches its native conformation or alternately, might terminally reside in an intermediate non-native state ('misfolded' state). One consequence of this phenomenon is the formation of toxic protein aggregates within the cell[18]. Not surprisingly, several human diseases can be correlated to protein misfolding and/or aggregation, including cystic fibrosis, antitrypsin deficiency and protein aggregation diseases such as Huntington's, Parkinson's, Alzheimer's and prion-associated diseases.

Apart from inaccuracies during *de novo* protein folding, misfolding can arise due to stochastic variations in the chemical environment of the cell, spontaneous errors in cellular processes such as transcription and translation, genetic mutations, environmental stresses such as elevated temperature and osmotic stress, toxic compounds, and defects in oligomeric assembly.

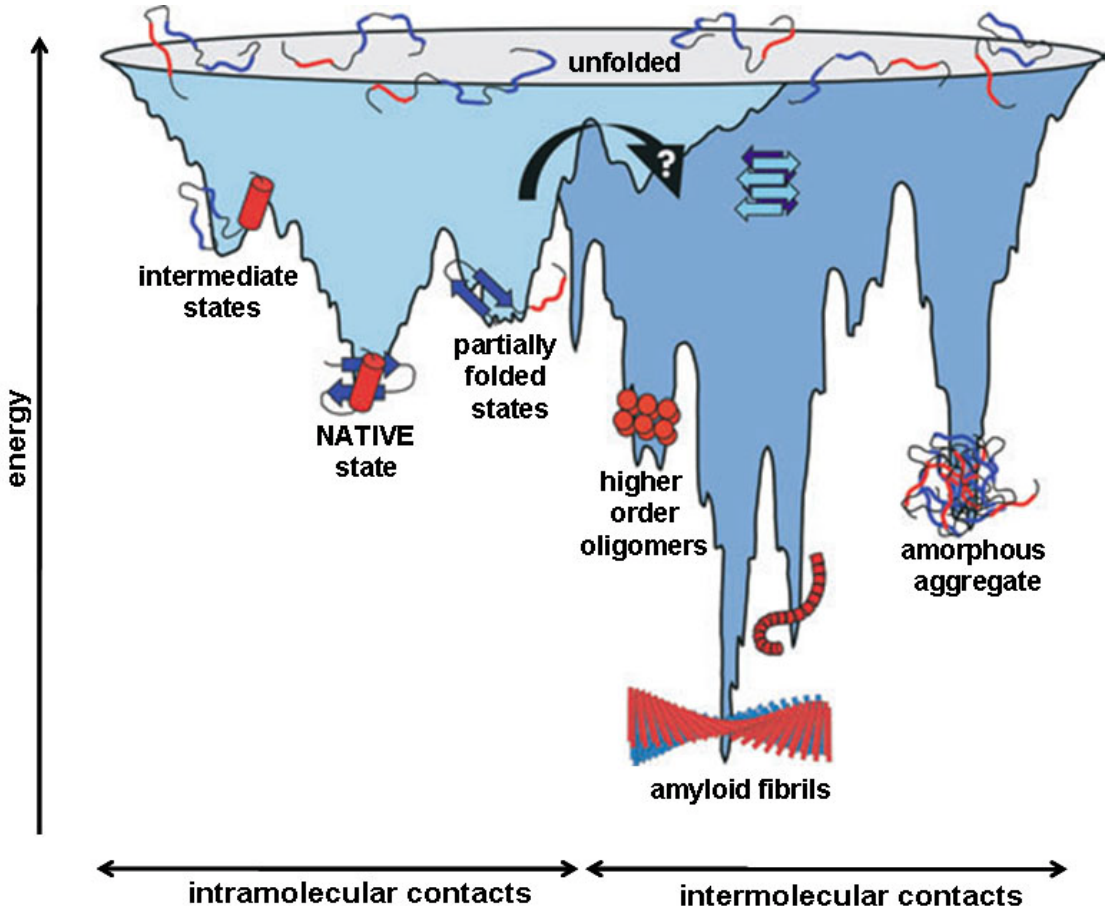

Figure 1: A schematic depiction of the folding energy landscape of a polypeptide chain.

The unfolded state of a protein is the highest energy state and is comprised of several conformations which are shown on the surface of the 'funnel'. As a protein folds into its native conformation via intramolecular contacts, it passes through intermediate states as well as partially folded states; each of these form energy traps and a protein might require the assistance of molecular chaperones to revert to the correct folding path. Alternately, a protein might begin to acquire intermolecular contacts to form homo-oligomers, heterogeneous aggregates, or amyloid fibrils; the exact mechanism by which this occurs is still unclear. It is important to note that the structures of most intermediate states are unknown.

The figure was adapted from Jahn and Radford, 2005[8].

To prevent misfolding-induced toxicity, cells have developed several quality control mechanisms to monitor protein folding, and in the case of terminal misfolding, to rapidly turn over the toxic species[19, 20]. One such preventive measure is the stress induction of a class of proteins called heat shock proteins (Hsps).

1.1 HEAT SHOCK PROTEINS

Hsps constitute a unique family of molecular chaperones that is found in all living organisms and in every subcellular organelle. They were initially classified according to molecular mass into Hsps of 70kDa, *i.e.,* Hsp70s, Hsps of 40 kDa, *i.e.,* Hsp40s, and so forth. Subsequently, as additional Hsps were identified, they were sorted into a particular subfamily predominantly based on their structural and functional similarity, not necessarily molecular mass. A second distinction was made between the inducible Hsps and the constitutively expressed Hscs; however, because the Hsps and Hscs are nearly indistinguishable at the levels of amino acid sequence and biochemical properties, the term Hsp in this dissertation will encompass all family members.

Hsp70s, Hsp40s and Hsp90s are some of the most abundant proteins in the cell (refer to Table 1 for a list of select members) and along with playing a role in protein folding, they participate in key signal transduction pathways[21, 22], assembly of multi-protein complexes[23-25], resolution of protein aggregates[26], protein translocation across membranes[24, 27, 28], endocytosis[29], protection against apoptosis[30, 31], and importantly, the recognition and targeting of misfolded proteins for degradation[5, 32, 33]. In the specific case of the Hsp70s and Hsp40s, where Hsp40s can act as cochaperones for Hsp70s, 3 Hsp70s and 6 Hsp40s have been characterized in bacterial

Table 1: Hsp90s, Hsp70s, Hsp70-like proteins and select Hsp70 co-factors found in the ER and cytosol

Component	Location	Yeast	Mammals
Hsp90	ER	-	GRP94
	Cytosol	Hsp82	Hsp90α, Hsp90β
Hsp70	ER	BiP/Kar2p	BiP/GRP78
	Cytosol	Ssa1-4p, Ssb1-2p	Hsc70, Hsp70-1, Hsp70-2, Hsp70-3
Hsp70-homologous nucleotide exchange factors	ER	Lhs1p	GRP170
	Cytosol	Sse1p	HSP110
Other Nucleotide Exchange Factors	ER	Sls1p/Sil1p	SIL1, BAP
	Cytosol	Fes1p, Snl1p	BAG1–2, HSPBP1
Hsp40	ER	Sec63p, Scj1p and Jem1p	ERj1, ERj2/SEC63, ERdj3, ERdj4, ERdj5, ERj6/p58^{IPK}
	Cytosol	Apj1p, Djp1p, Jjj1p, Jjj2p, Jjj3p, Sis1p, Swa2p, Xdj1p, Ydj1p, Zuo1p. Cwc23p, Hlj1p, Caj1p	HDJ1–2, HSJ1, DNJ3, Dj4, Djb4/HLJ1, MPP11, HSPF1, CSP, Auxilin
Other interacting proteins			
Lectin-like chaperones	ER	Cne1p/calnexin	Calnexin, Calreticulin
	ER	Yos9p	OS-9, XTBP3-B
Protein Disulfide Isomerase	ER	Eps1p and Pdi1p	PDI, ERp57, ERp72, ERdj5

cells, 14 Hsp70s and 22 Hsp40s in the budding yeast *Saccharomyces cerevisiae*, and 20 Hsp70s and > 50 Hsp40s in humans. Therefore, Hsp70s and Hsp40s appear to be required for more complex processes in higher eukaryotes and consequently, the intricacy of their interactions also increases.

A defined organelle to study the interactions between Hsp70s and Hsp40s is the endoplasmic reticulum (ER). The ER of yeast and mammals contains one Hsp70, the immunoglobulin heavy chain binding protein, BiP[34, 35]. BiP is also referred to as Kar2p in yeast due to its identification in a genetic screen for mutants defective for nuclear fusion during mating, *i.e.,* karyogamy[36-38], and glucose regulated protein of 78 kDa, GRP78, in humans, due to its induction by low serum glucose levels[39, 40]. Additionally, the yeast ER contains three well-characterized Hsp40s, Sec63p, Jem1p and Scj1p (refer to section 1.2.2), and possibly a fourth poorly-characterized Hsp40, ERj5[41], while the mammlian ER harbors six Hsp40s: MTJ1/ERj1[42], SEC63/ERj2[43, 44], HEDJ/ERj3/ERdj3[45-47], ERdj4[48, 49], ERdj5[50, 51] and p58^{IPK}/ERj6[52-54]. For the remainder of this chapter, I will discuss the multitude of functions performed by BiP in the ER, with an emphasis on its interactions with resident Hsp40 cochaperones.

1.2 BIP IS AN ER LUMENAL HSP70

A bacterial Hsp70, DnaK, and its cognate Hsp40, DnaJ, were amongst the first Hsp70s and Hsp40s discovered, due to their roles in bacteriophage lambda DNA replication[55-57]. Subsequent experiments showed that DnaK modulates the heat shock response in *Escherichia coli*[58]. As eukaryotic homologs began to be identified in the late 1970s and early 1980s, Munro and Pelham determined that ER-lumenal BiP[34] and GRP78[39, 40] were, in fact, the same protein, and that

BiP/GRP78 belonged to the Hsp70 subfamily of molecular chaperones; this was the first identification of a eukaryotic ER chaperone[35]. It was in 1989 that the laboratories of Rose and Sambrook independently established the identity of BiP in yeast and showed that the essential gene required for karyogamy, *KAR2*[36], encoded the yeast BiP homolog[36-38]. Since then, remarkable progress has been made toward understanding BiP functions and I describe a number of these below. Moreover, the discovery of non-Hsp40 cofactors that interact with BiP, and the correlation of BiP dysfunction to important human diseases, have opened up several new avenues of investigation with regard to this critical regulator of ER homeostasis.

1.2.1 Insights from Hsp70 structural studies

Hsp70s typically contain a ~44 kDa highly conserved N-terminal ATPase domain, followed by a less conserved ~ 18 kD a substrate binding domain, and a ~ 10 kDa variable C-terminal lid domain[24, 31, 59-62]. In the ATP-bound state, the 'open' conformation adopted by the Hsp70s results in low affinity and high release rates for substrates. The energy derived from subsequent ATP hydrolysis is utilized to drive a conformational change in the Hsp70s such that in the resulting ADP-bound 'closed' conformation, the Hsp70s exhibit high affinity and low release rates for substrates. Thus, through multiple cycles of ATP hydrolysis-driven substrate binding and release, Hps70s participate in protein folding by providing a protected environment for their substrates and preventing aggregation.

However, Hsp70s are poor ATPases, with specific activities in the range of 15-20 nmol ATP hydrolyzed/mg/min[63, 64] (as compared to strong ATPases such as myosin that exhibits an activity of 200-600 nmol ATP hydrolyzed/mg/min[65]). Therefore, two classes of cofactors activate the Hsp70 ATP hydrolysis cycle (Figure 2): J domain-containing Hsp40s and

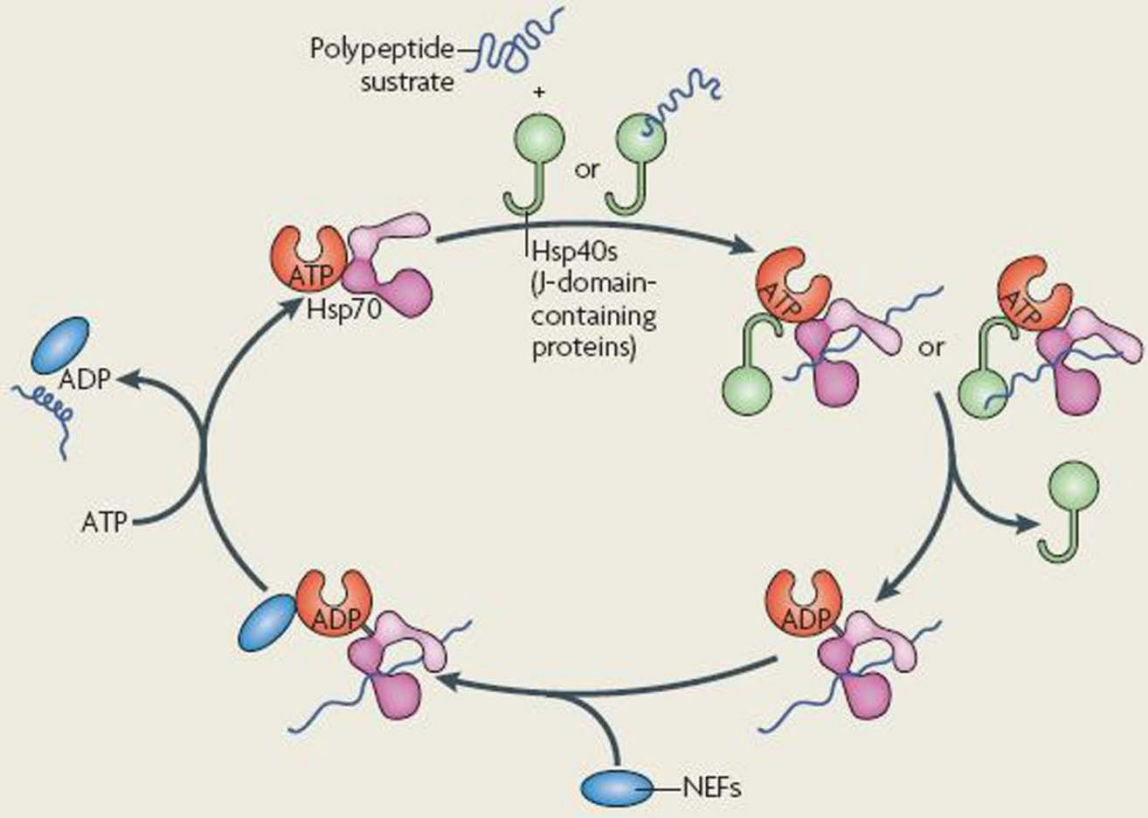

Figure 2: Hsp70 ATP hydrolysis cycle

The ATPase domain of the Hsp70 is depicted in orange, the substrate binding domain in red and the lid domain in pink. Binding of ATP in the nucleotide-binding pocket of the ATPase domain results in an Hsp70 conformation that exhibits low substrate affinity due to an 'open' lid domain. The interaction with a J domain-containing Hsp40, a polypeptide substrate, or a Hsp40-substrate complex, can stimulate the ATPase activity of the Hsp70 to generate a high substrate affinity ADP-bound conformation. In this state, the lid domain is 'closed' and encloses the substrate in the hydrophobic pocket of the substrate binding domain. The subsequent binding of NEFs to the ATPase domain engenders the exchange of ADP for ATP, and in the resultant ATP-bound conformation, the substrate is released. Therefore, through multiple cycles of ATP hydrolysis, the Hsp70 can assist in substrate folding.

The figure was adapted from Vembar and Brodsky, 2008[5].

Nucleotide Exchange Factors (NEFs). Hsp40s interact with the ATPase domain of Hsp70s through the highly conserved J domain (usually found at the N-terminus of Hsp40s) and promote ATP hydrolysis[66]; some Hsp40s also have the ability to bind to Hsp70 substrates via a C-terminal substrate binding domain and deliver them to Hsp70s[67, 68]. In contrast, the NEFs release ADP, which allows for ATP binding, and act synergistically with the Hsp40s to stimulate Hsp70 ATP hydrolysis[24]. Finally, substrate interaction can stimulate Hsp70 ATPase activity[69, 70]. Not surprisingly, the ATP hydrolysis rates of Hsp70s are maximally stimulated in the collective presence of the Hsp40s, NEFs and peptide substrates.

The first Hsp70-derived crystal structure was for the isolated ATPase domain of bovine Hsc70, crystallized in the presence of ATP[1] (Figure 3A). The ATPase domain is predominantly α-helical and can be sub-divided into two lobes, I and II, with a deep cleft in between them; each lobe is further composed of sub-domains a and b. Due to the presence of the bound nucleotide in the structure, the key residues that participate in nucleotide binding were mapped to the base of the cleft between subdomains Ia and IIa. Subsequent mutagenesis studies in various Hsp70s established the essentiality of these residues for function[24, 71-75]. Surprisingly, the tertiary structure of the nucleotide-binding pocket resembled the ATP and substrate binding regions of hexokinase[1], even though the structure adopted by the remainder of the ATPase domain was closer to that of actin[1]. However, the similarities to hexokinase suggested that the ATPase domain of Hsp70s might undergo a substantial conformational change upon ATP hydrolysis[76]. For example, this conformational change might occur in the presence of a substrate or an Hsp40, which could then be transmitted to the substrate binding domain to enable substrate binding. Importantly, this finding supported previous limited proteolysis studies that indicated that Hsp70 function may be allosterically regulated[77].

A

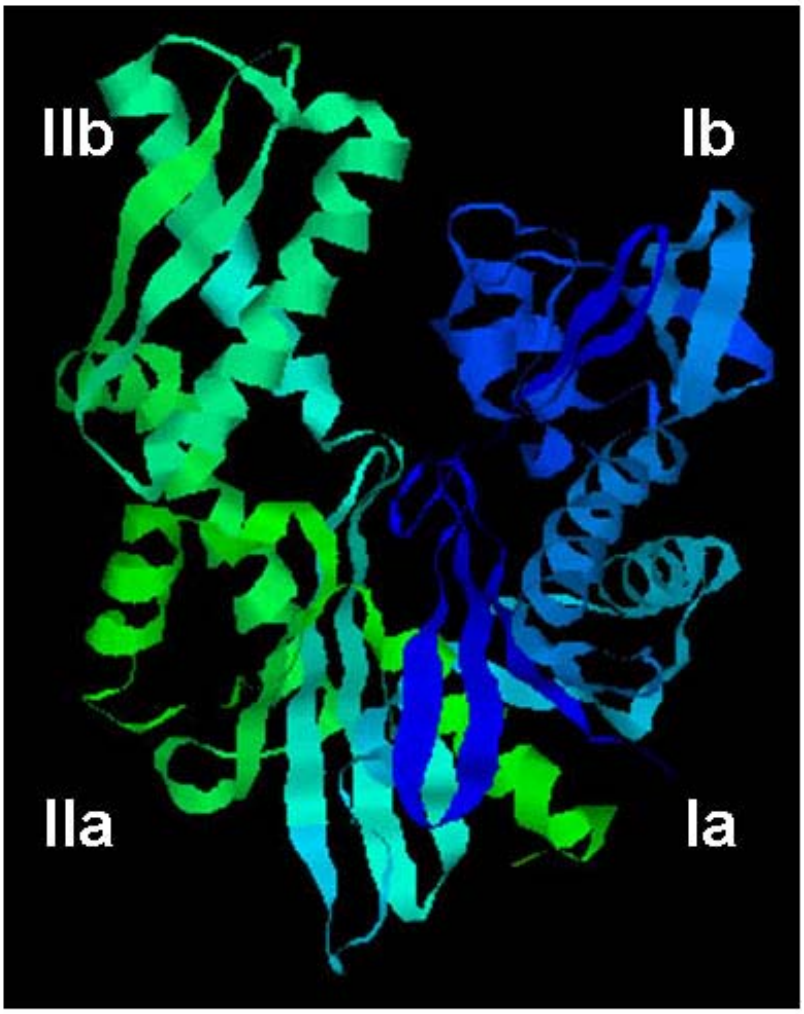

B

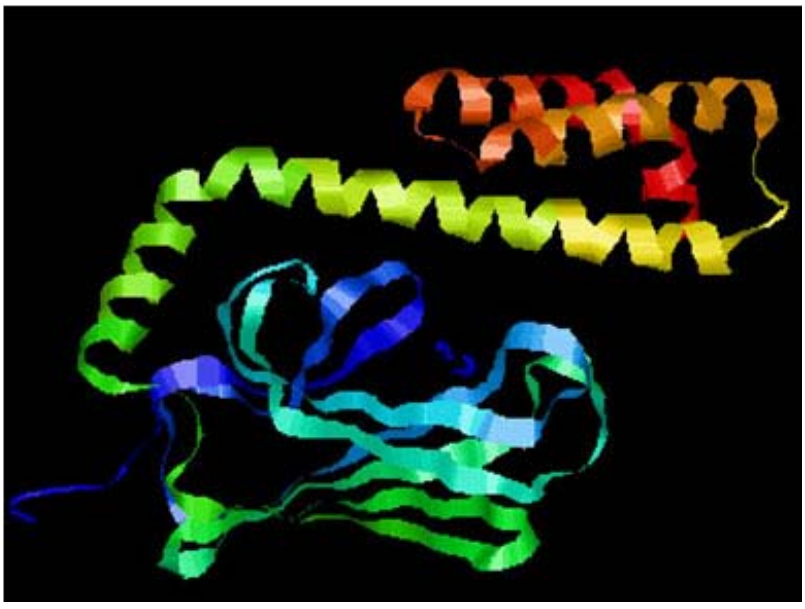

Figure 3: Crystal structures of isolated Hsp70 domains.

(A) The crystal structure of the ATPase domain of *Bos taurus* Hsc70 (Protein Data Bank ID: 3HSC) was solved at 2.2 Å resolution in the presence of ATP (not shown)[1]. The ATPase domain is predominantly α-helical and consists of two lobes, I and II, that can be further divided into subdomains a and b. ***(B)*** The crystal structure of the substrate binding and lid domains of *Escherichia coli* DnaK (Protein Data Bank ID: 1DKZ) was solved at 2.0 Å resolution in the presence of the peptide NRLLLTG[9]. The substrate binding domain is comprised of a β-sandwich structure followed by two α-helices. The lid domain terminates as an α-helical bundle. The peptide binds in an extended conformation to a hydrophobic cleft in the β-sandwich of the substrate binding domain.

The structures were generated using RasMol[11].

Next, the crystal structure of the C-terminal portion of bacterial DnaK (including the substrate binding domain and a part of the lid domain), was solved in the presence of the peptide NRLLLTG[9] (Figure 3B). The structure showed that the substrate binding domain was composed of a β sandwich followed by an α-helical bundle, while the lid domain was composed of α-helices. A hydrophobic pocket formed by the β sandwich directly bound to the peptide (which was present in an extended conformation) through numerous van der Waals interactions, while the α-helical portion did not contact the peptide; instead, this portion latched onto the β sandwich to capture the peptide. Moreover, the linker region between the ATPase and substrate binding domains remained exposed to solvent and therefore, was not ordered in the crystal. Based on a second crystal structure in which the α-helical portion appeared to be more mobile, the authors concluded that this mobility might be essential for the substrate to thread in and out of the β sandwich. Given these structural features, it is not surprising that the β sandwich portion of the Hsp70 substrate binding domain has a higher degree of sequence conservation amongst family members as compared to the α-helical portion.

In spite of the early structural resolution of individual Hsp70 domains, efforts to resolve the structure of a full-length Hsp70 have remained largely unsuccessful, probably because of the inherent flexibility of the various Hsp70 domains[24]. Instead, several studies have used nuclear magnetic resonance (NMR) and/or directed mutagenesis to designate similarities between the nucleotide-bound and nucleotide-free states of full-length Hsp70s, as well as to identify the residues required for inter-domain communication[78-81]. Based on these efforts, the inter-domain linker appears to be a key regulator of Hsp70 allostery. In the ATP-bound state, the linker binds in a hydrophobic cleft that is present between sub-domains Ia and IIa of the ATPase domain. This induces a conformational change in each Hsp70 domain such that the molecule as a whole

is compact and has weakened substrate binding. The ATP-bound state is therefore a state in which the Hsp70 molecule is less accessible to proteolytic cleavage. In the ADP-bound and nucleotide-free states, the linker is disordered and results in a conformation in which the ATPase and substrate binding domains are disjointed and can act independently of each other. In addition to the inter-domain linker, a universally conserved P residue (P143 in DnaK) in the ATPase domain regulates Hsp70 allostery[81]. The P is not only essential to stabilize the open conformation of the peptide binding pocket, but it also relays the change in the nucleotide-bound state of the ATPase domain to the substrate binding domain through an invariant R (R151 in DnaK) [81]. Lastly, mutagenesis studies have also identified the residues that are required for interactions between the lid and substrate binding domains and their contribution to inter-domain communication[82, 83].

More recently, the crystallization of 60 kD a truncation mutants of bovine Hsc70 in the nucleotide-free state[7] (Figure 4A) and rat Hsc70 in the ADP-bound state[12] (Figure 4B) have lent support to models that depict the mechanism for inter-domain communication. The structure of the bovine Hsc70 truncation supports the observation that the linker region is required for communication, and extensive mutagenesis studies of this region identified select residues required for Hsp70 function. On the other hand, the structure of the rat Hsc70 truncation supports the model in which the ATPase and substrate binding domains are disjointed in the ADP-bound state, and also provides evidence for the supposition that substrate binding can induce a similar change. Finally, the crystal structure of full-length ATP-bound Sse1p[14], a yeast Hsp110 which bears a high degree of sequence similarity to Hsp70s in the ATPase domain and acts as a NEF in the Hsp70 ATPase cycle[84, 85], has provided tremendous insight into the mechanism of allosteric regulation of Hsp70s (Figure 1-4C). For example, the binding of ATP in the ATPase domain of

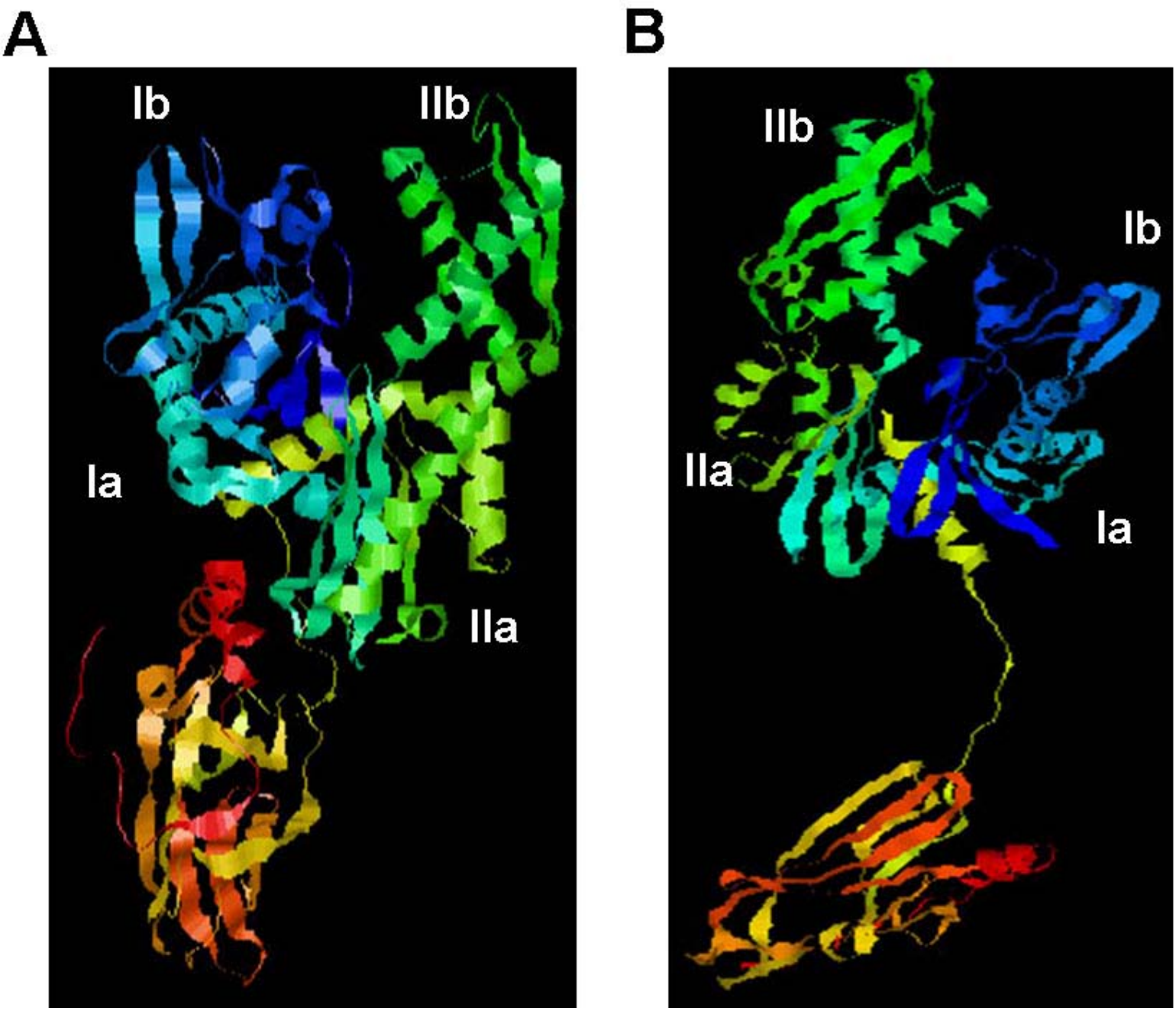
A
Ib
IIb
Ia
IIa
B
IIb
Ib
IIa
Ia

C

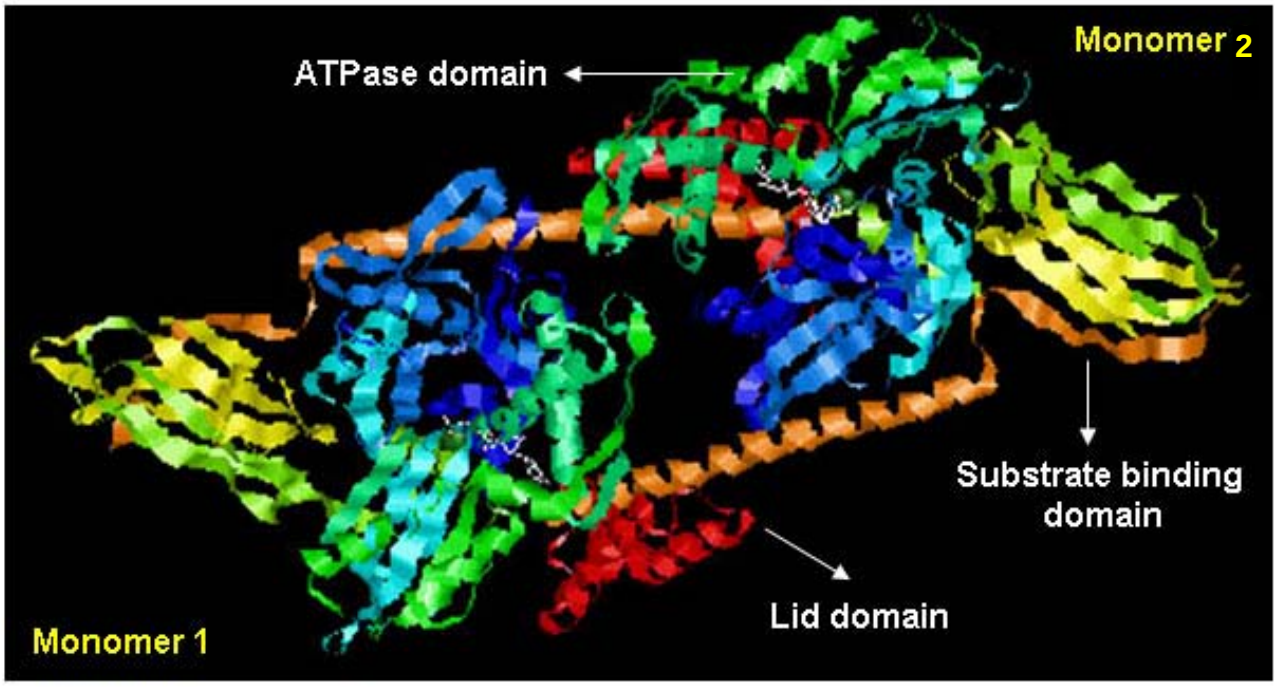
ATPase domain
Monomer 2
Substrate binding domain
Lid domain
Monomer 1

D

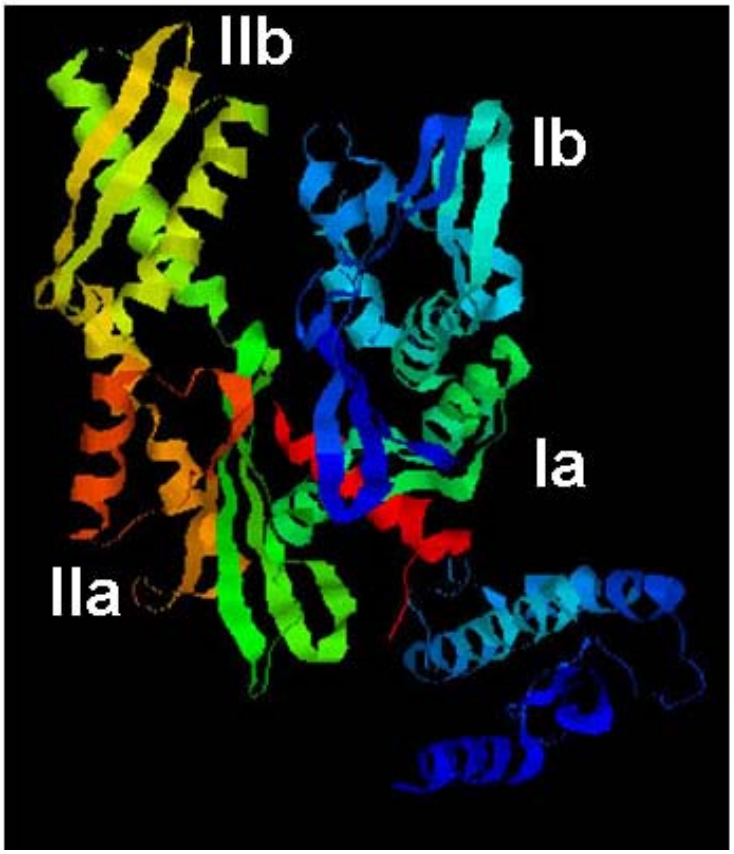
IIb
Ib
Ia
IIa

Figure 4: Crystal structures of select truncated Hsp70 isolates and Hsp70-like proteins.

(A) The crystal structure of a 60 kDa truncation mutant of *Bos taurus* Hsc70 (Protein Data Bank ID: 1YUW) was solved at 2.6 Å resolution and lacked nucleotide[7]. The ATPase domain is represented in blue and green while the substrate binding domain and a small portion of the lid domain is represented in red, yellow and orange. In this structure, the substrate binding and lid domains establish contacts with the interdomain linker as well as lobe I of the ATPase domain. ***(B)*** The crystal structure of a 60 kDa truncation mutant of *Rattus norvegicus* Hsc70 (Protein Data Bank ID: 2V7Z) was solved at 3.5 Å resolution in the presence of ADP and inorganic phosphate (not shown)[12]. The ATPase domain (represented in blue and green) is disjointed from the substrate binding and lid domains (represented in orange, yellow and red) via an exposed linker region. ***(C)*** The crystal structure of full-length *Saccharomyces cerevisiae* Sse1p (Protein Data Bank ID: 2QXL), a member of the related Hsp110 family, was solved at 2.4 Å resolution in the presence of ATP (depicted in white)[14]. In this structure, the ATPase domain is represented in blue and dark green, the substrate binding domain in yellow and light green, and the lid domain in red and orange. Sse1p was present as a dimer in the crystal structure with the substrate binding and lid domains of one monomer contacting the ATPase domain of the second monomer, thus stabilizing the structure. ***(D)*** The crystal structure of the ATPase domain of *Bos taurus* Hsc70 crosslinked to the J domain of *Bos taurus* auxilin (Protein Data Bank ID: 2QWR) was solved at 2.2 Å resolution in the presence of the ATP analog, AMPPNP (not shown)[15]. In this structure, the R171 residue of Hsc70 was altered to a C while the D 876 residue of auxilin was altered to a C to enable disulfide bridge-mediated crosslinking. The J domain of auxilin forms three predominant α-helices and is depicted in blue.

The structures were generated using RasMol[11].

Sse1p appears to be communicated to the hydrophobic peptide binding cleft of the substrate binding domain through hydrogen bonds that are formed not only between the catalytic residues and ATP, but also between the interdomain linker and the ATPase and substrate binding domains. Indeed, mutating the linker residues involved in hydrogen bond formation disrupted the function of Sse1p and the yeast cytosolic Hsp70, Ssa1p. However, because not all of the analogous mutations in DnaK and Ssc1p, a yeast mitochondrial Hsp70, disrupted function, the universality of this communication mechanism is unclear.

In addition to suggesting a mechanism for the allosteric coupling of the nucleotide binding and substrate binding domains, another facet of Hsp70 crystallography has addressed how Hsp70s interact with their cofactors. Structures of unique NEFs in complex with their cognate Hsp70 ATPase domains have been solved, and these studies have identified the Hsp70 residues that are involved in contacting the NEF[86-90]. Similarly, a crystal structure of the ATPase domain of bovine Hsc70 in complex with the J domain of auxilin, a cytosolic Hsp40 homolog, was recently solved in the presence of the ATP analog, AMPPNP[15] (Figure 4D). In this structure, the J domain of auxilin directed the Hsc70 interdomain linker onto a hydrophobic patch of the ATPase domain, hinting at a possible mechanism by which Hsp40s regulate Hsp70 allostery. However, to obtain a stable structure, the authors crosslinked the Hsc70 ATPase domain and the auxilin J domain via disulfide bridges by mutating a highly conserved R residue in the ATPase domain of bovine Hsc70, and an invariant D in the J domain of auxilin, to cysteines to enable crosslinking. Interestingly, the Hsc70 R maps to a region in the ATPase domain that is implicated in directly contacting the J domain of Hsp40s[91, 92].

Absent from these studies is the resolution of a BiP structure. While BiP exhibits a high degree of sequence conservation with several Hsp70s (for example, yeast BiP and *Escherichia*

coli DnaK share 50% overall sequence identity; yeast BiP and *Bos taurus* Hsc70, a cytosolic protein, share 61% overall sequence identity), the ER is more oxidizing than the cytosol; this might result in certain structural alterations that are unique to BiP. Furthermore, BiP participates in Ca^{2+} storage in the ER by directly binding to Ca^{2+} (refer to section 1.2.8).

Overall, a crystal structure of full-length Hsp70 in the presence of different nucleotides will be critical to better define the nucleotide-dependent allosteric change exhibited by these chaperones.

1.2.2 Yeast BiP's Hsp40 cochaperones

Yeast BiP interacts with three Hsp40 homologs to perform its various functions. The unique localization of these proteins within the ER and differences in domain organization might target BiP for specialized functions.

Sec63p, an essential protein, was initially discovered in a genetic screen targeted toward identifying yeast mutants defective for the ER translocation (refer to section 1.2.4) of a signal peptide-cytosolic enzyme hybrid protein[93]. Subsequent experiments demonstrated that *sec63* mutant yeast were defective for the translocation of a variety of soluble proteins[93, 94] and the translocation defect could be recapitulated *in vitro*[93]. The identification of an internal J domain in Sec63p indicated that it was a member of the Hsp40 sub-family of chaperones[94]; however, the J domain is the only region shared with the founding member of this protein class, DnaJ. Topology analysis next determined that Sec63p contains three transmembrane domains and that its J domain resided within the ER, ideally positioned to interact with BiP[95]. Since its identification, the vital role played by Sec63p during co- and post-translational translocation across the ER membrane (refer to section 1.2.4) has been addressed using *in vivo* and *in vitro* analyses, which

have revealed that Sec63p functions in translocation by: (i) residing in a complex with the Sec61 translocation channel (refer to section 1.2.4) in the ER membrane[95-100], (ii) by interacting with two proteins on the cytosolic face of the ER membrane, Sec71p and Sec72p[98, 101-106], which either assist the signal recognition particle in targeting ribosome-nascent polypeptide chain complexes to the translocation channel or directly participate in signal peptide recognition[103, 105], and (iii) by interacting with BiP in the ER lumen and directing it to nascent translocating polypeptide chains[98, 105-114]. Additionally, the interaction between mammalian SEC63 and BiP is required to localize BiP at the ER membrane so that it can function as a plug/gate for the translocation channel that opens into the ER[115, 116].

Scj1p (*Saccharomyces cerevisiae* DnaJ) was characterized in a genetic screen which was designed to identify genes that when overexpressed resulted in the missorting of a nuclear-targeted protein[117]. Scj1p shares 37% overall sequence identity with DnaJ and in addition to an N-terminal J domain, also contains a G/F-rich region and a cysteine-rich region similar to DnaJ. Subsequent studies determined that Scj1p was ER-localized and interacted with BiP in the ER lumen[118]; indeed, Scj1p's J domain contained the information required to specify BiP interaction because it could replace the J domain of Sec63p *in vivo*[118]. Further analyses revealed that Scj1p acted as a BiP cofactor during protein folding in the ER, especially under conditions of hypoglycosylation induced either by mutating components of the oligosaccharyl transferase (OST) complex (refer to section 1.2.5) or by treating cells with a small molecule inhibitor of glycosylation, *i.e.,* tunicamycin[119]. Finally, it was demonstrated that Scj1p and Jem1p (see below) participate in ER-associated degradation (ERAD; refer to section 1.2.6), either by assisting BiP in the recognition of misfolded substrates, or by targeting BiP-substrate complexes to the retrotranslocation channel[120]. Given that Scj1p has a substrate binding domain that bears

homology to DnaJ, it is possible that Scj1p directly binds to substrates and delivers them to BiP, as has been observed for the mammalian homolog, ERdj3 (refer to section 1.2.2.1). A critical role for Scj1p in the maintenance of ER protein homeostasis is further supported by the observation that *scj1Δ* yeast exhibit a high induction of the unfolded protein response[121] (UPR; refer to section 1.2.7).

When the *S. cerevisiae* genome was sequenced in 1996, several open reading frames encoding J domain-containing Hsp40 homologs were identified. One such open reading frame, *YJL073w*, was predicted to encode a J domain-containing protein with a putative membrane spanning domain and was named Jem1p (DnaJ-like protein of the ER membrane)[122, 123]. Targeted experiments determined that Jem1p is localized to the ER, and plays a role during karyogamy[122] (refer to section 1.2.8). Since J domain mutants of Jem1p were karyogamy-defective, the authors concluded that Jem1p's role in karyogamy depended on BiP interaction[122]. Subsequently, an overlapping role for Jem1p and Scj1p in ERAD was also described[120], and yeast deleted for *scj1* and *jem1* exhibit a synthetic temperature-sensitive growth phenotype[122]. Unlike most Hsp40s, Jem1p has an atypical domain arrangement wherein the J domain is located at the C-terminus and a putative substrate binding domain is N-terminal to the J domain. Moreover, since Jem1p might be membrane-associated[122, 123], it could target BiP-substrate complexes during ERAD by interacting with components of the retrotranslocation channel (refer to section 1.2.6).

Recently, a fourth ER-resident Hsp40 homolog, ERj5p, encoded by the *YFR041c* open reading frame[41], was identified in yeast. The function of this protein is unclear although it appears to be required to preserve the protein folding capacity of the ER, possibly by regulating BiP[41].

1.2.2.1 The human Hsp40, ERdj3

Compared to yeast, more Hsp40 cochaperones interact with BiP in the mammalian ER and six such factors have been identified to date (refer to section 1.1); one of these proteins is ERdj3. ERdj3 was initially described as a Scj1p homolog in dog pancreatic microsomes[45] and was subsequently isolated from human cells in a phenotypic cloning approach to identify genes that played a role in Shiga toxin trafficking[46]. Like Scj1p and DnaJ, ERdj3 has an N-terminal J domain followed by G/F-rich and C-rich regions and a substrate binding domain; the C-rich region might be involved in the formation of intramolecular disulfide bridges[124]. The key residues in ERdj3's substrate binding domain that are required for substrate binding have been identified[125] based on homology modeling to the substrate binding domain of Ydj1p[2], a yeast cytosolic Hsp40[126, 127]. These include residues constituting domain II of the substrate binding domain (spanning amino acids 160-200), a residue involved in dimerization, F326, and four residues in domain I, I134, V153, L208 and F223 that directly contact the substrate. It was also demonstrated that ERdj3 is expressed in all human tissues and stimulates BiP's ATPase activity, thus acting as a BiP cochaperone in the mammalian ER[46].

ERdj3 also co-purified as part of a multiprotein complex containing BiP, ER-resident molecular chaperones and incompletely folded immunoglobulin (Ig) heavy chains[128]. Follow-up biochemical experiments revealed that ERdj3 could directly bind to Ig heavy chains and other soluble substrates such as a non-secreted Ig κ light chain and a temperature-sensitive mutant of VSV-G[129]. Since the ERdj3-substrate association was lost upon the binding of BiP to substrate, a model was proposed in which ERdj3 binding helps to maintain substrates in a soluble, aggregation-free state until BiP binds to them[129]. More recently, this mechanism has been further elaborated[130]: ERdj3 recruits BiP to ERdj3-substrate complexes via a J domain-mediated

interactions and stimulates BiP's ATPase activity so that BiP has high substrate affinity. In the process, ERdj3 elicits its own dissociation from the chaperone-substrate complex. Given that another ER Hsp40, p58^{IPK}, adopts a similar mechanism to target BiP to its substrates[131], the authors on the papers speculate that Hsp40 substrate delivery to Hsp70s and stimulation of Hsp70 ATP hydrolysis are universally required to release substrates from Hsp40s.

1.2.3 Nucleotide Exchange Factors for yeast BiP and other BiP-interacting proteins

The yeast ER harbors two NEFs, Sls1p/Sil1p and Lhs1p; importantly, mammalian homologs/orthologs of both of these proteins exist (SIL1 and GRP170, respectively).

Yeast *SLS1* (synthetic lethal mutations with the 7S RNA mutation) was initially isolated in a genetic screen in the yeast *Yarrowia lipolytica* targeted toward identifying genes that demonstrated synthetic lethality with mutations in the signal recognition particle[132] (refer to section 1.2.4). Further analyses revealed that Sls1p localizes to the ER lumen and participates in protein translocation across the ER membrane as a BiP cofactor[132, 133]. When these data were recapitulated in *S. cerevisiae* and because Sls1p synergistically activated BiP's ATPase activity in the presence of the J domain of Sec63p[134], the authors concluded that Sls1p acted as a BiP NEF during protein translocation; this was the first identification of a BiP NEF. The Stirling group then determined that the overexpression of *S. cerevisiae SLS1/SIL1* suppressed the growth defect observed in *ire1Δlhs1Δ* yeast[135]. Ire1p is the signal transducer kinase/endoribonuclease for the unfolded protein response (refer to section 1.2.7) and Lhs1p is a second BiP NEF (see below)[135].

Lhs1p (Lumenal Hsp Seventy; *YKL073w*) was categorized as an ER-lumenal Hsp70-like protein when the yeast genome was sequenced in 1996[136, 137]. Although non-essential, synthetic

growth defects were observed in yeast lacking *lhs1* and containing *kar2* mutant alleles[136, 137]. These data suggested that BiP and Lhs1p might exhibit partially overlapping functions; indeed the *lhs1Δ* strain accumulated precursors of several secretory proteins, suggesting that Lhs1p played a role in protein translocation[136]. Lhs1p was also demonstrated to participate in the refolding of denatured substrates in the ER lumen[138]; it is still unclear whether this function is BiP dependent or not. Moreover, Lhs1p can act as a BiP NEF[139], similar to its mammalian ortholog, GRP170, which acts as a BiP NEF in the mammalian ER[140]. Taken together, the features of Lhs1p, *i.e.,* the sequence similarity of its ATPase domain to Hsp70s and the ability of Lhs1p to act as a BiP NEF, are reminiscent of other members of the Hsp110 family of chaperones[84, 85, 141]. Strikingly, the simultaneous deletion of *sls1* and *lhs1* is lethal, indicating that these NEFs confer an essential function in yeast, possibly during translocation[135].

BiP functions within the context of the crowded ER and hence, in addition to the Hsp40s and NEFs that are dedicated to BiP regulation, BiP genetically and physically interacts with several other proteins to ensure ER homeostasis. For example, a member of the protein disulfide isomerase (PDI) family of molecular chaperones, Eps1p, binds to BiP *in vitro* with a dissociation constant of $5.83 * 10^{-6}$ M[142]. Therefore, Eps1p and BiP might function in a coordinated manner *in vivo* in order to fold proteins that require the formation of disulfide bonds. Further evidence for a combinatorial role of BiP and PDIs comes from studies on a soluble misfolded substrate[143]. It was shown that a yeast PDI homolog, Pdi1p, functionally interacts with BiP during the targeting of the misfolded substrate to the retrotranslocation machinery during ERAD (refer to section 1.2.6). In addition, Rot1p, an essential ER membrane protein, is thought to act as a BiP cofactor during the folding of proteins involved in the maintenance of cell wall integrity and in the resolution of authophagic vesicles[144, 145]. Moreover, Yos9p, an ER lectin, forms a physical

ER-lumenal 'surveillance complex' with BiP and a membrane component, Hrd3p[3]. This complex targets terminally misfolded proteins to the retrotranslocation and/or ubiquitination machinery during ERAD (refer to section 1.2.6). Intriguingly, each member of this complex can individually recognize misfolded proteins, and whether this serves to distinguish between different non-native conformers within the same substrate, or to ensure the rapid clearance of toxic species, remains to be resolved.

1.2.4 BiP is required for co- and post-translational protein translocation across the ER membrane

In yeast, secretory proteins can be translocated into the ER as they are being translated, *i.e.,* co-translationally, or after they have been synthesized, *i.e.,* post-translationally[27]; a role for BiP has been described in both of these processes (Figure 5). The heterotrimeric Sec61 translocation channel (also known as the "translocon") is the conduit through which soluble and membrane-bound proteins enter the ER. The translocon is composed of Sec61p (Sec61α in mammals), Sbh1p (Sec61β in mammals), and Sss1p (Sec61γ in mammals). Sec61p is essential, possesses ten transmembrane segments and forms the aqueous translocation pore[96, 146]. The tail-anchored membrane protein Sss1p (Sec sixty-one suppressor) acts as an essential regulatory and Sec61p-stabilizing subunit[147, 148]. The role of the non-essential subunit, Sbh1p[149], during translocation is still unclear, though recent evidence suggests that its transmembrane domain is required primarily for cotranslational translocation (refer to Appendix A) and may regulate N-linked glysocylation (refer to section 1.2.5).

During co-translational translocation (Figure 5A), the signal peptide or transmembrane domain of a growing polypeptide chain is recognized by the signal recognition particle (SRP), a

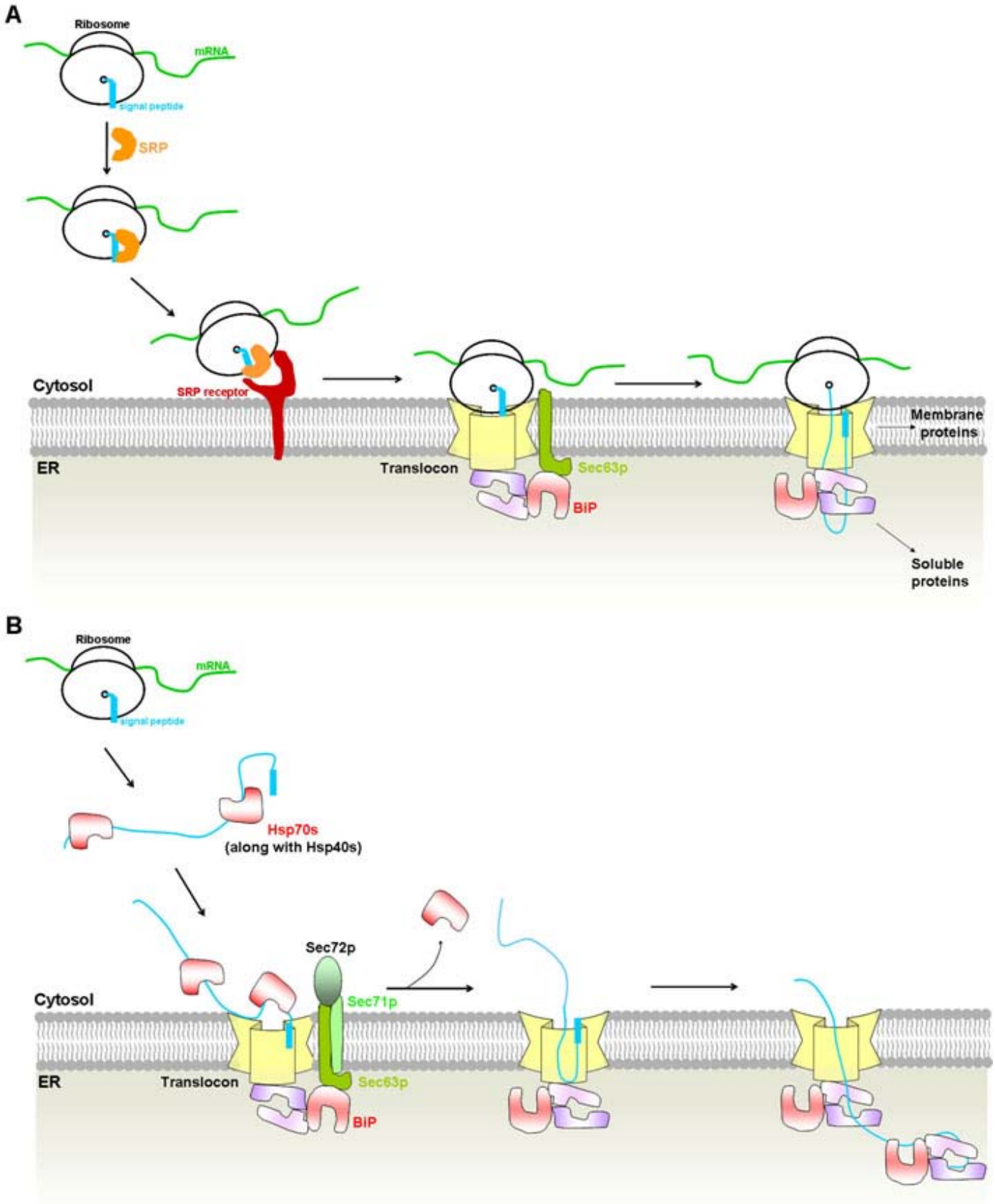
A
Ribosome
mRNA
signal peptide
SRP
SRP receptor
Cytosol
ER
Translocon
Sec63p
BiP
Membrane proteins
Soluble proteins
B
Ribosome
mRNA
signal peptide
Hsp70s
(along with Hsp40s)
Sec72p
Sec71p
Cytosol
ER
Translocon
Sec63p
BiP

Figure 5: Protein translocation across the endoplasmic reticulum membrane.

(A) During co-translational protein translocation, the signal recognition particle (SRP) binds to the signal peptide as it emerges from the ribosomal polypeptide tunnel. Next, the binding of SRP to its receptor at the ER membrane targets the ribosome-nascent polypeptide chain complex to the Sec61 translocation channel (Sec61 translocon). At the same time, BiP gates the ER-lumenal side of the translocon by interacting with its J domain-containing Hsp40 cochaperone, Sec63p. The release of SRP from the signal peptide, the interaction between the ribosome and Sec61p, resumption of translation, and subsequent BiP binding results in polypeptide translocation. Transmembrane segments can directly enter the ER membrane through a gate in the translocon (not shown). ***(B)*** During post-translational translocation, the polypeptide is completely synthesized in the cytosol, and the binding of Hsp70s and Hsp40s help to maintain the nascent protein in an aggregation-free state. The polypeptide is next targeted to the translocon by these cytosolic chaperones, and upon release, progresses into the translocation channel. The subsequent cleavage of the signal peptide and BiP binding ensures that the polypeptide chain travels into the ER via a Brownian ratchet mechanism. The interaction between BiP and Sec63p is essential to localize BiP to the translocating polypeptide. A critical role is also played by the membrane-bound translocon-associated protein, Sec62p (not shown in the figure).

ribonucleoprotein complex. This interaction results in a pause in translation. SRP then targets the ribosome-nascent polypeptide chain complex to the ER membrane by interacting with its membrane-bound receptor. Once the polypeptide chain has been transferred from SRP to the Sec61 channel, translation resumes and the tight binding between the ribosome and Sec61p ensures that the polypeptide chain translocates into the ER. By interacting with Sec63p, BiP localizes to the translocation channel and initially forms a gate to prevent the release of ions from the ER[115, 116]. When translocation is initiated, BiP binds to the polypeptide chain and promotes ER entry in an ATP-dependent manner. The genetic interactions observed between *sec61*, *sec63* and *kar2* temperature-sensitive mutant alleles, as well as the physical interactions between the corresponding wild-type proteins lend strong support for this model[93, 108-110, 114, 150]. Furthermore, *in vitro* translocation assays performed using reconstituted ER-derived microsomes lacking BiP[115] and synthetic proteoliposomes reconstituted with BiP mutants that are unable to interact with Sec63p or hydrolyze ATP[116], supports a role for BiP in co-translational translocation.

In yeast, several soluble proteins contain signal peptides that are poorly recognized by the SRP and therefore, they utilize a post-translational mode of translocation into the ER (Figure 5B). Prior to translocation, these proteins have to be maintained in a partially-unfolded aggregation-free state. Therefore, they associate with cytosolic Hsp70s and Hsp40 which are also responsible for delivering the substrates to the translocation channel. Once substrate handover has taken place, the cytosolic chaperones dissociate from the complex, and translocation is initiated, possibly through a Brownian ratcheting mechanism. This may be activated by Sec63p interaction with BiP and by BiP ATP hydrolysis, which ultimately 'pulls' the polypeptide into the ER[99, 105, 107, 111-113, 151]. Especially important for post-translational translocation is the interaction of Sec63p with Sec62p, an essential membrane-bound protein[93, 96, 97, 152, 153], and two

other non-essential, membrane-associated proteins, Sec71p and Sec72p[98, 101-106]. It is hypothesized that one or all of these proteins might contribute directly towards the recognition of a subset of signal peptides[103, 105]. In fact, BiP, Sec63p, Sec71p and Sec72p form the Sec63 complex which has been shown to participate in post-translational translocation[98]. Of note, secreted proteins in mammals almost always utilize the co-translational translocation pathway, and it is not surprising that mammalian homologs of Sec71p and Sec72p have not been identified to date. However, a mammalian Sec62p homolog exists[44, 154].

In addition to the signal peptidase complex and oligosaccharyl transferase complex, which are closely associated with the translocon (refer to section 1.2.5), unique membrane-bound components have been identified as regulators of translocation in mammalian cells. One glycoprotein, the translocon-associated membrane protein (TRAM) is essential for the translocation of a majority of proteins[155, 156]. Though the exact role played by TRAM is still unclear, given its transitory presence in the aqueous translocon pore and its interaction with translocating membrane proteins, it is possible that TRAM acts as a membrane chaperone[156, 157]. A second translocon-associated protein complex, TRAP, is also present in close proximity to the mammalian translocon, though its function has not been described[156, 158]. Additional membrane-associated components may also regulate the yeast Sec61 translocon. Recently, a nine-member complex called the ER membrane complex (EMC) has been implicated in the biogenesis and insertion of yeast membrane proteins into the ER[121].

1.2.5 BiP participates in nascent protein folding in the ER

As a protein traverses into the ER, there are two primary modifications that may occur co-translocationally: (i) cleavage of the signal peptide in soluble proteins which is catalyzed by the

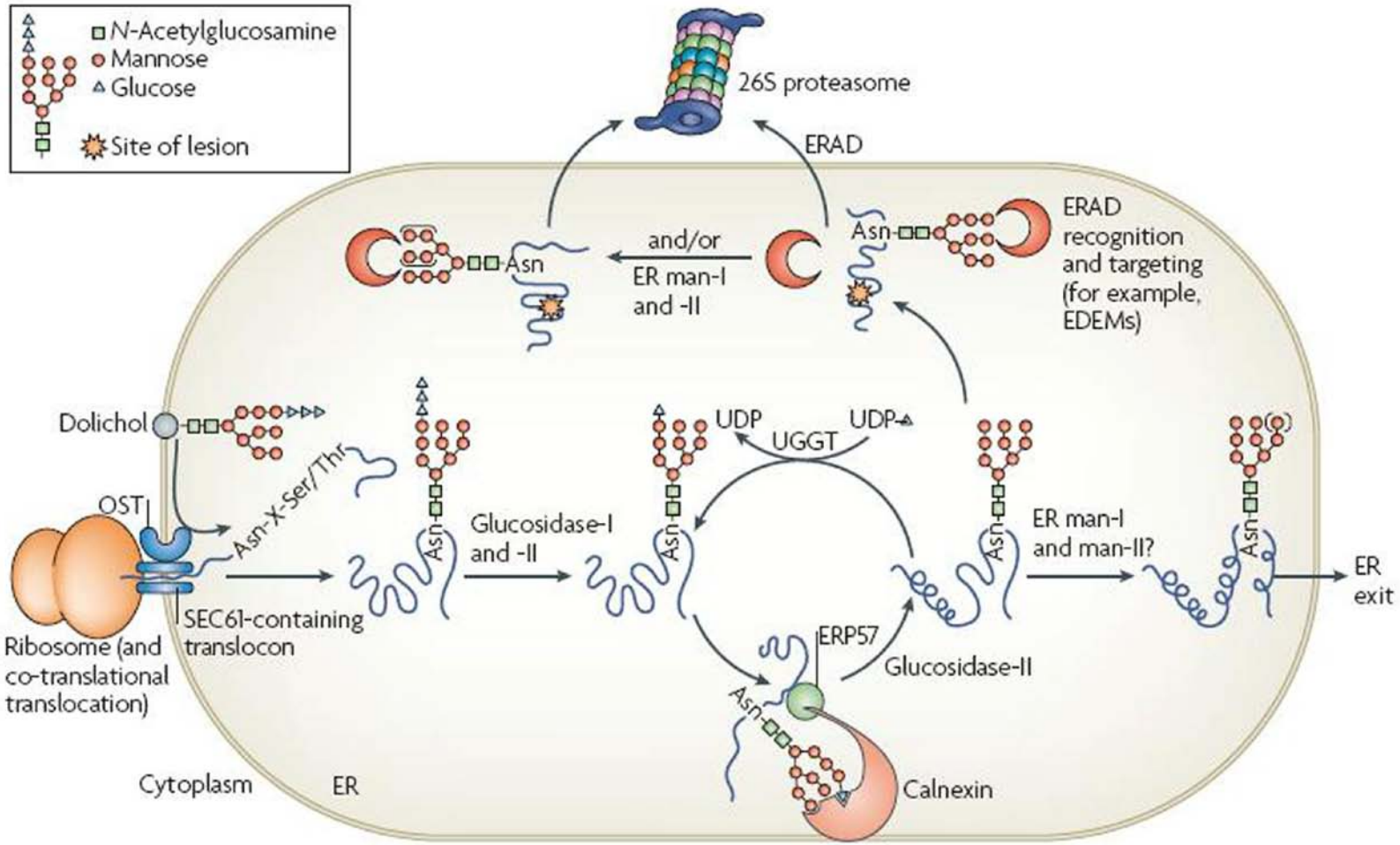
N-Acetylglucosamine
Mannose
Glucose
Site of lesion
26S proteasome
ERAD
ERAD recognition and targeting (for example, EDEMs)
and/or ER man-I and -II
Asn
Dolichol
OST
Asn-X-Ser/Thr
SEC61-containing translocon
Ribosome (and co-translational translocation)
Glucosidase-I and -II
UDP
UDP
UGGT
ER man-I and man-II?
ER exit
ERP57
Glucosidase-II
Calnexin
Cytoplasm
ER

Figure 6: N-linked glycosylation and the degradation of glycosylated proteins in the mammalian ER.

Proteins that enter the ER are often modified by the addition of a $GlcNAc_2$-Man_9-Glc_3 glycan to the side-chain nitrogen of N residues in the consensus N-X-S/T motif. First, the translocon-associated oligosaccharyl transferase (OST) complex co-translationally transfers $GlcNAc_2$-Man_9-Glc_3 glycans from dolichol to substrate proteins. Next, glucosidase-I and glucosidase-II sequentially remove two terminal glucoses, generating monoglucosylated substrates that are recognized by calnexin and calreticulin through their carbohydrate-binding globular domains (calreticulin is a soluble protein and is not shown). The interaction with calnexin and calreticulin facilitates folding. ERp57, a PDI homolog that is associated with the arm domain of calnexin and calreticulin, catalyzes disulphide bond formation. Following release from the calnexin–calreticulin cycle, the final glucose is trimmed by glucosidase-II. If glycoproteins have adopted their native conformations, they can be demannosylated (denoted by the use of parentheses around the mannoses) by ER mannosidases I and II (ER man-I and man-II) and exit the ER through coatomer protein complex-II vesicles. However, the folding of some glycoproteins requires multiple rounds of association with calnexin–calreticulin. Such proteins are reglucosylated by UDP-glucose:glycoprotein glucosyltransferase (UGGT), which recognize non-native states and transfers a glucose from UDP-glucose to the N-linked $GlcNAc_2$-Man_9 glycan. Re-monoglucosylation promotes re-entry into the folding cycle. Terminally misfolded glycoproteins might also be targeted for ERAD by calnexin and calreticulin or by other ERAD-requiring components such as EDEM (ER degradation enhancing α-mannosidase-like lectin), and in some cases, BiP. GlcNAc, *N*-acetylglucosamine; Man, mannose; Glc, glucose.

The figure was adapted from Vembar and Brodsky, 2008[5].

membrane-associated signal peptidase complex consisting of Sec11p, Spc1p, Scp2p and Spc3p[159-163], and (ii) N-linked glycosylation[164, 165] which is catalyzed by the oligosaccharyl transferase complex (OST) consisting of Ost1p, Ost2p, Ost3p, Ost5p, Swp1p and Wbp1p. The N-linked oligosaccharide, $GlcNAc_2$-Man_9-Glc_3, of which GlcNAc is N-acetylglucosamine, Man is mannose and Glc is glucose, is added onto an N in a consensus N-X-S/T motif (with X representing any amino acid) (Figure 6). The subsequent removal of terminal glucose residues by glucosidases, and facilitated folding by the carbohydrate-binding lectin-like chaperones calnexin and calreticulin, results in a glycoprotein that contains a $GlcNAc_2$-Man_9 moiety. Proteins with this sugar are competent for ER exit and can transit to their final destinations. In yeast, a calreticulin homolog is absent, and membrane-bound calnexin is non-essential, indicating that other proteins participate in the folding of glycosylated proteins, including BiP. In fact, BiP function is essential for the folding of the model glycosylated substrate, vacuolar carboxypeptidase Y (CPY)[166]. Furthermore, since folding of several proteins initiates co-translocationally[167, 168], a role for BiP becomes critical not only to promote correct folding, but also to prevent the formation of non-native conformers, which could occur when the N- and C-termini of certain substrates are unable to interact until the conclusion of translocation.

The method used by BiP to promote folding is well-established in mammalian cells, especially with regards to the folding and subsequent assembly of immunoglobulin heavy and light chains[169, 170]. Given that BiP was initially identified as part of immunoglobulin heavy chain complexes[34], BiP's requirement in this process is not surprising. BiP can recognize hydrophobic patches in its substrates[171, 172] either as part of unfolded polypeptide chains or on the surfaces of unassembled subunits. Through cycles of substrate binding and release mediated by ATP hydrolysis and interactions with its Hsp40 cofactors[119] and NEFs[138], BiP prevents protein

aggregation and retains substrates in the folding pathway. Interestingly, ATPase mutants of BiP can still bind to their substrates and maintain them in an aggregation-free state; however, they are unable to complete the folding cycle, and the substrates therefore cannot be folded to a secretion-competent state[74].

1.2.6 BiP-mediated recognition and targeting of misfolded proteins for ER-associated degradation

The ER is a unique protein folding environment and approximately one-third of all proteins in eukaryotes are targeted to this compartment[173, 174]. In addition to molecular chaperones, the ER contains unique enzymes that maintain an oxidizing environment relative to the cytoplasm (*i.e.,* PDIs) and catalyze co- and post-translational modifications (*i.e.,* enzymes in the N-linked glycosylation pathway). Therefore, to ensure that the ER assembly line manufactures products that meet the needs of the cell, secreted proteins are subject to ER quality control (ERQC)[175]. The primary mediators of ERQC are molecular chaperones that not only sample and help polypeptides to fold but also evaluate the conformations of their substrates. If a polypeptide has attained its native conformation, it might be targeted to its final destination. If folding is delayed or an illegitimate conformation arises, the substrate is either subjected to additional folding cycles or is selected for ERAD[176]. If, however, the concentration of these potentially toxic protein species increases, compensatory pathways are induced, including lysosomal degradation of bulk cytosolic proteins or even entire organelles, *i.e.,* autophagy[177]. The individual steps during ERAD (Figure 1-7) include substrate recognition, targeting, retrotranslocation, ubiquitination and proteasomal degradation[5].

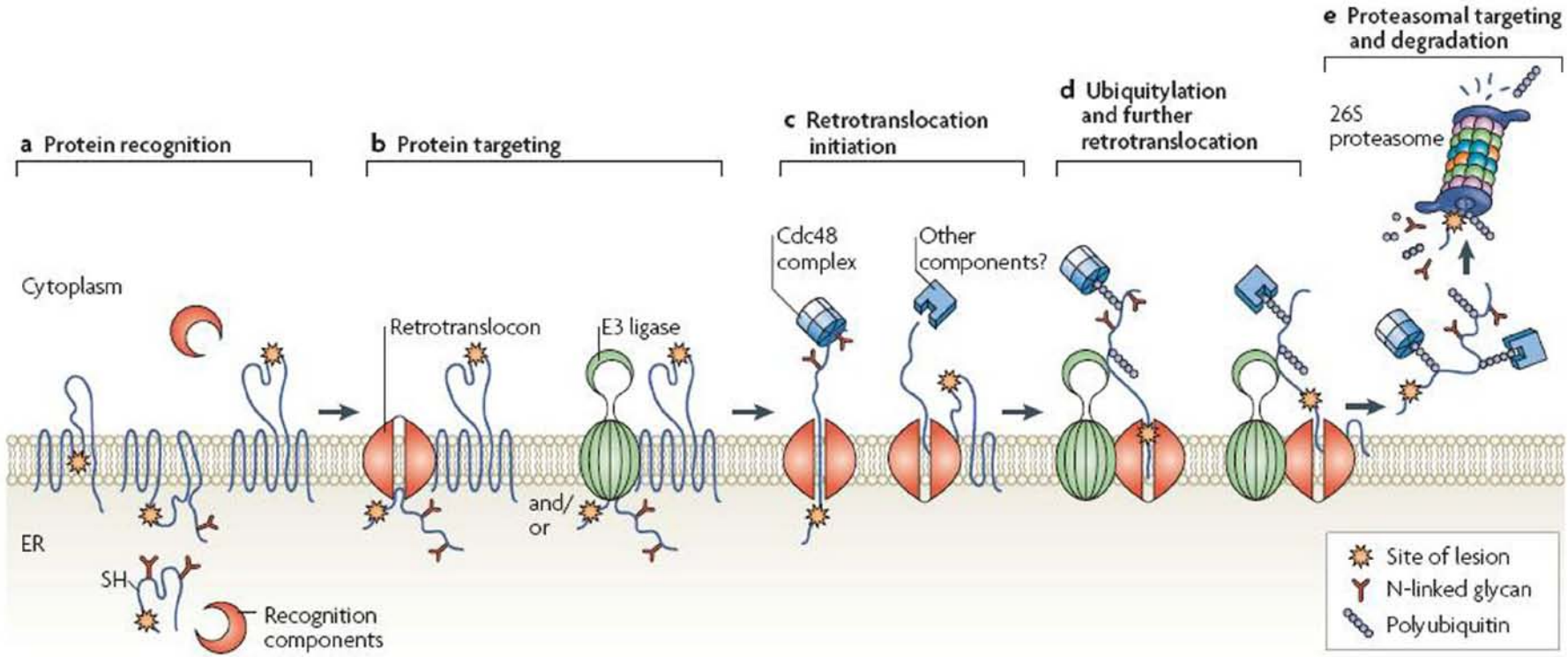
a Protein recognition
b Protein targeting
c Retrotranslocation initiation
d Ubiquitylation and further retrotranslocation
e Proteasomal targeting and degradation
Cytoplasm
ER
SH
Recognition components
Retrotranslocon
E3 ligase
and/or
Cdc48 complex
Other components?
26S proteasome
Site of lesion
N-linked glycan
Polyubiquitin

Figure 7: A step-by-step illustration of endoplasmic reticulum-associated degradation.

(A) *Protein recognition*. Misfolded proteins containing cytoplasmic, intramembrane or ER-lumenal lesions are recognized by cytoplasmic and lumenal chaperones and associated factors, such as Hsp70s, calnexin and calreticulin, and PDIs. ***(B)*** *Protein targeting*. ERAD substrates are targeted to the retrotranslocation machinery (the retrotranslocon) and/or to ubiquitin ligases. ***(C)*** *Retrotranslocation initiation*. Substrate retrotranslocation into the cytoplasm might be initiated in part by the cell-division cycle-48 (Cdc48p) complex; other components, such as molecular chaperones or the proteasome, might also be required for this step. The energy derived from ATP hydrolysis by Cdc48p, which is a AAA+ ATPase, is coupled to retrotranslocation. ***(D)*** *Ubiquitination and further retrotranslocation*. As proteins exit the retrotranslocon they are polyubiquitinated by ubiquitin ligases. This promotes further retrotranslocation and is aided by cytoplasmic ubiquitin-binding protein complexes. ***(E)*** *Proteasomal targeting and degradation*. Once a polyubiquitinated substrate is displaced into the cytoplasm, it is recognized by receptors in the 19S cap of the 26S proteasome. De-ubiquitinating enzymes (not shown) remove the polyubiquitin tag, and peptide N-glycanase (not shown) might also be required for efficient degradation. The substrate is then threaded into the 20S catalytic core of the proteasome where it is broken down into peptide fragments. Ubiquitin that is generated by this process can be recycled for subsequent rounds of modification.

The figure was adapted from Vembar and Brodsky, 2008[5].

BiP participates in the recognition of substrates with misfolded lesions in the ER lumen by binding to hydrophobic patches[171, 172]. In the native conformation, hydrophobic patches are usually buried within the interior of soluble proteins in order to maintain the lowest energy state[8]. However, since the misfolded state is not the most energetically favorable state, these patches can become exposed, which can lead to aggregation. Indeed, various groups have demonstrated that BiP, either independently or with its Hsp40 co-factors, is required for the recognition of a variety of misfolded substrates in mammalian and yeast systems, including unglycosylated invertase and misfolded prolactin[178], unassembled immunoglobulin light chains[179], misfolded human surfactant protein C[180], and mutant forms of yeast CPY (CPY*) and pre-pro-alpha factor (ΔgpαF), the yeast mating pheromone[120, 181]. However, the role of the NEFs that interact with BiP during ERAD in yeast is ill-defined.

In mammalian cells, another well-described aspect during ERAD recognition is the crosstalk between BiP and the lectin-like proteins, calnexin and calreticulin. For example, some substrates interact sequentially with BiP and calnexin/ calreticulin in the cell[182], whereas calnexin and BiP synergistically suppress the aggregation of a non-glycosylated substrate *in vitro*[183]. Furthermore, BiP can compensate for the absence of the calnexin–calreticulin cycle by binding to glycosylated substrates with which it does not normally interact[184]. In some cases, the two chaperone systems even have unique effects on the fate of a substrate[185-188]. Additionally, BiP cooperates with the PDIs during ERAD[5]. As previously stated, BiP and Pdi1p recognize a misfolded substrate in yeast and target it for retrotranslocation[143]. Another novel component of ERAD in mammalian cells is the recently characterized Hsp40 homolog, ERdj5, which not only contains a J domain for BiP interaction, but also contains four canonical thioredoxin-like active-site Cys-X-X-Cys motifs, suggesting that it can function as a PDI[189]. Indeed, in a BiP-dependent

manner, ERdj5 regulates the degradation of null Hong Kong (NHK), a disease-causing α1-antitrypsin variant, by accelerating the formation of degradation competent NHK monomers from disulfide-linked dimers. Therefore, the complexity of BiP interactions necessary to catalyze ERAD in mammals is increased relative to yeast.

Soluble ERAD substrates must first be selected (*i.e.,* targeted) for retrotranslocation to the cytosol because the enzymes required for ubiquitination (Figure 1-8) reside in this compartment. However, substrate recognition and targeting can become indistinguishable because ERAD substrates might not be passed between distinct recognition and targeting complexes. Recent observations suggest that factors required for recognition reside within multiprotein complexes that are also essential for targeting. For example, as noted above (refer to section 1.2.4) yeast BiP is tethered to the ER membrane by virtue of its interaction with Sec63p, which in turn resides in a multiprotein ensemble that includes Sec61p, a candidate for the retrotranslocation channel[190-192]. Therefore, a complex containing BiP, Scj1p, Jem1p and misfolded substrates could directly target substrates for retrotranslocation through the Sec61 channel. Alternately, as discussed above (section 1.2.3), BiP forms a complex with Yos9p and membrane-bound Hrd3p, a protein that interacts with the ubiquitin ligase, Hrd1p, a second candidate for the retrotranslocation channel[193], and this complex might suffice for the targeting of glycosylated and unglycosylated substrates. In mammals, a recent study implicated a transmembrane ER-resident protein, Herp, as a receptor for non-glycosylated BiP substrates[194]. As Herp coprecipitates with Derlin-1[195], a third candidate for the retrotranslocation channel[196, 197], and with ubiquitinated proteins and the 26S proteasome[195], this targeting factor might bridge the ER-recognition machinery to the cytoplasmic ubiquitin–proteasome system. A Herp

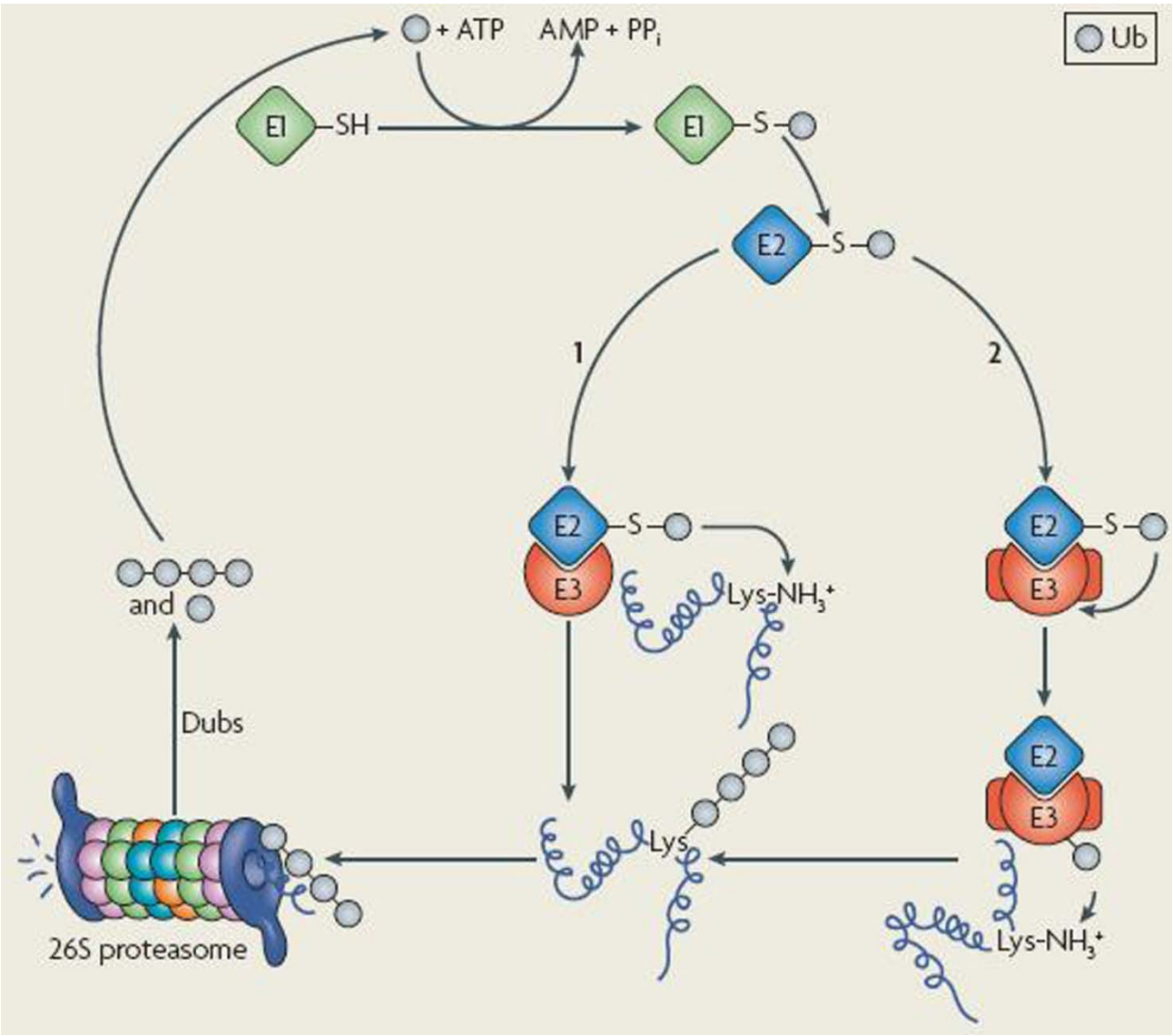
+ ATP
AMP + PPi
Ub
E1
SH
E1
S
E2
S
1
2
E2
S
E3
Lys-NH3+
E2
S
E3
and
Dubs
E2
E3
Lys
26S proteasome
Lys-NH3+

Figure 8: The ubiquitin-proteasome system.

Ubiquitin (Ub), a 76 amino-acid peptide, is covalently attached through an isopeptide bond to ε-amino groups of K in substrates. Ub itself contains several K residues, but the covalent linkage through K48 seems to be a hallmark for proteasome-mediated degradation. Degradation also requires at least a tetra-Ub chain[6].

Ub conjugation first requires an E1 Ub-activating enzyme. The C-terminal G of Ub is adenylated by the E1 and then displaced following the nucleophilic attack of a conserved C residue in the E1, resulting in a thioester linkage between the E1 and Ub. The next step involves the transfer of Ub to an E2 Ub-conjugating enzyme through the formation of another thioester linkage. The covalent attachment of Ub to substrates is catalysed by E3 Ub ligases, such as RING, U-box and HECT domain-containing proteins. The RING and U-box domain E3s facilitate the transfer of Ub from the E2 to selected substrates (step 1). The HECT domain E3s are covalently coupled to Ub by a thioester bond in the HECT domain. The subsequent interaction with substrates is required for Ub modification (step 2). Once polyubiquitinated, a substrate can be targeted to the 26S proteasome and degraded[13].

The figure was adapted from Vembar and Brodsky, 2008[5].

homolog, Usa1p, exists in yeast and has been shown to interact with the yeast Derlin homolog, Der1p, and also with Hrd1p[198].

Given the various roles of BiP during ERAD, it will become important to characterize the structural features in BiP that aid in the recognition of misfolded substrates. Notably, it will be necessary to discover the mechanism by which BiP distinguishes between unfolded and misfolded proteins. This specificity of function might largely depend on the Hsp40-containing complexes in which BiP resides.

1.2.7 BiP is required for the induction of the unfolded protein response

Under conditions of ER stress, misfolded protein accumulation in the ER can lead to the induction of the UPR, which reduces ER-protein load by several elaborate mechanisms[199-202]: the volume of the ER expands by up regulated lipid synthesis, the concentration of molecular chaperones and enzymes required for post-translational modifications rises, the transcription of components of the ERAD machinery increases in order to enhance misfolded protein clearance, protein translation and ER translocation decrease, and protein transport through the secretory pathway probably increases, thereby emptying this compartment of potentially toxic polypeptides. UPR induction might also result in the cleavage of ER-associated mRNAs that encode secreted proteins[203].

The existence of a UPR pathway in yeast was first revealed by the identification of a 22 bp *cis*-acting element in the promoter region of BiP which was transcriptionally responsive to the accumulation of unfolded proteins in the ER[204, 205] (*i.e.,* the unfolded protein response element or UPRE). The subsequent discovery of the ER membrane-bound inositol-requiring protein-1 (Ire1p), a transmembrane Ser/Thr kinase and site-specific endoribonuclease, as an essential

component of the response pathway[206, 207], and the observation that activated Ire1p could cleave an unspliced intron in the mRNA of the transcriptional activator Hac1p[208, 209] (homologous to ATG6/CREB), implicated Ire1p directly in signal transduction. The next step was to establish the mechanism of Ire1p activation. Based on the observation that BiP and Ire1p physically interact under normal growth conditions, and that this interaction is lost under conditions of ER stress[210], it was hypothesized that the titration of BiP away from Ire1p, due to an accumulation of unfolded proteins, could trigger Ire1p oligomerization, and hence UPR induction[211-213]. This hypothesis was supported by the analysis of BiP mutants that dissociated from Ire1p at restrictive temperatures leading to an induction of the UPR[214] as well as *ire1* alleles that were defective for BiP interaction and therefore exhibited a sustained UPR[215]. However, it is also becoming clear that Ire1p itself can directly bind to unfolded proteins. The first evidence for this came from the crystal structure of the Ire1p ER lumenal domain, which was found to resemble the binding pocket of the major histocompatibility complex I (MHCI) protein for its peptide antigens[216]. Follow-up experiments demonstrated that the lumenal domain of Ire1p could indeed bind to unfolded polypeptides[217, 218].

Based on all of these data, a working model for the induction of the UPR is as follows (Figure 9): Under unstressed conditions, BiP binds to Ire1p in the ER lumen and maintains the enzyme in an inactive state. When BiP is titrated away from Ire1p to bind to misfolded substrates, Ire1p is activated (Figure 9, step 1). Ire1p also dimerizes and binds to misfolded proteins owing to the formation of a peptide-binding pocket in the ER-lumenal domain, thus resulting in further activation (Figure 9, step 2). Ire1p activation involves the transphosphorylation of its cytoplasmic domain, which triggers endoribonuclease activity and splices an intron in the mRNA that encodes Hac1p, the dedicated UPR transcriptional activator.

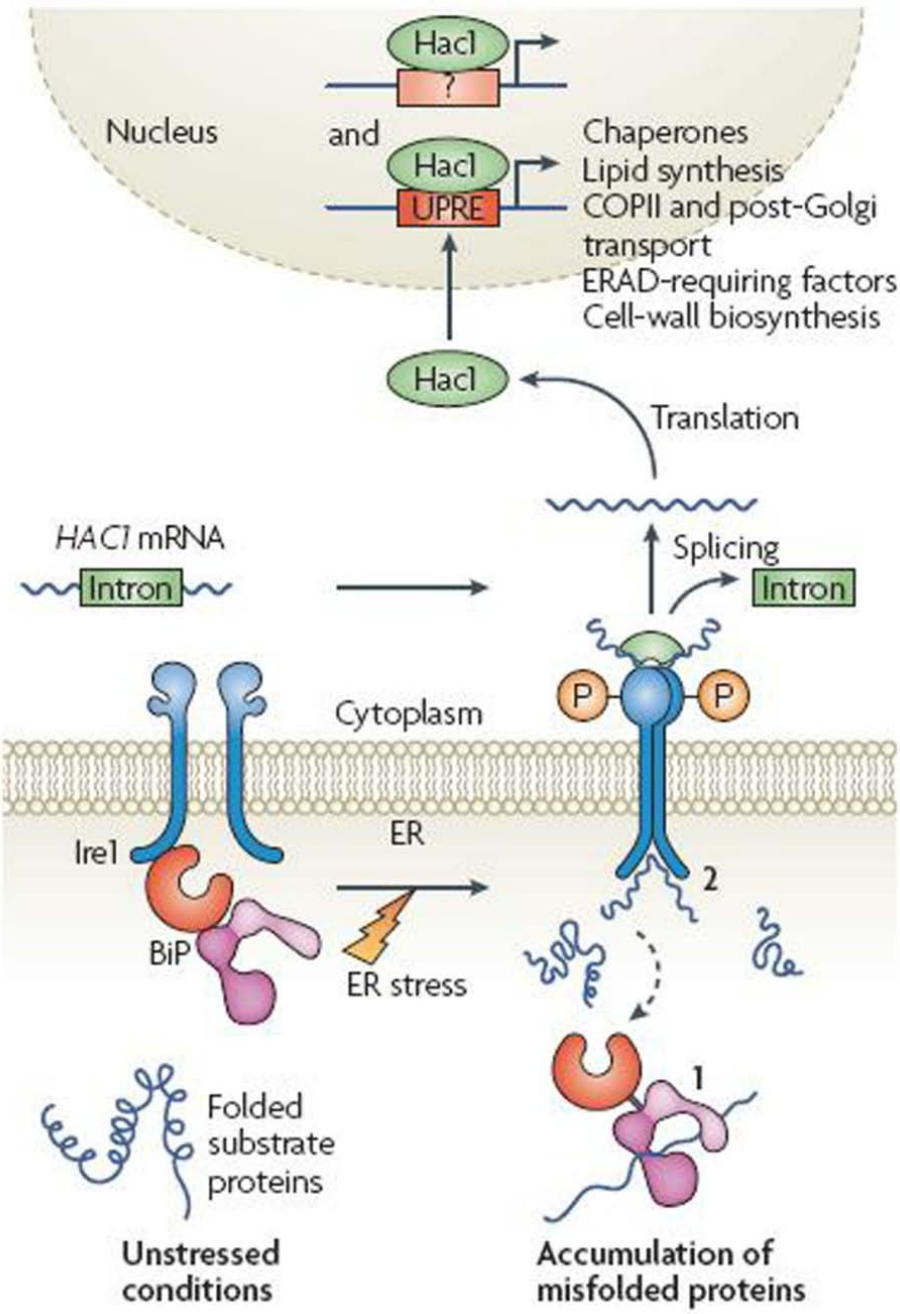
Hac1
?
Nucleus
and
Hac1
UPRE
Chaperones
Lipid synthesis
COPII and post-Golgi transport
ERAD-requiring factors
Cell-wall biosynthesis
Hac1
Translation
HAC1 mRNA
Intron
Splicing
Intron
P
P
Cytoplasm
Ire1
ER
2
BiP
ER stress
1
Folded substrate proteins
Unstressed conditions
Accumulation of misfolded proteins

Figure 9: Induction of the unfolded protein response (UPR) in yeast.

Under unstressed conditions, BiP binds to Ire1p and maintains it in an inactive state, *i.e.*, Ire1p cannot function as an endoribonuclease. Consequently, an intron in the mRNA of *HAC1* remains unprocessed and forms a hairpin structure that inhibits Hac1p translation (not shown). When the ER is stressed due to an accumulation of misfolded proteins, two phenomena occur: 1) BiP titrates away from Ire1p to bind to its misfolded substrates either to prevent them from aggregating or to target them for ERAD, and 2) Ire1p dimerizes or polymerizes and directly binds to misfolded proteins due to the presence of an ER-lumenal peptide binding pocket. This results in Ire1p trans-autophosphorylation and subsequent activation of its endoribonuclease activity. Active Ire1p cleaves the inhibitory intron in the mRNA of *HAC1*, permitting Hac1p translation. Hac1p translocates into the nucleus to upregulate UPR-responsive genes (listed in the figure).

The figure was adapted from Vembar and Brodsky, 2008[5].

The processed mRNA is re-ligated by a tRNA ligase, Trl1p, and translated[219]. Hac1p then translocates into the nucleus, binds to UPREs and possibly other sequences in the promoter region of target genes, including those regulated by Gcn4p[220], and upregulates their expression.

Making the signaling mechanism more intricate, in the past year, two reports have demonstrated that the cytosolic domain of Ire1p forms multimers (not dimers as had been previously hypothesized), and upon activation, Ire1p multimers localize to discrete foci in the ER membrane[221, 222]. This phenomenon appears to be essential to recruit the unspliced form of the mRNA of Hac1p for subsequent cleavage. Finally, the mammalian ER harbors two additional signal transducers, PERK and ATF6, and the intricacy of their interactions with BiP changes specific aspects of the responses elicited by the mammalian UPR[223-225].

1.2.8 Other BiP functions

In addition to the functions described above, BiP also participates in the maintenance of ER calcium stores (in yeast and mammals), as well as in nuclear fusion during mating in yeast; each of these functions is briefly discussed in this section. The possibility that other BiP-regulated processes remain to be discovered cannot be ruled out.

The role of BiP in calcium storage is best established in mammalian cells. The concentration of calcium in the mammalian ER is nearly a thousand-fold higher as compared to the cytosol, and ER calcium storage is vital to maintain ER homeostasis as well as for rapid physiological signaling[226]. Besides the employment of signaling receptors and ER calcium pumps, the primary mechanism to maintain a high ER calcium concentration is through the binding of calcium to low-affinity calcium binding proteins such as calnexin, calreticulin and GRP94, the ER-lumenal Hsp90, and high-affinity calcium binding proteins such as reticulocalbin

and calstorin[227]. Also amongst this ensemble of calcium binding proteins is BiP[228]. Due to its abundance in the ER, and the presence of acidic amino acid clusters in BiP's sequence that are common to other calcium binding proteins, it was determined that BiP contributes to nearly 25% of the ER calcium stores[170, 229]. Furthermore, BiP's calcium binding activity appeared to be independent of its chaperoning activity because a BiP mutant lacking the substrate binding and lid domains successfully maintained ER calcium levels[229]. Interestingly, drugs (for example, thapsigargin[230]) that inactivate the family of sarco-ER-Ca^{2+} ATPases, *i.e.,* SERCA, which pumps calcium into the ER[230], also activate the UPR[231]. This suggests that proteins that fold in the ER, in a BiP and calnexin/calreticulin dependent manner, require high levels of calcium to attain their native conformations. Finally, the anti-apoptotic function exhibited by BiP in transformed cells could be correlated to the maintenance of calcium stores in the ER by BiP[39, 232, 233].

During the sexual cycle of *S. cerevisiae*, nuclear fusion or karyogamy is essential to produce diploid progeny[234]. The first gene characterized to participate in karyogamy, *KAR1*, was also required during mitosis and conjugation, possibly for the function and formation of intra- and extra-nuclear microtubules[235, 236]. A random mutagenesis screen was subsequently performed to isolate additional mutants that were defective for karyogamy, and two other genes, *KAR2* and *KAR3*, were identified[36]. The characterization of *KAR2* as the yeast BiP homolog[37], and the implication of the Sec63 complex containing Sec63p, BiP, Sec71p and Sec72p in nuclear fusion[237], supported a role for BiP during karyogamy. Furthermore, the genetic interactions exhibited by *kar2* alleles with *kar8/jem1*[238], and the nuclear fusion defects observed in *jem1Δ* yeast[122], strongly suggest that the formation of a functional BiP-Jem1p pair is essential for nuclear fusion. Since the yeast ER is contiguous with the nuclear envelope, it is not surprising

that ER proteins play a role during karyogamy. However, the mechanistic details of this process remain ill-defined.

1.2.9 BiP and human disease

Given the multiple processes in which BiP partakes, as well as the diverse proteins with which it interacts, BiP function must be tightly regulated. Indeed, BiP dysfunction, either due to BiP up- or down-regulation or due to mutations in its interacting partners, correlates with several disease states[239, 240] (Table 2).

For example, some toxic strains of *E. coli* produce toxins such as the Shiga toxin and subtilase AB (or AB_5 toxin) which enter the cell through endocytosis and subsequently traffic to the ER by retrograde transport via the secretory pathway. In the ER, the A subunit of the toxin, which possesses serine protease activity, proteolytically cleaves BiP and inactivates it[241, 242]; the resulting loss of BiP function is lethal to the infected cells. Moreover, BiP plays a role in the entry of Coxsackie B and Dengue Fever viruses by serving as a cell surface receptor for these viruses[243, 244]. Several studies have shown that BiP trafficks to the cell surface of mammalian cells and participates in signaling cascades and antigen presentation, possibly by binding to unfolded polypeptide substrates[239].

In addition, autosomal dominant polycystic liver disease is an inherited disorder which has been linked to mutations in the *SEC63* gene[245]; patients present with the progressive development of multiple biliary epithelial liver cysts. Though the mechanism that results in the disease state is unclear, it is proposed that the loss of SEC63 function results in the mislocalization of secretory proteins required for the regulation of liver cell growth and proliferation. This leads to an expansion of the liver epithelium, in turn forming cysts. Also, the

Table 2: Select human diseases related to BiP malfunction.

Protein	Related Disease	Causative phenomenon	Reference
SEC63	Polycystic liver disease	Genetic mutations	Davila *et al.,* 2004[245]
	Hereditary nonpolyposis colorectal cancer (HNPCC)-associated malignancies (*i.e.,* small bowel cancer)	Frameshift mutations due to DNA mismatch repair deficiencies	Schulmann *et al.,* 2005[246]
	Gastric cancer	Biallelic mutations due to microsatellite instability	Mori *et al.,* 2002[247]
SIL1	Marinesco-Sjçgren syndrome	Genetic mutations	Annesi *et al.,* 2007[248]
SEC62	Prostate and colorectal cancers	Gene amplification	Jung *et al.,* 2006[249]
HERP	Sporadic inclusion-body myositis	Upregulation	Nogalska *et al.,* 2006[250]
	Alzheimer's disease	Upregulation	Sai *et al.,* 2002[251]
BP	Shiga toxinogenic *Escherichia coli* infection	BiP sequestration and proteolysis	Falguieres and Johannes, 2006[242]; Paton et al., 2006[241]
	Dengue Virus and Coxsackie B viral infections	BiP acts as receptor for the virus during viral entry	Jindadamrongwech *et al.,* 2004[244]; Triantafilou *et al.,* 2002[243]
	Several kinds of cancers	BiP upregulation due to an induction of the unfolded protein response; Increased expression of BiP on the cell surface of cancer cells	For reviews: Lee, 2007[252]; Wang *et al.,* 2009[253]
	Diabetes	Defects in UPR signaling	For a review: Scheuner and Kaufman, 2008[254]

autosomal recessively inherited neurodegenerative disease, Marinesco-Sjçgren syndrome, is caused by mutations in the *SIL1* gene that result either in its truncation or inactivation[248]; SIL1 is the homolog of yeast Sls1p, one of BiP's NEFs (Table 1) [255]. The disease state probably results from a reduction in functional BiP pools in the ER due to SIL1 malfunction.

Beyond these infectious and inherited diseases, mutations in *SEC63* have been linked to several cancers that exhibit defects in DNA mismatch repair, and overproduction of SEC62 has been linked to prostate cancers (Table 2). BiP expression levels can also be directly correlated to different cancers[252, 253]; in particular, BiP participates in tumor proliferation, metastasis and in some cases, resistance to therapies. Since cancer cells are under high levels of oxidative, nutritional and other environmental stresses, it is not surprising that upregulated BiP levels are essential for cancer cell survival. Indeed, BiP can be found on the cell surface of cancer cells[252, 253], and this population may be used as a target for the development of cancer therapies. In addition, recent studies have linked defective UPR signaling to the failure of pancreatic beta cells to secrete insulin in diabetic individuals[254]. This effect may be BiP-dependent because the overexpression of BiP in pancreatic beta cells in an *in vitro* system is sufficient to increase insulin secretion[256]. Finally, given the connections between the UPR and neurodegenerative diseases including Alzheimer's, Huntington's and Parkinson's diseases[257, 258], and BiP's role in the induction of the UPR (refer to section 1.2.7.), ameliorating the UPR by modulating BiP function might provide a novel therapeutic strategy for curing these diseases.

1.3 A PREVIEW OF CHAPTERS 2 AND 3

I chose to focus this chapter on yeast BiP and its functions within the ER, with an emphasis on the three well-characterized Hsp40s with which it interacts. However, the diversity of Hsp70s and Hsp40s increases in higher eukaryotes and in some other subcellular compartments. For example, the yeast cytosol contains six Hsp70s and 13 Hsp40s[259]. Thus, there is an intricate network of Hsp70-Hsp40 interactions. In the particular case of the yeast cytosol, members of the Ssa Hsp70 sub-family (Ssa1p, Ssa2p, Ssa3p and Ssa4p) are not essential when individually deleted; however, the deletion of *ssa1, ssa2* and *ssa4* results in yeast inviability unless Ssa3p is overexpressed from the *SSA2* promoter[260]. This indicates that cytosolic Hsp70s can perform overlapping functions and that the level of protein expression determines their essentiality. In contrast, a subset of the cytosolic Hsp40s has been classified as 'generalized cochaperones' since these proteins can substitute for each other to enable cell survival, while others are considered to be 'specialized', since they are indispensable for yeast growth[261]. This is probably not surprising because the specialized Hsp40s may contain unique domains that are vital for their functionality[259, 261]. Based on these observations, an understanding of a less complex system, *i.e.,* BiP function within the ER, might shed light on the general mechanisms through which Hsp70s and Hsp40s interact in order to perform diverse functions. Alternately, by understanding the requirements for a divergent Hsp40 to function in a non-native environment, it may become possible to identify features that distinguish individual Hsp40s from one another.

In Chapter 2, in order to better dissect BiP function and its interaction with Hsp40 partners and substrates, I generated three yeast BiP mutants and characterized them *in vitro* and *in vivo*. I identified a mutant, R217A BiP, which was defective for protein translocation into the ER, owing to a reduction in functional activation by Sec63p. This result suggested that BiP

possesses inherent properties that enable it to differentiate between its various Hsp40 cochaperones. I then utilized a screen to identify genes that exhibited genetic interactions with R217A BiP and discovered a previously uncharacterized ER membrane protein, Ilm1p, as a potential regulator of translocation.

In Chapter 3, in order to understand the minimal requirements for Hsp40 function in the yeast cytosol, I expressed wild-type and mutant versions of ERdj3, a mammalian ER-lumenal Hsp40, and tested the ability of these diverse ERdj3 forms to substitute functionally for two yeast cytosolic Hsp40s, Hlj1 and Ydj1. I found that the J domain-mediated interactions of ERdj3 with the yeast Hsp70s, as well as efficient Hsp70-independent substrate binding, were essential for ERdj3 to function in the yeast cytosol. This result suggested that Hsp40s are not just Hsp70 cochaperones but can perform cellular functions that require specialized properties.

2.0 THE TRANSLOCATION-SPECIFIC BIP MUTANT, R217A, GENETICALLY INTERACTS WITH ILM1, A NOVEL PLAYER IN CO-TRANSLOCATIONAL PROTEIN TRANSLOCATION ACROSS THE ER MEMBRANE

The endoplasmic reticulum (ER) is the major site of protein synthesis in the eukaryotic cell, with nearly one-third of all cellular proteins being targeted to their final destinations in the secretory pathway via the ER[173, 174]. Owing to the high protein load encountered by the ER, there are several quality control mechanisms in place to ensure that only correctly folded proteins reside within or exit from the ER[5, 175, 262-264]. The primary line of defense is formed by molecular chaperones such as Hsp70s, calnexin/calreticulin and protein disulfide isomerases, which assist in protein folding as well as in protein quality control[33, 175, 264, 265].

One such molecular chaperone, the ER lumenal Hsp70, BiP/Grp78/Kar2p[34, 35, 37, 266, 267], is referred to as the 'master regulator' of the ER[169, 170] and constitutes a large proportion of the soluble protein in the ER[173]. BiP participates in multiple cellular processes, including polypeptide translocation across the ER membrane[98, 100, 105, 107-111, 113, 114, 150, 268-270], maintenance of the permeability barrier of the ER during translocation[115, 116], protein folding[74, 166, 267, 270-277], recognition and targeting of misfolded proteins for retrotranslocation during ER-associated degradation (ERAD)[3, 120, 181, 190, 278, 279], induction of the unfolded protein response (UPR)[210, 213-215, 217, 218, 223, 280-284], calcium homeostasis[228, 229], and karyogamy in yeast[36, 37, 237, 285]. Therefore, most proteins that traverse the secretory pathway are bound to encounter BiP at some point

during their maturation. BiP's essentiality is further underscored by the variety of human diseases that have been correlated to BiP dysfunction[239, 240].

Like all Hsp70s[24], BiP is comprised of a highly conserved N-terminal ATPase domain (divided into subdomains Ia, Ib, IIa and IIb) followed by a substrate binding domain and a C-terminal lid domain. BiP uses the energy derived from ATP hydrolysis to bind to hydrophobic sequences within its substrates[171, 172, 271, 286]. In the ATP-bound conformation, BiP exhibits low affinity and high release rates for substrates, while in the ADP-bound conformation, it binds to substrates with high affinity, thus providing an environment for the substrate to attain its native three-dimensional fold and preventing aggregation. Since BiP is a poor ATPase (turnover number of 0.18 sec^{-1}), it interacts with two classes of cofactors to enhance its ATP hydrolytic cycle: J domain-containing Hsp40s that stimulate ATPase activity due to an interaction between the resident J domain and the ATPase domain of BiP, and Nucleotide Exchange Factors (NEFs) that exchange ADP for ATP. The interaction with peptide substrates is also sufficient to stimulate BiP's ATPase activity[70, 171].

In yeast, the interaction with the membrane-bound Hsp40 homolog, Sec63p, is indispensable for BiP's role in co- and post-translational protein translocation[95, 97, 98, 105, 107-112, 114], whereas the interaction with the membrane-associated Hsp40, Jem1p, and the soluble Hsp40, Scj1p, is critical for BiP's function during the ERAD of soluble substrates, though the exact contributions of these Hsp40s during ERAD are unclear[120]. Moreover, a competent BiP-Scj1p interaction catalyzes protein folding in the ER[119] while a functional BiP-Jem1p pair is required for karyogamy[122, 238]. In turn, the NEFs, Sls1p/Sil1p and Lhs1p, assist BiP and increase protein translocation efficiency[133-136].

Another important role for BiP is during the induction of the UPR[210, 213-215, 217, 218, 223, 280-284]. Under normal unstressed cellular conditions, BiP binds to the UPR-dedicated signal transducer kinase, Ire1p, and maintains it in an inactive state[214, 215]. However, when there is an increased load of unfolded proteins in the ER, for example, in the presence of a reducing agent, BiP is titrated away from Ire1p and binds to unfolded substrates, in turn activating Ire1p[210, 217, 218]. The end result of Ire1p signaling is the upregulation of genes involved in protein folding (including BiP), lipid synthesis and transport of secreted proteins to later compartments. These events mitigate the unfolded protein load of the ER[199]. Therefore, Ire1p-mediated UPR induction is often used as an indicator of ER homeostasis[224, 225]. Recently, the BiP residues that either directly interact with Ire1p or are located proximal to a region that interacts with Ire1p were mapped onto subdomain Ib of BiP's ATPase domain[287].

While the significance of BiP's ATPase activity for most of its functions is well-established[73, 74, 151], the amino acid residues that contribute to BiP's interactions with its Hsp40 cofactors are less defined. The Brodsky lab recently demonstrated that the mutation of residues in BiP's substrate binding domain that reduce substrate affinity specifically affects ERAD[181]. To understand this further, I report on the characterization of BiP mutants that exhibit defects in Hsp40 interaction and/or substrate binding. Specifically, I identified a point mutation in BiP, R217A, which resulted in defective Sec63p interaction *in vitro* and a translocation-specific defect *in vivo*. When the genetic interactions between R217A BiP and a subset of the yeast knockout collection were examined in a UPR-based screen, I then discovered a novel player in protein translocation, Ilm1p, which has thus far been poorly characterized. Taken together, I conclude that the utilization of function-specific alleles of essential genes in a targeted genetic screen can provide new insights into essential cellular processes.

2.1 MATERIALS AND METHODS

2.1.1 Yeast strains and plasmids

All strains and plasmids used in this study are listed in Tables 4 and 5, respectively. Unless otherwise indicated, standard conditions were used for plasmid manipulation and yeast growth[288].

For the heterologous expression of mutant BiP proteins in *Escherichia coli*, the *KAR2* coding sequence contained in pMR2623[151] was mutagenized using the Quikchange site-directed mutagenesis kit (Stratagene) with the following primer pairs (underlined letters represent the altered sequence): (i) R217A:- 5' primer: GCTGGTTTGAACGTTTGGCAATTGTTAATGAACCAACCGC, and 3' primer: GCGGTTGTTCATTAACAATTGCCAAAACGTTCAAACCAGC; (ii) K584X:- 5' primer: GGCCAAGGTGAATCTAGAAACTAATTAGAAAACTACGCTCAC, and 3' primer: GTGAGCGTAGTTTTCTAATTAGTTTCTAGATTCAACCTTGGCC; (iii) S493F:- 5' primer: CGAGGTGAAAGAGCCATGTTTAAGGACAACAATCTATTAGG, and 3' primer: CCTAATAGATTGTTGTCCTTAAACATGGCTCTTTCACCTCG. The resultant plasmids were transformed into *E. coli* RR1 cells for large-scale purification.

For the expression of wild-type BiP protein from the galactose-inducible P_{GAL1} promoter in yeast, the coding sequence for wild-type BiP was amplified from pMR713 (*CEN4*, *LEU2*, P_{KAR2}-*KAR2*) with the following primer pair (italicized letters indicate the *BamH1* recognition site on the 5' primer and the *XhoI* recognition site on the 3' primer):- 5' primer: GTA*GGATCC*CCAGAGTAGTCTCAA, and 3' primer:

TAC*CTCGAG*CTACAATTCGTCGTGTTC. The resulting PCR product was inserted into the pYES2 vector (2μ *URA3*; Invitrogen) to generate pGAL1-*KAR2*. The primer pairs described above were then used to introduce the R217A, K584X and S493F mutations into pGAL1-*KAR2*. Next, the diploid yeast strain MMY2[181] (*MAT***a**/α, *his3-Δ200/his3-Δ200, leu2-Δ1/leu2-Δ1, ura3-52/ura3-52, trp1-Δ63/trp1-Δ63, KAR2/kar2::HIS3*) was transformed with wild-type or mutant pGAL1-*KAR2* vectors and sporulated and tetrads were dissected on yeast extract-peptone-galactose medium. Haploid spores with the following genotype were selected: *MAT*α, *his3-Δ200, leu2-Δ1, ura3-52, trp1-Δ63, kar2::HIS3,* pGAL1-*KAR2* (wild-type or mutant) resulting in the *GAL-KAR2*, *GAL-R217A*, *GAL-K584X* and *GAL-S493F* yeast strains.

For the expression of wild-type BiP from the P_{TEF1} and P_{CYC1} promoters in yeast, the DNA sequence encoding BiP was removed from the pGAL1-*KAR2* vector using the restriction enzymes *BamH1* and *Xho1*. Next, the plasmids p414TEF1 (*CEN4/ARS*, *TRP1,* P_{TEF1}) and p414CYC1 (*CEN4/ARS*, *TRP1,* P_{CYC1})[289] were independently digested with the restriction enzymes *BamHI* and *Sal1*, and the BiP coding sequence was inserted. The ligation mixture was transformed into the yeast strain MMY8-2 (*MAT*α, *his3-Δ200, leu2-Δ1, ura3-52, trp1-Δ63, kar2::HIS3,* pMR397 (2μ, *URA3, KAR2*))[181] and transformants were selected on synthetic complete medium lacking uracil and tryptophan and containing 2% glucose. Positive clones were then plated onto selective synthetic complete medium lacking tryptophan and containing 2% glucose and 1 mg/ml 5-fluoroorotic acid (5-FOA). Clones that survived in the presence of 5-FOA had the genotype: *MAT*α, *his3-Δ200, leu2-Δ1, ura3-52, trp1-Δ63, kar2::HIS3,* pTEF1-*KAR2* (*CEN4/ARS*, *TRP1,* P_{TEF1}-*KAR2*) or *MAT*α, *his3-Δ200, leu2-Δ1, ura3-52, trp1-Δ63, kar2::HIS3,* pCYC1-*KAR2* (*CEN4/ARS*, *TRP1,* P_{CYC1}-*KAR2*) and were called *TEF1-KAR2* and *CYC1-KAR2* respectively. The *TEF1-R217A*, *TEF1-K584X* and *TEF1-S493F* strains were

similarly created. In order to generate an isogenic control strain in which *KAR2* was expressed from its endogenous promoter, pMR713 (*CEN4*, *LEU2*, P_{KAR2}-*KAR2*) was introduced into MMY8-2 and transformants were selected on synthetic complete medium lacking uracil and leucine and containing 2% glucose. In a manner similar to that described above, the plasmid pMR397 was cured using 5-FOA generating the strain MMY713 (*MATα*, *his3-Δ200, leu2-Δ1, ura3-52, trp1-Δ63, kar2::HIS3,* pMR713).

To create the *TEF1-KAR2 jem1Δ* and *TEF1-R217A jem1Δ* strains, the *NATMX6* cassette was amplified from pFA6a-NATMX6[290] with primers bearing homology to flanking regions of the *JEM1* open reading frame (the underlined sequence indicates homology to regions upstream and downstream of *JEM1*):- 5' primer:

TGTATTACTAAGGCCGATCTTAACGTCTACGAAACGAAGTCGGATCCCCGGGTTAAT

TAA and 3' primer:

TGTTGTGGTATCCTAGTTAATGGGCATAGAATGTATTTCAGAATTCGAGCTCGTTTA

AAC. The resulting PCR product was transformed into *TEF1-KAR2* or *TEF1-R217A*, and transformants were selected on yeast extract-peptone-dextrose medium supplemented with the antibiotic nourseothricin at a final concentration of 100 μg/ml (CloNAT; Werner BioAgents, Germany). Positive clones were confirmed by PCR. The *TEF1-KAR2 scj1Δ* and *TEF1-R217A scj1Δ* strains were created in an analogous manner but the PCR primers that were used complemented the flanking regions of the *SCJ1* open reading frame (the underlined sequence indicates homology to regions upstream and downstream of *SCJ1*):- 5' primer:

CCAGAAGAGCGTGCATTGGCTGGCGAAAAGATCGAGGACACGGATCCCCGGGTTAA

TTAA and 3' primer:

CTATCTATATATGCATGTGTGCGTACGTAGGATTATCTGTGAATTCGAGCTCGTTTAA AC.

To generate FLAG-tagged Ilm1p, the *ILM1* coding sequence including the open reading frame and ~350 basepairs of 3'-UTR was amplified from genomic DNA extracted from BY4742 wild-type yeast utilizing the primer pair (italicized letters represent the *PvuII* recognition site on the 5' primer and *BamHI* recognition site on the 3' primer):- 5' primer: GAATGGTAGTGTAA*CAGCTG*ACAACATAAT, and 3' primer: CGAATGTGC*GGATCC*ATTCGTGATGA. The resulting PCR product was inserted into pFA6a-NATMX6 immediately upstream of the *NATMX6* coding sequence to produce the plasmid pILM1-UTR-NAT. Next, a 3XFLAG epitope was introduced at the 3' end of the *ILM1* open reading frame in pILM1-UTR-NAT using a modified site-directed mutagenesis protocol[291] with the following primer pair:- 5' primer: GATGGGAAAGATGAGAAAGGTGACTACAAGGACGATGACGATAAGAGGCCCGACT ACAAGGACGATGACGATAAGAGGCCCGACTACAAGGACGATGACGATAAGAATGA TGATAGCGATGCAAAA, and 3' primer: TTTTGCATCGCTATCATCATTCTTATCGTCATCGTCCTTGTAGTCGGGCCTCTTATCGT CATCGTCCTTGTAGTCGGGCCTCTTATCGTCATCGTCCTTGTAGTCACCTTTCTCATCT TTCCCATC, to create pILM1-3XFLAG. For homologous recombination, the resulting *ILM1-3XFLAG-UTR-NAT* sequence was amplified using the primer pair (the underlined sequence indicates homology to regions upstream and downstream of *ILM1*):- 5' primer: GTATCGCATTCAGCAAAAGTAAAGAATAAATTCTAAGAAAATGGCTCAAGCCTTGA ACTC, and 3' primer:

GTCTATATCTACATACATACACAGGTATCTACTATAAGAGAATTCGAGCTCGTTTAA AC, and transformed into BY4741 wild-type yeast (*MAT**a**, his3-Δ1, leu2-Δ0, ura3-Δ0, met15-Δ0)*. Positive clones (*ILM1-FLAG-NAT*) were selected on yeast extract-peptone-dextrose medium supplemented with nourseothricin and analyzed for FLAG-tagged Ilm1p expression by immunoblotting with anti-FLAG antibodies (Santa Cruz Biochemicals).

2.1.2 Protein purification

Hexahistidine-tagged wild-type and mutant BiP proteins expressed from pMR2623 were purified from *E. coli* RR1 cells using a previously optimized protocol[151]. GST-tagged J domains of Sec63p (Sec63'J')[111] and Jem1p (Jem1'J')[181] were purified from *E. coli* BL21(DE3) and *E. coli* TG1 cells, respectively, according to previously established protocols.

For heterologous expression of Scj1p in *E. coli,* a plasmid construct (pET-*SCJ1*) was generated by introducing the DNA fragment that corresponds to mature Scj1p lacking the ER retention signal (amino acid residues 23-373) into pET21a (Novagen) between the *NdeI* and *Not1* restriction enzyme sites (a kind gift from S. Nishikawa, Nagoya University, Japan). Upon transformation of pET-*SCJ1* into *E. coli* BL21(DE3) cells and addition of isopropyl-β-D-1-thio-galactopyranoside (IPTG), a C-terminally hexahistidine-tagged Scj1p was expressed. For large-scale purification, logarithmic phase cells (OD_{600} = 0.8 to 1.0) in a volume of 1 L were induced with 1 mM IPTG for 4 h at 37°C. The cells were harvested, washed with sterile double distilled water and resuspended in 20 ml of denaturing lysis buffer (10 mM Tris, pH 8.0, 300 mM NaCl, 8 M urea and 10 mM imidazole) supplemented with the protease inhibitors pepstatin, leupeptin and phenylmethylsulphonyl-fluoride (PMSF) at a concentration of 1 mM each. Next, the cells were lysed on ice by sonication (4 time, 30 s), and subjected to two rounds of centrifugation to remove

unbroken cells and cell debris: the first round was for 10 min at 13000 rpm at 4°C, and the second round was for 20 min at 16000 rpm at 4°C. The cleared lysate was loaded onto a 2 ml Ni^{2+}-NTA agarose column (Qiagen) prequilibrated in lysis buffer and proteins were allowed to bind. All subsequent steps were performed at 4°C. The column was then washed with 20 ml of 10 mM Tris, pH 8.0, 300 m M NaCl and 10 m M imidazole, and 10 ml of 10 m M Tris, pH 8.0, 300 mM NaCl and 20 mM imidazole. Proteins were eluted with a linear imidazole gradient from 25 mM to 500 mM in 10 mM Tris, pH 8.0 and 300 mM NaCl which was set up using a gradient maker, and 1 ml fractions were collected. Once the peak fractions were detected by SDS-PAGE analysis, the protein was dialyzed into 50 mM Tris, pH 7.4, 50 mM NaCl, 2 mM $MgCl_2$, and 0.8 mM DTT. The protein concentration of the dialysate was determined using the Bradford reagent (BioRad) and protein aliquots were stored at -80°C. The purity of the enriched protein samples was determined by silver staining.

2.1.3 ATP hydrolysis and limited proteolysis assays

Steady state-like ATPase assays were performed as described[127, 151]. The amount of BiP present in each reaction and the ratios of the J domain-containing cofactors or peptide p5[292] (CLLLSAPRR) to BiP are indicated in the figure legends. The J domain-containing cofactors and peptide were pre-incubated with BiP on ice for 10 min in the absence of radiolabeled ATP before starting the assay at 30°C.

Limited proteolysis assays were performed with Proteinase K (Sigma) by slightly modifying the conditions described by McClellan *et al.*, 1998[151]. Briefly, each reaction mixture contained 5 μg of wild-type or mutant BiP and 5 mM ATP or ADP as indicated, made up to a volume of 64 μl in reaction buffer (20 mM HEPES, pH 7.2, 25 mM KCl, 2 mM $MgCl_2$, 0.1 mM

EDTA and 0.5 mM DTT). After incubating the reaction mixture at 20ºC for 1 h to allow for BiP-nucleotide binding, proteolysis was initiated by the addition of 2 µl of a 1 mg/ml Proteinase K solution in reaction buffer. The digestion reaction was carried out at 30ºC for 10 min and quenched with 25 µl of a solution of 10 mM PMSF and 90% tri-chloro acetic acid (TCA). Finally, proteins were precipitated, resolved by SDS-PAGE and analyzed by Coomassie Brilliant Blue staining.

2.1.4 Serial dilutions

The *GAL-KAR2*, *GAL-R217A*, *GAL-K584X* and *GAL-S493F* strains were grown to logarithmic phase (OD_{600} = 0.6 to 0.8) in selective synthetic complete medium containing 2% galactose for 16-24 h. Ten-fold serial dilutions of equivalent ODs of each strain were spotted onto solid medium and cultured at the indicated temperatures for 2 d. Where indicated, the growth medium was supplemented with 8 mM dithiothreitol (DTT) or 0.2% glucose.

The *TEF1-KAR2*, *CYC1-KAR2*, *TEF1-R217A*, *TEF1-K584X*, *TEF1-S493F*, *TEF1-KAR2 jem1Δ* and *TEF1-KAR2 scj1Δ*, *TEF1-R217A jem1Δ* and *TEF1-R217A scj1Δ* strains were grown to logarithmic phase in selective synthetic complete medium containing 2% glucose for ~16 h and analyzed in a manner similar to that described above. (The *GAL-S493F* and *TEF1-S493F* strains are slow-growing and required longer incubation periods to reach the logarithmic phase of growth.)

2.1.5 Preparation of yeast cell extracts and immunoblotting

To detect expression of the wild-type and mutant BiP proteins *in vivo,* protein extracts of cells in the logarithmic phase of growth were prepared using a previously established TCA precipitation protocol[293].

For immunoblotting, the following antibodies were used: anti-BiP[98], anti-Sec61[294], anti-Sec63'J' against the J domain of Sec63p (a kind gift from R. Schekman, University of California, Berkeley), anti-Sec71[102], anti-Sec72[98], anti-FLAG (Sigma and Santa Cruz Biochemicals), anti-Ssh1 (a kind gift from T. Rapoport, Harvard Medical School), anti-G6PDH (Sigma) and anti-HA (Roche). Primary, bound antibodies were decorated with the appropriate horseradish peroxidase-conjugated secondary antibody and signals were detected using the SuperSignal® West Pico Chemiluminescent Substrate (Thermo Scientific).

2.1.6 Pulse-labeling of cells and immunoprecipitation

To measure the stability of BiP in wild-type and mutant *TEF1-KAR2* strains, cells were radioactively labeled and chased as previously described[295]. Briefly, 20 ODs of logarithmic phase cells were harvested, washed and resuspended in synthetic complete medium lacking methionine to 10 ODs/ml. After recovery at 30°C for 30 min, the cells were labeled with 25 µl of Express ^{35}S labeling mix (Perkin-Elmer) for 10 min. Next, cycloheximide was added at a concentration of 200 µg/ml to stop protein translation, and samples were collected at 0, 20, 40, 60 and 90 min. At each time point, 4 ODs of cells were harvested, quenched with 0.1 M sodium azide, and cell extracts were prepared using glass bead lysis in the presence of protease inhibitors. The radioactivity of each sample was measured using a scintillation counter, and for

each sample, a total volume corresponding to 5 million radioactive counts per minute (cpm) was treated with polyclonal anti-BiP antisera. Immunoprecipitated proteins were resolved by SDS-PAGE and the radiolabeled proteins were detected by autoradiography. Relative amounts of radioactivity, which corresponded to protein levels, were quantified using Image Gauge (FujiFilm).

To analyze pre-pro-alpha factor (ppαF) translocation *in vivo*, the *TEF1-KAR2* and *TEF1-R217A* strains were transformed with the plasmid pSM36-ΔgppαF-HA[296], which expresses an HA-tagged version of mutant pre-pro-alpha factor lacking the core consensus glycosylation sequences. Transformants were grown to logarithmic phase, labeled and chased as described above, except that samples were collected at 0 and 10 min. Immunoprecipitation of a sample volume corresponding to 10 million cpm was performed with an anti-HA monoclonal antibody (Roche) and analyzed as above.

To evaluate the effects of the *KAR2* mutations on CPY* degradation, a plasmid encoding an HA-tagged version of CPY*, pDN431[201], was transformed into wild-type and mutant *TEF1-KAR2* strains. Transformants were grown to logarithmic phase, labeled, chased and immunoprecipitates were analyzed as above.

To examine CPY folding efficiency, wild-type and mutant *TEF1-KAR2* strains were assayed using a slightly modified pulse-labeling protocol[145]. Eight ODs of cells grown to logarithmic phase were harvested and resuspended in 800 µl of synthetic minimal medium supplemented with all amino acids except cysteine and methionine. After recovery at 30°C for 15 min, cells were labeled with 10 µl of Express ^{35}S labeling mix (Perkin-Elmer) for 10 min. A solution of unlabeled cysteine and methionine was added to start the chase and time points were taken at 0 and 30 min. Cell extracts were prepared using glass bead lysis and a sample volume

corresponding to 10 million cpm was treated with anti-CPY antibodies (Molecular Probes) to immunoprecipitate CPY. The immunoprecipitates were analyzed as described above. In the case of *kar2-113*, a *kar2* mutant strain that served as a positive control[166], the folding defect was induced by a temperature shift from 30°C to 37°C for 30 min, after which the cells were labeled and chased at 37°C.

To determine the effects of deleting *ILM1* on the translocation efficiency of select proteins *in vivo*, wild-type and *ilm1Δ* cells were labeled for 10 min as described above and either chased for 0 and 20 min or immediately harvested. Proteins from cell extracts were immunoprecipitated with anti-BiP (5 million cpm), anti-DPAP-B (10 million cpm; a kind gift from R. Gilmore, University of Massachusetts Medical School), anti-Pho8p (10 million counts; Invitrogen) or anti-ppαF (10 million cpm; a kind gift of R. Schekman, University of California, Berkeley) antisera as indicated.

2.1.7 β-galactosidase assays to measure the induction of the UPR

Wild-type and mutant *TEF1-KAR2* strains were transformed with the UPR reporter plasmid, pJC104[208], which contains the β-galactosidase gene downstream of four unfolded protein response elements (UPREs). The readout for UPR induction is β-galactosidase expression which was assayed using a standard protocol[297]. The conditions that were tested for the various strains include: cells grown to logarithmic phase at 30°C, cells shifted to 37°C for 1 h, and cells treated with 8 mM DTT for 1 h at 30°C.

2.1.8 *In vitro* translocation and ERAD assays

To measure the translocation and ERAD efficiencies corresponding to wild-type and mutant forms of ppαF, ER-derived vesicles, *i.e.,* microsomes[107], were prepared from the *TEF1-KAR2, TEF1-R217A, TEF1-K584X* and *TEF1-S493F* strains. In brief, 2000-3000 ODs of logarithmic phase cells were harvested, washed and subjected to lyticase treatment in order to digest the cell wall. After digestion, spheroplasts lacking the cell wall were collected using 0.8 M sucrose, 1.5% Ficoll 400, 20 mM HEPES-NaOH, pH 7.4. Next, the spheroplasts were homogenized in 0.1 M sorbitol, 50 mM KOAc, 2 mM EDTA, 20 mM HEPES-NaOH, pH 7.4, supplemented with protease inhibitors, and microsomes were collected using 1.0 M sucrose, 50 mM KOAc, 20 mM HEPES-NaOH, pH 7.4, 1 mM DTT. Finally, the microsomes were washed and resuspended in HEPES-NaOH, pH 6.8, 150 mM KOAc, 5 mM MgOAc, 250 mM sorbitol at a protein concentration of 10-12 mg/ml. Single use aliquots were stored at -80°C.

Next, radiolabeled ppαF and ΔgppαF were synthesized using the plasmid templates pDJ100[298] and pGem2α36-3Q[176], respectively, with Promega's TnT® Coupled Reticulocyte Lysate System. Each plasmid template was mixed on ice with Express ^{35}S labeling mix, ribonuclease inhibitor, and supplied SP6 RNA polymerase, amino acid mixture (lacking methionine), and rabbit reticulocyte lysate, according to manufacturer's instructions. The reaction mixture was incubated at 30°C for 90 min and the resultant radiolabeled translation product was aliquoted and stored at -80ºC. Translation efficiency was analyzed by SDS-PAGE and autoradiography.

For *in vitro* translocation assays, microsomes derived from wild-type or mutant *TEF1-KAR2* strains were mixed with radiolabeled ppαF and an ATP regenerating system, and the assay was performed as previously described[107].

For *in vitro* ERAD assays[176], translocation of ΔgppαF was initially carried out by incubating radiolabeled ΔgppαF with microsomes prepared from wild-type or mutant *TEF1-KAR2* strains and an ATP regenerating system. Next, to measure ERAD efficiency, microsomes containing translocated ΔgpαF were harvested, washed and either mixed with 0.5 mg/ml of cytosol derived from RSY607 yeast, and an ATP regenerating system, or directly resuspended in reaction buffer (20 mM HEPES, pH 6.8, 150 mM KOAc, 250 mM sorbitol, and 5 mM MgOAc). The reaction mixture was incubated at 30°C for 20 min, after which proteins were TCA-precipitated, resolved by SDS-PAGE and analyzed by autoradiography. The data were quantified using Image Gauge (FujiFilm).

2.1.9 Purification of the Sec63 complex

The Sec63 complex containing Sec63p, BiP, Sec71p and Sec72p was purified from microsomes derived from *TEF1-KAR2* and *TEF1-R217A* yeast under non-denaturing conditions using a three-step chromatography protocol which has been described previously[98]. The only modification involved replacing the Superose 6 resin that was recommended for size exclusion chromatography with a 32 ml Sephacryl S-300 column (Amersham Biosciences) that was run under gravity. After purification, the components of the complex were detected by Coomassie Brilliant Blue staining and immunoblotting.

2.1.10 UPR-based genetic analysis

To generate strains amenable for genetic analysis in the UPR-based screen, the *KAR2* locus of BY4741 wild-type yeast was tagged with the *NATMX6* casssette as described in Appendix B to create the *KAR2::NAT* strain. Using a similar strategy, the *kar2-R217A::NAT* strain was generated. Next, the *KAR2::NAT* and *kar2-R217A::NAT* strains were individually mated with 350 yeast strains (listed in Table 6 in Appendix B); each of these 350 strains carried a deletion in a specific non-essential gene (*yfg::KANMX*) and maintained a GFP-based UPR reporter plasmid[121]. Next, synthetic genetic array (SGA) analysis was performed in the laboratory of Jonathan Weissman at the University of California, San Francisco, to generate haploid strains with the following genotypes: *KAR2::NAT, yfg::KANMX,* pUPRE-GFP or *kar2-R217A::NAT, yfg::KANMX,* pUPRE-GFP. To measure the levels of UPR induction in the resultant haploid strains, flow cytometry was performed and the results analyzed according to Jonikas *et al.,* 2009. Based on computational analyses, a correlation coefficient was generated which indicates the similarity of genetic interactions exhibited by *KAR2::NAT* or *kar2-R217A::NAT* and *yfg::KANMX*. Deletion strains that displayed the highest correlation coefficient values were considered most similar to *KAR2::NAT* or *kar2-R217A::NAT* and could be grouped functionally with either strain. A second value was also generated which corresponds to the likelihood of genetic interactions between *KAR2::NAT* or *kar2-R217A::NAT* and *yfg::KANMX*. Again, the more positive this value, the higher the probabiltity that *KAR2::NAT* or *kar2-R217A::NAT* and *yfg::KANMX* genetically interact.

2.1.11 Native immunoprecipitations of FLAG-tagged Ilm1p

To identify proteins that interact with Ilm1p, a FLAG-tagged version of Ilm1p was generated (refer to section 2.1.1). Next, native immunoprecipitations were performed as described[3], except that the ER membrane preparation protocol was modified[299]. In brief, 2 L of BY4741 and *ILM1-FLAG* yeast grown to an OD_{600} of 2-3 were harvested, washed with sterile double distilled water and stored at -20°C. The next day, the cell pellets were thawed on ice and resuspended in 20 ml of lysis buffer (20 mM HEPES, pH 7.4, 50 mM KOAc, 2 mM EDTA, 0.1 M sorbitol and 1 mM DTT) supplemented with protease inhibitors. Glass beads were added up to the meniscus and the cells were disrupted by agitation on a Vortex mixer (ten times for 30 s with 1 min incubation on ice between each round). The resulting lysate was layered onto 20 mM HEPES, pH 7.4, 50 mM KOAc, 1.0 M sucrose, and 1 mM DTT, and centrifuged for 10 min at 6000 rpm at 4°C in an HB-6 rotor (Sorvall). The supernatant was collected and further centrifuged at 16000 rpm for 30 min at 4°C in an SS-34 rotor (Sorvall) to isolate the ER-enriched membrane fraction. The membranes were washed once in IP buffer (50mM HEPES, pH 6.8, 150mM KOAc, 2 mM MgOAc, and 1 mM $CaCl_2$) supplemented with protease inhibitors, and immunoprecipitation was performed using anti-FLAG agarose beads (Sigma) as described[3]. Proteins in the precipitate were resolved by SDS-PAGE and analyzed by immunoblotting.

2.1.12 Cycloheximide-chase ERAD assays

To measure the ERAD efficiency of *ilm1Δ* yeast, the following plasmids were transformed into the BY4742-based *ilm1Δ* strain: CPY*-3HA[300] (*CEN/ARS*, *URA3, prc1-1:3HA*), p425-Ste6p*-HA (2μ, *LEU2,* P_{PGK1}*-ste6-166:HA*) (refer to section 3.1.6), pSM1152[293] (2μ, *URA3,* P_{PGK1}-

CFTR:HA) and pSLW1-B29[301] (2μ, *URA3, P_{GAL1}-APOB29:HA*). Transformants were selected, grown to logarithmic phase and cycloheximide chase analysis was carried out at the indicated temperature according to an established protocol[299]. The resulting cell extracts were resolved by SDS-PAGE and immunoblotted with an anti-HA antibody to detect the HA-tagged ERAD substrates. The amount of HA-tagged substrate present in each sample was quantified using the Image Station software (Kodak) and was normalized to the level of glucose-6-phosphate dehydrogenase (G6PDH), which served as a loading control.

2.1.13 Data analysis

The experimental average of three or more independent replicates and the corresponding experimental error were calculated in Microsoft Excel 2003 using the average (AVG) and standard error (STEYX) functions, respectively. All of the graphs were plotted using Kaleidograph (version 3.0.4; Synergy software).

2.2 RESULTS

2.2.1 Generation of the yeast BiP mutants, R217A, K584X and S493F

As stated above, a previous genetic screen in the lab identified BiP mutants that were defective for substrate binding, but not for interaction with the J domains of Hsp40s[181]. Intriguingly, *in vivo* expression of these mutants resulted specifically in ERAD defects, Therefore, in order to better understand the requirements for J domain interaction and substrate binding in BiP

function, three yeast BiP mutants, R217A, K584X and S493F, were generated (Figure 10A). The invariant R217 residue lies in subdomain IA of BiP's ATPase domain and maps to the positively charged lower cleft that is thought to directly contact the J domain[91, 92]. Several studies have demonstrated that mutating this residue in Hsp70s results in reduced interaction with Hsp40 cochaperones[91, 116, 302]. The K584X mutation generates a truncated protein that lacks part of the lid domain. *In vitro* studies showed that K584X BiP (amino acids 43-583) binds to the same range of peptide substrates as wild-type BiP but exhibits a higher off-rate for the peptides[303]. The S493F mutant was isolated in a genetic screen directed to identify BiP mutants defective for ERAD[181], but was not reported (Kabani, M. and Brodsky, J.L., unpublished data). This mutation is predicted to disrupt a salt bridge between BiP's susbtrate binding and lid domains, and may affect peptide binding.

Hexahistidine-tagged wild-type and mutant proteins were purified from *E. coli* and their endogenous ability to hydrolyze ATP was examined. I observed that R217A BiP hydrolyzed ATP to similar levels as the wild-type protein whereas the K584X and S493F mutants exhibited reduced activity (Figure 10B). The specific activity of wild-type BiP was 1.48 $\pm$ 0.06 nmol ATP hydrolyzed/ mg/ min while that of R217A, K584X and S493F was 1.47 $\pm$ 0.09, 0.78 $\pm$ 0.12 and 0.53 $\pm$ 0.09, respectively. This suggested that mutations in the substrate binding and lid domains affected the activity of BiP to a greater extent than a mutation in an ATPase domain surface residue. To determine whether the effects on ATPase activity were due to altered protein conformation, the protease susceptibility patterns of the wild-type and mutant proteins were compared. I found that the protease digestion pattern of the R217A mutant was similar to wild-type BiP; however, the K584X mutant exhibited an increased susceptibility to protease irrespective of the bound nucleotide (Figure 10C). This suggested that K584X BiP might have

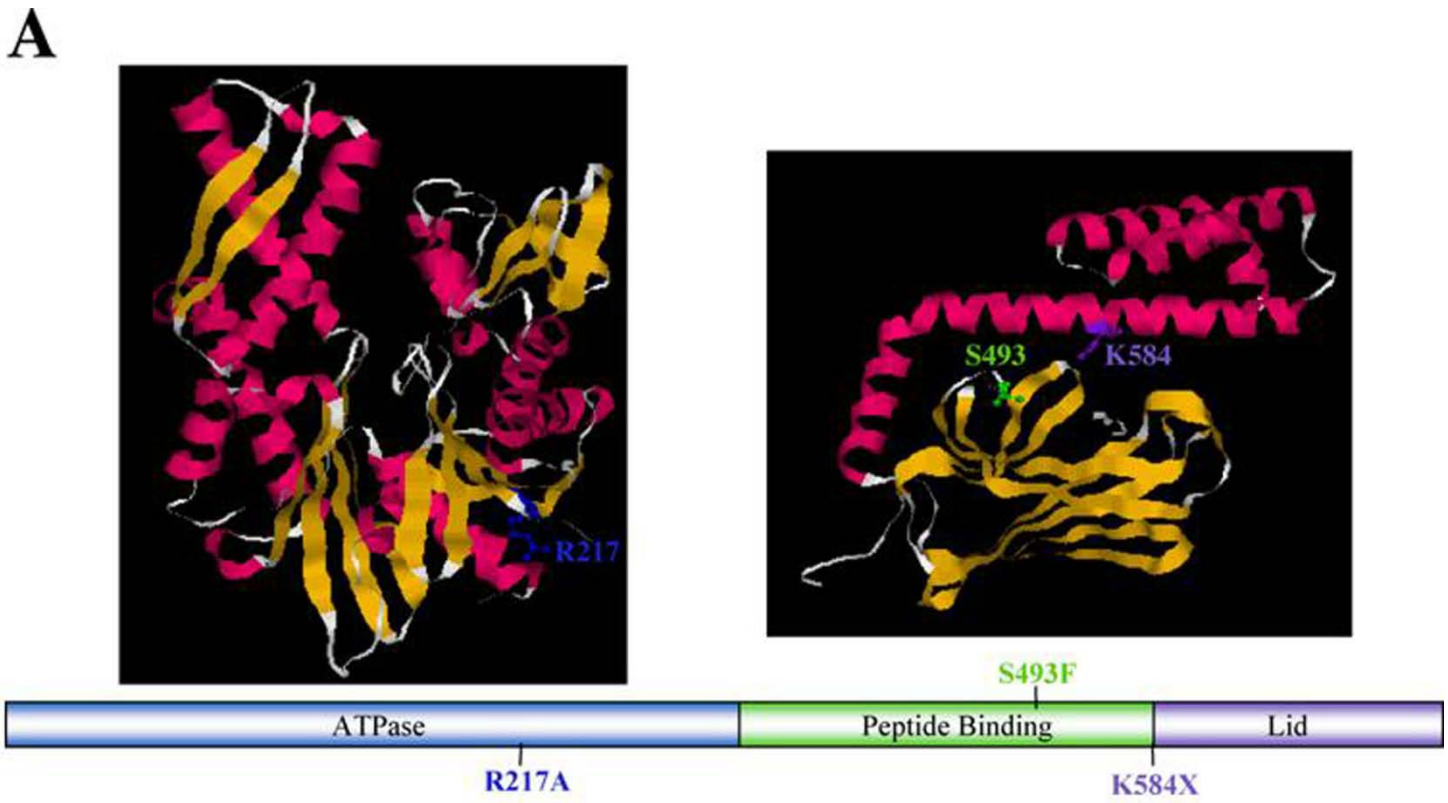
A
R217
S493
K584
S493F
ATPase
Peptide Binding
Lid
R217A
K584X

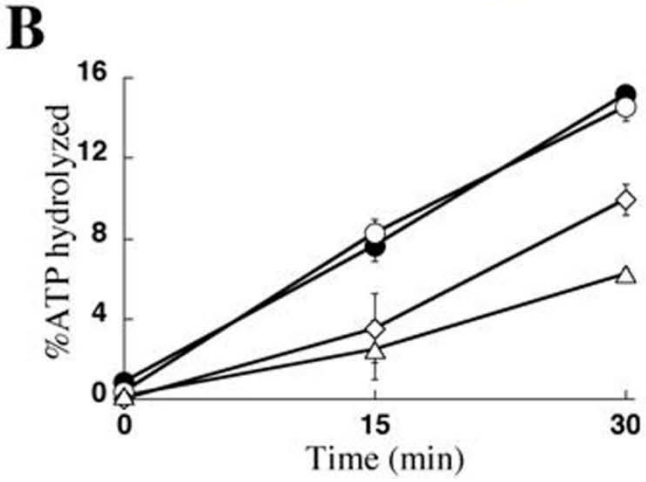
B
%ATP hydrolyzed
16
12
8
4
0
0
15
30
Time (min)

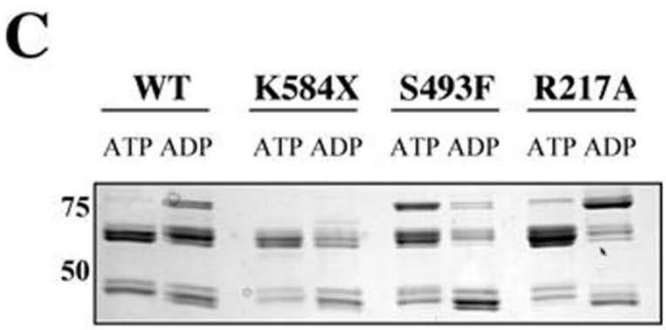
C
WT
K584X
S493F
R217A
ATP ADP
ATP ADP
ATP ADP
ATP ADP
75
50

Figure 10: Three yeast BiP mutants: R217A, S493F and K584X.

(A) The residue R217 was mapped onto the crystal structure of the ATPase domain of bovine Hsc70[1] after aligning the sequences of BiP and Hsc70. This residue is conserved between BiP and Hsc70. The residues S493 and K584 were mapped onto the crystal structure of the peptide binding and lid domains of the bacterial Hsp70, DnaK[9], after aligning the BiP and DnaK sequences. While K584 is conserved in DnaK, serine at 493 is an alanine in DnaK. Also included is a linear representation of the mutations on BiP's secondary structure. ***(B)*** The endogenous ATPase activities of 3 μg of wild-type (●) and mutant BiP isolates (R217A (O), K584X (△) and S493F (◇)) were measured at 30°C. ATPase activity is expressed as nmoles of ATP hydrolyzed per milligram of protein. Data represent the means of a minimum of three independent experiments ± standard errors. *(C)* Protease susceptibility assays were performed at 30°C on wild-type and mutant BiP isolates in the presence of 5 mM ATP or ADP, as indicated. Data are representative of a minimum of three independent experiments.

reduced stability *in vitro*. In contrast, the protease susceptibility pattern of S493F BiP was different from wild-type BiP in both the ATP- and ADP-bound states (Figure 10C), implying that S493F BiP adopts a non-native conformation. This could, in turn, account for its observed defect in ATP hydrolysis.

2.2.2 R217A BiP exhibits defective interaction with Sec63p and Scj1p

Next, I analyzed the ability of the wild-type and mutant BiP proteins to functionally interact with the J domains of BiP's cognate JDPs, Sec63p, Jem1p and Scj1p. To this end, the J domains of Sec63p (Sec63'J') and Jem1p (Jem1'J'), and full-length Scj1p (Scj1) were expressed and purified from *E. coli* and tested in ATPase assays. As expected, wild-type BiP's ATP hydrolsysis activity was robustly stimulated by all three JDPs (Figure 11). In contrast, R217A BiP exhibited a specific defect for interaction with Sec63'J' (Figures 11A and 11D) and Scj1 (Figures 11C and 11F), but its ATPase activity was efficiently stimulated by Jem1'J' (Figures 11B and 11E). Taken together, these results suggest that a unique point mutation in the ATPase domain of BiP is sufficient to confer differential recognition towards the J domains of cognate JDP cochaperones. Furthermore, the ATPase activity of K584X and S493F BiP was proficiently stimulated by Sec63'J' and Jem1'J', with the observed fold-stimulation being greater than wild-type levels (Figures 11A and 11B); however, these mutants were defective for Scj1 stimulation (Figure 11C). One possible explanation for this observation is that the interactions of K584X and S493F with the J domains of Sec63p and Jem1p, but not with full-length Scj1p, might shift the stabilities/conformations of these mutants toward a state which resembles the wild-type protein. Hence, they are now competent to hydrolyze ATP at rates similar to wild-type BiP.

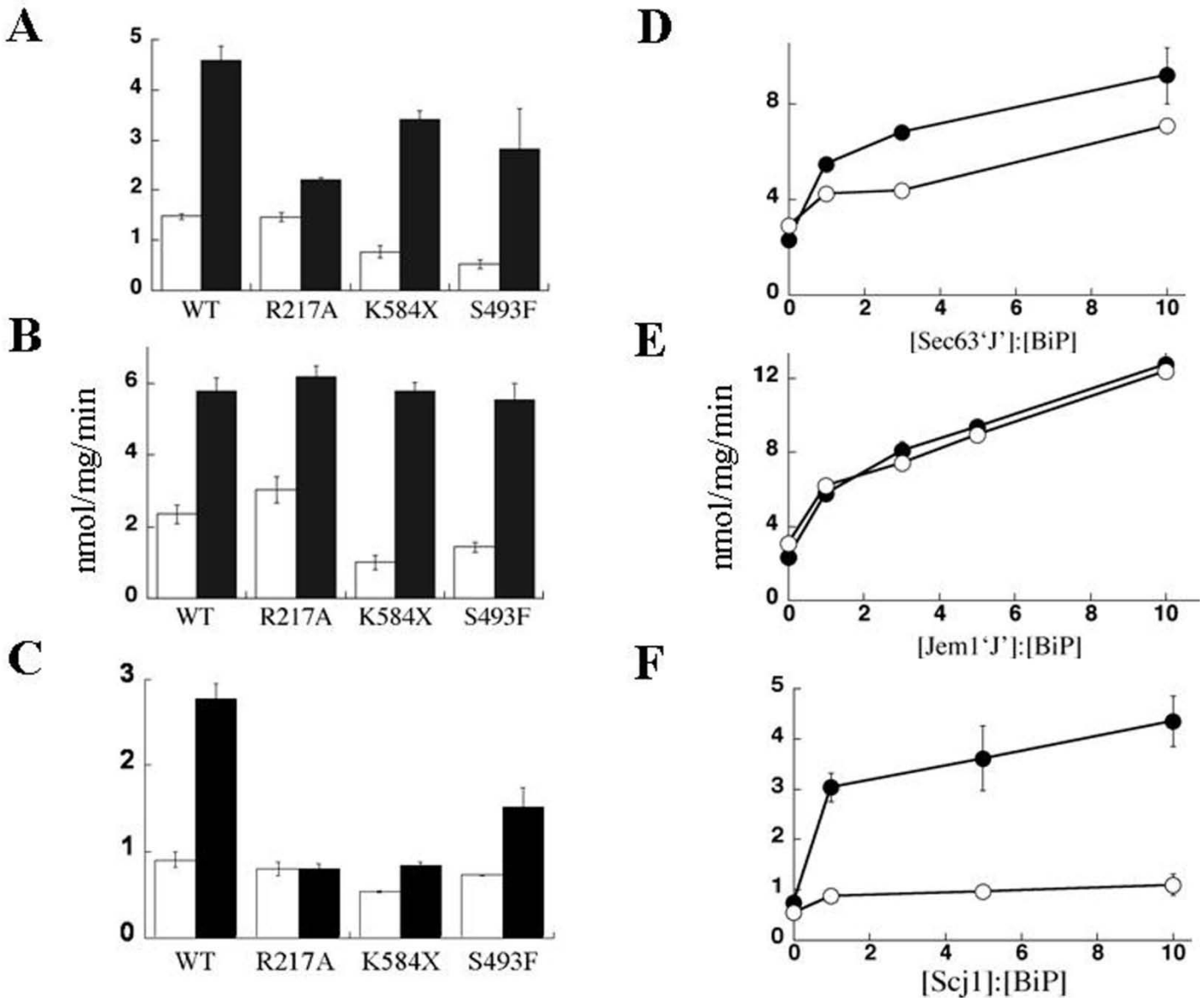
A
B
C
D
E
F
nmol/mg/min
WT
R217A
K584X
S493F
[Sec63'J']:[BiP]
[Jem1'J']:[BiP]
[Scj1]:[BiP]

Figure 11: R217A is compromised for stimulation of ATPase activity by the J domain of Sec63p and full-length Scj1p, but not by the J domain of Jem1p.

ATPase assays were performed either in the absence (white bars) or presence (black bars) of ***(A)*** the J domain of Sec63p (Sec63'J'), ***(B)*** the J domain of Jem1p (Jem1'J'), or ***(C)*** full-length Scj1p (Scj1). Wild-type or mutant BiP proteins (3 μg) and the JDP constructs were present in equimolar amounts in the reactions. By increasing the molar amounts of ***(D)*** Sec63'J', ***(E)*** Jem1p'J', or ***(F)*** Scj1 present in the reaction, the stimulation of R217A BiP's ATPase activity (**O**) by these JDPs was specifically compared to WT (●). The ATPase activity is expressed as nmoles of ATP hydrolyzed per mg of protein per min. Data represent the means of a minimum of three independent experiments ± standard errors.

Next, I examined the ability of the peptide $p5^{292}$ (CLLLSAPRR) to activate the ATP hydrolysis rates of wild-type and mutant BiP isolates. By analyzing a range of p5 concentrations, I observed that wild-type and R217A BiP interacted productively with p5 (Figure 12). However, the two peptide binding domain mutants, K584X and S493F, exhibited significantly reduced p5-stimulated ATPase activities (Figure 12). These data suggest that the presence of a lid domain and the ability of the lid domain to clamp onto the substrate binding domain are both critical for BiP to functionally interact with peptide substrates.

Overall, my *in vitro* analyses indicate that K584X and S493F BiP are primarily defective for substrate binding, whereas R217A BiP exhibits a specific defect in the interaction with two of BiP's JDP cochaperones, Sec63p and Scj1p.

2.2.3 High level expression of BiP mutants results in yeast strains displaying varied sensitivity to elevated temperature and ER stress

Next, I genetically engineered yeast to express the R217A, K584X or S493F BiP mutants in order to examine the consequences of these mutations on BiP function. Initially, the genes encoding the wild-type and mutant BiP proteins were expressed from the galactose-inducible P_{GAL1} promoter to generate the strains: *GAL-KAR2, GAL-R217A, GAL-K584X* and *GAL-S493F* (Figure 13A). Because the ability of a protein to support cellular growth is an important measure of its function, I tested the ability of these wild-type and mutant *kar2* strains to grow in the presence of environmental stresses. *GAL-KAR2, GAL-R217A, GAL-K584X* and *GAL-S493F* cells were serially diluted onto selective medium and exposed to a range of temperatures. I found that the expression of wild-type BiP from P_{GAL1} did not affect yeast growth at all the temperatures tested (Figure 13B), as expected. However, expression of R217A, K584X and S493F BiP from

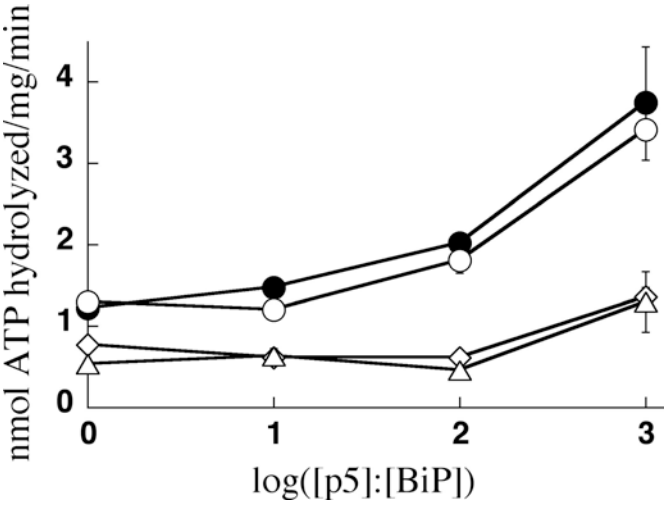

Figure 12: K584X and S493F are defective for peptide stimulation of ATPase activity.

ATPase assays were performed in the presence of increasing molar ratios of peptide p5 (CLLLSAPRR). 1 μg of wild-type (●), R217A (**O**), K584X (△) or S493F (◇) BiP isolates was present in each reaction. The ATPase activity is expressed as nmoles of ATP hydrolyzed per mg of protein per min. Data represent the means of a minimum of three independent experiments ± standard errors.

P_{GAL1} resulted in a growth defect at 37°C (Figure 13B). In fact, the S493F mutant was unable to support growth even at 30°C (Figure 13B), indicating that the presence of this mutation was unfavorable for cellular homeostasis under normal growth conditions. Furthermore, the growth defect of the *GAL-R217A* and *GAL-K584X* mutant strains was exacerbated in the presence of DTT, a reducing agent that induces ER stress (Figure 13C), even though the wild-type *GAL-KAR2* grew robustly in the presence of DTT. This suggested that the *GAL-R217A* and the *GAL-K584X* mutant strains were unable to mount an adequate UPR to counteract the damaging effects of DTT.

To determine whether the observed defects could be attributed to differential levels of protein expression from P_{GAL1} (and also due to variations in plasmid copy number), I prepared cell extracts from wild-type and mutant strains and compared BiP levels by immunoblotting with a polyclonal anti-BiP antiserum. As shown in Figure 13D, R217A BiP is expressed two-fold higher than wild-type BiP while the S493F mutant is expressed three-fold higher. In contrast, the K584X BiP mutant is expressed three-fold lower than wild-type, after having accounted for a two-fold reduction in antibody recognition for this truncation mutant. This was determined by analyzing equal amounts of purified wild-type and K584X BiP proteins by immunoblotting with the anti-BiP antiserum (data not shown).

Taken together, these data indicate that the growth defects resulting from mutant BiP expression could be explained in two ways: (i) the level of mutant protein expression determines the viability of the yeast strain; for example, high levels of S493F BiP may be detrimental to yeast survival, or (ii) the BiP mutants are functionally defective and are unable to completely substitute for wild-type BiP *in vivo*; for example, R217A BiP which shows specific defects *in vitro*. To test the first possibility, the wild-type and mutant strains were serially diluted onto

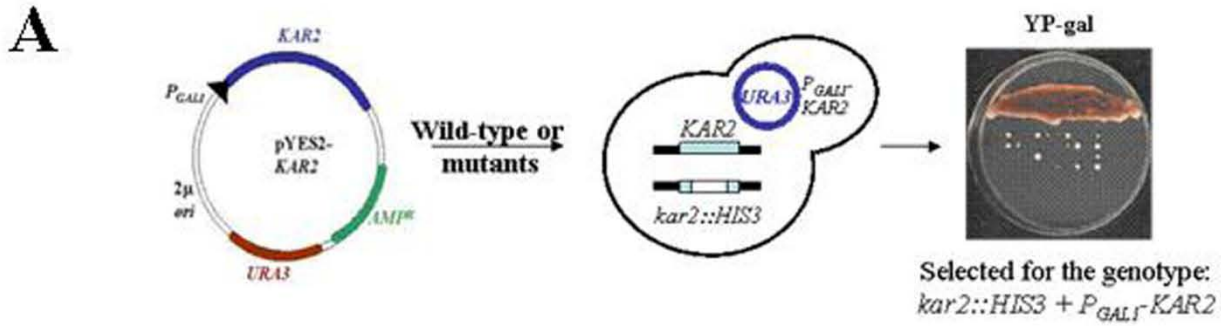
A
KAR2
P_{GAL1}
pYES2-
KAR2
2μ
ori
AMP^R
URA3
Wild-type or
mutants
URA3
P_{GAL1}
KAR2
KAR2
kar2::HIS3
YP-gal
Selected for the genotype:
kar2::HIS3 + P_{GAL1}-KAR2

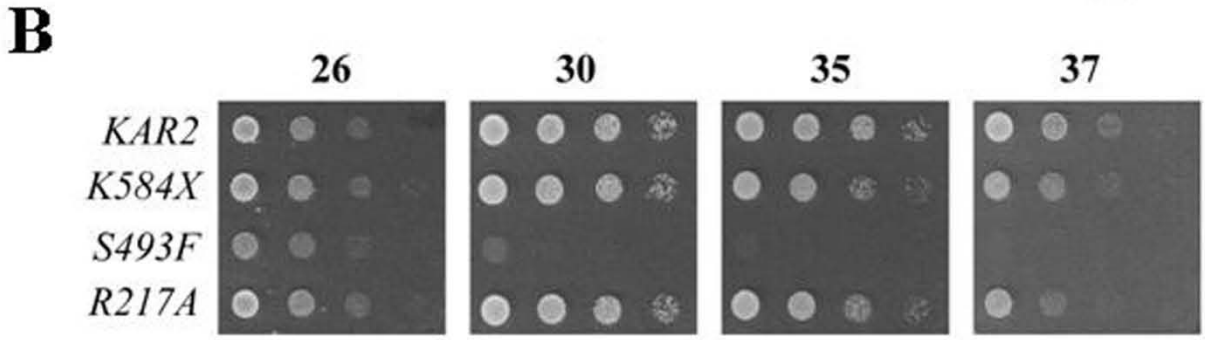
B
26
30
35
37
KAR2
K584X
S493F
R217A

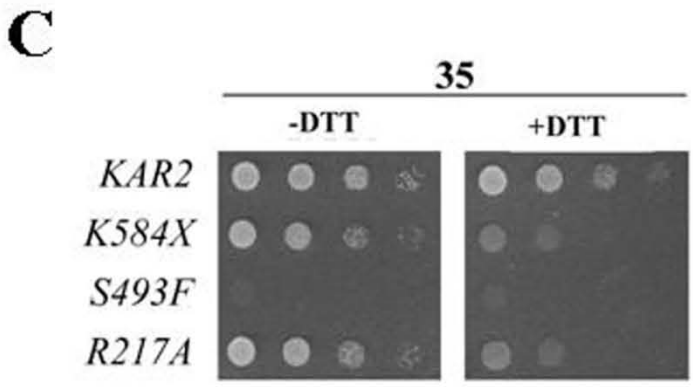
C
35
-DTT
+DTT
KAR2
K584X
S493F
R217A

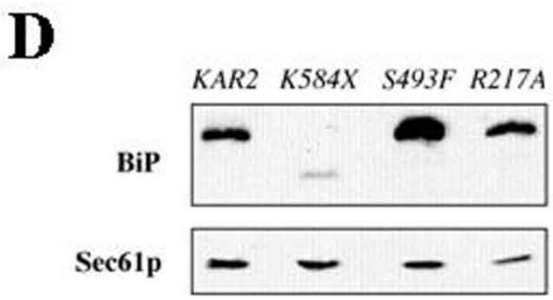
D
KAR2
K584X
S493F
R217A
BiP
Sec61p

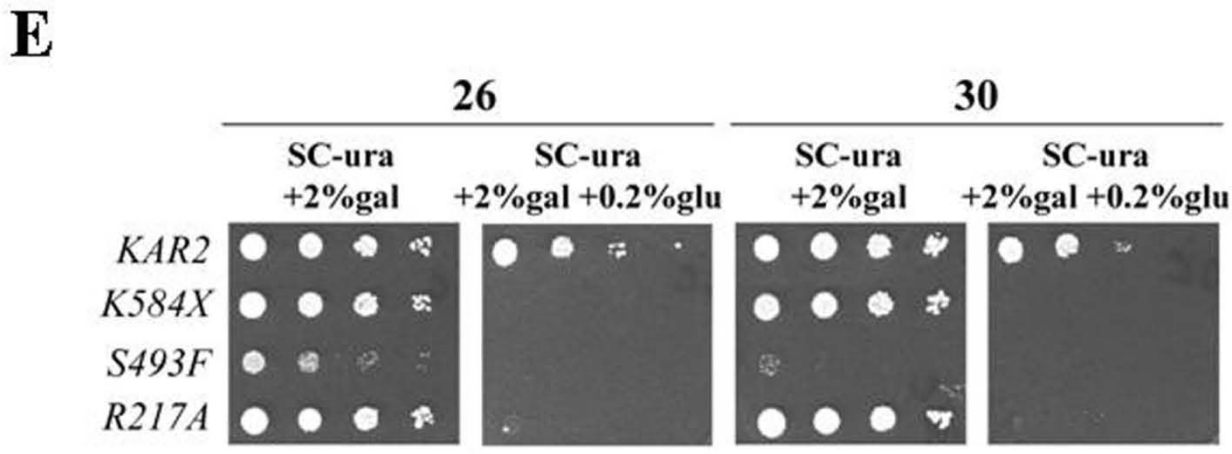
E
26
30
SC-ura
+2%gal
SC-ura
+2%gal +0.2%glu
SC-ura
+2%gal
SC-ura
+2%gal +0.2%glu
KAR2
K584X
S493F
R217A

Figure 13: Expression of BiP mutants from the galactose-inducible P_{GAL1} promoter results in yeast strains exhibiting varied sensitivities to elevated temperature and ER stress.

(A) An outline of the methodology used to construct yeast strains expressing wild-type and mutant BiP proteins from the P_{GAL1} promoter. ***(B)*** Ten-fold serial dilutions of the P_{GAL1}–based *kar2* wild-type and mutant strains (denoted here as *KAR2, R217A, K584X* and *S493F*) were plated onto selective medium containing 2% galactose as the only carbohydrate source. Plates were incubated at 26, 30, 35 and 37°C, for 2 d. ***(C)*** Ten-fold serial dilutions of the wild-type and mutant strains were plated onto selective medium lacking (-DTT) or containing 8mM DTT (+DTT) and containing 2% galactose as the only carbohydrate source. Plates were incubated at 35°C for 2 d. ***(D)*** Cell extracts were prepared from wild-type or mutant strains grown at 30 °C in medium containing 2% galactose as the only carbohydrate source and immunoblotted with polyclonal anti-BiP antisera. The level of Sec61p in cell extracts served as a loading control. ***(E)*** Ten-fold serial dilutions of the wild-type and mutant strains were plated onto selective medium containing 2% galactose (SC -ura +2%gal) or a mixture of 2% galactose and 0.2% glucose (SC –ura +2% gal +0.2%glu). Plates were incubated at 26 or 30°C for 2 d.

medium containing 2% galactose which was supplemented with 0.2 % glucose to reduce expression from the P_{GAL1} promoter[304]. To my surprise, reducing the levels of each of the three mutant proteins by glucose-mediated P_{GAL1} repression resulted in inviability even though, again, the wild-type *GAL-KAR2* strain grew in the presence of glucose (Figure 13E). This observation lent strong support to the second possibility that the BiP mutants are functionally defective and that high levels of protein expression are required to compensate for any functional defects. Given the potential drawbacks of using a galactose-inducible promoter on a multicopy plasmid for protein expression, I decided to use an alternative BiP expression system.

2.2.4 Lower level expression of the K584X and S493F BiP mutants results in yeast strains exhibiting sensitivity to elevated temperature and ER stress

For lower and, ideally, comparable levels of expression, the genes encoding the wild-type and mutant BiP proteins were engineered under the control of the constitutive P_{TEF1} promoter, which drives moderate levels of protein expression on a *CEN4/ARS* plasmid, p414TEF[289]. The resulting strains were denoted *TEF1-KAR2, TEF1-R217A, TEF1-K584X* and *TEF1-S493F* (Figure 14A). Similarly, I attempted to engineer these genes under the control of the constitutive P_{CYC1} promoter which drives even lower levels of protein expression[289]. However, I was unsuccessful in obtaining strains in which the mutant proteins were expressed from P_{CYC1}, even though I was able to generate the wild-type *CYC1-KAR2* strain. This further supported the observation that a reduction in the levels of the mutant proteins results in inviability (Figure 13E).

I first compared the expression levels of BiP in *TEF1-KAR2, TEF1-R217A, TEF1-K584X* and *TEF1-S493F* yeast and observed that the level of wild-type BiP expressed from the P_{TEF1} promoter was identical to that from BiP's endogenous promoter (Figure 14B; compare WT and

TEF1-KAR2). Thus, the *TEF1-KAR2* strain can be treated as a wild-type strain for the purposes of this study. Next, I found that the mutant proteins were expressed at levels similar to wild-type BiP in the P_{TEF1}-based *kar2* strains (Figure 14B), although the K584X mutant was expressed two-fold lower, even after accounting for the reduced recognition by the anti-BiP antiserum. I therefore tested whether K584X BiP was unstable *in vivo*. To measure stability, I radioactively labeled the wild-type and mutant P_{TEF1}-based *kar2* strains and assayed the level of BiP by performing a chase analysis and immunoprecipitating BiP from cell extracts at various time-points. As anticipated, K584X was turned over more rapidly than the wild-type protein (Figure 14C), confirming that this mutant has a reduced stability *in vivo*. This observation suggests that BiP's lid domain confers stability. The stabilities of R217A and S493F were similar to wild-type (Figure 14C), consistent with the behavior of these proteins in limited proteolysis assays (Figure 10C).

I next tested the ability of the wild-type and mutant P_{TEF1}-based *kar2* strains to grow at elevated temperatures or in the presence of DTT. I found that the *TEF1-KAR2* strain grew robustly at all temperatures tested as well as in the presence of DTT (Figures 14D and 14E). The *CYC1-KAR2* strain, on the other hand, grew slowly at 26°C and 37°C, and in the presence of DTT (Figures 14D and 14E). Since half as much BiP is present in the *CYC1-KAR2* strain as compared to the *TEF1-KAR2* strain (data not shown), these data indicated that a reduction in the levels of wild-type protein is sufficient to create a cellular stress, which is exacerbated by non-optimal growth conditions. I then compared the mutant *kar2* strains and found that the growth of *TEF1-R217A* yeast was most similar to the wild-type strain (Figures 14D and 14E). However, the *TEF1-K584X* and *TEF1-S493F* strains showed modest and strong temperature-sensitive and DTT-sensitive growth defects, respectively (Figures 14D and 14E).

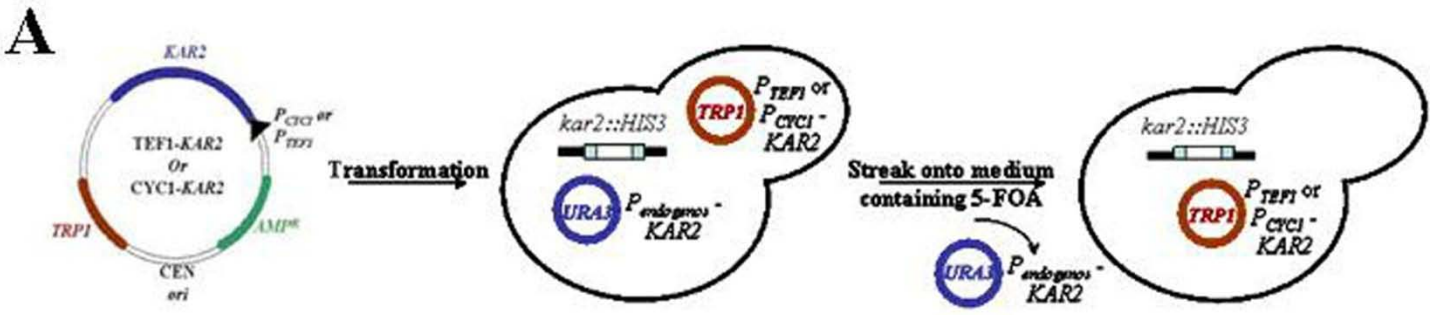
A
KAR2
TEF1-KAR2
Or
CYC1-KAR2
TRP1
CEN
ori
Transformation
kar2::HIS3
TRP1
URA3
Streak onto medium
containing 5-FOA
kar2::HIS3
TRP1

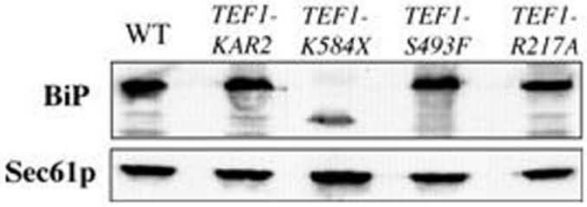
B
WT
TEF1-KAR2
TEF1-K584X
TEF1-S493F
TEF1-R217A
BiP
Sec61p

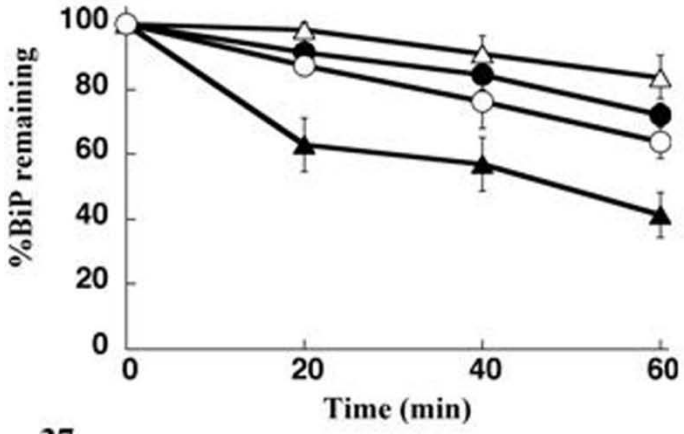
C
%BiP remaining
100
80
60
40
20
0
0
20
40
60
Time (min)

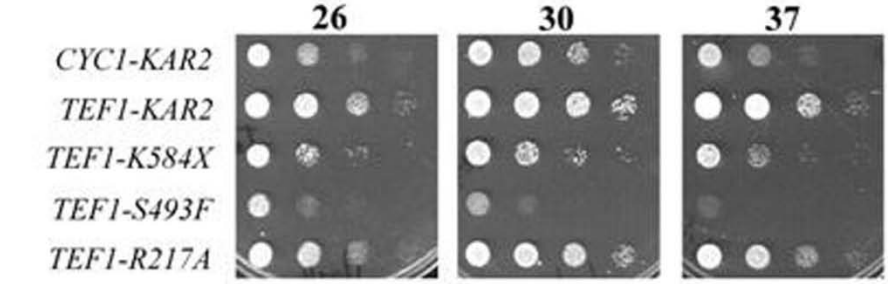
D
26
30
37
CYC1-KAR2
TEF1-KAR2
TEF1-K584X
TEF1-S493F
TEF1-R217A

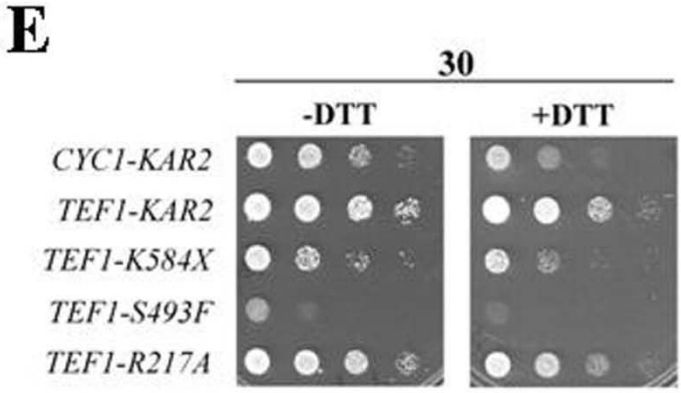
E
30
-DTT
+DTT
CYC1-KAR2
TEF1-KAR2
TEF1-K584X
TEF1-S493F
TEF1-R217A

F

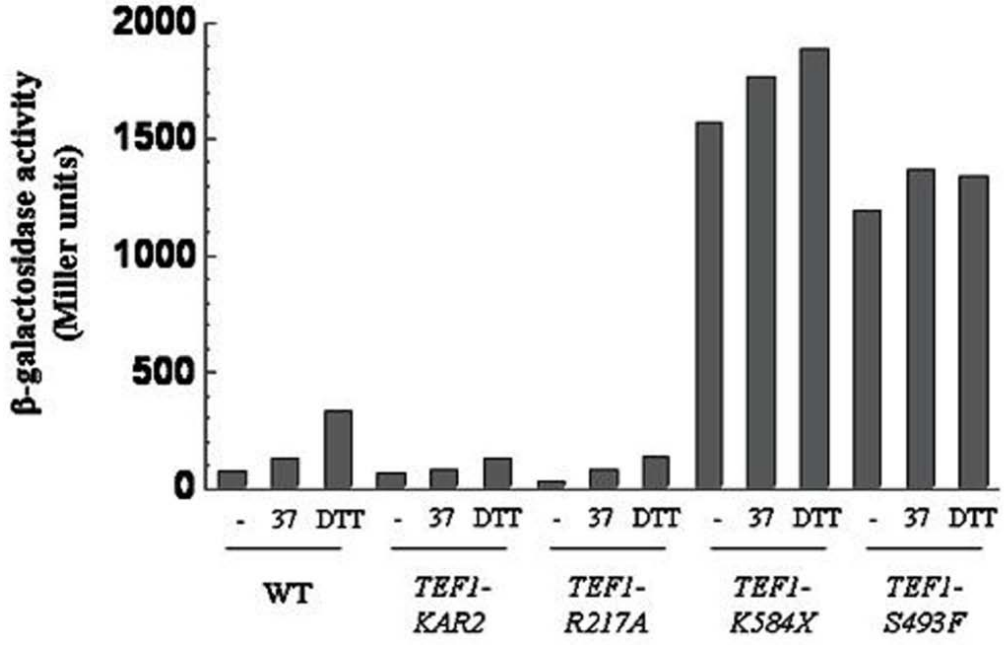
β-galactosidase activity (Miller units)
2000
1500
1000
500
0
- 37 DTT
WT
TEF1-KAR2
TEF1-R217A
TEF1-K584X
TEF1-S493F

Figure 14: Expression of K584X and S493F BiP from the constitutive P_{TEF1} promoter results in yeast strains exhibiting sensitivity to elevated temperature and ER stress.

(A) An outline of the methodology used to construct yeast strains expressing wild-type and mutant BiP proteins from the constitutive P_{TEF1} and P_{CYC1} promoters. ***(B)*** Cell extracts prepared from the P_{TEF1}-based *kar2* wild-type or mutant strains grown at 30 °C were resolved by SDS-PAGE and immunoblotted with polyclonal anti-BiP antisera. The level of Sec61p served as a loading control. ***(C)*** Pulse-chase followed by immunoprecipitation assays were performed on *TEF1-KAR2* (●), *TEF1-R217A* (**O**), *TEF1-K584X* (▲) and *TEF1-S493F* (△) strains grown at 30°C using anti-BiP antisera. Data represent the means of three or more independent experiments ± standard errors. ***(D)*** Ten-fold serial dilutions of the wild-type and mutant strains were plated onto selective medium. Plates were incubated at 26, 30 and 37 °C for 2 d. ***(E)*** Ten-fold serial dilutions of the wild-type and mutant strains were plated onto selective medium without (-DTT) or with 8mM DTT (+DTT). Plates were incubated at 30 °C for 2 d. ***(F)*** Induction of the unfolded protein response (UPR) in wild-type and mutant P_{TEF1}–based strains was analyzed using β-galactosidase reporter assays. Cells were incubated either at 30°C (-), shifted to 37°C for one hour (37), or treated with 8mM DTT for one hour at 30°C (DTT). Where indicated, WT corresponds to the MMY713 strain (refer to section 2.1.1).

Note that the exacerbated growth defect of the *TEF1-K584X* strain relative to the *TEF1-S493F* strain probably arises from different stabilities of the corresponding BiP mutant proteins.

Since the Brodsky lab previously showed that the expression of BiP mutants deficient for substrate binding resulted in a DTT-sensitive growth phenotype due to a constitutive induction of the UPR[181], I asked whether yeast expressing K584X and S493F BiP, mutants that exhibit reduced peptide interaction (Figure 12), also display high, constitutive UPR levels. Therefore, a UPR reporter plasmid was transformed into the P_{TEF1}-based *kar2* wild-type and mutant strains and UPR induction levels were measured using a β-galactosidase assay. As expected, the *TEF1-K584X* and *TEF1-S493F* strains showed a greater than 10-fold higher induction of the UPR at 30°C when compared to the *TEF1-KAR2* strain (Figure 14F; compare columns labeled '-' of the wild-type and mutant strains). Moreover, stressors such as elevated temperature and DTT did not exaggerate the level of UPR induction in *TEF1-K584X* and *TEF1-S493F* yeast (Figure 14F; compare columns labeled '-' to those labeled '37' and 'DTT'). These data suggest that the UPR is maximally induced in these mutant strains. Consequently, the growth defects exhibited by *TEF1-K584X* and *TEF1-S493F* yeast may be explained by their inability to mount a greater UPR at elevated temperatures and in the presence of DTT.

Taken together, these observations suggest that mutations in the substrate binding domain predominantly affect BiP's ability to bind to substrates, and the expression of such mutants in yeast may result in large-scale protein unfolding in the ER, thus inducing the UPR. However, a mutation that affects J domain interaction and does not alter substrate binding has no effect on growth under stress conditions.

2.2.5 The *TEF1-R217A* strain exhibits a defect in protein translocation across the ER membrane, but is proficient for ERAD and ER protein folding

Protein translocation across the ER membrane is the first commitment step in the secretory pathway. Given that BiP plays a role during co- and post-translational protein translocation (refer to section 1.2.4), I measured the translocation efficiencies of the *TEF1-KAR2, TEF1-R217A, TEF1-K584X* and *TEF1-S493F* strains. I therefore prepared ER-derived microsomes from these strains and performed *in vitro* translocation assays for a well-characterized substrate, the yeast mating pheromone precursor, pre-pro-alpha factor (ppαF)[298, 305-308]. Upon translocation into the ER, the 'pre' signal sequence of ppαF is cleaved[309] by the catalytic subunit of the signal peptidase complex, Sec11p[159], and the resulting protein is triply N-glycosylated to the 3gpαF form[305]. These transformations can be assessed by altered electrophoretic mobilities on a denaturing polyacrylamide gel.

When microsomes derived from *TEF1-KAR2* wild-type yeast were incubated with ppαF, a translocation efficiency of ~50% was obtained (Figure 15A). This efficiency is comparable to the level in microsomes prepared from the MMY713 wild-type strain (data not shown). However, microsomes containing R217A BiP were half as efficient (Figure 15A). This result could be partly explained by my observation that R217A BiP is defective for interaction with the J domain of Sec63p, the Hsp40 cochaperone dedicated to translocation (Figures 11A and 11D). Moreover, microsomes containing the substrate binding mutants, K584X and S493F BiP, were defective for translocation (Figure 15A), although the mutant proteins interacted competently with Sec63p (Figure 11A). In fact, microsomes containing S493F had negligible levels of translocation, similar to a previously characterized *kar2* mutant with a lesion in the ATPase

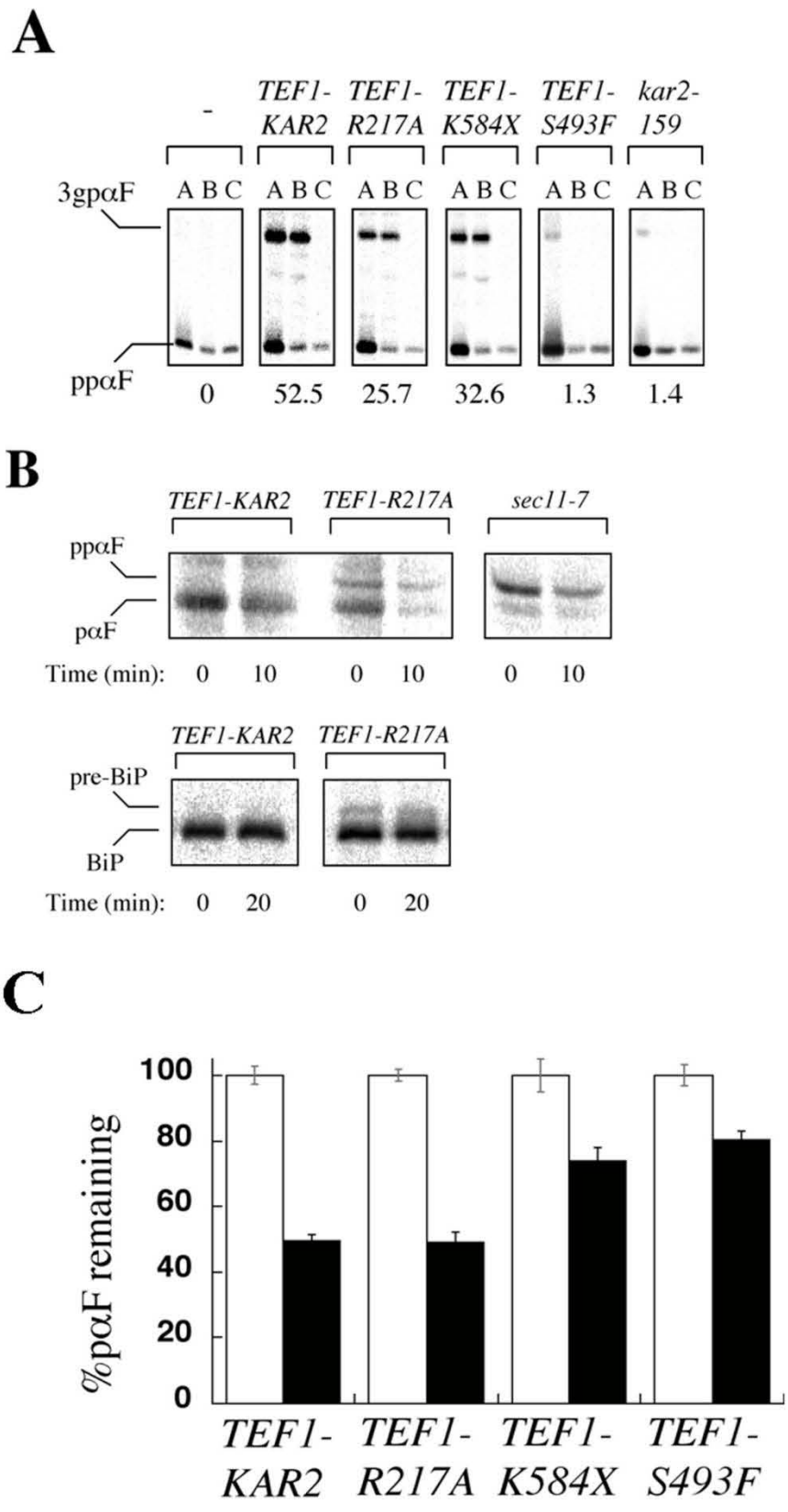
A
-
TEF1-KAR2
TEF1-R217A
TEF1-K584X
TEF1-S493F
kar2-159
A B C
3gpαF
ppαF
0
52.5
25.7
32.6
1.3
1.4
B
TEF1-KAR2
TEF1-R217A
sec11-7
ppαF
pαF
Time (min): 0 10 0 10 0 10
TEF1-KAR2
TEF1-R217A
pre-BiP
BiP
Time (min): 0 20 0 20
C
%pαF remaining
100
80
60
40
20
0
TEF1-KAR2
TEF1-R217A
TEF1-K584X
TEF1-S493F

D

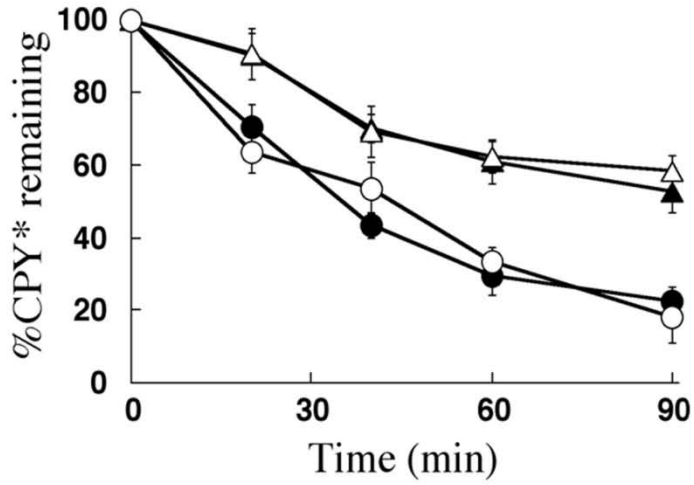
%CPY* remaining
100
80
60
40
20
0
0
30
60
90
Time (min)

E

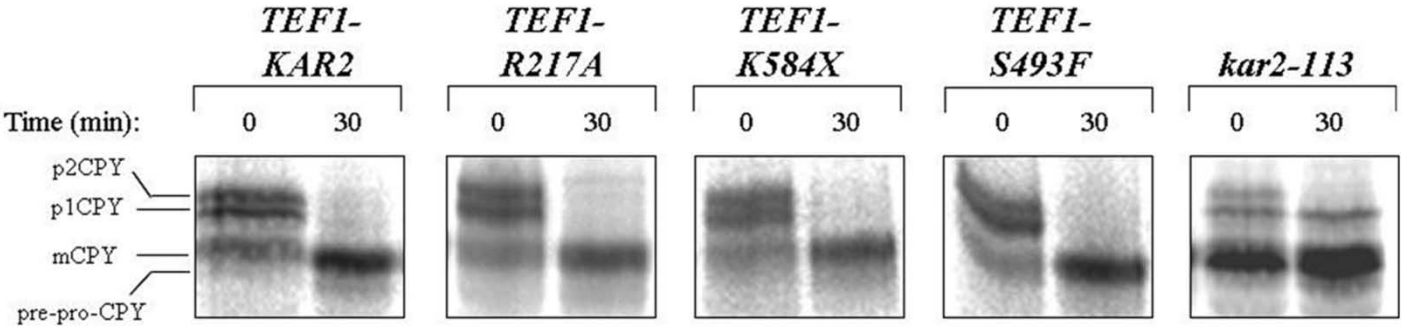
TEF1-KAR2
TEF1-R217A
TEF1-K584X
TEF1-S493F
kar2-113
Time (min):
0
30
p2CPY
p1CPY
mCPY
pre-pro-CPY

Figure 15: Yeast expressing R217A BiP exhibit translocation, but not ERAD or ER folding defects.

(A) *In vitro* ppαF translocation assays were performed using microsomes derived from wild-type and mutant P_{TEF1}–based strains. Two controls included reactions lacking microsomes (-) and microsomes derived from a *kar2* mutant strain, *kar2-159*. After translocation, each reaction was divided and treated in one of three ways: A-buffer, B-trypsin, C-trypsin and Triton X-100. The percent translocation efficiency is indicated below each panel. Data are representative of a minimum of four independent experiments. ***(B)*** Accumulation of ppαF or signal sequence-containing pre-BiP was analyzed at the indicated time-points during a pulse-chase immunoprecipitation experiment to determine the translocation efficiencies of the *TEF1-KAR2* and *TEF1-R217A* strains. *sec11-7* was used as a positive control. ***(C)*** *In vitro* ERAD assays assessing the degradation of ΔgpαF were performed using microsomes from wild-type and mutant P_{TEF1}–based strains. Reactions were carried out in the absence (white bars) or presence (black bars) of an ATP regeneration system and 0.5 mg/ml of yeast cytosol. Data represent the means of a minimum of three independent experiments ± standard errors. ***(D)*** Pulse-chase followed by immunoprecipitation assays were used to analyze the degradation of a soluble ERAD substrate, CPY*, in the *TEF1-KAR2* (●), *TEF1-R217A* (**O**), *TEF1-K584X* (▲) and *TEF1-S493F* (Δ) strains. Data represent the means of a minimum of three independent experiments ± standard errors. ***(E)*** CPY folding was examined in the wild-type and mutant P_{TEF1}–based strains by pulse-labeling the cells and performing a chase for 30 min. *kar2-113* served as a positive control. Data are representative of three independent experiments. The various CPY forms are described in the text.

All of the experiments were performed at 30°C.

domain, kar2-159p[268]. These data suggest that both Sec63p J domain interaction and substrate affinity are important determinants of BiP's ability to support translocation.

To verify the observed translocation defects *in vivo*, I examined the translocation efficiency of the *TEF1-KAR2* and *TEF1-R217A* strains. These strains are of the *MAT*α mating type and I initially immunoprecipitated ppαF from radiolabeled cell extracts using anti-ppαF antiserum. However, I was unable to observe an accumulation of ppαF in the *TEF-R217A* strain (data not shown) either due to low levels of expression of this protein or inefficient immunoprecipitation. Therefore, I transformed these strains with a plasmid encoding an HA-tagged version of a ppαF mutant (ΔgppαF) and performed immunoprecipitations with anti-HA antiserum. ΔgppαF cannot be N-glycosylated as it translocates across the ER membrane; however, the signal sequence can be cleaved to generate ΔgpαF, which becomes an ERAD substrate[176, 310]. Based on this analysis, I observed that ΔgppαF accumulated in the *TEF1-R217A* strain (Figure 15B). This species was also present in the control strain, *sec11-7*[159], which carries a mutant allele in the *SEC11* gene (Figure 15B). Furthermore, I observed that the signal sequence-containing form of BiP, *i.e.,* pre-BiP, also accumulated in the *TEF1-R217A* strain (Figure 15B). Taken together, these data demonstrate that the expression of R217A BiP in yeast results in translocation defects.

Next, I evaluated the ability of microsomes containing either the wild-type or mutant BiP proteins to degrade ΔgpαF via ERAD and observed that microsomes prepared from the *TEF1-R217A* strain degraded ΔgpαF to a similar extent as microsomes derived from the wild-type strain (Figure 15C). This result was initially surprising because R217A BiP was defective for interaction with Scj1p, one of two JDP cochaperones required for ERAD (Figures 11C and 11F), but not Jem1p (Figures 11B and 11E). However, given the fact that Scj1p and Jem1p exhibit

overlapping functions during the ERAD of $\Delta gp\alpha F^{120}$, it follows that the interaction of R217A BiP with Jem1p is sufficient to support ERAD. In contrast, microsomes derived from the *TEF1-K584X* and *TEF1-S493F* strains demonstrated defects in mutant pαF degradation (Figure 15C). Again, since K584X and S493F BiP efficiently interacted with Jem1p (Figure 11B), but not Scj1p (Figure 11C), this defect can be directly attributed to their substrate binding incompetence (Figure 12).

To confirm these data, I measured the ability of the wild-type and mutant P_{TEF1}-based strains to degrade the model ERAD substrate, CPY*, which is a mutant form of the vacuolar protease, carboxypeptidase Y (CPY). As above, the *TEF1-K584X* and *TEF1-S493F* strains exhibited defects in the ERAD of CPY* (Figure 15D) whereas the *TEF1-KAR2* and *TEF1-R217A* strains efficiently degraded CPY*. Taken together, these results suggest that substrate binding is an important determinant of BiP's ability to support ERAD.

I then examined the ability of the BiP mutants to support ER protein folding by following the *in vivo* maturation of $CPY^{311\text{-}313}$. Upon translocation into the ER, the signal sequence of pre-pro-CPY is cleaved to generate pro-CPY, which is N-glycosylated to the 'p1CPY' ER precursor form. Subsequent trafficking to the Golgi results in additional sugar modifications, generating the 'p2CPY' Golgi precursor form. Finally, the "pro" sequence is cleaved in the vacuole, resulting in the mature and active mCPY form. mCPY has a molecular mass similar to the immature pre-pro-CPY form while p2CPY and p1CPY have higher molecular masses and hence migrate at a slower rate on a denaturing polyacrylamide gel. Defects in CPY folding in the ER result in an accumulation of the p1CPY ER precursor form.

CPY was immunoprecipitated from *TEF1-KAR2*, *TEF1-R217A*, *TEF1-K584X* and *TEF1-S493F* yeast that were pulse-labeled for 10 min at 30°C and then chased for 30 min (Figure 15E).

The temperature-sensitive *kar2* mutant strain, *kar2-113*, served as a positive control[166]. As expected, in the wild-type *TEF1-KAR2* strain, bands corresponding to the p1CPY, p2CPY and mCPY forms were observed after 10 min of pulse-labeling (Figure 15E; lane marked '0'), and at the end of the 30 min chase, the p1CPY and p2CPY forms matured to the mCPY form (Figure 15E); since signal peptide cleavage occurs co-translocationally, the pre-pro-CPY form cannot be detected in a wild-type strain. In the *kar2-113* mutant strain, on the other hand, the pre-pro-CPY and p1CPY forms persisted at 30 min, confirming that this strain has a translocation as well as folding defect (Figure 6E). Surprisingly, the CPY folding profile in the *TEF1-R217A*, *TEF1-K584X* and *TEF1-S493F* strains at 30 min resembled that of the wild-type strain (Figure 15E) suggesting that these strains were not deficient for CPY folding. This was unexpected because I had observed that the R217A, K584X and S493F BiP mutants were defective for *in vitro* interaction with Scj1p (Figure 2C). Scj1p cooperates with BiP to fold ER proteins under conditions of stress induced by hypoglycosylation[119], and exhibits genetic interactions with several *kar2* alleles[118, 119]. However, it is possible that the expression of these *kar2* mutants has no effect on N-linked glycosylation and hence these mutants are not dependent on Scj1p cooperation for folding CPY. Also, in the absence of Scj1p, it has been observed that Jem1p can take over as a folding cofactor for BiP[119], and none of these mutants are defective for Jem1p interaction (Figure 11B). Furthermore, even though the K584X and S493F BiP mutants exhibit substrate binding defects, they induce the UPR to very high levels (Figure 14F), which might be sufficient to compensate for folding problems in the ER.

Overall, I have identified a BiP mutant, R217A, which exhibits a translocation-specific defect when expressed in yeast. However, owing to its competent interaction with Jem1p, the R217A mutant does not exhibit ERAD defects. I have also identified two substrate binding

mutants, K584X and S493F, which show defects in both translocation and ERAD, suggesting that substrate binding is important for multiple BiP functions.

2.2.6 Sec63 complex formation is reduced for R217A BiP

The translocation complex in yeast is composed of the core proteins Sec61p (Sec61α), Sbh1p (Sec61β), and Sss1p (Sec61γ)[93, 96, 146], which are associated with Sec62p[152, 153] and the Sec63 complex[98]. The Sec63 complex contains Sec63p, BiP, Sec71p and Sec72p. Each of these complexes can be purified under non-denaturing conditions from yeast microsomes[96, 98, 100] and it has been demonstrated that BiP and Sec63p copurify in equal amounts as part of the Sec63 complex[98]. The interaction between BiP and Sec63p is thought to be critical to localize BiP at the ER membrane, where it can catalyze protein translocation.

Since I observed a defect in the interaction of R217A BiP with the J domain of Sec63p *in vitro* (Figures 11A and 11D), I wanted to determine the stoichiometry of the Sec63 complex in the *TEF1-R217A* strain. To this end, microsomes were prepared from *TEF1-KAR2* or *TEF1-R217A* yeast, solubilized in a non-ionizing detergent, and subjected to ion-exchange, size exclusion and mixed mode ion-exchange chromatography to isolate the Sec63 complex. Individual components of the complex were identified using Coomassie blue staining or immunoblotting after SDS-PAGE. As previously reported[98], I found that wild-type BiP and Sec63p were present in equal amounts in the Sec63 complex purified from the *TEF1-KAR2* wild-type strain (Figure 16). However, there was a 40-50% reduction in the amount of R217A BiP that copurified with Sec63p when the complex was analyzed from the *TEF1-R217A* strain (Figure 16). This observation, along with the results from Figures 11A and 11D, provides an

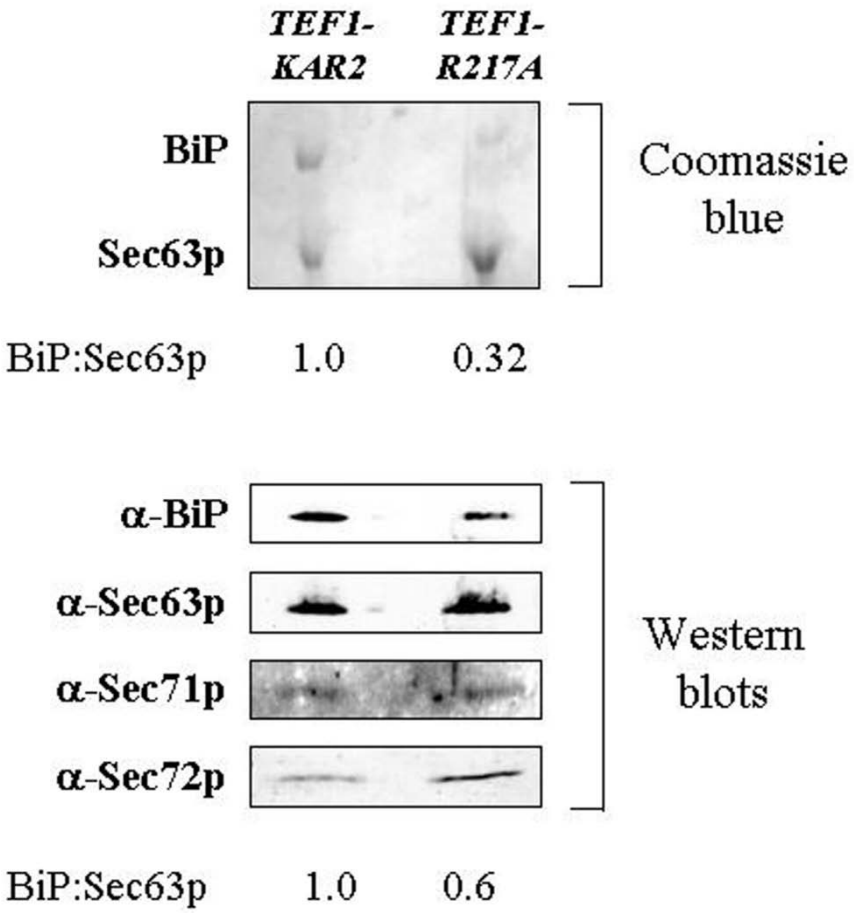

Figure 16: The translocation defect in *TEF1-R217A* yeast is due to reduced complex formation between Sec63p and R217A.

The Sec63p complex containing Sec63p, BiP, Sec71p and Sec72p, was purified from microsomes derived from the *TEF1-KAR2* and *TEF1-R217A* strains, resolved by SDS-PAGE and subjected to Coomassie Brilliant Blue staining or immunoblotting. The ratio of BiP to Sec63p is indicated below each panel.

explanation for the translocation defect exhibited by *TEF1-R217A* yeast (Figures 15A and 15B).

2.2.7 Scj1p and Jem1p function redundantly in *TEF1-R217A* yeast

The observation that: (i) R217A BiP was defective for *in vitro* Scj1p interaction (Figures 11C and 11F) but not Jem1p interaction (Figures 11B and 11E), and (ii) *TEF1-R217A* yeast degraded soluble ERAD substrates efficiently (Figures 15C and 15D), suggested that a competent interaction between Jem1p and R217A BiP was sufficient to support ERAD in the *TEF1-R217A* strain. Therefore, I hypothesized that if this interaction between Jem1p and R217A BiP were to be disrupted, it would result in an ERAD defect. To test this hypothesis, I created *TEF1-R217A* yeast strains lacking a functional copy of either *JEM1* or *SCJ1*, thus generating the *TEF1-R217A jem1Δ* and *TEF1-R217A scj1Δ* strains. As controls, I also generated the *TEF1-KAR2 jem1Δ* and *TEF1-KAR2 scj1Δ* strains.

The resulting strains were initially tested for their ability to grow at elevated temperature or in the presence of DTT. I found that the deletion of *jem1* or *scj1* in either *TEF1-KAR2* or *TEF1-R217A* yeast did not affect growth at elevated temperatures (Figure 17A), although the *TEF1-R217A scj1Δ* strain showed reduced growth at 37°C. Moreover, deletion of *scj1*, but not *jem1*, in the *TEF1-KAR2* and *TEF1-R217A* strains resulted in DTT sensitivity (Figure 17B). This was not surprising because previous studies demonstrated that *scj1Δ* yeast cannot grow efficiently in the presence of ER stress-inducing agents such as tunicamycin and β-mercaptoethanol, whereas *jem1Δ* yeast can grow in the presence of these compounds[119].

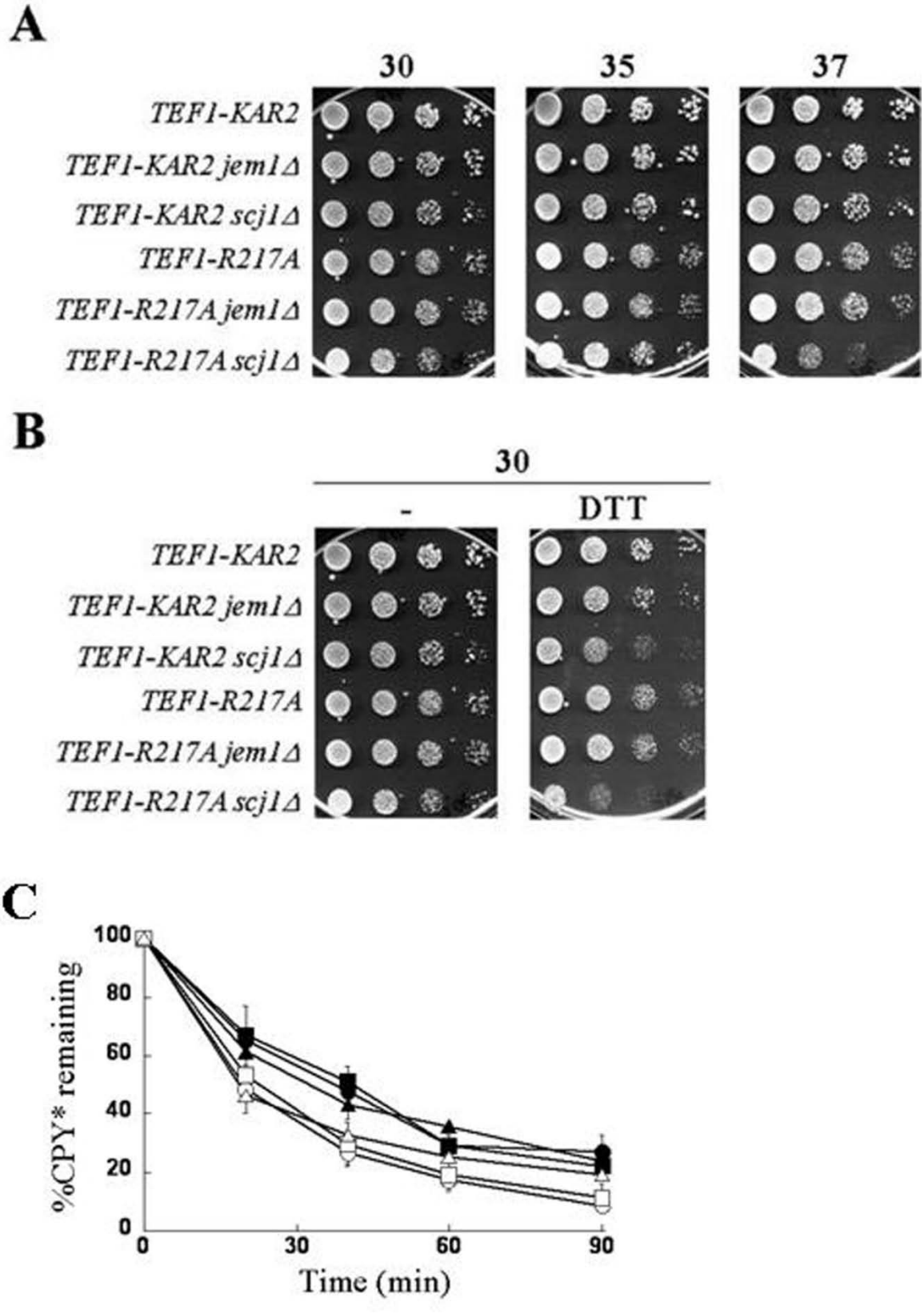
A
30
35
37
TEF1-KAR2
TEF1-KAR2 jem1Δ
TEF1-KAR2 scj1Δ
TEF1-R217A
TEF1-R217A jem1Δ
TEF1-R217A scj1Δ
B
30
-
DTT
TEF1-KAR2
TEF1-KAR2 jem1Δ
TEF1-KAR2 scj1Δ
TEF1-R217A
TEF1-R217A jem1Δ
TEF1-R217A scj1Δ
C
%CPY* remaining
100
80
60
40
20
0
0
30
60
90
Time (min)

Figure 17: Jem1p and Scj1p function redundantly to support ERAD in the *TEF1-R217A* strain.

(A) Ten-fold serial dilutions of the indicated strains were plated onto selective medium and incubated at 30, 35 or 37 °C for 2 d. ***(B)*** Ten-fold serial dilutions of the indicated strains were plated onto selective medium without (-) or with 8mM DTT (DTT). Plates were incubated at 30° C for 2 d. ***(C)*** Pulse-chase immunoprecipitation experiments were used to analyze the degradation of CPY* in *TEF1-KAR2* (●), *TEF1-R217A* (**O**), *TEF1-KAR2 jem1Δ* (■), *TEF1-KAR2 scj1Δ* (▲), *TEF1-R217A jem1Δ* (□) *and TEF1-R217A scj1Δ* (△) strains at 30°C. Data represent the means of a minimum of three independent experiments ± standard errors.

Next, I measured the ERAD efficiencies of the *TEF1-KAR2 jem1Δ, TEF1-KAR2 scj1Δ*, *TEF1-R217A jem1Δ* and *TEF1-R217A scj1Δ* strains by examining the degradation rate of CPY*. I found that the individual deletions of *jem1* or *scj1* in the *TEF1-KAR2* strain did not affect CPY* degradation efficiency (Figure 17C), consistent with their overlapping roles during ERAD[120]. Moreover, the deletion of *scj1* in *TEF1-R217A* yeast did not result in an ERAD defect, in keeping with my hypothesis (Figure 17C). However, contrary to my expectation, the deletion of *jem1* in *TEF1-R217A* yeast had no effect on CPY* degradation (Figure 17C). A possible explanation for this result is that even though R217A BiP and Scj1p are unable to interact with each other, as was observed *in vitro* (Figures 11C and 11F), in the absence of Jem1p, the two proteins might cooperate to an extent that is sufficient to support ERAD. In fact, the UPR is induced upon deletion of Jem1p (data not shown) and this might be sufficient to compensate for ERAD defects in *TEF1-R217A jem1Δ* cells. Alternately, R217A BiP and Scj1p might independently, but simultaneously, bind to CPY* and other misfolded proteins during ERAD and maintain them in a soluble, retrotranslocation-competent state. Indeed, Scj1p has a substrate binding domain that is similar to that of bacterial DnaJ, the founding member of the Hsp40 family[314], and to Ydj1, a yeast cytosolic Hsp40 that requires its substrate binding properties to function efficiently in the cell[315]. In addition, the contribution of ERj5, a newly characterized yeast ER Hsp40 (refer to section 1.2.2), during ERAD might explain this discrepancy. Finally, I cannot discount the possibility that the results that were obtained *in vivo* might not fully mirror the *in vitro* defects observed for the interaction between R217A BiP and Scj1p.

2.2.8 Identification of genetic interactions specific for the *R217A* BiP allele

In order to better understand the range of cellular functions altered by R217A BiP expression, I decided to take an unbiased genetic approach. This genetic approach might also identify novel players in translocation and/or other BiP-regulated processes. To this end, 350 gene deletions were selected which resulted in a constitutive induction of the UPR (Table 6 in Appendix B; Jonikas *et al.,* 2009). These gene deletions not only included those expected to alter the ER folding environment such as ER and cytosolic chaperones, components of the N-linked glycosylation machinery, and ERAD, but also included genes encoding factors required for O-mannosylation, GPI anchor synthesis, vesicular trafficking, vacuole function, lipid biosynthesis and, intriguingly, cytoskeletal organization and chromatin remodeling. I asked whether deleting these genes in combination with *kar2-R217A::NAT* (Appendix B) produced unusually high or low levels of UPR, as assessed through the use of a fluorescent UPR reporter (see Table 7 in Appendix B). This approach was chosen due to a higher sensivtivity than a growth-based genomic analysis (J.S.Weissman, personal communication).

Next, a *kar2-R217A::NAT* genetic interaction profile was generated (Figure 18B) as recently detailed[121]. The efficacy of this approach was verified by the fact that *hac1Δ* and *ire1Δ* were epistatic to all other examined interactions. An initial comparison of the wild-type *KAR2::NAT* and *kar2-R217A::NAT* genetic interaction profiles (Figure 18; datapoints on the horizontal blue line) showed that the *kar2-R217A::NAT* allele masked the UPR induction otherwise observed in a subset of deletion strains, including *las21Δ, opi3Δ, ilm1Δ, vps53Δ, yur1Δ, spc1Δ, sys1Δ, rav1Δ, vtc4Δ* and *mtc1Δ* (refer to Table 6 in Appendix B for a description of these genes). These data suggest that the *kar2-R217A::NAT* allele is epistatic to these gene

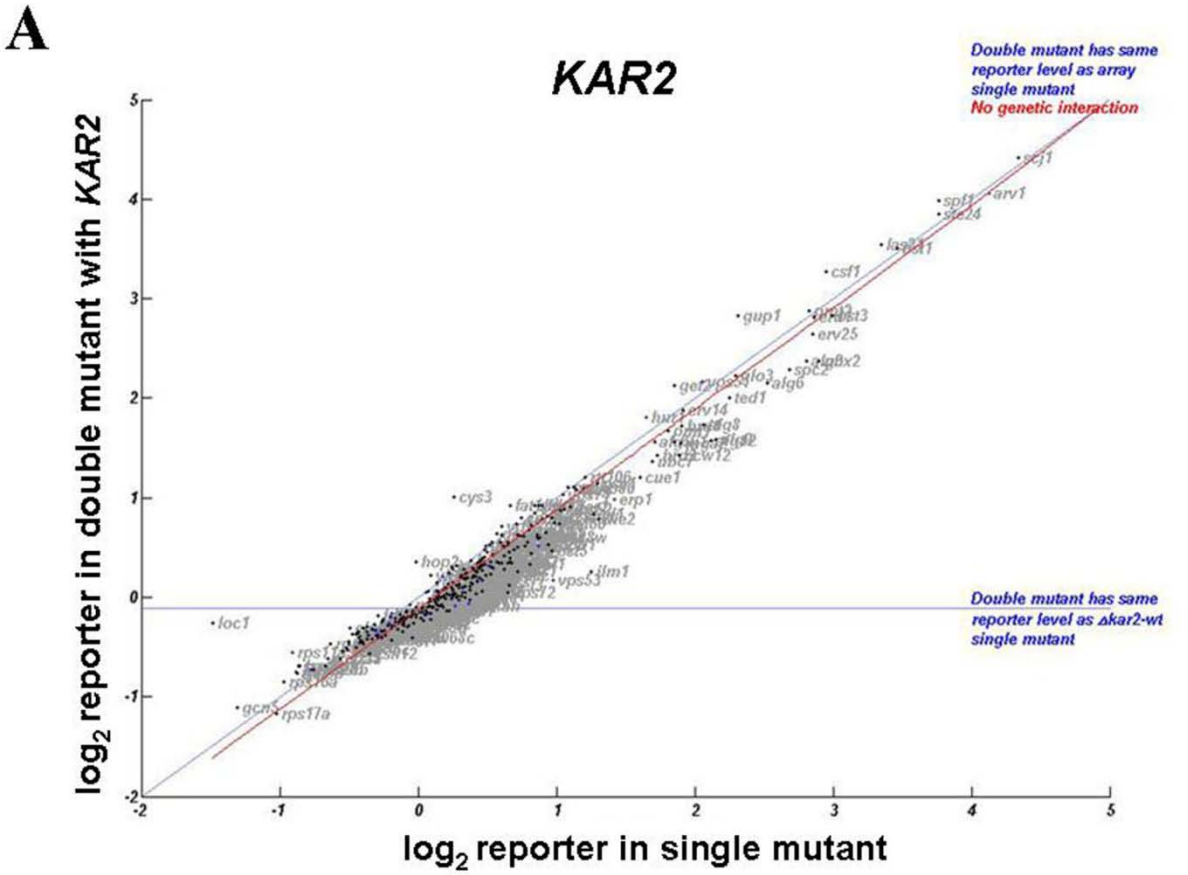
A
KAR2
Double mutant has same reporter level as array single mutant
No genetic interaction
Double mutant has same reporter level as Δkar2-wt single mutant
log2 reporter in double mutant with KAR2
log2 reporter in single mutant
B
kar2:R217A
Double mutant has same reporter level as array single mutant
No genetic interaction
Double mutant has same reporter level as Δkar2-r217a single mutant
log2 reporter in double mutant with kar2:R217A
log2 reporter in single mutant

Figure 18: Genetic interaction profile of *kar2-R217A::NAT* with 350 gene deletions that induce the UPR.

The levels of UPR induction in the 350 gene deletion strains was measured using a fluorescent reporter either in the absence (values represented on the x-axis) or presence (values represented on the y-axis) of ***(A)*** wild-type *KAR2::NAT*, or ***(B)*** the *kar2-R217A::NAT* mutant, with each datapoint on the graph corresponding to a unique gene deletion. The horizontal blue line represents the basal level of UPR induction observed in the *KAR2::NAT* or *kar2-R217A::NAT* strains. The diagonal blue line represents the expected values of UPR induction in each of the individual deletion strains if the presence of *KAR2::NAT* or *kar2-R217A::NAT* does not induce an additional ER stress. The red line represents the 'best fit' curve to the predicted values in the double mutant strains when each gene deletion is combined with either *KAR2::NAT* or *kar2-R217A::NAT*.

deletions. Additionally, when the *kar2-R217A::NAT* genetic interaction profile was compared to interaction profiles previously collected for the 350 gene deletions (Jonikas *et al.,* 2009), a very high correlation was noted to the set of genetic interactions exhibited by the *sec71Δ* and *sec72Δ* strains, consistent with a translocation-specific defect in this mutant. Moreover, the *kar2-R217A::NAT* allele lacked a characteristic signature shared by genes required for ERAD, including aggravating interactions with *cne1Δ, rer1Δ* and *yur1Δ*. Therefore, using a novel method of genetic analysis, I was able to recapitulate the translocation-specific defect that was observed for the *R217A* allele of BiP (Figure 15).

2.2.9 Ilm1p is a novel player during protein translocation across the ER membrane

Owing to the similarity of the *kar2:R217A, sec71Δ* and *sec72Δ* genetic interaction profiles, I postulated that gene deletions that showed significant genetic interactions with each of these strains might also be defective for translocation. Based on the strength of their genetic interactions and based on the fact that these mutants were relatively uncharacterized, I then selected three strains, *ilm1Δ, erd1Δ* and *sur4Δ*, for further analyses (Table 3). Ilm1p (Increased loss of mitochondrial DNA) is an uncharacterized protein that is predicted to possess three transmembrane domains and localize to the ER. Erd1p (ER retention defect) is a poorly-characterized ER transmembrane protein; deletion of *erd1* results in increased secretion of ER lumenal proteins, though the mechanism is unknown[316, 317]. Sur4p (Suppressor of *rvs161* and *rvs167* mutations) is an ER-resident protein that is involved in the synthesis of very long chain fatty acids[318, 319].

Table 3: Quantification of the genetic interactions between individual deletion strains (columns) and the indicated query strain (rows).

* A positive genetic interaction value means that the double mutant strain had a lower level of UPR induction than what was predicted.

** A positive genetic interaction value which is statistically significant is highlighted in red.

*** Note that the value for the absence of a genetic interaction is ~0[121].

**** N/A indicates either that the double mutant strain was inviable or that a value was not obtained due to experimental error.

Mutant	*ilm1Δ*	*erd1Δ*	*sur4Δ*	*ccw12Δ*	*vtc4Δ*
kar2:R217A	1.2534	1.3922	0.9569	0.6068	0.4451
sec71Δ	-0.1357	1.4758	0.3603	#N/A	0.0184
sec72Δ	0.778	0.3587	0.4122	0.4514	#N/A

To determine whether the *ilm1Δ, erd1Δ, sur4Δ* strains had translocation-related phenotypes, I examined the *in vivo* translocation efficiencies of ppαF and BiP in these strains (Figure 19A). I found that pre-BiP accumulated only in the *ilm1Δ* strain, suggesting that Ilm1p might play a role in translocation. However, because ppαF did not accumulate in *ilm1Δ* yeast (Figure 19A), I decided to look at the translocation efficiency of two other well-characterized substrates, dipeptidyl aminopeptidase-B (DPAP-B) and the repressible vacuolar alkaline phosphatase, Pho8p. Upon translocation into the ER, pre-DPAP-B is N-glycosylated at multiple sites resulting in an increase in the molecular mass from ~95 kDa to 130 kDa[320]. Pre-Pho8p is N-glycosylated at a single site after its translocation resulting in an increase in molecular mass from ~68 kDa to 72 kDa[321]. When I analyzed the translocation of DPAP-B and Pho8p in wild-type and *ilm1Δ* yeast cells, I did not see an accumulation of pre-DPAP-B or pre-Pho8p as compared to the control strain, *sec65-1*[322], which contains a mutant allele in the Sec65p subunit of the signal recognition particle (SRP; Figure 19A). Therefore, of the four substrates that I examined, the deletion of *ilm1* uniquely affected the translocation of pre-BiP.

The induction of the UPR results in BiP upregulation and attenuation of translocation across the ER membrane[199]. It is therefore possible that the pre-BiP-specific translocation defect observed in *ilm1Δ* yeast is an artefact of the high levels of UPR induction observed in this strain[121]. To rule out this possibility, I examined BiP translocation in another deletion strain that induces the UPR to very high levels, *scj1Δ*[121]. I found that pre-BiP did not accumulate in the *scj1Δ* strain, even though the *ilm1Δ* strain, again, accumulated pre-BiP (Figure 19A, bottom row). Taken together, these observations suggest that Ilm1p either plays a specific role in BiP translocation, or that it might be required for the translocation of a unique subset of proteins, which includes BiP.

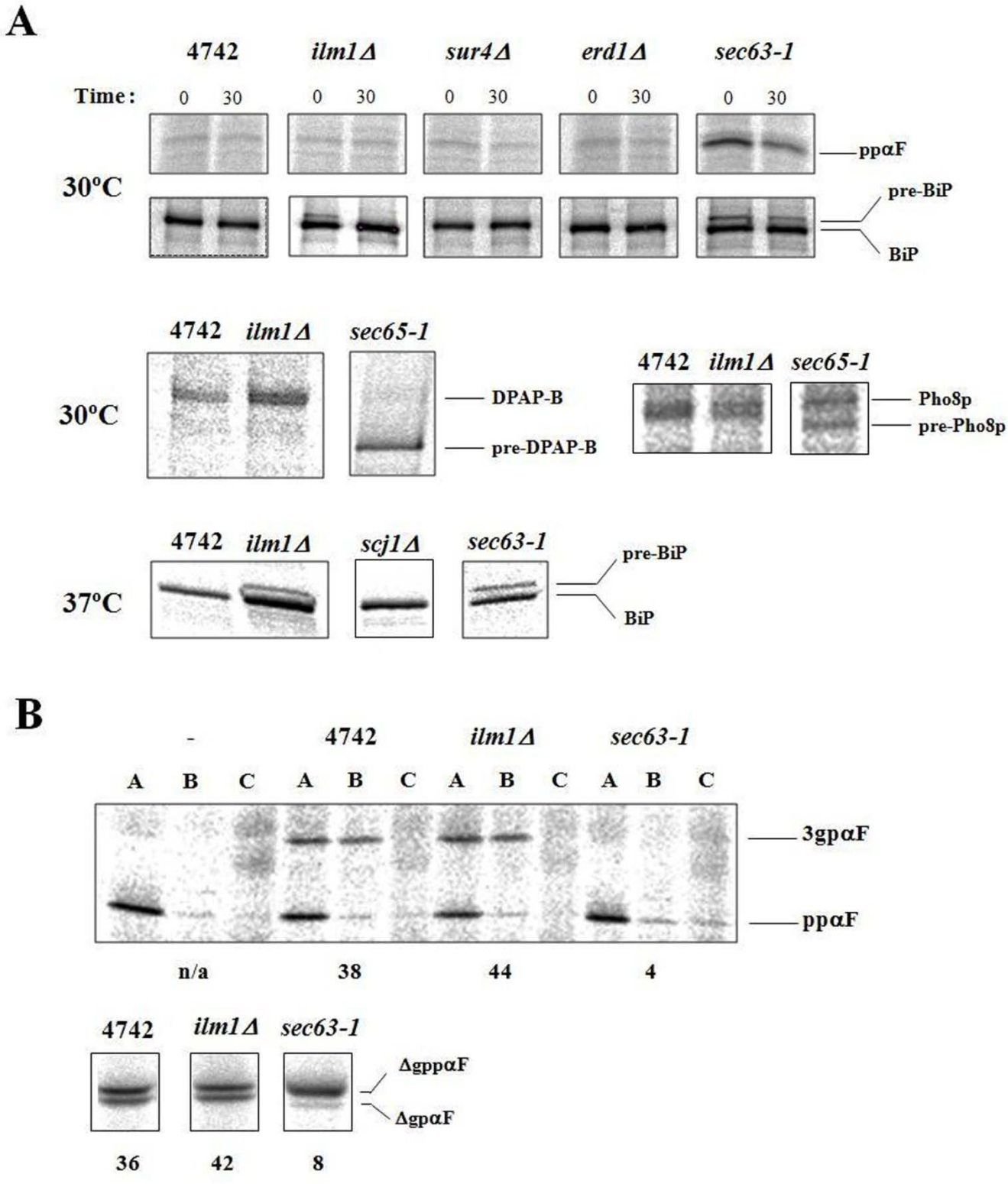
A
4742
ilm1Δ
sur4Δ
erd1Δ
sec63-1
Time:
0
30
30°C
ppαF
pre-BiP
BiP
4742
ilm1Δ
sec65-1
30°C
DPAP-B
pre-DPAP-B
4742
ilm1Δ
sec65-1
Pho8p
pre-Pho8p
4742
ilm1Δ
scj1Δ
sec63-1
37°C
pre-BiP
BiP
B
-
4742
ilm1Δ
sec63-1
A
B
C
3gpαF
ppαF
n/a
38
44
4
4742
ilm1Δ
sec63-1
ΔgppαF
ΔgpαF
36
42
8

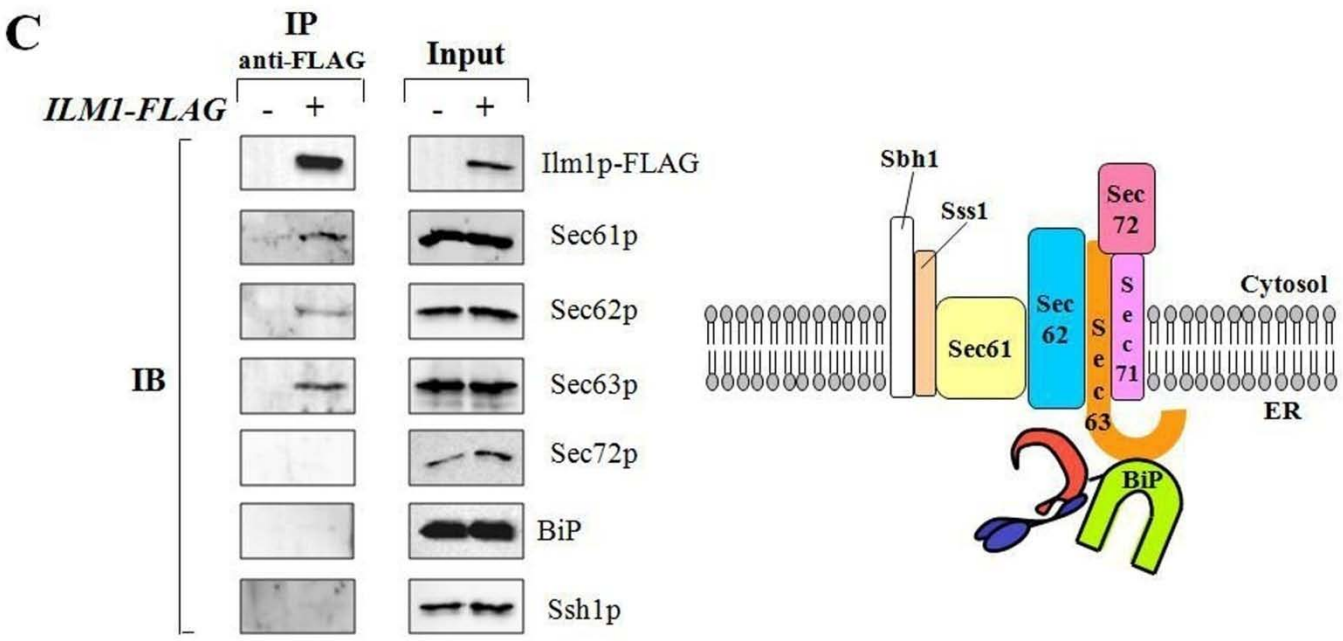

Figure 19: Ilm1p is required for the efficient translocation of BiP and interacts with components of the translocation machinery.

(A) The translocation efficiency of ppαF, BiP, DPAP-B and Pho8p was assessed in the indicated wild-type and mutant strains by performing a pulse-chase immunoprecipitation assay at the specified temperatures. The *sec63-1* strain which carries a translocation-defective allele of *SEC63,* and the *sec65-1* strain which carries a temperature-sensitive allele of *SEC65,* served as positive controls. ***(B)*** The ability of microsomes derived from the indicated strains to translocate ppαF and ΔgppαF was evaluated at 20°C. After translocation, each sample was divided and treated in one of three ways: A-buffer, B-trypsin, C-trypsin and Triton X-100. The percent translocation efficiency is indicated below each panel. Data are representative of three independent experiments. ***(C)*** Native immunoprecipitations using anti-FLAG-agarose beads against Ilm1p-FLAG were performed as described[3]. The BY4741 wild-type strain containing an untagged copy of *ILM1* served as a negative control. Input: 5% of the material that was immunoprecipitated; IP: Immunoprecipitation; IB: Immunoblotting. The components of the Sec61 complex are depicted pictorially.

Next, I examined microsomes derived from the *ilm1Δ* strain for the translocation of ppαF and mutant ΔgppαF. In agreement with my *in vivo* results, microsomes lacking Ilm1 were as efficient as wild-type microsomes for ppαF and ΔgppαF translocation (Figure 19B).

Finally, I tested whether Ilm1p interacted with components of the translocation machinery. For this purpose, I generated a chromosomal version of FLAG-tagged *ILM1* in the BY4741 strain background. Pre-BiP did not accumulate in this strain (data not shown), indicating that FLAG-tagged Ilm1p is functional. Next, I immunoprecipitated Ilm1p-FLAG-associated protein complexes from yeast cells in the presence of Triton X-100, resolved proteins in the precipitate by SDS-PAGE, and performed immunoblot analysis with antisera against the the FLAG epitope, Sec61p, Sec62p, Sec63p, Sec72p and BiP. As shown in Figure 19C, Sec61p, Sec62p and Sec63p co-immunoprecipitated with Ilm1p, suggesting that these proteins form a complex with Ilm1p. Furthermore, the absence of Sec72p and BiP from this complex emphasizes the specificity of the Ilm1p-Sec61-Sec62-Sec63 interaction. As a control, I also examined whether Ssh1p, a Sec61p homolog[323], resided in the immunoprecipitated complex, but this species was absent (Figure 19C). This result indicates that Ilm1p cooperates with the Sec61 complex, but probably not the Ssh1 complex, to enable the translocation of distinct factors.

2.2.10 Deletion of *ilm1* does not result in ERAD defects

To test if Ilm1p plays a specific role in translocation, but not in ERAD, I measured the ability of the *ilm1Δ* strain to degrade different classes of ERAD substrates: (i) substrates with ER lumenal lesions, such as CPY*; (ii) integral membrane substrates with cytosolic lesions, such as Ste6p*, a mutant form of the yeast **a**-factor transporter[324], and CFTR (cystic fibrosis transmembrane

conductance regulator[325]); and (iii) co-translocational substrates such as ApoB29 (a truncated version of human apolipoprotein B [301]). I observed that Ste6p*, CFTR and ApoB29 were degraded efficiently in *ilm1Δ* yeast (Figure 20B, 20C and 20D, respectively) although there was a slight reduction in the degradation of CPY* (Figure 20A). However, since the genetic interaction profile of *ilm1Δ* yeast lacks an ERAD-specific signature[121], I do not consider this effect to be significant. Furthermore, when I measured the degradation of mutant ΔgpαF using microsomes derived from the *ilm1Δ* strain, I found that ΔgpαF was degraded comparably to microsomes derived from the wild-type BY4742 strain (Figure 11E). Taken together, I can conclude that *ilm1Δ* yeast do not exhibit ERAD defects.

2.3 DISCUSSION

BiP is a highly conserved, essential protein in eukaryotes; for example, the yeast and mammalian BiP homologs share greater than 65% sequence identities. Several human diseases including Alzheimer's disease, Marinesco-Sjögren syndrome, autosomal dominant polycystic liver disease, Wolcott-Rallison syndrome, and a variety of cancers may result from either the overexpression of BiP or the malfunction of BiP and/or its cofactors[239, 240]. Hence, insights into the function of this protein, in particular its interactions with various cofactors, are critical toward understanding the etiology of these various diseases. Owing to the amenability of *Saccharomyces cerevisiae* to genetic manipulations and the availability of specific biochemical assays to evaluate BiP function, this model organism is an excellent starting point to characterize the determinants of BiP-cofactor interaction.

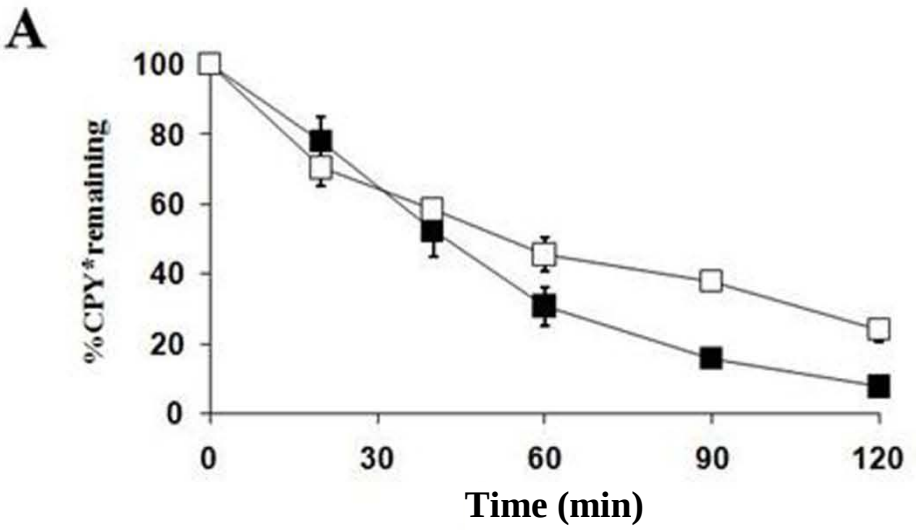
A
100
80
60
40
20
0
%CPY*remaining
0
30
60
90
120
Time (min)

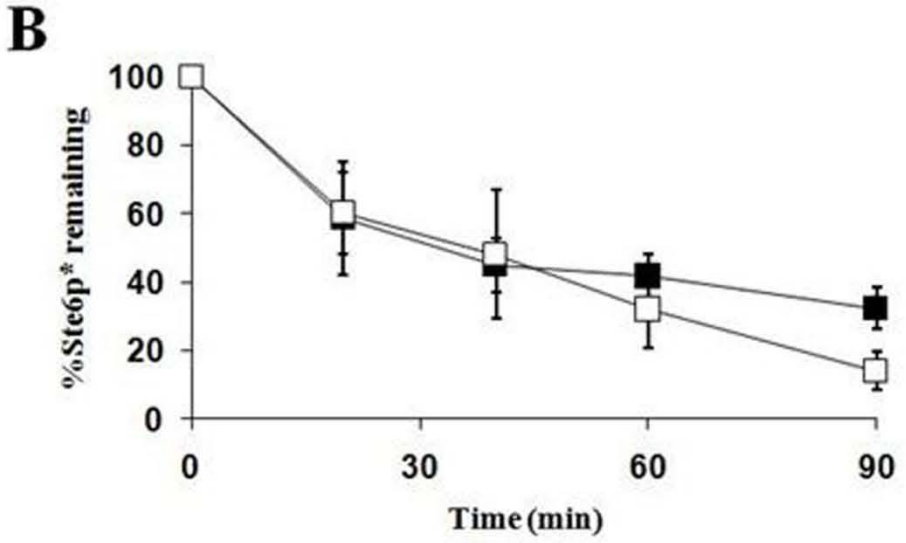
B
100
80
60
40
20
0
%Ste6p* remaining
0
30
60
90
Time (min)

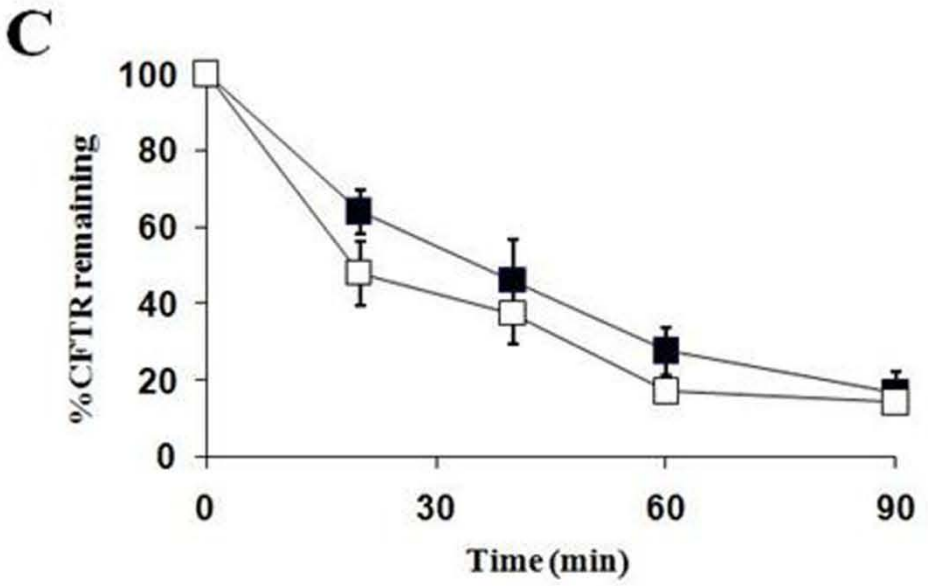
C
100
80
60
40
20
0
%CFTR remaining
0
30
60
90
Time (min)

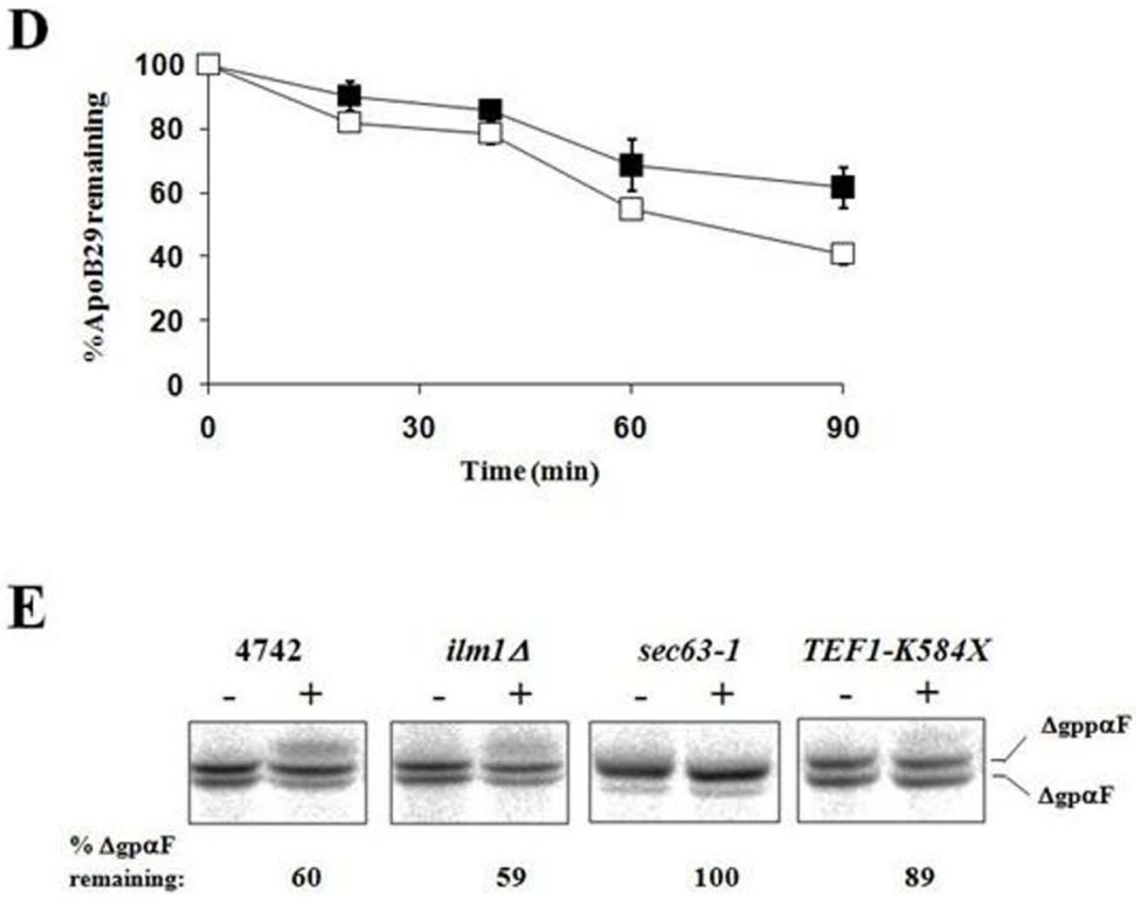

Figure 20: Deletion of *ilm1* has no effect on ERAD.

The ERAD efficiencies of wild-type (BY4742) (■) and *ilm1Δ* (□) yeast were compared using a cycloheximide chase assay for the substrates ***(A)*** CPY* (assayed at 30°C), ***(B)*** Ste6p* (assayed at 37°C), ***(C)*** CFTR (assayed at 40° C), and ***(D)*** ApoB29 (assayed at 30°C). Data represent the means of a minimum of three independent experiments ± standard errors. ***(E)*** *In vitro* ERAD assays using microsomes derived from wild-type and *ilm1Δ* yeast was performed either in the absence (-) or presence (+) of an ATP regenerating system and 0.5 mg/ml of yeast cytosol at 30°C. Microsomes derived from the *sec63-1* and *TEF1-K584X* strains served as positive controls. The percent ΔgpαF remaining after 20 min was calculated by normalizing the amount of ΔgpαF present in the '+' lane to the amount present in the corresponding '-' lane. Data are representative of three independent experiments ± standard errors.

2.3.1 Identification of a translocation-specific BiP mutant, R217A

I have demonstrated that a specific mutation in the putative J domain interacting surface of yeast BiP/Kar2p, R217A, results in a protein that differentially interacts with its cognate Hsp40 cochaperones. Specifically, R217A BiP competently interacts with Jem1p but is defective for maximal ATPase stimulation by Sec63p and Scj1p. This might seem surprising given that the J domains of Sec63p and Scj1p share a lower sequence identity (*i.e.,* 34%) than the sequence identity shared by the J domains of Sec63p and Jem1p (*i.e.,* 40%), and by the J domains of Scj1p and Jem1p (*i.e.,* 40%; Figure 21). However, the observation that the J domains of Sec63p and Scj1p are interchangeable *in vivo*[118] indicates that the context of the J domain and perhaps individual amino acids within this domain are as important as the overall sequence and percent conservation. Notably, the *in vitro* studies utilized the J domain alone from Sec63p (~70 amino acids), the J domain with its flanking sequences from Jem1p (~110 amino acids), but full-length Scj1p (~350 amino acids). Therefore, one cannot rule out the possibility that residues in the J domain other than the HPD motif might also be required for optimal BiP-Hsp40 interaction, as has been observed for other Hsp70-Hsp40 pairs[66, 326]. Formally, it is also possible that the J domains of BiP's cognate Hsp40s have diverged so that they can target BiP to function specifically in the ER.

I also found that the expression of R217A BiP in yeast reduced translocation efficiency across the ER membrane, and this could be explained by a reduced complex formation between Sec63p and BiP. Since Sec63p interaction helps to localize BiP at the ER for binding to translocating polypeptide chains this result is not surprising. Taken together with my observations that the ERAD and folding efficiencies of yeast expressing R217A BiP remain unaltered, I conclude that a unique mutation in BiP's ATPase domain is sufficient to affect a

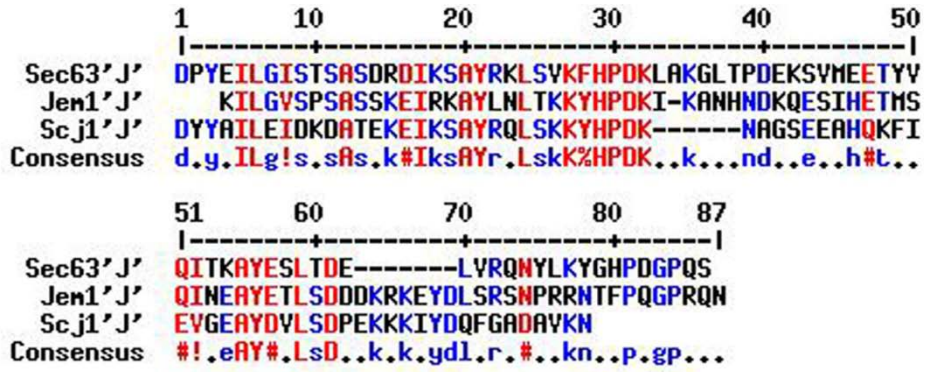

Figure 21: An alignment of the J domains of Sec63p, Jem1p and Scj1p.

The amino acid sequences corresponding to the J domains of Sec63p (amino acids 125-203), Jem1p (amino acids 541-623) and Scj1p (amino acids 23-94) were aligned using the program Multalin[4]. The highest conservation is observed at the canonical HPD motif. Amino acid notations in the row labeled "consensus" include:!- isoleucine or valine; $- leucine or methionine; %- phenylalanine or tyrosine; #- asparagine, aspartate, glutamine or glutamate.

specific BiP function, *i.e.,* translocation. Also, because yeast cells expressing R217A BiP do not induce the UPR, and can be sensitized to induce the UPR by treatment with DTT, I surmise that this mutant is not defective for Ire1p interaction. Indeed, the R217 residue is distal to the putative Ire1p-interacting surface of BiP[287].

Prior studies have addressed the effects of mutating the analogous arginine residue in DnaK[91], the bacterial Hsp70, and Chinese hamster BiP/Grp78[116, 302]. In fact, the R167A mutant of DnaK was identified in a screen directed toward identifying suppressors of a mutation in the bacterial Hsp40, DnaJ, which negatively affected DnaK interaction; this was the first report of an Hsp70 mutant that was defective for J domain interaction[91]. Recent studies in which the analogous R197 of Chinese hamster BiP was altered to diverse amino acids with unique chemical properties further emphasized the contributions of R197 towards interaction with ERdj3, the ER-lumenal Hsp40[116, 302], and possibly toward inter-domain communication between the ATPase and substrate binding domains[302]. However, none of these studies addressed whether the mutant Hsp70s demonstrated Hsp40 binding specificity. Further implications of the R217A mutation on BiP function are discussed in Chapter 4.

Finally, the closely-related family of Hsp110s and Grp170, including BiP's cofactor Lhs1p, contain an alanine in place of this invariant Hsp70 arginine, and it is not surprising that the ATPase activity of Lhs1p cannot be stimulated by the ER-resident Hsp40s[139].

2.3.2 Substrate binding mutants of BiP affect ER homeostasis and multiple BiP functions

Two mutations in BiP's substrate binding domain, K584X that lacks the lid domain and S493F that destroys a salt bridge between the substrate binding and lid domains, were defective for functional substrate interaction as determined in a peptide-stimulated ATPase assay. K584X BiP

also exhibited reduced stability *in vitro* and *in vivo*, while S493F BiP adopted an alternate conformation from wild-type BiP. Since these mutants maintained their ability to interact with two of BiP's Hsp40s, Sec63p and Jem1p, I speculate that mutations in the substrate binding domain only affect BiP's ability to bind to substrates. To further confirm the inability of K584X and S493F BiP proteins to bind to substrates, I intend to perform peptide binding assays using a fluorescently-labeled peptide substrate according to a previously established protocol[181].

Interestingly, the expression of these mutants in yeast resulted in both translocation and ERAD defects. This was in contrast to the ERAD-defective substrate binding mutants, P515L and T473F, which the Brodsky laboratory identified in a previous genetic screen[181]. However, in the current study, the mutant BiP proteins were expressed from the constitutive P_{TEF1} promoter, whereas in the previous study, the mutants were expressed from BiP's endogenous promoter which contains heat shock[204] and UPR elements[204, 205]; therefore, the expression of P515L and T473F was sensitive to ER stress. Since the expression of substrate binding BiP mutants results in UPR induction (Ref. 174 and Figure 5), it is formally possible that the mutant proteins in the previous study were expressed at sufficiently high levels from the endogenous promoter to suppress translocation defects. This could also account for the inability to identify translocation-specific mutants in the same genetic screen. The contribution of substrate binding to BiP function is further elaborated upon in Chapter 4.

2.3.3 Characterization of the genetic interactions of R217A BiP

To understand the range of functions altered by R217A BiP *in vivo*, I utilized an unbiased genetic approach in which I analyzed the effect of R217A BiP expression on the UPR induction in 350 individual gene deletions that perturb the ER folding environment. Since R217A BiP

expression does not in itself induce the UPR (Figure 14E), I hypothesized that this BiP mutant might exacerbate or alleviate the UPR when combined with another deletion with which it genetically interacts. Accordingly, I found that *kar2-R217A::NAT* masked the UPR induction normally observed in a subset of gene deletions, indicating that R217A BiP was epistatic to these gene deletions; one such deletion was *spc1Δ*. Spc1p is a component of the signal peptidase complex[160, 161]. This was not surprising because signal sequence cleavage occurs after polypeptide translocation has been initiated[27], and BiP is required for the latter process, especially during co-translational protein translocation. I also determined that in the presence of R217A BiP, the UPR induction in the *sls1Δ* strain (also known as *sil1Δ*) was slightly exacerbated. This is again consistent with BiP and Sls1p playing a coordinated role in translocation, although whether Sls1p simply acts as a BiP NEF, or plays another role, is still unclear[133-135]. Interestingly, I was unable to analyze data for the *lhs1Δ* strain, suggesting either that the *kar2-R217A::NAT lhs1Δ* double mutant is inviable, in agreement with a role for Lhs1p in translocation[135, 136, 138], or that the *kar2-R217A::NAT* and the *lhs1Δ* strains might have mating/sporulation incompatibility. Since the genes encoding Kar2p and Lhs1p are located on different chromosomes, the possibility of polar effects can be ruled out. Finally, I found that UPR levels were alleviated in the *hlj1Δ* strain in the presence of R217A BiP, suggesting that the corresponding proteins function in the same or parallel pathways. This result is intriguing because the only known function for Hlj1p that has been identified thus far is in ERAD[324, 327]. However, my data suggest that Hlj1p may also play a role in translocation (or even translation).

Furthermore, by comparing the genetic interaction profile of R217A BiP to the 350 gene deletions, we found that, strikingly, R217A BiP's profile closely resembled the genetic interactions exhibited by two other translocation components, Sec71p and Sec72p. Not only did

this confirm that the expression of R217A BiP *in vivo* specifically affects translocation, it also encouraged us to identify the gene deletions that exhibited the highest levels of interactions with the three translocation-related alleles, and test their translocation efficiency; one such candidate was *ilm1Δ*.

2.3.4 Ilm1p, a previously uncharacterized protein, plays a role in the translocation of BiP

Ilm1p was first characterized in a genetic screen targeted toward the identification of yeast mutants that were sensitive to filamentous growth induced by slowed-DNA synthesis; it was suggested that Ilm1p plays a role in the maintenance of mitochondrial DNA[328]. But, given its localization to the ER membrane[329], and the observed genetic interactions with R217A BiP, *sec66Δ* and *sec72Δ* (Table 3), I speculated that Ilm1p may play a role in translocation. Consistent with my expectations, I found that *ilm1Δ* yeast exhibit a specific defect for pre-BiP translocation. Furthermore, Ilm1p, an integral membrane protein, interacts with other integral membrane components of the translocation machinery, *i.e.,* Sec61p, Sec62p and Sec63p, indicating that it is present at the right location in the ER membrane. However, I was unable to observe a translocation defect for three other substrates, ppαF, DPAP-B and Pho8p. Previous studies have demonstrated that while ppαF uses an SRP-independent post-translational translocation pathway to get into the ER, DPAP-B and Pho8p use a SRP-dependent co-translational translocation mechanism[330]. Interestingly, BiP uses both modes of translocation, and only one other substrate, Och1p, a mannosyltranferase of the cis-Golgi apparatus, was shown to behave similar to BiP[330]. Therefore, it is possible that *ilm1Δ* yeast may also be defective for Och1p translocation. If this were the case, Ilm1p might be the linchpin that mediates the recognition of substrates that require

the post-translational and co-translational modes of translocation. However, this hypothesis remains to be tested.

An interesting feature of BiP's signal sequence is its unusual length, *i.e.,* 42 amino acids, compared to the average signal sequence length of ~20-30 amino acids[331]. In fact, only five other yeast proteins have predicted signal sequences of comparable or greater length, as compiled from the Signal Peptide database (http://proline.bic.nus.edu.sg/spdb/). Therefore, an alternate explanation for Ilm1p's unique effects on pre-BiP translocation may be that Ilm1p either directly binds to or facilitates the recognition of a subset of signal sequences in a length-dependent manner. A second explanation could be that signal sequences of a certain chemical nature might require Ilm1p for their recognition. Previous studies have demonstrated that signal sequences are typically comprised of an N-terminal basic domain, followed by a core hydrophobic region and a C-terminal slightly polar domain. Other than these features, signal sequences lack significant homology[332], and whether there are additional determinants that classify signal sequences is currently unknown. It is also possible that Ilm1p might be dedicated to the translocation of BiP, one of the most abundant proteins in the ER, and our observation that *kar2:R217A* was epistatic to *ilm1Δ* supports this hypothesis (Figure 18B). This could also provide an explanation for the observed UPR induction upon *ilm1* deletion. Each of these hypotheses remains to be tested.

2.3.5 Perspective

Recently, a large number of novel, high-throughput genetic screening technologies have been developed for yeast[333-345]. However, the application of these technologies to understand yeast biology is in its infancy and can easily be extended to key metabolic pathways. As a specific example, I demonstrate that the careful investigation of unique mutant alleles of an essential

multi-functional gene when combined with a targeted genetic screen can lead to the identification of novel players in an otherwise well-studied cellular process. Moreover, during the course of such a study, functions can also be assigned to poorly characterized open reading frames. Based on my success, it is not hard to conjecture the widespread application of this technique.

Taking this study one step further, I can also examine the genetic interactions of the same mutant alleles with the entire yeast deletion series (~4800 genes), possibly identifying a number of new interactions.

Additional future directions are discussed in Chapter 4.

3.0 COMPLEMENTATION OF HSP40-DEPENDENT YEAST PHENOTYPES DIFFER IN THEIR REQUIREMENTS FOR THE J DOMAIN AND SUBSTRATE BINDING ACTIVITIES OF A MAMMALIAN HOMOLOG

Hsp70s constitute a highly conserved family of molecular chaperones that are found in all organisms and in all cellular organelles. Due to their ability to bind to unfolded regions on nascent polypeptides or unassembled subunits of heteromeric complexes in a nucleotide-dependent manner, these chaperones play critical roles in diverse cellular processes[35, 346]. Two distinct sets of cofactors tightly monitor Hsp70 action by regulating ATPase activity[24, 347]: J domain containing proteins (JDPs) of the Hsp40/DnaJ family and nucleotide exchange factors (NEFs). The highly conserved ~70 amino acid J domain of JDPs contacts Hsp70's nucleotide binding domain and enhances ATPase activity by inducing a conformational change[92, 348]. This leads to enhanced binding of Hsp70s to substrates. Moreover, some JDPs directly bind to unfolded regions on substrate proteins through their substrate binding domain and deliver the unfolded protein to the ATP-bound form of their Hsp70 partner[67, 68], while others contain atypical domains that specify exclusive functions[189, 349]. The NEFs, on the other hand, release bound ADP, which triggers ATP rebinding and subsequent substrate release from the Hsp70.

The JDPs can be classified into three groups[66, 350]: (i) Type I JDPs are most similar to DnaJ and contain a J domain followed by a glycine/phenylalanine-rich region and a cysteine-rich region with four repeats of a CxxCxGxG-type zinc finger; (ii) Type II JDPs lack the cysteine-

rich region and are unable to coordinate Zn2+; (iii) Type III JDPs only have the J domain in common with DnaJ. Notably, the number of JDPs exceeds the number of Hsp70s and NEFs in most organisms/ organelles. In fact, a single Hsp70 can interact with different JDPs to form unique Hsp70-JDP pairs that participate in specific cellular functions[261, 350]. Despite the high conservation of the J domain, JDPs are not necessarily interchangeable between organelles or organisms[66, 351], further suggesting that there is specificity in the interaction between Hsp70s and JDPs. Specificity might be essential for substrate recognition and delivery, for the targeting of Hsp70 to distinct cellular locations, and/or for catalyzing protein folding in distinct chemical environments within organelles.

To begin to address this hypothesis, a recent study tested the ability of 13 different JDPs to interact with resident Hsp70s in the yeast cytoplasm[261]. In many cases, the ability of a JDP to stimulate the ATPase activity of a particular Hsp70 was sufficient to constitute a functional pair. However, distinct features of JDPs, such as the ability to interact with substrates, might also be required for specific functions[67, 151, 315, 352]. To better resolve this apparent discrepancy, I have compared the abilities of two type I JDPs, a mammalian, ER-lumenal protein (ERdj3), and a yeast cytosolic protein (Ydj1) to functionally substitute for each other (refer to Figures 22 and 23 for the domain organization and sequence comparison of ERdj3 and Ydj1). The data obtained in this study, combined with those of a previous study[261], suggest that both the binding of JDPs to substrates and their association with Hsp70s are essential to support cell viability and chaperone-dependent functions.

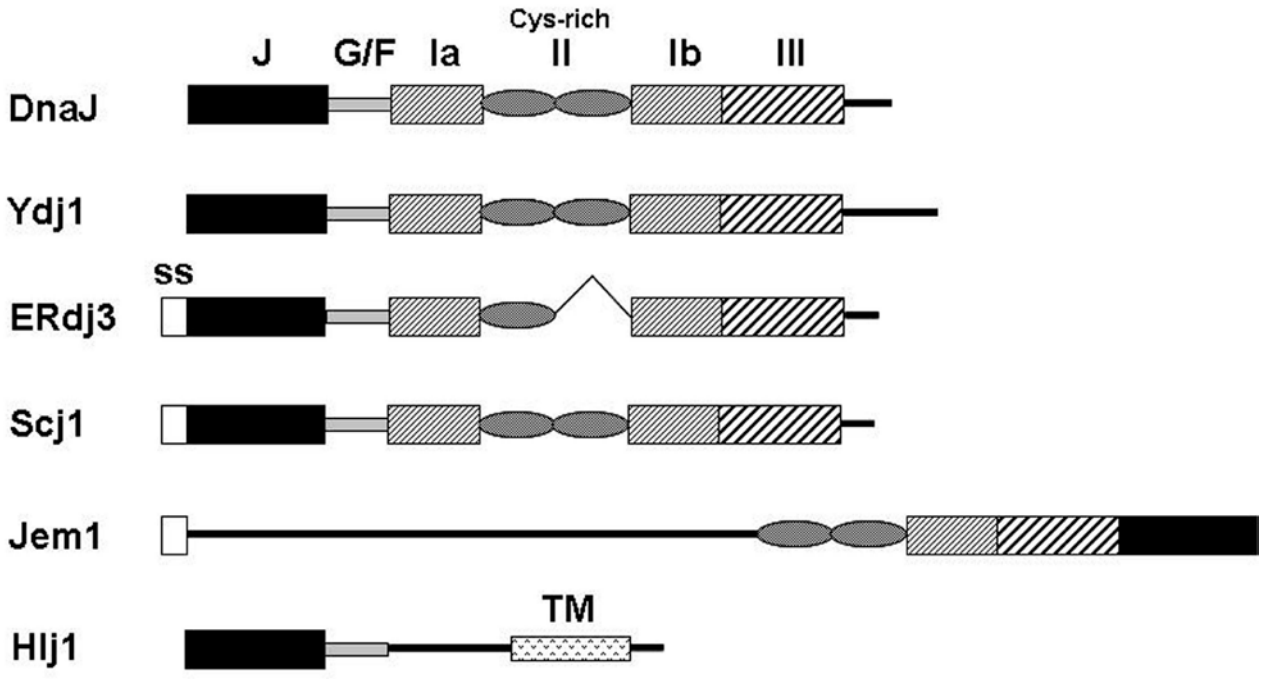

Figure 22: A schematic representation of select JDPs.

DnaJ, the founding member of this family of chaperones, is a bacterial Type I JDP. Ydj1, ERdj3 and Scj1 are Type I JDPs found in the yeast cytosol, mammalian ER and yeast ER, respectively. Hlj1 is a Type II JDP found in the yeast cytosol whereas Jem1 is a Type III JDP found in the yeast ER with an atypical domain organization. The domains are indicated by: J - J domain; G/F - glycine/phenylalanine rich region; Ia, II, Ib, III - various subdomains of the substrate binding domain based on Ydj1's crystal structure[2]; Cys-rich - cysteine rich region containing the Zn^{2+}-finger motifs; ss - signal sequence; TM - transmembrane domain, and are not drawn to scale.

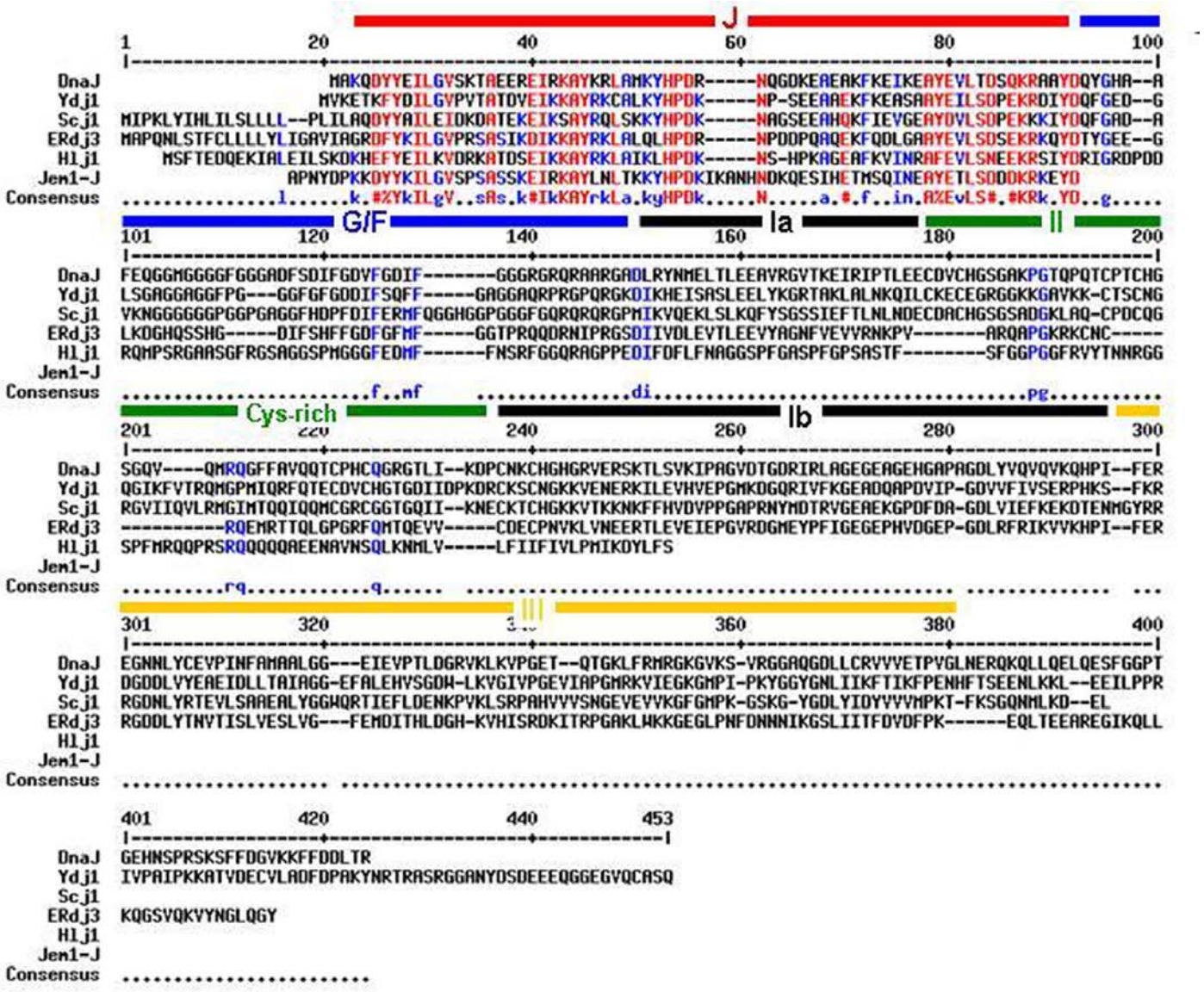
J
G/F
Ia
II
Cys-rich
Ib
III
DnaJ
Ydj1
Sc j1
ERdj3
Hlj1
Jen1-J
Consensus

Figure 23: Sequence comparison of DnaJ, Ydj1, Scj1, ERdj3, Hlj1 and the J domain of Jem1.

The protein sequences of DnaJ (AAC73126), Ydj1 (CAA95937), Scj1 (CAA41529), ERdj3 (NP_057390), Hlj1 (NP_013884) and the J domain of Jem1 (amino acids 531-645; NP_012462) were aligned using the software Multalin[4]. The numbers in parantheses indicate NCBI accession numbers. The various domains are represented by: J- J domain; G/F- glycine/ phenylalanine rich domain; Ia and Ib- domain I; II- domain II; III- domain III. Amino acid notations in the row that indicates the consensus sequence include:!- isoleucine or valine; $ - leucine or methionine; % - phenylalanine or tyrosine; # - asparagine, aspartate, glutamine or glutamate. Where indicated throughout the main text, % sequence identity was calculated using the program Kalign[10].

3.1 MATERIALS AND METHODS

3.1.1 Preparation of Ydj1 and ERdj3 constructs

The plasmids utilized in this study are listed in Table 5. Unless otherwise indicated, the plasmids were constructed by Yi Jin, a graduate student in the laboratory of Linda Hendershot at St. Jude Children's Hospital, Memphis.

To target Ydj1 to the mammalian ER, a signal sequence (ss) was engineered onto the N-terminus of Ydj1 using pAV4[353] as a template and the following PCR primers (lower case letters represent the inserted ss and the italics indicate a *BamHI* site):- 5' primer: CG*GGATCC*atggctccgcagaacctgagcacctttgcctgttgctgctatacctcatcggggcggtgattgccGTTAAAGAA ACTAAGTTTTACGATATTCTAGGTGTTCC and 3' primer: CG*GGATCC*TCATTGAGATGCACATTGAACACCTTC. The PCR product was digested with *BamHI* and inserted into 3HA-DSL, a mammalian expression vector which was modified from the original pSG5 vector (Neupogen) by the addition of several unique restriction enzyme recognition sequences to the multiple cloning site (mcs) and a triple-HA sequence at the 3' end of the mcs. After determining the directionality of insertion, the translation 'STOP' codon in ssYdj1-3HA-DSL was destroyed using the Quikchange site-directed mutagenesis kit (Stratagene) with the following primers:- 5' primer: GAAGGTGTTCAATGTGCATCTCAAGGATCCCCGGAATTCCTCGAG and 3' primer: CTCGAGGAATTCCGGGGATCCTTGAGATGCACATTGAACACCTTC. Next, a ribosomal-binding Kozak sequence (underlined, see below) was inserted immediately upstream of the

translation start site of ssYdj1 using the Quikchange site-directed mutagenesis kit with the following primers:- 5' primer: GTTTAAACGGATCCACCCGGGACAGAGGAACCATGGCTCCGCAGAAC and 3'primer: GTTCTGCGGAGCCATGGTTCCTCTGTCCCGGGTGGATCCGTTTAAAC. Finally, a second construct was made in which the farnesylation acceptor site in ssYdj1 was mutated (denoted by the underlined sequence) with the primer pair:- 5' primer: GGTGGCGAAGGTGTTCAAAGTGCATCTCAAGGATCCCCG and 3' primer: CGGGGATCCTTGAGATGCACTTTGAACACCTTCGCCACC, to generate ssYdj1C406S.

To express ERdj3 in yeast, two constructs were produced under the control of the P_{GPD} promoter in the multi-copy pGPD426 vector[289]: (i) Full-length human ERdj3 containing its endogenous ER-targeting signal sequence was amplified by PCR from the ERdj3-3HA-DSL vector[125] with the following primer pair (the italicized letters represent the *EcoRI* and *BamH*I sites introduced for cloning purposes):- 5' primer: C*GGAATTC*GGACCCGGGAC and 3' primer: C*GGGATCC*ATATCCTTGCAGTCCATTGTATACCTTCTG. The resulting PCR product was digested with *EcoRI* and *BamHI* and inserted into pGPD426; (ii) For cytosolic expression, CaaX-ERdj3 was generated using the following primer pair with ERdj3-3HA-DSL serving as the template (the underlined letters on the 5' primer represent the beginning of the coding sequence for the mature ERdj3 protein without its signal sequence, while the underlined sequence on the 3' primer represents the farnesylation sequence; the italicized letters represent the restriction sites used for cloning):- 5' primer: CG*GGATCC*GGAACCATGGGACGAGATTTCTATAAGATCTTGGGG and 3' primer: CCC*AAGCTT*TCATTGAGATGCACATTGCAGTCCATTGTATACCTTCTGC. The resulting PCR product lacked the N-terminal signal sequence, and contained a 'CASQ' farnesylation

sequence in lieu of the final two C-terminal amino acids (GY) in ERdj3. Next, the PCR product was digested with *BamHI* and *HindIII* and inserted into pGPD426. All CaaX-ERdj3 mutants were generated by Quikchange site-directed mutagenesis using primer pairs previously described, except for the H53Q and D55N mutants[125]. I generated these mutants with the primer pairs: (i) H53Q:- 5' primer: CTAGCCCTGCAGCTTCAGCCCGACCGGAACCCTGATGATC, and 3' primer: GATCATCAGGGTTCCGGTCGGGCTGAAGCTGCAGGGCTAG; (ii) D55N:- 5' primer: CTAGCCCTGCAGCTTCATCCCAAGCGGAACCCTGATGATC, and 3' primer: GATCATCAGGGTTCCGGTTGGGATGAAGCTGCAGGGCTAG.

3.1.2 Expression and detection of Ydj1 in mammalian cells

Cells were transfected with the indicated vectors using the FuGENE 6 transfection reagent (Roche). A vector that encodes Chinese hamster BiP has previously been described[74]. For immunofluorescence[255], transfected cells grown on coverslips were fixed and stained with an anti-HA antibody to detect ssYdj1 followed by FITC-labeled secondary antibody. Grp94, an abundant ER lumenal protein, served as an ER marker and was detected with an anti-Grp94 antiserum[255] followed by a TRITC-conjugated secondary antibody.

To detect interactions between JDPs and either BiP or substrate, 48 h post-transfection, cells were labeled with ^{35}S Translabel (Amersham Biosciences) for 3 h, and cell lysates were prepared[125]. To stabilize protein complexes, cells were treated with 150 µg/ml 3,3'-dithio-bis-propionic acid N-hydroxysuccinimide ester (DSP) for 1 h on ice and lysed in a non-ionic lysing buffer (50 mM Tris-HCl, pH 7.5, 150 mM NaCl, 0.5% DOC and 0.5% NP-40) after first quenching the crosslinker with 100 µl of 1M glycine. Solubilized proteins were incubated with the indicated antisera and precipitated with Protein A-Sepharose beads. The immunoprecipitated

complexes were subjected to denaturing gel electrophoresis and after enhancing with Amplify (Amersham Bioscience), the signals were detected by chemiluminescence.

3.1.3 Protein expression, purification and ATPase assays

Hexahistidine-tagged recombinant wild-type and mutant human ERdj3[125] and hamster BiP[354] proteins were expressed in *E. coli* M15 cells and purified under non-denaturing conditions using Ni^{2+}-NTA agarose (Qiagen QIAexpress System) as described. The following proteins were purified using previously established protocols: Ssa1p[151], Ydj1[127], GST-tagged J domain of Hlj1[327], hexahistidine-tagged Kar2[151], and the GST-tagged J domain of Sec63[111].

Steady-state ATPase assays using the indicated molar ratios of the JDP to Hsp70 were performed as described[127, 151].

3.1.4 Rescue of the slow growth phenotype of mutant yeast strains

The following *Saccharomyces cerevisiae* yeast strains were used for complementation studies: *SCJ1JEM1* (MATα *lys2-801 leu2-3,112 his3-Δ200 trp1-Δ901 ura3-52 suc2-Δ9*) and *scj1Δ jem1Δ* (MATα *ade2-1 leu2-3,112 his3-11,15 trp1-1 ura3-1 can1-100 scj1Δ::TRP1 jem1Δ::LEU2*)[122]; *YDJ1 (MATα ade2-1 leu2-3,112 his3-11,15 trp1-1 ura3-1 can1-100)* and *ydj1Δ (MATα ade2-1 leu2-3,112 his3-11,15 trp1-1 ura3-1 can1-100 ydj1-2::HIS3)*[355]; *HLJ1YDJ1* (MATα *ade2-1 leu2-3,112 his3-11,15 trp1-1 ura3-1 can1-100*) and *hlj1Δydj1-151* (MATα *ade2-1 leu2-3,112 his3-11,15 trp1-1 ura3-1 can1-100 hlj1Δ::TRP1 ydj1-2::HIS3 LEU2::ydj1-151*)[327]. The yeast strains were grown to logarithmic phase at 26°C in yeast extract–peptone–dextrose medium containing 2% glucose and transformed with the indicated plasmids

using lithium acetate[356]. The resulting transformants were selected and grown to logarithmic phase at 26°C in selective synthetic complete medium containing 2% glucose. Ten-fold serial dilutions were spotted onto solid medium and cultured at the indicated temperatures for 2 d. Where indicated, NaCl was included in the medium at a final concentration of 0.4M, sorbitol at a final concentration of 1M and DTT at a final concentration of 8 mM.

3.1.5 Detection of ERdj3 in yeast

Wild-type cells transformed with an empty vector or plasmids expressing either ERdj3 or CaaX-ERdj3 were grown to logarithmic phase (OD_{600} of 0.8 -1.0) in selective synthetic complete medium containing 2% glucose. A total of ~200 OD_{600} equivalents of cells were harvested, and ER-derived microsomal membranes were prepared as previously described[299]. For protein detection, ~20 μg of membranes were resolved by SDS-PAGE and immunoblots were analyzed using a polyclonal anti-ERdj3 antiserum[129].

For indirect immunofluorescence microscopy, wild-type and mutant yeast expressing the various ERdj3 constructs were analyzed according to an established protocol[357].

3.1.6 Assays for ER-Associated Degradation (ERAD)

The gene encoding HA-tagged Ste6p* was sub-cloned from pSM1911 (*2μ URA3* P_{PGK} *ste6-166::HA*)[324] into pRS425 (*2μ LEU2*)[358] to generate the p425-Ste6p*-HA plasmid. In brief, pSM1911 was digested with the restriction enzymes *HindIII* and *Sac I* to generate products of size 5.5 kb (corresponding to P_{PGK} *ste6-166::HA*) and 6.2 kb (corresponding to the vector backbone); the products were resolved by agarose gel electrophoresis. Next, the P_{PGK} *ste6-*

166::HA fragment was extracted from the agarose gel using Qiagen's Gel Extract kit, and inserted into pRS425, also treated with *HindIII* and *SacI*. After many unsuccessful attempts at transforming *E. coli* with the ligation mixture, I transformed the ligation mixture into *HLJ1YDJ1* yeast and selected transformants on synthetic complete medium lacking leucine. To identify positive clones, cell extracts were prepared from select transformants, resolved by SDS-PAGE and immunoblotted with anti-HA antibodies to detect Ste6p*-HA expression. After identifying positive clones, genomic DNA was prepared from these strains, transformed into *E. coli* XL1-Gold ultracompetent cells and selected on Luria-Bertini-agar medium supplemented with ampicillin (50 μg/ml). The resulting *E. coli* strains harbored the p425-Ste6p*-HA plasmid.

To enable selection of p425-Ste6p*-HA in the *hlj1Δydj1-151* strain, the *LEU2* gene was replaced with the *NATMX6* cassette, which confers resistance to the antibiotic nourseothricin, using PCR-mediated gene disruption[359]. Briefly, the *NATMX6* cassette was amplified from the pFA6a-NATMX6 plasmid (Table 5) with the primer pair:- 5' primer: GCTATTTCTGATGTTCGTTCCAATGTCAAGTTCGATTTCGCGGATCCCCGGGTTAATT AA, and 3' primer: GGCAAGTTCAATGACAATTTCAACATCATTGCAGCAGACAGAATTCGAGCTCGTTTA AAC. The resulting PCR product was transformed into *hlj1Δydj1-151* yeast and transformants were selected on yeast extract-peptone-dextrose-agar medium supplemented with nourseothricin. Positive clones were confirmed by PCR, thus generating the *hlj1Δydj1-151 leu2::NAT* strain.

Cycloheximide chase assays to measure the degradation efficiency of Ste6p* were performed as described[299] at 37°C.

3.2 RESULTS

3.2.1 Ydj1 expressed in the mammalian ER functions as an Hsp70 cofactor

To better understand the restrictions guiding the formation of functional Hsp70-JDP pairs, I first asked whether Ydj1, a cytosolic yeast JDP, could interact with BiP/GRP78, the mammalian ER-lumenal Hsp70. Ydj1 is a type I JDP and bears an overall sequence identity of 37% to ERdj3, a cognate BiP JDP (Figures 22 and 23). For this set of experiments, COS cells were transfected with plasmids expressing BiP along with either a C-terminally HA-tagged form of ERdj3 as a positive control, or with two different Ydj1 constructs engineered with an N-terminal ER signal-sequence for targeting to the ER and a C-terminal HA tag for detection. In one construct, Ydj1's farnesylation site was removed (ssYdj1C406S) and in the other, it was retained (ssYdj1). In yeast, farnesylation enables Ydj1 to associate with the cytosolic surface of the ER and is essential for Ydj1's function at elevated temperatures[353].

Post-transfection, the ER localization of the two Ydj1 isoforms was confirmed using indirect immunofluorescence (Fig 24A). The transfected cells were metabolically labeled, treated with a cross-linking agent to stabilize multiprotein complexes and lysed. Proteins were immunoprecipitated with antisera against BiP, or a monoclonal antibody against HA, to detect Ydj1. I found that the two Ydj1 isoforms efficiently associated with BiP, at levels similar to those observed for ERdj3 (Figure 24B). Importantly, interaction between BiP and Ydj1 was detected regardless of whether the immunoprecipitation was performed with anti-BiP or anti-HA antibodies. Given that BiP is more abundant than the JDPs in the ER and that the anti-BiP antiserum is inefficient for immunoprecipitation, it was not surprising that I detected a stronger BiP signal when the JDPs were immunoprecipitated with the anti-HA antibody.

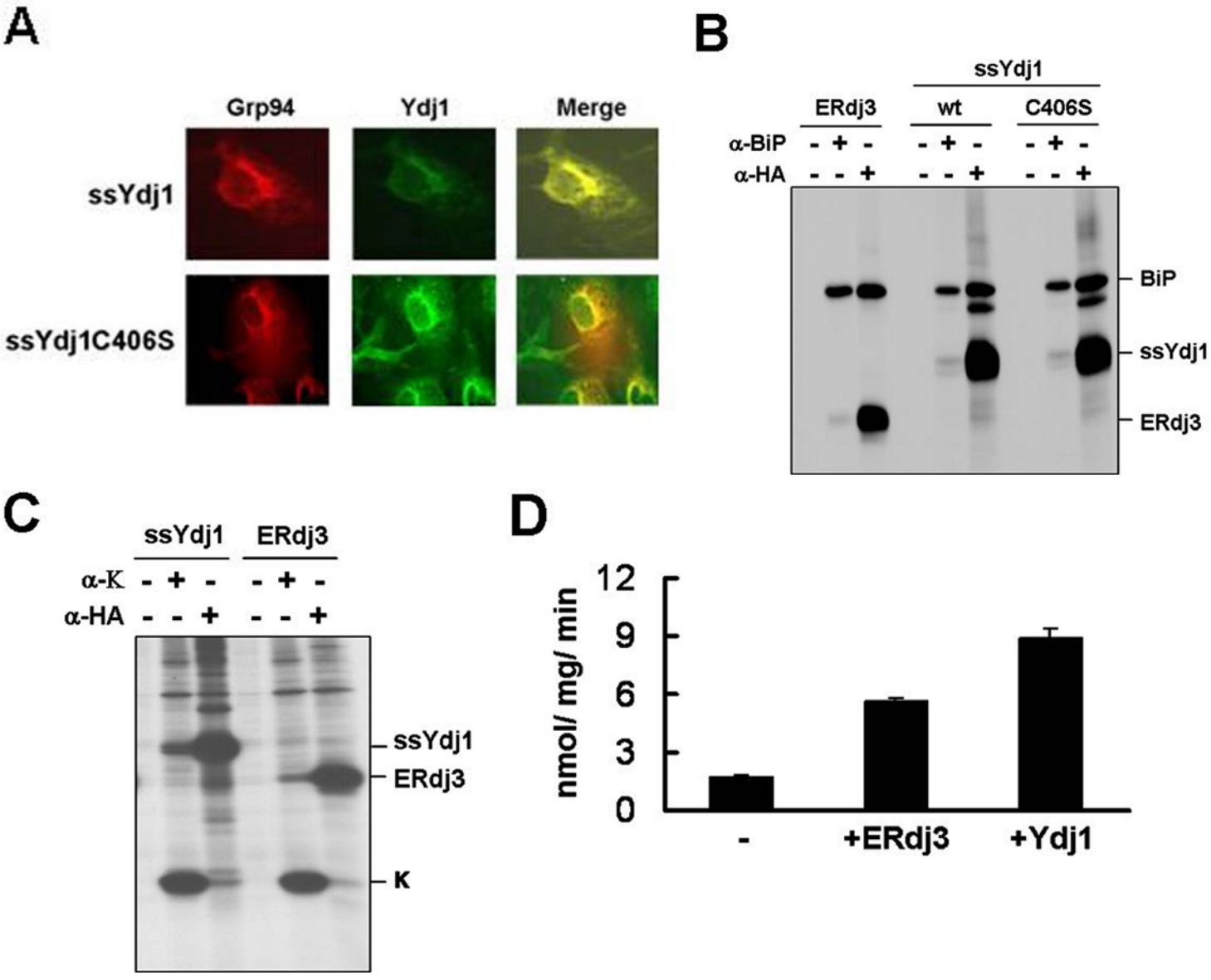
A
Grp94
Ydj1
Merge
ssYdj1
ssYdj1C406S
B
ssYdj1
ERdj3
wt
C406S
α-BiP
α-HA
BiP
ssYdj1
ERdj3
C
ssYdj1
ERdj3
α-K
α-HA
ssYdj1
ERdj3
K
D
nmol/ mg/ min
12
9
6
3
0
-
+ERdj3
+Ydj1

Figure 24: Ydj1 interacts with both BiP and κLC in the mammalian ER.

(A) COS cells transfected with HA-tagged ssYdj1 or ssYdj1-C306S were grown on coverslips, fixed and stained with an anti-HA antibody to detect the Ydj1 isoforms. Grp94 served as an ER marker. ***(B)*** COS cells were co-transfected with cDNAs encoding BiP and the indicated HA-tagged ERdj3 or Ydj1 constructs. Metabolically labeled, DSP cross-linked cell lysates were immunoprecipitated with anti-HA or anti-BiP antibodies, or Protein A Sepharose alone. Isolated proteins were separated by denaturing gel electrophoresis. ***(C)*** COS cells were co-transfected with cDNAs encoding κLC and either ERdj3 or ssYdj1. Cell lysates were immunoprecipitated wth anti-κ or anti-HA antibodies, or Protein A Sepharose alone. Samples were analyzed as described in (B). ***(D)*** The ATPase activity of BiP was measured in the absence (-) or presence of either ERdj3 or Ydj1. Reactions contained 1 μg of BiP and an eight-fold molar excess of ERdj3 or Ydj1. ATPase activity is expressed as nmoles of ATP hydrolyzed per milligram of protein per minute. Data represent the means of a minimum of three independent experiments $\pm$ standard errors.

The experiments in part A-C were performed by YiJin in the laboratory of Linda Hendershot at St. Jude Chidren's Hospital, Memphis.

Next, when COS cells were co-transfected with plasmids expressing Ydj1 and immunoglobulin κ light chain (κLC), which is normally a BiP and ERdj3 substrate[129], Ydj1 interacted with κLC to the same extent as ERdj3 (Figure 24C). Taken together, these data suggested that Ydj1 attains its native conformation in the mammalian ER, and is active. Finally, I observed that Ydj1 robustly stimulated BiP's ATP hydrolysis activity to an even greater degree than ERdj3 (Figure 24D). Thus, Ydj1 when targeted to the mammalian ER can function as a BiP cofactor. This result was intriguing, because the Brodsky lab had previously shown that Ydj1 does not bind to or functionally interact with the yeast ER-lumenal Hsp70, BiP/Kar2, *in vitro*[151].

3.2.2 Overexpression of cytosolically localized ERdj3 rescues the temperature-sensitive growth defect of *hlj1Δydj1-151* yeast

In yeast, Scj1 and Jem1 are two ER-localized JDPs[118, 122] that interact with Kar2, the yeast BiP homolog, and are required for multiple ER functions, including protein folding[119] and ER-associated degradation (ERAD)[120]. Scj1 is a soluble type I JDP (Figure 22) whose structural organization is similar to ERdj3, although its overall sequence is only 30% identical to that of ERdj3 (Figure 23). Jem1 is a membrane-associated type III JDP (Figure 22), and owing to its non-canonical domain arrangement, the sequence comparison of Jem1 and ERdj3 was limited to that of the J domains, which revealed that they share 35% sequence identity (Figure 23). Loss of both Scj1 and Jem1 (*scj1Δjem1Δ*) reduces the degradation efficiency of soluble ERAD substrates[120] and induces the unfolded protein response (UPR)[119, 122]. In addition, the *scj1Δjem1Δ* strain exhibits a slow growth phenotype at elevated temperatures[122].

Since ERdj3 is ER-localized and contains intramolecular disulfide bonds[124], I initially tested whether this JDP can substitute for Scj1 and Jem1 in the yeast ER. Two ERdj3 constructs

were created for strong, constitutive expression from the P_{GPD} promoter[289]. One contains an ER-targeting signal sequence (wild-type ERdj3), whereas the other lacks this sequence but possesses a CASQ farnesylation sequence at the C-terminus that attaches the protein to the cytosolic side of the ER membrane (CaaX-ERdj3); the farnesylation sequence is the same as that found in Ydj1[353]. When the constructs were introduced into wild-type *SCJ1JEM1* yeast, they did not affect growth, indicating that the overexpression of these heterologous proteins is not toxic (Figure 25A). As expected, when cytosolically-targeted CaaX-ERdj3 was overexpressed in the *scj1Δjem1Δ* strain, it did not restore growth at elevated temperatures, however, neither did ERdj3 (Figure 25A). To determine whether the lack of an effect on *scj1Δjem1Δ* growth was due to ineffective Kar2-ERdj3 interaction, I measured ERdj3's ability to stimulate Kar2's ATPase activity. As shown in Figure 25B, ERdj3 only weakly stimulated the ATP hydrolysis rate of Kar2, as compared to Sec63, a cognate Kar2 JDP that is essential for nascent polypeptide translocation across the ER membrane[98, 109, 111]. Moreover, the lack of an effect was not due to ERdj3 being unstable in yeast cells, as I was able to detect its expression by western blotting (Figure 25C). Taken together, these observations suggest that ERdj3 is unable to functionally interact with Kar2 and hence cannot substitute for Scj1 and Jem1 *in vivo*.

Based on my observation that a yeast cytosolic JDP could function in the mammalian ER (Figure 24), I next asked if ERdj3 was able to function in the yeast cytosol. The yeast cytosol contains 13 JDPs of which the best characterized is Ydj1. *YDJ1* deletion results in slow growth at 30°C and inviability at elevated temperatures[126]. However, the slow growth of the *ydj1Δ* strain can be rescued by the overexpression of at least five other cytosolic JDPs[261]. Interestingly,

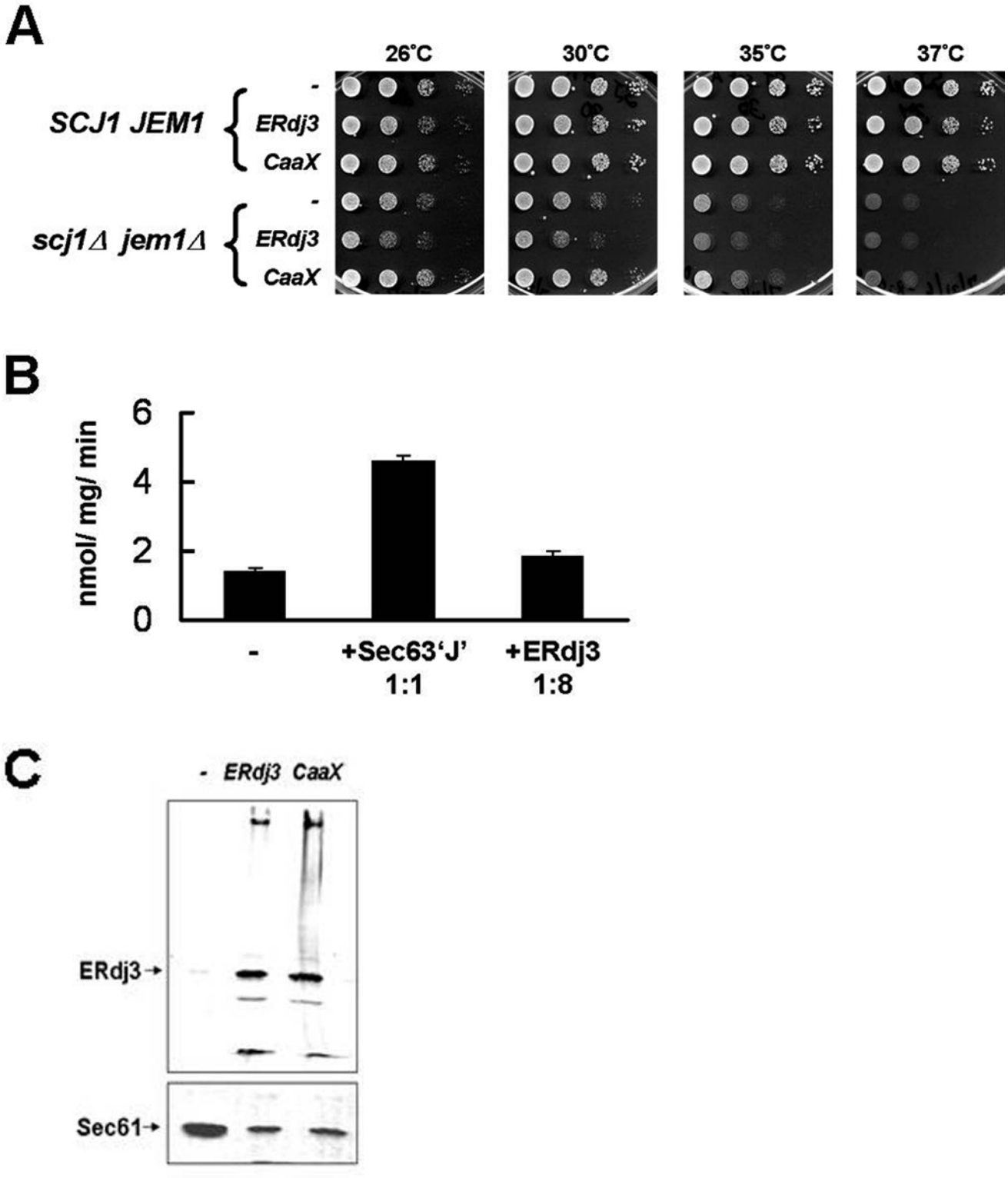
A
26°C
30°C
35°C
37°C
SCJ1 JEM1
-
ERdj3
CaaX
scj1Δ jem1Δ
-
ERdj3
CaaX
B
nmol/ mg/ min
6
4
2
0
-
+Sec63'J'
1:1
+ERdj3
1:8
C
- ERdj3 CaaX
ERdj3
Sec61

Figure 25: ER expressed ERdj3 is unable to rescue the growth phenotype of the *scj1Δjem1Δ* strain.

(A) Ten-fold serial dilutions were performed for wild-type (*SCJ1JEM1*) and mutant (*scj1Δjem1Δ*) yeast strains containing an empty vector (-), a vector for the expression of an ER-targeted form (*ERdj3*), or a vector encoding a cytosolically localized form (*CaaX*) of full-length ERdj3. Cells were plated onto selective medium and incubated for 2 d at the indicated temperatures. ***(B)*** The ATPase activity of Kar2 was measured alone (-) or in the presence of equimolar amounts of the J domain of Sec63 or an eight-fold molar excess of ERdj3 as described in the legend to Figure 24 D**.** Data represent the means of a minimum of three independent experiments ± standard errors. ***(C)*** Microsomal membranes were prepared from wild-type yeast strains that were transformed with an empty vector (-) or vectors encoding either ERdj3 or CaaX-ERdj3. ERdj3 was detected using anti-ERdj3 antisera and primarily migrates at its predicted molecular mass of 42 kDa. Sec61, as detected using anti-Sec61 antiserum, served as a loading control.

expression of the J domain alone of these five JDPs is sufficient to substitute for Ydj1 at 30°C, suggesting that the J domain-mediated activation of Hsp70 ATPase activity is critical to support the growth of *ydj1Δ* yeast[261].

To determine whether ERdj3 could substitute for Ydj1, I first asked whether ERdj3 could stimulate the ATPase activity of Ssa1, an essential cytosolic Hsp70 that interacts with Ydj1 to execute key cellular functions[324, 327, 351, 360-364]. I discovered that ERdj3 proficiently stimulated Ssa1's ATP hydrolysis rate, to a similar extent as Ydj1 and Hlj1, another J domain containing Ssa1 cofactor (Figure 26A; see below). Next, I performed serial dilution analyses on wild-type *YDJ1* and mutant *ydj1Δ* yeast strains transformed with plasmids expressing either ERdj3 or CaaX-ERdj3. ERdj3 did not rescue the slow growth phenotype of *ydj1Δ* yeast, which was anticipated due to its expression in the ER lumen rather than on the cytosolic face of the ER. However, contrary to my expectations, neither did cytosolically targeted CaaX-ERdj3 (Figure 26B). These data suggest that in spite of its ability to be expressed in yeast (Figure 25C), and to stimulate the ATPase activity of Ssa1 *in vitro* (Figure 26A), cytosolic expression of ERdj3 is not sufficient to overcome the strong impairment of cellular homeostasis that results from deleting the *YDJ1* locus.

I therefore decided to utilize an alternate yeast strain, *hlj1Δydj1-151*, which contains a temperature-sensitive allele of *YDJ1* and lacks another ER-associated JDP with a cytosolic J domain, Hlj1[327]. Hlj1 is a type II JDP and bears 27% overall sequence identity to ERdj3 (Figures 22 and 23). The *hlj1Δydj1-151* yeast strain exhibits a tight temperature-sensitive growth phenotype but not the slow growth displayed by *ydj1Δ* yeast; this strain also exhibits defects in the ERAD of select integral membrane proteins, such as a mutant form of the yeast **a**-factor transporter, Ste6p (i.e., Ste6p*)[324] and the cystic fibrosis transmembrane conductance regulator

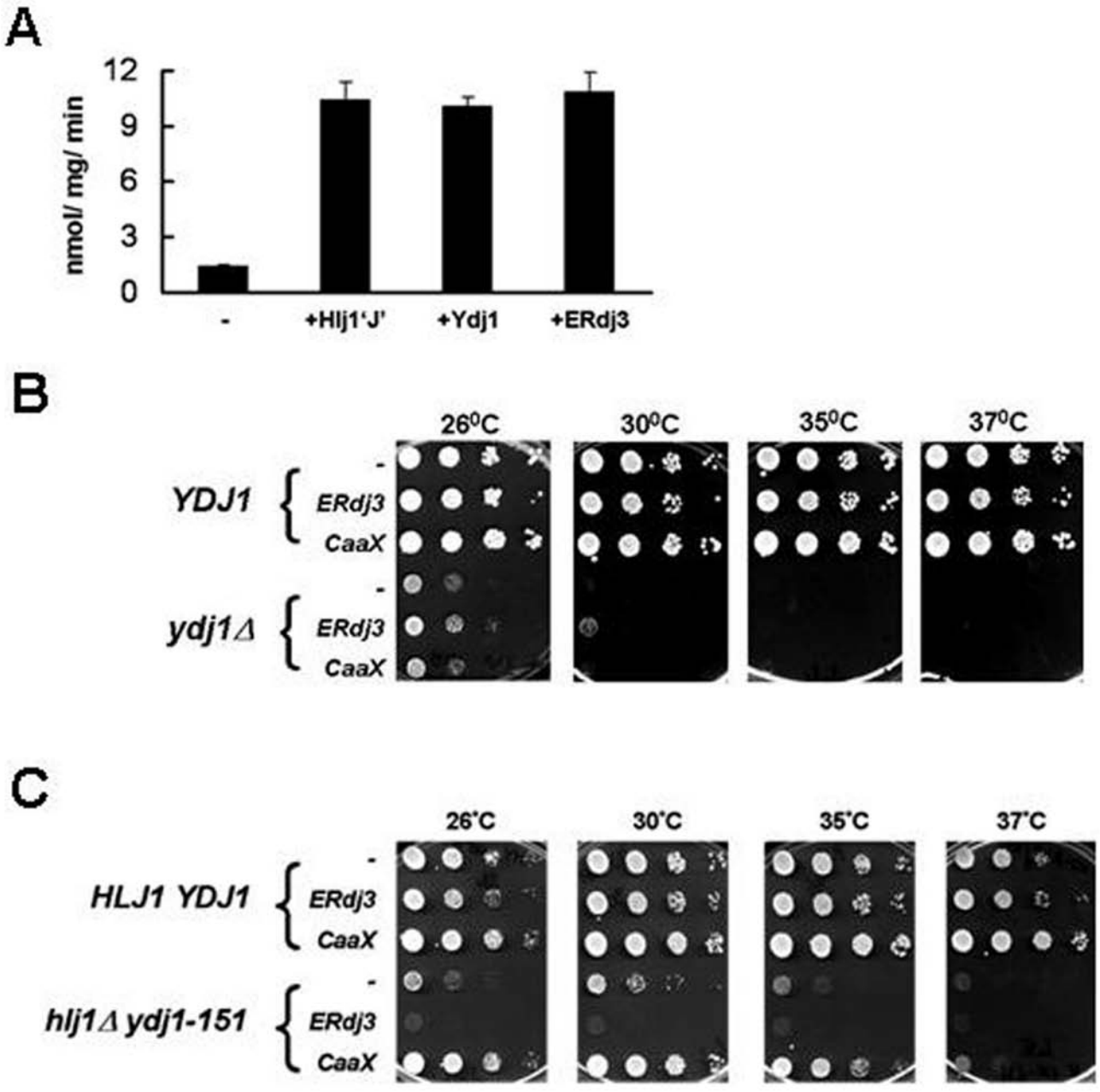
A
12
9
6
3
0
nmol/ mg/ min
-
+Hlj1'J'
+Ydj1
+ERdj3
B
26°C
30°C
35°C
37°C
YDJ1
-
ERdj3
CaaX
ydj1Δ
-
ERdj3
CaaX
C
26°C
30°C
35°C
37°C
HLJ1 YDJ1
-
ERdj3
CaaX
hlj1Δ ydj1-151
-
ERdj3
CaaX

Figure 26: Cytosolic expression of ERdj3 rescues the temperature-sensitive growth phenotype of the *hlj1Δydj1-151* strain.

(A) The ATPase activity of Ssa1 was measured either alone (-) or in the presence of Ydj1, Hlj1 or ERdj3 as described in the legend to Figure 24D**.** The molar ratio of Ssa1 to the JDPs was 1:2. Data represent the means of a minimum of three independent experiments ± standard errors. ***(B & C)*** Either an empty vector (-), or a vector containing an ER-targeted form (*ERdj3*) or a vector engineered to produce an ER-tethered, cytosolically localized form (*CaaX*) of ERdj3 was transformed into ***(B)*** wild-type (*YDJ1*) and mutant (*ydj1Δ*) yeast strains, or ***(C)*** wild-type (*HLJ1YDJ1*) and mutant (*hlj1Δydj1-151*) yeast strains. The resulting transformants were serially diluted onto selective medium and incubated as described in the legend to Figure 25A.

(CFTR)[327]. To this end, plasmids engineered for the expression of ERdj3 and CaaX-ERdj3 were transformed into *HLJ1YDJ1* and *hlj1Δydj1-151* yeast strains and indirect immunofluorescence microscopy was performed to confirm that the proteins were expressed (Figure 27). Next, serial dilution analyses were performed to analyze the growth of the transformed strains at various temperatures. In contrast to the results using *ydj1Δ* yeast, I observed that cytosolic CaaX-ERdj3, but not ER-targeted ERdj3, restored the growth of *hlj1Δydj1-151* cells at temperatures up to 37°C (Figure 26C). In fact, the ER lumenally expressed ERdj3 actually exacerbated the growth defect of the *hlj1Δydj1-151* strain (Figure 26C), probably due to its drastic effect on ER morphology (Figure 27). These results indicate that CaaX-ERdj3 functions as a cochaperone for Ssa1 *in vivo* and can compensate for Hlj1 and Ydj1, but only in the presence of a partially functional copy of Ydj1.

3.2.3 The substrate binding domain of ERdj3 is required to rescue the slow growth phenotype of *hlj1Δydj1-151* yeast

Previous studies showed that substrate binding is essential for Ydj1 to optimally function *in vivo* and *in vitro*[315, 352, 365], and Ydj1 and ERdj3 have similar substrate binding domains (Figure 23). The Hendershot lab recently demonstrated that the binding of ERdj3 to substrates requires three features: (i) the presence of domain II (Figure 22), (ii) the pocket formed by hydrophobic amino acids in domain I, and (iii) dimerization, which occurs through interactions in the C-terminal region and requires the presence of phenylalanine 326[125].

Having established a new system to assay the function of ERdj3, I next wished to determine whether substrate interaction is required for CaaX-ERdj3 to rescue the growth of

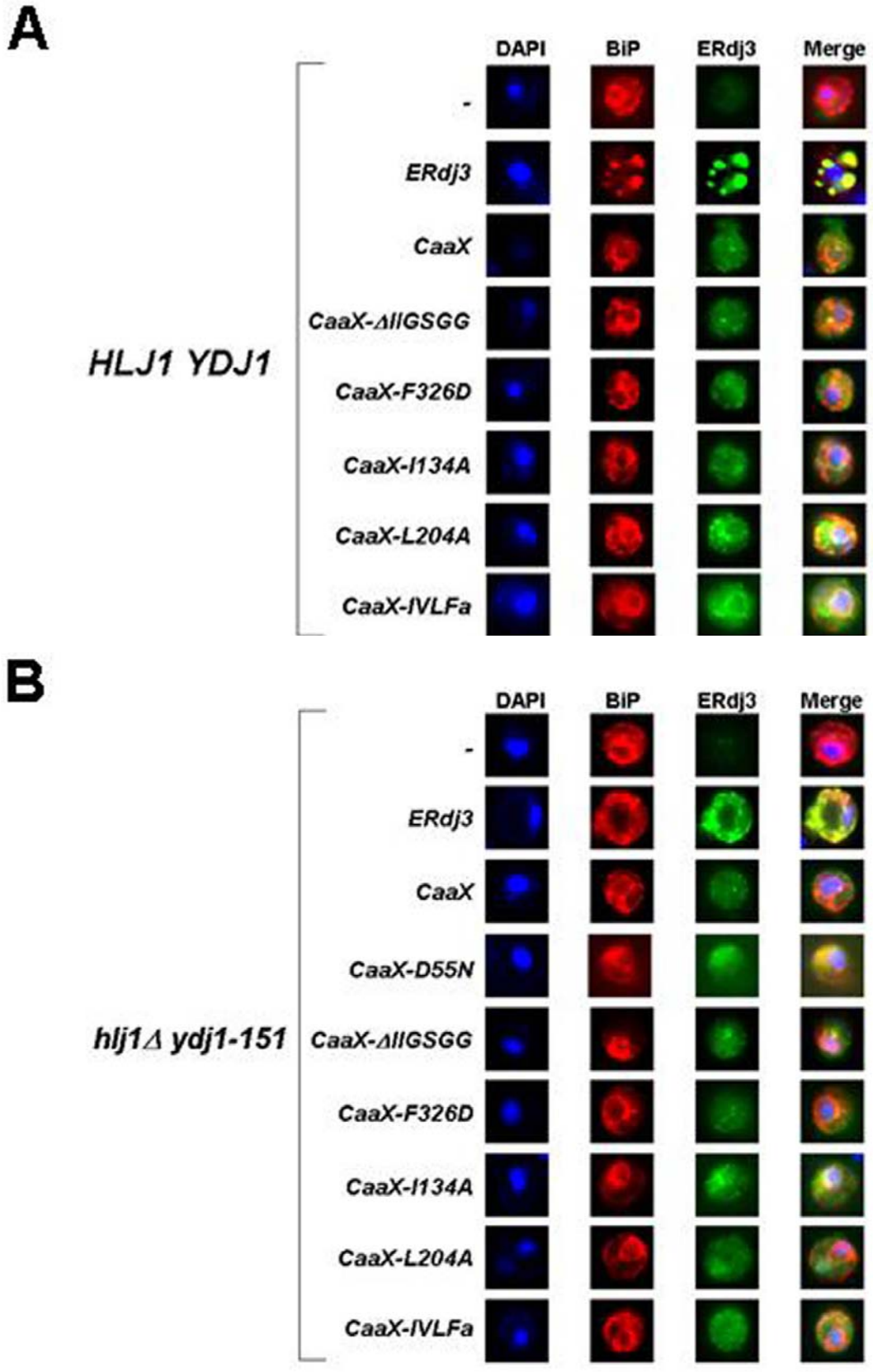
A
DAPI
BiP
ERdj3
Merge
-
ERdj3
CaaX
CaaX-ΔIIGSGG
HLJ1 YDJ1
CaaX-F326D
CaaX-I134A
CaaX-L204A
CaaX-IVLFa
B
DAPI
BiP
ERdj3
Merge
-
ERdj3
CaaX
CaaX-D55N
hlj1Δ ydj1-151
CaaX-ΔIIGSGG
CaaX-F326D
CaaX-I134A
CaaX-L204A
CaaX-IVLFa

Figure 27: Detection of the various wild-type and mutant ERdj3 proteins in yeast by indirect immunofluorescence.

Wild-type *HLJ1YDJ1* and mutant *hlj1Δydj1-151* yeast strains containing an empty vector (-), or expression vectors for an ER-targeted form of ERdj3 (*ERdj3*), an ER-tethered cytosolically localized form of full-length ERdj3 (CaaX) or CaaX mutants (*CaaX-D55N, CaaX-ΔII-GSGG, CaaX-F326D, CaaX-L204A* and *CaaX-IVLFa*) were stained with antibodies against ER-lumenal Kar2 (TRITC-labeled secondary antibody) and ERdj3 (FITC-labeled secondary antibody). DAPI was used to visualize the nuclear DNA.

hlj1Δydj1-151 yeast. I therefore expressed seven CaaX-ERdj3 substrate binding mutants in this strain. These included mutants in which domain II, spanning amino acids 160-200, was deleted (ΔII) or was replaced by a "GSGG" linker (ΔII-GSGG), two mutants in which dimerization was inhibited (F326A and F326D), single amino acid substitution mutants in domain I (I134A and L208A), and a mutant in which four hydrophobic residues in domain I that affect substrate binding, including I134A and L208A, were altered (IVLFa). In addition, I expressed two versions of CaaX-ERdj3 that are defective for Hsp70 interaction, H53Q and D55N[129, 130]. These mutations lie in the invariant HPD motif of the J domain[366].

Expression of the mutant CaaX-ERdj3 proteins in wild-type *HLJ1YDJ1* yeast did not affect cell growth (Figure 28A), indicating that these proteins do not exert a dominant negative effect. Moreover, none of the substrate binding mutants rescued the temperature-sensitive phenotype of the *hlj1Δydj1-151* strain, even though CaaX-ERdj3 was again able to improve growth up to 37°C (Figure 28B). The failure of the substrate binding mutants to rescue the growth phenotype was not due to their inability to stimulate the ATPase activity of Ssa1, since a member of each mutant class stimulated Ssa1 ATP hydrolysis to levels comparable to wild-type ERdj3 (Figure 28C and data not shown); however, the IVLFa mutant stimulated Ssa1's ATPase activity only about half as efficiently as wild-type ERdj3. I also noted that the mutant proteins were expressed at similar levels as CaaX-ERdj3 as determined by indirect immunofluorescence microscopy (Figure 27B and data not shown).

In contrast to the inability of the substrate binding mutants to restore viability, the J domain mutants rescued the growth of the *hlj1Δydj1-151* strain as efficiently as wild-type CaaX-ERdj3 (Figure 28B). As anticipated, these mutant proteins were unable to stimulate Ssa1's ATPase activity *in vitro* (Figure 28C). Taken together, these data argue that the substrate

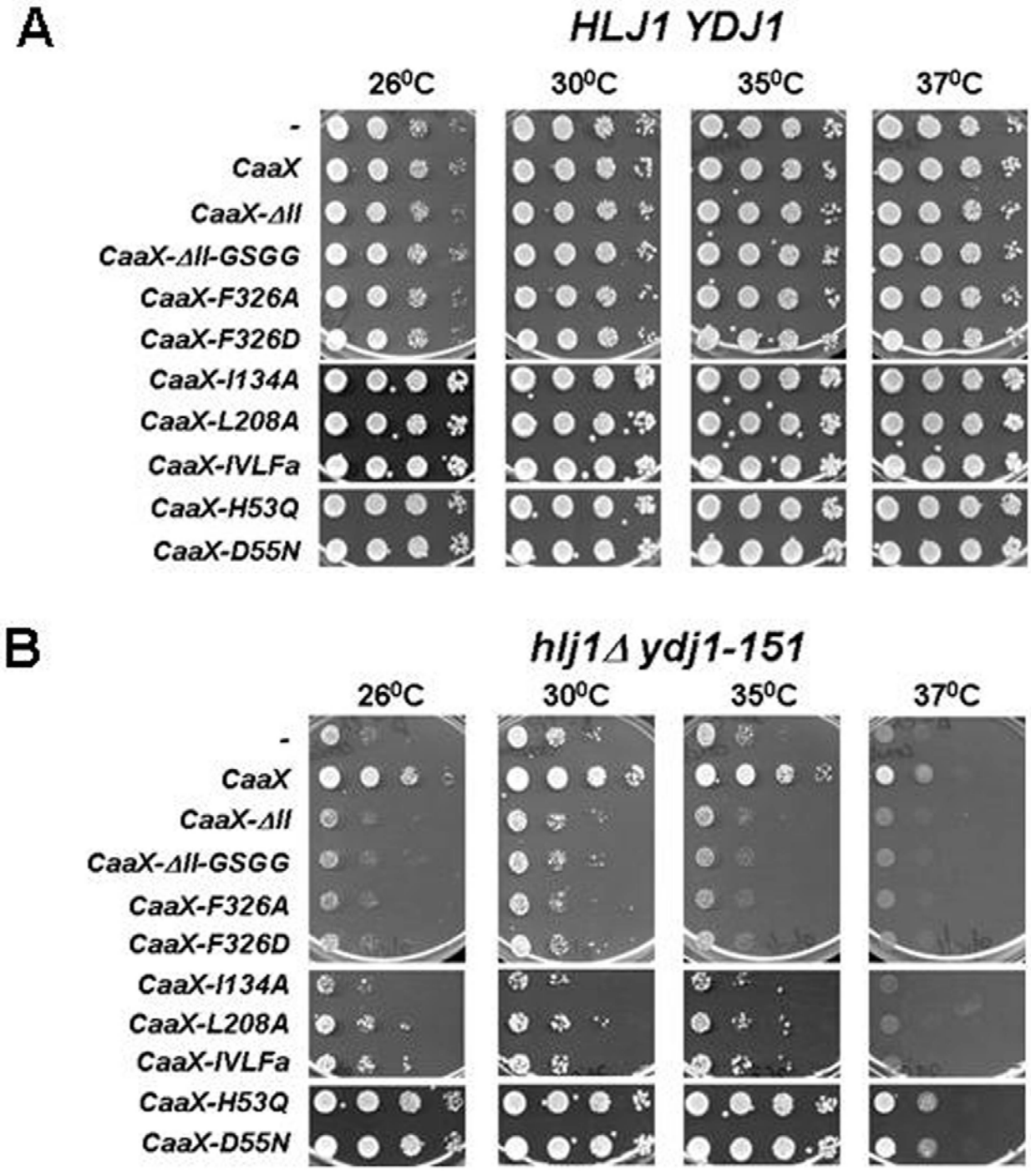
A
HLJ1 YDJ1
26⁰C
30⁰C
35⁰C
37⁰C
-
CaaX
CaaX-Δll
CaaX-Δll-GSGG
CaaX-F326A
CaaX-F326D
CaaX-I134A
CaaX-L208A
CaaX-IVLFa
CaaX-H53Q
CaaX-D55N
B
hlj1Δ ydj1-151
26⁰C
30⁰C
35⁰C
37⁰C
-
CaaX
CaaX-Δll
CaaX-Δll-GSGG
CaaX-F326A
CaaX-F326D
CaaX-I134A
CaaX-L208A
CaaX-IVLFa
CaaX-H53Q
CaaX-D55N

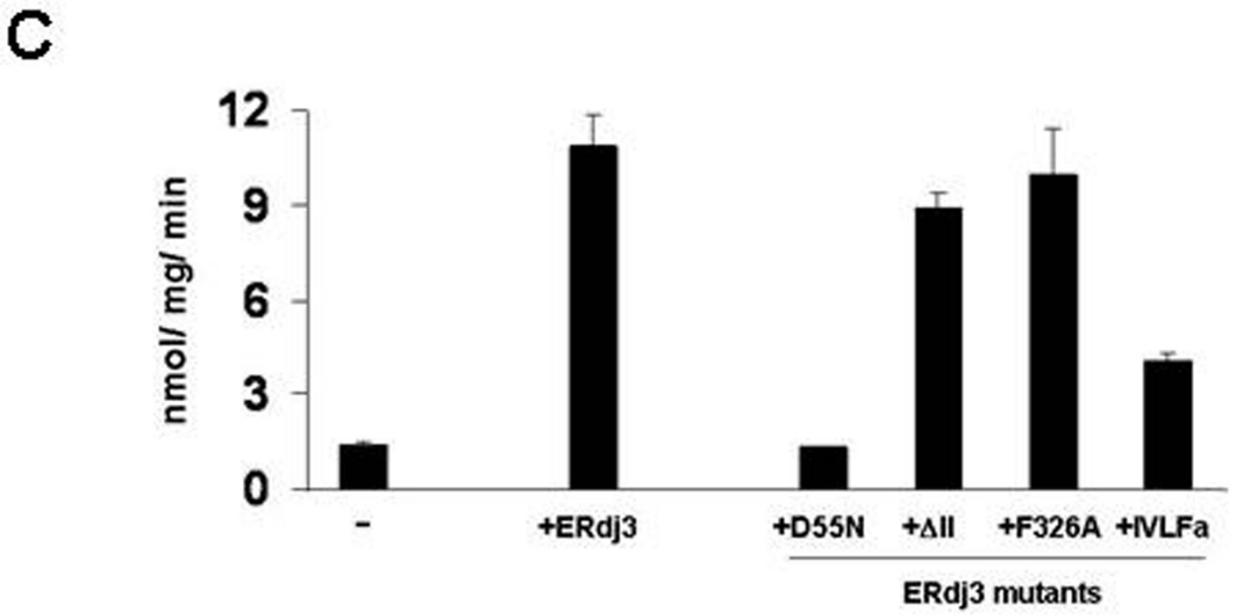

Figure 28: ERdj3 substrate binding mutants fail to enhance the growth of *hlj1Δydj1-151* yeast.

Cytosolic forms (CaaX) of wild type or mutant ERdj3 were expressed in *HLJ1YDJ1* wild type ***(A)*** or *hlj1Δydj1-151* mutant ***(B)*** yeast strains. Cells were plated and incubated as described in the legend to Figure 25A. ***(C)*** The ATPase activity of Ssa1 was measured in the absence (-) or presence of the indicated wild-type and mutant ERdj3 proteins as described in the legend to Figure 25D**.** The molar ratio of Ssa1 to the indicated JDPs was 1: 2. Data represent the means of a minimum of three independent experiments $\pm$ standard errors.

binding properties of CaaX-ERdj3 are required to complement the growth defect of the *hlj1Δydj1-151* strain, and that this does not simply depend on (or even require) the functional interaction of JDPs with a cognate Hsp70.

3.2.4 Cytosolically expressed ERdj3 compensates for cell wall defects in the *hlj1Δydj1-151* strain

Yeast cells are fortified by a cell wall that is comprised of two layers: an inner layer composed of β-1,3-glucans, β−1,6-glucans and small amounts of chitin, and a protective outer layer composed of glycosylphosphatidylinositol (GPI) and Pir glycoproteins. Cell wall integrity, which is essential during growth, cell division and stress, is maintained by the coordinated action of several signaling pathways[367]. Recently, the Brodsky lab demonstrated that Ydj1 also plays a role in the maintenance of cell wall integrity[355]. For example, the growth of *ydj1Δ* mutant yeast was rescued by osmostabilizing agents such as sodium chloride (NaCl) and sorbitol. However, the role of Ydj1 in cell wall integrity appeared to be independent of Ssa1 function because yeast cells carrying a temperature-sensitive mutant allele in *SSA1*, *ssa1-45*, did not exhibit these phenotypes. Based on these data, I next asked if *hlj1Δydj1-151* yeast demonstrated cell wall defects, and if so, whether CaaX-ERdj3 expression could rescue these phenotypes.

First, *HLJ1YDJ1* and *hlj1Δydj1-151* cells were transformed with a vector control and serially diluted on growth medium supplemented with NaCl or sorbitol. I found that the growth of *hlj1Δydj1-151* was partially restored at 37°C under these conditions (Figure 29, row labeled '-'), suggesting that the mutant strain has a cell wall phenotype. Next, *hlj1Δydj1-151* yeast were transformed with plasmids expressing either wild-type or mutant versions of CaaX-ERdj3 and

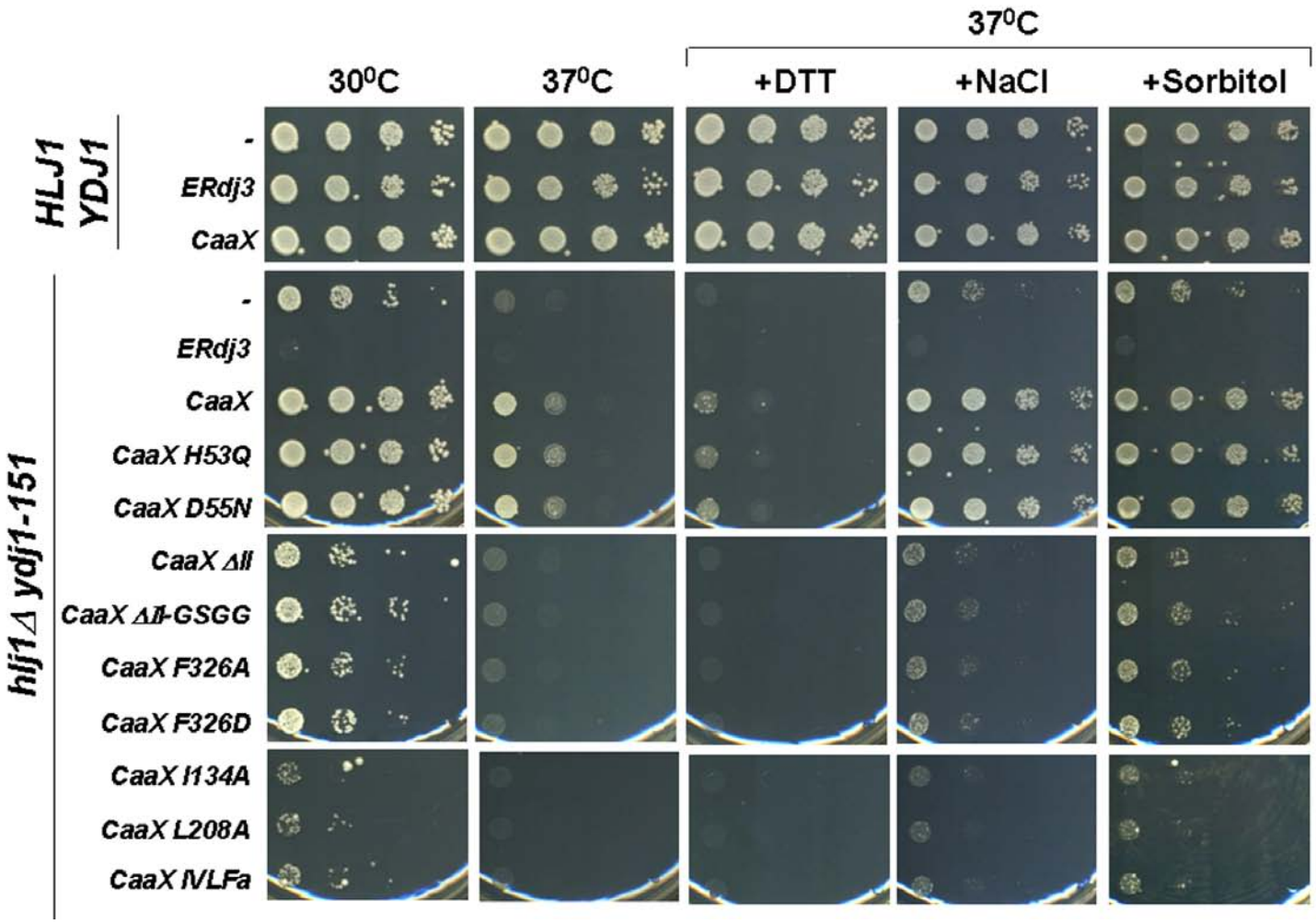

Figure 29: CaaX-ERdj3 complements the cell wall phenotype of the *hlj1Δydj1-151* strain.

Either an empty vector (-), a vector containing an ER-targeted form (*ERdj3*), or a vector engineered to produce a cytosolically localized form (*CaaX*) of ERdj3 was transformed into wild-type (*HLJ1YDJ1*) and mutant (*hlj1Δydj1-151*) yeast strains. In addition, cytosolic forms (*CaaX*) of mutant ERdj3 were expressed in *hlj1Δydj1-151* yeast. Cells were serially diluted onto selective medium containing or lacking 8 mM DTT, 0.4M NaCl or 1 M sorbitol, and were incubated as described in the legend to Figure 25A.

were tested for growth on NaCl- or sorbitol-supplemented medium. I observed that the expression of wild-type and J domain mutants of CaaX-ERdj3, but not the substrate binding mutants, significantly rescued the cell wall defects of *hlj1Δydj1-151* yeast (Figure 29). These data further support the hypothesis that Ydj1's role in the maintenance of cell wall integrity is not reliant upon its interaction with Ssa1[355].

Finally, I tested whether di-thio-threitol (DTT), a reducing agent that causes acute ER stress, affected the growth of *hlj1Δydj1-151* yeast expressing wild-type and mutant CaaX-ERdj3 proteins. I found that, at normal growth temperatures, *i.e.,* 30°C, the *hlj1Δydj1-151* strain transformed with an empty vector did not exhibit sensitivity to DTT (data not shown) suggesting that *hlj1Δydj1-151* yeast are able to mount an adequate UPR to combat ER stress. In contrast, at elevated temperatures and at a DTT concentration of 8 mM, the *hlj1Δydj1-151* strain is inviable (Figure 29, row labeled '-'), and the expression of wild-type or mutant CaaX-ERdj3 proteins was unable to rescue this growth defect (Figure 29). One implication of these observations is that CaaX-ERdj3 adopts its correct three-dimensional structure by forming intramolecular disulfide bridges[124] in the yeast cytosol, an environment that is less oxidizing than the mammalian ER, and it takes the addition of a reducing agent to induce unfolding and abrogate ERdj3 function. Alternately, it is possible that the combination of DTT and elevated temperature is a highly unsuitable growth condition for *hlj1Δydj1-151* yeast, and even the overexpression of cytosolic ERdj3 is unable to compensate for this.

3.2.5 CaaX-ERdj3 expression restores ERAD in *hlj1Δydj1-151* yeast

In the previous section, I found that ERdj3 rescues a JDP-dependent cellular process that is independent of Ssa1. Next, I wished to examine the effects of ERdj3 on an Hsp70-dependent process, namely ERAD. ERAD is a quality control process during which misfolded ER-localized proteins are retrotranslocated to the cytosol and targeted to the 26S proteasome for degradation[5]. The Brodsky lab previously showed that Hlj1 and Ydj1 act as Ssa1 cofactors during the ERAD recognition and targeting of integral membrane proteins such as Ste6p* and CFTR, and that the *hlj1Δydj1-151* strain is defective for the ERAD of these substrates[324, 327]. To determine whether CaaX-ERdj3 could substitute for Hlj1 and Ydj1 during ERAD, I co-expressed wild-type or mutant CaaX-ERdj3 proteins with Ste6p* in the *hlj1Δydj1-151* strain and performed a cycloheximide chase analysis to measure the degradation efficiency of Ste6p*. Although the *hlj1Δydj1-151* strain degraded Ste6p* poorly, I found that CaaX-ERdj3 overexpression significantly accelerated the degradation of Ste6p* (Figure 30A). In contrast, none of the ERdj3 mutants were as efficient as wild-type CaaX-ERdj3 in compensating for the ERAD defect in the *hlj1Δydj1-151* strain (Figure 30B). However, the strongest defect was observed when the ability of the D55N J domain mutant form of CaaX-ERdj3 was tested, which is unable to stimulate Ssa1's ATPase activity (Figure 28C). These data indicate that CaaX-ERdj3's ability to improve ERAD is primarily dependent on its interaction with the cytosolic Hsp70, but that direct interaction with substrates is also important.

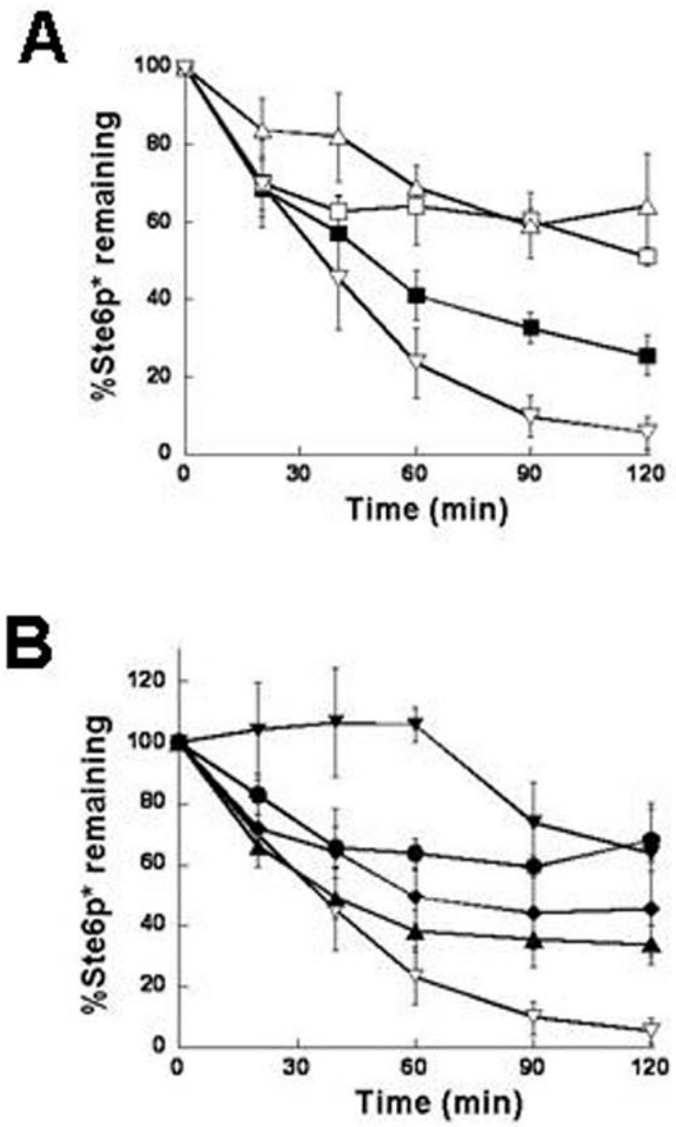

Figure 30: CaaX-ERdj3 substitutes for Hlj1 and Ydj1 during ERAD.

Cycloheximide chase assays were performed to measure the degradation of Ste6p* in **(A)** wild-type (*HLJ1YDJ1*) yeast transformed with an empty vector (■) and *hlj1Δydj1-151* yeast transformed with either an empty vector (□), a vector containing an ER-lumenal form of ERdj3 (△), or a vector engineered to produce a cytosolically localized form of ERdj3 (▽), or **(B)** in *hlj1Δydj1-151* yeast transformed with vectors engineered to produce cytosolically localized forms of wild-type (▽) and the following mutant ERdj3 proteins: D55N (▼), ΔII-GSGG (●), F326D (◆), and IVLFa (▲). Data represent the means of a minimum of three independent experiments ± standard errors.

3.3 DISCUSSION

Ydj1 and ERdj3 are Type I JDPs and share a similar domain organization (Figure 22). However, the chemical environments within their resident organelles are significantly different. Ydj1 resides in the yeast cytosol, an environment that is relatively less oxidizing than ERdj3's native milieu, the mammalian ER. Consequently, ERdj3's cysteines are involved in intramolecular disulfide bridges[124], while the cysteine-rich region of Ydj1 coordinates Zn^{2+}, similar to other Type I DnaJ homologs[368]. Given these differences and the low overall sequence identity shared by Ydj1 and ERdj3 (*i.e.,* 37%), one might expect that these JDPs would be unable to substitute for one another *in vivo*. Surprisingly, I observed that Ydj1 could function in the mammalian ER and ERdj3 could function in the yeast cytosol, indicating that these JDPs attain their native or near-native conformations in diverse environments. In contrast, ERdj3 was unable to compensate for two ER-localized yeast JDPs, Scj1 and Jem1, most likely due to its failure to efficiently stimulate the ATPase activity of the yeast BiP homolog, Kar2 (Figure 25B). Together, these results demonstrate that Ydj1 and ERdj3 associate productively with Hsp70s in unique subcellular compartments and can exhibit a relaxed Hsp70 specificity. In addition, given the previous observation that Ydj1 cannot interact productively with Kar2[151], these data also indicate that Kar2 is more fastidious than Ssa1 or BiP with regards to JDP association.

I also discovered that although cytosolically expressed ERdj3 could complement the temperature-sensitive growth of the *hlj1Δydj1-151* strain, it could not rescue the slow growth phenotype of *ydj1Δ* yeast. This was somewhat surprising given that the overexpression of isolated J domains is sufficient to compensate for the loss of Ydj1[261]. This phenomenon probably

arises due to the activation of the ATPase activity of cytosolic Hsp70s by the examined J domains, and I show that ERdj3 robustly stimulates the ATPase activity of a cytosolic Hsp70, Ssa1 (Figure 26A). However, since the level of J domain expression also influences the efficiency of *ydj1Δ* growth rescue[261], it is possible that CaaX-ERdj3 was not expressed to sufficiently high levels *in vivo* either to interact with Ssa1 or localize correctly, and hence was unable to compensate for the loss of Ydj1. Alternately, the interaction of ERdj3 with another cytosolic Hsp70 such as Ssb1[369] may be required to complement *ydj1Δ* growth, and ERdj3 might be unable to stimulate the activity of this Hsp70. It is also formally possible that ERdj3 is more suited to complement the functions of Hlj1 than those of Ydj1; because Hlj1-specific functions and phenotypes have not been reported, there is no ready way to test this possibility.

I determined that ERdj3 mutants that fail to associate with Ssa1 are competent to rescue the temperature-sensitive and cell wall phenotypes associated with *hlj1Δydj1-151* mutant yeast. This suggests that these phenotypes result from defects in processes that are independent of Ssa1 interaction. Based on the observation that substrate binding mutants of ERdj3 were unable to rescue *hlj1Δydj1-151* phenotypes (Figure 28 and 29), and that *hlj1Δ* yeast do not exhibit slow growth and cell wall phenotypes (data not shown) but *ydj1Δ* do[126, 355], I surmise that cell wall function and robust growth at elevated temperature are linked to the ability of Ydj1 to bind to specific substrates. Formally, the cell wall phenotypes may also arise from the ability of Ydj1 to partner with Hsp82, the cytosolic Hsp90 which plays a role in high osmotic stress response in yeast[355, 370, 371] and functions in conjunction with Ydj1 in the folding and maturation of certain client proteins[368, 372, 373]. The cell wall phenotype may additionally arise from altered association with Sse1, the cytosolic Hsp110[370], which has previously been shown to genetically interact with *YDJ1*[141].

The substrate binding dependent effects of ERdj3 expression on *hlj1Δydj1-151* growth, but not on *ydj1Δ* growth, are reminiscent of prior studies suggesting that although Ydj1 and Sis1, an essential yeast cytosolic JDP[374], perform unique essential cellular activities, they also exhibit substrate binding promiscuity: (i) Ydj1 overexpression is unable to support the viability of *sis1Δ* yeast, although Sis1 overexpression rescues the growth defect of the *ydj1Δ* strain[261, 374]; and, (ii) the substrate binding domains of either Ydj1 or Sis1, but not both, are required for optimal yeast growth and survival[315]. Taken together with my results, I infer that while certain substrate proteins can interact with multiple JDPs for delivery to cognate Hsp70s for folding/assembly, others may require specific JDPs for cellular targeting or protein folding.

To my knowledge, this study is the first demonstration that a full-length mammalian JDP can function in a non-native organelle in a divergent organism. Several other reports have analyzed the effects of overexpressing the J domains of cognate or non-cognate JDPs in related/divergent model systems[261, 375, 376], but rarely has the specific impact of the JDP substrate binding domain been investigated. My data, together with those of others, reveal novel insights into the biology of DnaJ family proteins. For example, since isolated J domains can complement a subset of JDP-related defects[261], it appears that for many cellular processes, the JDP-stimulated high affinity binding of partner Hsp70s to substrates is sufficient. In other cases (*i.e.,* ERAD), the JDP must interact both with the substrate and the Hsp70, presumably to aid in the recruitment of the Hsp70 to its substrate. Finally, for other functions (*i.e.,* cell wall integrity), the JDPs do not have to interact with an Hsp70, but merely need to recognize their substrates. In keeping with these diverse models/pathways, ERdj3 was able to function both in ERAD and in maintaining cell wall integrity, arguing that this JDP is able to perform both Hsp70 dependent and Hsp70 independent functions through its substrate binding activity. Very recently, a novel class of Type

IV JDPs has been identified, constituting proteins that lack the canonical HPD motif that is essential for interacting with Hsp70s but possess putative substrate binding domains[377]. Thus, this group of JDPs may have evolved to simply bind to substrates, presumably in an Hsp70 independent fashion.

Finally, this study opens-up a new avenue to determine the functions of mammalian JDPs in ERAD. In particular, the Brodsky lab is now positioned to examine the ability of any JDP to substitute for cytosolic homologs during this quality control process.

4.0 CONCLUSIONS AND PERSPECTIVES

The diversity of Hsp70s and Hsp40s increases in higher eukaryotes and varies between sub-cellular compartments. Therefore, the pathways and networks coordinated by these chaperones are intricate and essential for cell survival. In order to better understand the rules that govern the formation of functional Hsp70-Hsp40 pairs, I utilized a two-pronged approach. First, I examined the properties of the ER-lumenal Hsp70, BiP, that contribute toward the recognition of its Hsp40 cochaperones, Sec63p, Scj1p and Jem1p, in the yeast ER. Second, I evaluated the capacity of a mammalian ER-lumenal Hsp40, ERdj3, to function in yeast and addressed the importance of ERdj3's substrate binding activity. The results from these studies have not only provided insights into the mechanisms utilized by Hsp70s and Hsp40s to achieve optimal function, but have also resulted in the formulation of novel hypotheses, which I discuss below.

BiP differentially interacts with its Hsp40 cochaperones

In the yeast ER, BiP interacts with: (i) Sec63p to catalyze protein translocation across the ER membrane, (ii) Scj1p to chaperone protein folding, (iii) Jem1p to facilitate karyogamy, and (iv) both Scj1p and Jem1p to recognize misfolded proteins and target them for ERAD. However, the specific properties of BiP that enable it to distinguish between its Hsp40 cochaperones are unknown. During the course of my studies, I discovered that mutating a conserved R in sub-domain Ia of BiP's ATPase domain to an A resulted in a protein that was defective for Sec63p

and Scj1p interaction, but maintained its ability to interact with Jem1p (refer to section 2.2.2). This result suggests that surface residues in sub-domain Ia of BiP's ATPase domain, including R217, are vital for targeting BiP to specific cochaperones, possibly by forming unique sets of hydrogen bonds, electrostatic interactions and/or van der Waals interactions. To test this hypothesis, conserved residues that are located adjacent to R217 could be mutated and the resulting proteins examined for their ability to interact with the J domains of Sec63p, Scj1p and Jem1p. However, since charged surface residues in subdomain Ia of Hsp70s may form hydrogen bonds with residues in the inter-domain linker[7, 15], it is possible that altering these conserved amino acids in BiP's ATPase domain might result in a loss of the allosteric regulation mediated by all Hsp40 cochaperones. Conversely, it is possible that the J domains of Sec63p, Scj1p and Jem1p have evolved to contact different residues in BiP's ATPase domain. These variations may explain the low sequence similarities shared by these and other J domains (refer to section 2.3.1). To address this hypothesis, non-conserved residues in the J domains of Sec63p, Scj1p and Jem1p, which are adjacent to the conserved, invariant HPD motif could be mutated and the resulting proteins analyzed for BiP interaction. Finally, each of these Hsp40 cochaperones might reside within unique multiprotein complexes and therefore enhance BiP's ability to participate in specific functions. One such complex has been identified for membrane-bound Sec63p, which is is positioned to interact with components of the Sec61 translocation machinery (refer to section 1.2.4), and target BiP to nascent, translocating polypeptide chains.

I also found that the expression of R217A BiP in yeast resulted in translocation-specific defects (refer to section 2.2.5). While this result could be correlated to a reduced interaction between R217A BiP and Sec63p (refer to sections 2.2.2 and 2.2.6), it is formally possible that R217A BiP is defective for interacting with other proteins. For example, R217A BiP might be

unable to efficiently associate with BiP's NEFs, Sls1p and Lhs1p, which assist in protein translocation (refer to section 1.2.3). This hypothesis could be evaluated by performing large-scale pulldowns to identify BiP-associated proteins from wild-type and mutant *kar2* strains. Alternately, a genetic screen can be performed to discover similarities/dissimilarities in genetic interactions between wild-type and mutant *kar2* alleles. In fact, I employed this approach to identify a gene that appears to play a unique role in translocation (see below and refer to section 2.2.8 and Appendix B).

Taken together with previous studies that analyzed mutants of DnaK[91] and Chinese hamster BiP[302] that were defective for cognate Hsp40 interaction, the behavior of the R217A mutant of yeast BiP has improved our knowledge of the structural determinants required for Hsp40 recognition. However, the aforementioned studies did not address whether this unique mutation differentially affected the recognition of every potential Hsp40. These studies also failed to address whether the conserved mutation affected multiple functions performed by the Hsp70.

Substrate binding is a key determinant of yeast BiP function

A previous study showed that the overexpression of the substrate binding and lid domains of bacterial DnaK in *E. coli* abrogates cell viability[378], possibly because this isolated fragment can bind to substrates but is unable to fold them[379]. The random mutagenesis of this substrate binding and lid domain fusion led to the identification of residues important for substrate binding, including G400D, L459P, G443D, G443S, S398F, G539D, P419L, P419S, E444K, M408I, G405S, G406D, E402K, A488T, and D526N[378]. Intriguingly, while none of these residues directly contact the peptide, many of them cluster to a specific region in the substrate binding domain consisting of loop $L_{1,2}$, loop $L_{4,5}$, and the β1 strand. Moreover, these are conserved in

several Hsp70s. The authors surmised that these residues are involved in the stabilization of DnaK-substrate interaction and are therefore important for the *in vivo* function of DnaK. Since the mutations were isolated by mutagenizing a DnaK fragment that lacked the ATPase domain, they most likely do not contribute to Hsp70 allostery.

I also constructed and identified two mutations in BiP, K584X and S493F in the substrate binding domain that affected BiP's ability to functionally interact with substrates (refer to section 2.2.2). Neither of these mutations maps to the hydrophobic cleft that binds to substrates, but instead the K584X mutation results in a loss of the lid domain while the S493F mutation alters a putative link between the substrate binding and lid domains. My results with K584X and S493F BiP indicate that modifications distal to the hydrophobic peptide binding cleft also alter BiP's substrate recognition properties. Moreover, because the *in vivo* expression of K584X and S493F BiP resulted in translocation and ERAD defects, as well as an induction of the UPR, I suggest that BiP's ability to bind to substrates is primarily controlled by interactions between the substrate binding and lid domains. To further address this hypothesis, mutations in BiP analogous to those identified in the study described above could be constructed and examined.

Hsp70 interaction and substrate binding determine ERdj3's ability to function in yeast

In the mammalian ER, an environment that is relatively more oxidizing than the cytosol, ERdj3 functions as a BiP cofactor during the folding of several proteins, including immunoglobulin subunits (refer to section 1.2.2.1). It has been observed that ERdj3 mutants that are unable to interact with BiP robustly bind to substrates[129], and conversely, ERdj3 mutants that are defective for substrate binding maintain their ability to cooperate with BiP[125] and stimulate BiP's ATPase activity (personal communication, Jin, Y. and Hendershot, L.M.). However, because the mammalian ER harbors five other Hsp40 homologs that act as BiP cofactors, the interpretation

of results obtained from ERdj3 overexpression studies becomes complicated. Therefore, I used a yeast expression system to understand the cellular requirements for ERdj3 function.

When wild-type ERdj3 was expressed in the yeast ER, I observed that it was unable to substitute for Scj1p and Jem1p, possibly because of its poor functional interaction with yeast BiP (refer to section 3.2.2). This result was initially surprising because ERdj3 normally resides in the ER. Nonetheless, yeast BiP is fastidious with regards to its Hsp40 interactions[151]. Hence, I postulate that ERdj3 does not possess the correct recognition elements to form a functional pair with yeast BiP, even though it may bind to yeast BiP substrates. For example, during a process such as ERAD, ERdj3 might be defective for targeting BiP to misfolded substrates, even though it may be competent to interact with these substrates. Alternately, it is possible that ERdj3 overexpression in the yeast ER is toxic, which was observed as reduced growth and aberrant ER morphology (refer to section 3.2.2 and Figure 27). Taken together, these data indicate that not all Hsp70s and Hsp40s can function in a coordinated manner, and that these chaperones possess inherent abilities to distinguish between their partners. To further understand the structural properties of Hsp40s that are recognized by yeast BiP, point mutants in ERdj3 could be generated by random mutagenesis, with the goal of identifying mutations that enhance BiP binding and ATPase activation. I predict that ERdj3 mutants with these properties will be competent to restore the growth of *scj1Δjem1Δ* yeast at 37°C.

In contrast, when wild-type ERdj3 was targeted to the yeast cytosol, it complemented the growth defects of the *hlj1Δydj1-151* strain, which contains mutations in two cytosolic Hsp40s, Hlj1p and Ydj1p (refer to section 3.2.2). One explanation for this observation may be the ability of ERdj3 to stimulate the ATPase activity of the cytosolic Hsp70, Ssa1p (refer to section 3.2.2). However, since ERdj3 was unable to rescue the growth defects of *ydj1Δ* yeast (refer to section

3.2.2) unlike other overexpressed J domains[261], other endogenous properties of ERdj3 must be required for function. Accordingly, I found that substrate binding mutants of ERdj3 were unable to substitute for Hlj1p and Ydj1p (refer to section 3.2.3), possibly because they fail to fold/traffic specific substrates that normally depend upon Hlj1p and Ydj1p. Moreover, because ERdj3 mutants that were defective for Hsp70 interaction maintained their ability to complement *hlj1Δydj1-151* temperature-sensitive growth, I speculate that substrate binding is a critical determinant of ERdj3 function. Therefore, a careful structure/function analysis of the substrate binding properties of unique Hsp40s, as well as the identification of the substrate ensemble targeted by each Hsp40, is necessary to fully understand Hsp40 function.

A genetic screen leads to the identification of novel players in ER protein translocation

To further examine the *in vivo* ramifications of R217A BiP expression, I utilized a targeted UPR-based genetic screen. In brief, yeast strains expressing R217A BiP were crossed against a set of 350 deletion strains (refer to section 2.2.8 and Appendix B). The strains were chosen because the UPR is constitutively induced, which is indicative of a reduction in ER homeostasis[121]. From this analysis, I determined that the genetic interaction profile of *kar2-R217A* resembled the profiles of two other mutants, *sec71Δ* and *sec72Δ*, which also exhibit defects in translocation. Moreover, *kar2-R217A* genetically interacted with a subset of the gene deletion strains; one such strain was *ilm1Δ*. My subsequent analyses of this strain defined a role for Ilm1p, a previously uncharacterized integral membrane protein, during the translocation of pre-BiP. I also identified an association of Ilm1p with components of the translocation machinery, notably Sec61p, Sec62p and Sec63p (refer to section 2.2.9). However, given that *ilm1Δ* yeast efficiently translocated three other substrates (ppαF, DPAP-B and Pho8p) it will be vital to: (i) characterize

the translocation efficiencies of other substrates, including CPY, Och1p and Gas1p (a β-1,3-glucanosyltransferase involved in cell wall assembly), in *ilm1Δ* yeast, (ii) determine whether Ilm1p plays a specific role in the recognition of pre-BiP, which will be completed by attaching the signal sequence from pre-BiP to other proteins and assessing Ilm1p-dependence, and (iii) evaluate whether *ilm1* mutants exhibit genetic interactions with components of the signal recognition and ER translocation machinery. I have begun experiments toward each of these goals.

My data suggest that the function of the yeast translocon may be regulated by Ilm1p, a phenomenon that is reminiscent of the regulation of the mammalian translocation apparatus by integral membrane proteins such as TRAM and TRAP (refer to section 1.2.4). Although Ilm1p homologs are only found in other fungi, Ilm1p physically interacts with an uncharacterized but essential integral membrane protein encoded by *YNL181w*. *YNL181w* is highly conserved in all eukaryotes. Since Ynl181p is predicted to possess oxidoreductase activity, I conjecture that this protein acts as a membrane chaperone for translocating polypeptide chains; Ilm1p may either assist Ynl181p during translocation, or perform an independent function prior to translocation initiation, such as signal sequence recognition for a subset of proteins. Because *YNL181w* is essential, and mutant alleles of this gene are not available, I am presently characterizing the translocation efficiency of a strain harboring a hypomorphic allele of *YNL181w*.

What next?

In the genetic screen described in this study, I utilized an approach wherein I chose specific *kar2* alleles and examined their genetic interactions with a subset of the yeast genome. To elaborate on *KAR2*'s genetic interactions, it will become important to screen the entire yeast genome,

including essential and non-essential genes. Strains carrying hypomorphic alleles of essential genes[344, 380] (~940 in number) and deletions of non-essential genes[381, 382] (~4800 in number) are available, and the effects of mutant BiP expression on the growth of these strains could now be analyzed. I hypothesize that this study will not only lead to an enhanced understanding of BiP-regulated processes but will also help establish the function of uncharacterized genes. This screen might also identify new BiP-catalyzed processes in cells.

The UPR-based screen can also be utilized to assign properties to novel *kar2* alleles, especially those that do not affect cellular growth. For example, I found that the expression of the translocation-defective BiP mutant, R217A, from the P_{TEF1} promoter did not result in temperature-sensitive or DTT-sensitive growth phenotypes (refer to sections 2.2.4 and 2.2.5). However, the genetic interaction profile of *kar2-R217A* in the UPR-based screen resembled the profiles of other gene deletions that exhibit translocation defects (refer to section 2.2.8). Therefore, analyzing the genetic interaction profiles of novel *kar2* alleles in this screen might lead to the identification of BiP mutants that exhibit specific functional defects. As a proof of principle, such an analysis was applied to characterize the genetic interactions of the *kar2-P515L* allele, which exhibits ERAD-specific defects *in vitro*[181] (Appendix B).

Extrapolating my observations to human BiP function

Not only do the yeast and human versions of BiP share 70% overall sequence identity, the cofactors that interact with these proteins are also conserved (Table 1). For example, human homologs or orthologs of Sec63p, Scj1p, Jem1p, Sls1p and Lhs1p exist, and importantly, some of these proteins have been linked to human diseases (refer to section 1.2.9). I propose that an understanding of the interactions of yeast BiP with its cofactors can be extrapolated to comprehend the BiP interaction network in humans. In addition, if the amino acid residues in

BiP's structure that determine cofactor recognition and discrimination were identified, small molecule inhibitors could be designed to modulate unique BiP-cofactor interactions. These inhibitors could then be used as novel therapeutic agents to alleviate disease states that arise from the misregulation of BiP or its cofactors. Moreover, the essential contribution of substrate binding to BiP function underscores the possibility that peptide mimics can be used as a first line of therapy to treat cancers that arise due to BiP overexpression. Based on the observation that ERdj3's substrate binding property is critical to its function in the yeast cytosol (refer to section 3.2.3), I predict that substrate binding also determines ERdj3's ability to function in the human ER. Because ERdj3 acts upstream to BiP in the folding of several substrates, disrupting ERdj3 function by targeting its substrate binding domain might provide an alternate mechanism to more specifically alter BiP function in human cells.

Several open questions on our understanding of BiP biology in humans remain unanswered. For example, the mechanism by which mammalian BiP trafficks to the cell surface to participate in signal transduction pathways is unknown[239]. Though yeast BiP is not normally expressed at the cell surface, under high levels of UPR induction[205], and in mutant strains that are defective for Golgi to ER retrograde transport[316, 317, 383], BiP is secreted. Therefore, yeast can be used as a model system to understand the BiP trafficking mechanism. This becomes important because several cancer cells exhibit elevated surface BiP levels[252, 253]. In addition, it is unknown whether BiP's anti-apoptotic properties[39, 232, 233] can be correlated to its role in UPR induction or calcium storage.

Overall, my studies have hopefully helped to better define the functions of this complex protein.

Table 4: Strains used in this study

Strain name	Genotype	Source/ Reference
MMY2	*MAT***a**/α, *his3-Δ200/his3-Δ200, leu2-Δ1/leu2-Δ1, ura3-52/ura3-52, trp1-Δ63/trp1-Δ63, KAR2/kar2::HIS3*	Kabani *et al.*, 2003
GAL-KAR2	*MAT*α, *his3-Δ200, leu2-Δ1, ura3-52, trp1-Δ63, kar2::HIS3*, pGAL1-*KAR2*	This study
GAL-R217A	*MAT*α, *his3-Δ200, leu2-Δ1, ura3-52, trp1-Δ63, kar2::HIS3*, pGAL1-*R217A*	This study
GAL-K584X	*MAT*α, *his3-Δ200, leu2-Δ1, ura3-52, trp1-Δ63, kar2::HIS3*, pGAL1-*K584X*	This study
GAL-S493F	*MAT*α, *his3-Δ200, leu2-Δ1, ura3-52, trp1-Δ63, kar2::HIS3*, pGAL1-*S493F*	This study
MMY8-2	*MAT*α, *his3-Δ200, leu2-Δ1, ura3-52, trp1-Δ63, kar2::HIS3*, pMR397	Kabani *et al.*, 2003
TEF1-KAR2	*MAT*α, *his3-Δ200, leu2-Δ1, ura3-52, trp1-Δ63, kar2::HIS3*, pTEF1-*KAR2*	This study
TEF1-R217A	*MAT*α, *his3-Δ200, leu2-Δ1, ura3-52, trp1-Δ63, kar2::HIS3*, pTEF1-*R217A*	This study
TEF1-K584X	*MAT*α, *his3-Δ200, leu2-Δ1, ura3-52, trp1-Δ63, kar2::HIS3*, pTEF1-*K584X*	This study
TEF1-S493F	*MAT*α, *his3-Δ200, leu2-Δ1, ura3-52, trp1-Δ63, kar2::HIS3*, pTEF1-*S493F*	This study
CYC1-KAR2	*MAT*α, *his3-Δ200, leu2-Δ1, ura3-52, trp1-Δ63, kar2::HIS3*, pCYC1-*KAR2*	This study
MMY713	*MAT*α, *his3-Δ200, leu2-Δ1, ura3-52, trp1-Δ63, kar2::HIS3*, pMR713	This study
TEF1-KAR2 jem1Δ	*MAT*α, *his3-Δ200, leu2-Δ1, ura3-52, trp1-Δ63, kar2::HIS3, jem1Δ::NAT*, pTEF1-*KAR2*	This study
TEF1-KAR2 scj1Δ	*MAT*α, *his3-Δ200, leu2-Δ1, ura3-52, trp1-Δ63, kar2::HIS3, scj1Δ::NAT*, pTEF1-*KAR2*	This study
TEF1-R217A jem1Δ	*MAT*α, *his3-Δ200, leu2-Δ1, ura3-52, trp1-Δ63, kar2::HIS3, jem1Δ::NAT*, pTEF1-*R217A*	This study

Strain name	Genotype	Source/ Reference
TEF1-R217A scj1Δ	*MATα, his3-Δ200, leu2-Δ1, ura3-52, trp1-Δ63, kar2::HIS3, scj1Δ::NAT,* pTEF1-*R217A*	This study
RSY607	*MATα, leu2-3, 112, ura3-52, PEP4::URA3*	R. Schekman
sec11-7	*MAT***a**, *sec11-7, ura3-52, leu2-3, his4-619*	Bohni *et al.*, 1988
kar2-159	*MATα, ura3-52, ade2-101, leu2-3,112, kar2-159*	M. Rose
kar2-113	*MATα, ura3-52, ade2-101, leu2-3,112, kar2-113*	M. Rose
BY4742	*MATα, his3-Δ1, leu2-Δ0, ura3-Δ0, lys2-Δ0*	Lab stock
ilm1Δ	*MATα, his3-Δ1, leu2-Δ0, ura3-Δ0, lys2-Δ0, ilm1Δ::KANMX*	Yeast Knockout Collection
erd1Δ	*MATα, his3-Δ1, leu2-Δ0, ura3-Δ0, lys2-Δ0, erd1Δ::KANMX*	Yeast Knockout Collection
sur4Δ	*MATα, his3-Δ1, leu2-Δ0, ura3-Δ0, lys2-Δ0, sur4Δ::KANMX*	Yeast Knockout Collection
sec63-1	*MATα sec63-1 leu2-3, 112 ura3-52*	R. Schekman
sec65-1	*MAT***a**, *sec65-1, ade2, his3, leu2, trp1, ura3*	Wilkinson *et al.*, 1997
scj1Δ	*MATα, his3-Δ1, leu2-Δ0, ura3-Δ0, lys2-Δ0, scj1Δ::KANMX*	Yeast Knockout Collection
BY4741	*MAT***a**, *his3-Δ1, leu2-Δ0, ura3-Δ0, met15-Δ0*	J. S. Weissman
ILM1-FLAG	*MAT***a**, *his3-Δ1, leu2-Δ0, ura3-Δ0, met15-Δ0, ILM1-3XFLAG::NAT*	This study
SCJ1 JEM1	MATα, *lys2-801, leu2-3,112, his3-Δ200, trp1-Δ901, ura3-52, suc2-Δ9,*	Nishikawa and Endo, 1997
scj1Δ jem1Δ	MATα *ade2-1 leu2-3,112 his3-11,15 trp1-1 ura3-1 can1-100 scj1Δ::TRP1 jem1Δ::LEU2*	Nishikawa and Endo, 1997

Strain name	Genotype	Source/ Reference
YDJ1 and *HLJ1 YDJ1 (*W303*)*	*MATα, ade2-1, leu2-3,112, his3-11,15, trp1-1, ura3-1, can1-100*	Lab stock
ydj1Δ	*MATα, ade2-1, leu2-3,112, his3-11,15, trp1-1, ura3-1, can1-100, ydj1-2::HIS3*	Wright *et al.*, 2007
hlj1Δ ydj1-151	*MATα, ade2-1, leu2-3,112, his3-11,15, trp1-1, ura3-1, can1-100, hlj1Δ::TRP1, ydj1-2::HIS3, LEU2::ydj1-151*	Youker *et al.*, 2004
hlj1Δ ydj1-151 leu2::NAT	*MATα, ade2-1, leu2-3,112, his3-11,15, trp1-1, ura3-1, can1-100, hlj1Δ::TRP1, ydj1-2::HIS3, leu2::NAT::ydj1-151*	This study
BY4743	*MAT***a**/α, *his3-Δ0/his3-Δ0, leu2-Δ0/leu2-Δ0, ura3-Δ0/ura3-Δ0, TRP1/TRP1, LYS2/lys2-Δ0, MET15/met15-Δ0*	J. S. Weissman
KAR2::NAT	*MAT***a**, *his3-Δ1, leu2-Δ0, ura3-Δ0, met15-Δ0, KAR2::NAT*	This study
kar2-R217A::NAT	*MAT***a**, *his3-Δ1, leu2-Δ0, ura3-Δ0, met15-Δ0, kar2-R217A::NAT*	This study
kar2-P515L:NAT	*MAT***a**, *his3-Δ1, leu2-Δ0, ura3-Δ0, met15-Δ0, kar2-P515L::NAT*	This study
kar2-DamP::NAT	*MAT***a**, *his3-Δ1, leu2-Δ0, ura3-Δ0, met15-Δ0, kar2-DamP::NAT*	This study
kar2-P515L-DamP::NAT	*MAT***a**, *his3-Δ1, leu2-Δ0, ura3-Δ0, met15-Δ0, kar2-P515L-DamP::NAT*	This study
vtc4Δ	*MATα, his3-Δ1, leu2-Δ0, ura3-Δ0, lys2-Δ0, vtc4Δ::KANMX*	Yeast Knockout Collection
ylr104wΔ	*MATα, his3-Δ1, leu2-Δ0, ura3-Δ0, lys2-Δ0, ylr104wΔ::KANMX*	Yeast Knockout Collection
SLS1 (RSY801)	*MAT***a,** *ade2-101, leu2-3,113, ura3-52*	R. Schekman
sls1Δ	*MAT***a,** *ade2-101, leu2-3,113, ura3-52, sls1::URA3*	Kabani *et al.*, 2000

Table 5: Plasmids used in this study

Plasmid name	Details	Source/Reference
pMR2623(wt)	IPTG-inducible His_6-BiP expression	M. Rose
pMR2623(R217A)	IPTG-inducible His_6-R217A BiP expression	This study
pMR2623(K584X)	IPTG-inducible His_6-K584X BiP expression	This study
pMR2623(S493F)	IPTG-inducible His_6-S493F BiP expression	This study
pMR713	*CEN4/ARS*, *LEU2*, P_{KAR2}-*KAR2*	M. Rose
pYES2	2μ, *URA3*	Invitrogen
pGAL1-*KAR2*	2μ, *URA3*, P_{GAL1}-*KAR2*	This study
pGAL1-*R217A*	2μ, *URA3*, P_{GAL1}-*kar2-R217A*	This study
pGAL1-*K584X*	2μ, *URA3*, P_{GAL1}-*kar2-K584X*	This study
pGAL1-*S493F*	2μ, *URA3*, P_{GAL1}-*kar2-S493F*	This study
p414TEF1	*CEN4/ARS*, *TRP1*, P_{TEF1}	Mumberg *et al.*, 1995
p414CYC1	*CEN4/ARS*, *TRP1*, P_{CYC1}	Mumberg *et al.*, 1995
pTEF1-*KAR2*	*CEN4/ARS*, *TRP1*, P_{TEF1}-*KAR2*	This study
pCYC1-*R217A*	*CEN4/ARS*, *TRP1*, P_{TEF1}-*kar2-R217A*	This study
pTEF1-*K584X*	*CEN4/ARS*, *TRP1*, P_{TEF1}-*kar2-K584X*	This study
pTEF1-*S493F*	*CEN4/ARS*, *TRP1*, P_{TEF1}-*kar2-S493F*	This study
pFA6a-NATMX6	*E. Coli oriC*, *NATMX6*, AMP^R	J. S. Weissman
pILM1-UTR-NAT	*E. Coli oriC*, *ILM1::NATMX6*, AMP^R	This study
pILM1-3XFLAG	*E. Coli oriC*, *ILM1-3XFLAG::NATMX6*, AMP^R	This study
pET-SCJ1	IPTG-inducible Scj1-His_6 expression	S. I. Nishikawa

Plasmid name	Details	Source/Reference
pSM36-ΔgppαF-HA	Yeast expression vector for HA-tagged mutant pre-pro-alpha factor (asparagines of the three consensus glycosylation sites mutated to glutamine), *URA3*	D. Ng
pDN431	*CEN4/ARS, URA3,* P_{PRC1}*-prc1-1:HA*	Ng *et al.*, 2000
pJC104	2μ, *URA3,* P_{4XUPRE}*-lacZ*	Cox and Walter, 1996
pDJ100	pSP65 vector containing pre-pro-alpha factor under the SP6 promoter; AMP^R	Hansen *et al.*, 1986
pGem2α36-3Q	Vector containing mutant pre-pro-alpha factor under the SP6 promoter, AMP^R	Mccracken and Brodsky, 1996
pCPY*-3HA	*CEN4/ARS, URA3,* P_{PRC1}*-prc1-1:3HA*	Bhamidipati *et al.*, 2005
pSM1911	2μ, *URA3,* P_{PGK1}*-ste6-166:HA*	Huyer e*t al.*, 2004
p425-Ste6p*HA	2μ, *LEU2,* P_{PGK1}*-ste6-166:HA*	This study
pSM1152	2μ, *URA3,* P_{PGK1}*-CFTR:HA*	Zhang *et al.*, 2002
pSLW1-B29	2μ, *URA3,* P_{GAL1}*-APOB29:HA*	Hrizo *et al.*, 2007
pAV4	*CEN4/ARS, URA3,* P_{YDJ1}*–YDJ1*	Caplan *et al.*, 1992
pssYdj1-3HA-DSL	A modified pSG5 vector (Stratagene) for mammalian expression of signal sequence -containing Ydj1 with a 3HA tag at the C-terminus	This study
pssYdj1-C406S-3HA-DSL	pssYdj1-3HA-DSL with the C406S mutation in Ydj1 (disrupts the farnesylation of Ydj1)	This study
pGPD426	2μ, *URA3,* P_{GPD}	Mumberg *et al.*, 1995
pGPD426-ERdj3	2μ, *URA3,* P_{GPD}*-ERdj3*	This study
pGPD426-CaaX	2μ, *URA3,* P_{GPD}*-(Δss)ERdj3-CASQ*	This study
pGPD426-CaaX-ΔII	pGPD426CaaX with a deletion of domain II in ERdj3	This study

Plasmid name	Details	Source/Reference
pGPD426-CaaX-ΔII-GSGG	pGPD426CaaX with the GSGG linker replacing domain II in ERdj3	This study
pGPD426-CaaX-F326A	pGPD426CaaX with the F326A mutation in ERdj3	This study
pGPD426-CaaX-F326D	pGPD426CaaX with the F326D mutation in ERdj3	This study
pGPD426-CaaX-I134A	pGPD426CaaX with the I134A mutation in ERdj3	This study
pGPD426-CaaX-L208A	pGPD426CaaX with the L208A mutation in ERdj3	This study
pGPD426-CaaX-IVLFa	pGPD426CaaX with the I134A, VL208A, mutations in ERdj3	This study
pGPD426-CaaX-H53Q	pGPD426CaaX with the H53Q mutation in ERdj3	This study
pGPD426-CaaX-D55N	pGPD426CaaX with the D55N mutation in ERdj3	This study
pKAR2-UTR-NAT	*E. Coli oriC*, *KAR2-UTR::NATMX6, AMP*^{R}	This study
pkar2-DamP-NAT	*E. Coli oriC*, *kar2-DamP::NATMX6, AMP*^{R}	This study
pkar2-R217A-UTR-NAT	*E. Coli oriC*, *kar2-R217A::NATMX6, AMP*^{R}	This study
pkar2-R217A-DamP-NAT	*E. Coli oriC*, *kar2-R217A-DamP::NATMX6, AMP*^{R}	This study
pkar2-P515L-UTR-NAT	*E. Coli oriC*, *kar2-P515L::NATMX6, AMP*^{R}	This study
pkar2-P515L-DamP-NAT	*E. Coli oriC*, *kar2-P515L-DamP::NATMX6, AMP*^{R}	This study

APPENDIX A

THE TRANSMEMBRANE DOMAIN OF EITHER SBH1p OR SBH2p IS SUFFICIENT TO COMPENSATE FOR N-GLYCAN TRIMMING DEFECTS OBSERVED IN *sbh1Δ sbh2Δ* YEAST

This work was performed in collaboration with the laboratories of Jussi Jantti at the University of Helsinki, Finland and Karin Römisch at Cambridge University, U.K. and is published:

*Feng, D., Zhao, X., Soromani, C., Toikkanen, J., Römisch, K., Vembar, S.S., Brodsky, J.L., Keränen, S., Jäntti, J. The transmembrane domain is sufficient for Sbh1p function, its association with the Sec61 complex, and interaction with Rtn1p. J Biol Chem **282**, 30618-28 (2007).*

The function of Sbh1p[100, 149], the β-subunit of the yeast Sec61 translocation complex, and its homologue, Sbh2p[149, 323] which forms part of a second yeast translocation complex, the Ssh1 complex, is not clearly understood. Sbh1p is an 82 amino acid protein with a single transmembrane domain. Several groups have demonstrated that: (i) Yeast lacking *sbh1* and *sbh2* are temperature-sensitive and accumulate secretory precursors, especially those that require co-translational translocation to get into the ER[149, 323]; (ii) Sbh1p interacts with subunits of the signal peptidase complex[384] and oligosaccharyl transferase complex[385]; (iii) Sbh1p may act as a guanine-nucleotide exchange factor for the GTPase subunit of the SRP receptor[386]; (iv) Sbh1p

mediates the interaction between Sec61p and the exocyst complex[387, 388], although the significance of this interaction is still unknown. The exocyst complex includes of Sec3p, Sec5p, Sec6p, Sec8p, Sec10p, Sec15p, Exo70p, and Exo84p, and along with select small Rab GTPases such as Sec4p, it participates in the tethering of secretory vesicles to the plasma membrane during exocytosis[389]. Therefore, it is possible that Sbh1p acts as a guanine-nucletotide exchange factor for these essential GTPase.

To elaborate the role of Sbh1p and Sbh2p during translocation, our collaborators first examined the translocation efficiency of *sbh1Δsbh2Δ* yeast. They recapitulated the observations that Sbh1p and Sbh2p are required for co-translational protein translocation into the ER, but not for post-translational protein translocation. Second, they showed that the deletion of Sbh1p and Sbh2p affected the N-glycan trimming of proteins that are glycosylated upon entry into the ER (refer to section 1.2.5 and Figure 6); this effect was independent of whether the substrate was co- or post-translationally translocated across the ER membrane. Third, to establish the minimal domain requirements for Sbh1p and Sbh2p function, they expressed different fragments of either protein in *sbh1Δsbh2Δ* yeast and examined the rescue of temperature-sensitive growth. Intriguingly, the overexpressed transmembrane domain of either protein was sufficient to complement the growth defect of *sbh1Δsbh2Δ* yeast, and this effect could be directly correlated to a rescue of co-translational protein translocation in *sbh1Δsbh2Δ* cells.

To determine whether the defect in N-glycan trimming could be also rescued by overexpression of the Sbh1p or Sbh2p transmembrane domain (*i.e.,* Sbh1p-TM or Sbh2p-TM), I examined the efficiency of pre-pro-alpha factor translocation into microsomes derived from *sbh1Δsbh2Δ* yeast transformed either with an empty vector, or expression vectors for Sbh1p, Sbh2p, Sbh1p-TM or Sbh2p-TM. As shown in Figure 31, the overexpression of the

transmembrane domain of either Sbh1p or Sbh2p was sufficient to support N-glycan trimming in *sbh1Δsbh2Δ* yeast, further emphasizing the sufficiency of the transmembrane domain of either Sbh1p or Sbh2p for Sbh function. In agreement with these results, a recent report examined the species specificity of Sbh1p homologs from *Schizosaccharomyces pombe*, *S. cerevisiae* and humans[390], and observed that the transmembrane domains of these homologs were sufficient to substitute for one another during translocation and other Sbh1-regulated processes.

Finally, our collaborators established a novel correlation between Sbh1p and the exocyst complex. They showed that Sbh1p exists as two subpopulations within the cell, one that interacts with Sec61p and the other that interacts with Rtn1p. Rtn1p is an ER membrane protein belonging to the highly conserved reticulon A-like family that regulates cortical ER morphology by interacting with Sec6p, a component of the exocyst complex[391].

Figure 31: Complementation of the N-glycan trimming defect of *sbh1Δsbh2Δ* yeast by either Sbh1p or Sbh2p.

Microsomes derived from the *sbh1Δsbh2Δ* strain transformed with either an empty vector (-) or vectors harboring the indicated *SBH* constructs were tested in duplicate for their ability to translocate pre-pro-alpha factor (ppαF), thus generating the glycosylated pro-alpha factor form (3gpαF). Assays were performed at 20°C for 20 min. Data are representative of three independent experiments. TM=transmembrane domain.

APPENDIX B

ANALYSIS OF THE GENETIC INTERACTIONS OF TWO BIP MUTANTS, R217A AND P515L, WITH A SUBSET OF YEAST GENES THAT REGULATE ER FOLDING HOMEOSTASIS

This work was performed in collaboration with Martin Jonikas, a graduate student in the laboratory of Jonathan Weissman at the University of California, San Francisco.

In recent years, it has become evident from several *S. cerevisiae* genomic and proteomic analyses[173, 333-345, 392-394] that most proteins in the cell either function in the context of multiprotein complexes or affect multiple cellular pathways. Proteomic studies such as protein localization[173] and protein-protein interaction analyses[392, 393] have examined the features of essential and non-essential genes, and have been successful in assigning putative functions to select uncharacterized open reading frames. However, most genomic studies have utilized the haploid Yeast Knockout (YKO) collection[381, 382], a set of strains in which each of ~4800 non-essential genes has been individually deleted with an antibiotic-resistance cassette, consequently neglecting the essential genes. The limited genomic analyses that have been performed with essential genes have utilized hypomorphic 'decreased abundance by mRNA perturbation' or '*DamP*' alleles wherein the 3' untranslated region (3'UTR) of these genes has been disrupted

with an antibiotic-resistance cassette[344, 380]. But, given that the efficacy of *DamP*ing is dependent on mRNA stability and copy number as well as transcription and translation rates[344], the results obtained for each essential gene varies. Moreover, in some cases, *DamP*ing is lethal[344, 380], while in others it may affect specific functions of a multifunctional gene[333]. One solution to this problem could be the utilization of mutant alleles of an essential gene which are known to be defective for specific functions. Accordingly, in this section, I describe the application of a novel UPR-based genetic screen to dissect the genetic interaction profiles exhibited by unique alleles of the essential gene, *KAR2*. To highlight any differences, I also utilized '*DamP*'ed versions of the wild-type and mutant *KAR2* alleles.

As described in Chapter 2, R217A BiP (encoded by *kar2-R217A*) exhibits a specific defect for translocation into the ER which can be attributed to its reduced interaction with Sec63p, the Hsp40 cochaperone dedicated to translocation; this is the first identification of a translocation-specific BiP mutant. Conversely, the Brodsky lab had previously characterized a point mutant, P515L, in BiP's substrate binding domain that was deficient for substrate binding, and the expression of this protein resulted in an ERAD-specific defect *in vivo*[181].

Given the functional distinction exhibited by R217A and P515L BiP, I hypothesized that these mutant BiP proteins might function in the context of unique protein complexes, or exhibit unique sets of genetic interactions with other cellular components that are required to maintain ER homeostasis. To test this hypothesis, I chose to examine the genetic interactions between R217A BiP and P515L BiP with 350 other non-essential genes. The deletions of these 350 genes lead to a constitutive induction of the UPR[121], and can be measured in a defined assay[121]. This set of 350 genes includes ER and cytosolic chaperones, components of the N-linked glycosylation machinery and ERAD, and genes required for O-mannosylation, GPI anchor synthesis, vesicular

trafficking, vacuole function, lipid biosynthesis, cytoskeletal organization and chromatin remodeling. This study is ongoing and I summarize the results that I have obtained thus far.

B.1. CONSTRUCTION OF *KAR2* STRAINS FOR UPR-BASED GENETIC ANALYSIS

To generate wild-type and mutant *kar2* strains amenable to manipulation in the UPR-based genetic screen, the first step involved the construction of vectors in which the wild-type *KAR2* gene, lacking or containing the nucleotide sequence corresponding to the 3'UTR, was inserted upstream of the *NATMX6* antibiotic resistance cassette. To do this, the *KAR2* gene lacking the 3' UTR (henceforth referred to as *kar2-DamP*) was amplified from yeast genomic DNA with the primer pair (the underlined sequence in the 5' primer represents the *PvuII* recognition site and in the 3' primer represents the *BamHI* recognition site):- 5'primer:
GTCCCCAAGAGCAGCTGCAAGGGAAA, and 3' primer:
CAACCTTGAAGGATCCAGCAGCAAAA, whereas the *KAR2* gene containing the 3'UTR (henceforth referred to as *KAR2-UTR*) was amplified with the primer pair (the underlined sequence in the 5' primer represents the *PvuII* recognition site and in the 3' primer represents the *BamHI* recognition site):- 5' primer: GTCCCCAAGAGCAGCTGCAAGGGAAA, and 3' primer: CAATAGTGATGGGATCCGATGAGATGA. The resultant PCR products were digested with the indicated restriction enzymes and inserted into the plasmid pFA6a-NATMX6 to generate pkar2-DamP-NAT and pKAR2-UTR-NAT, respectively. Next, the *kar2-DamP-NAT* or *KAR2-UTR-NAT* cassette was amplified with the primer pair:- 5' primer:
AAAGATTAACGTGTTACTGTTTTACTTTTTTAAAGTCCCCAAGAGTAGTCTCAAGGG
AAAAAGCGTATC, and 3' primer:

CCATTTCAGTATTAGGTTCTCGAGCCTTTCAACTCTCTCTGTTATAATGTGAATTCGA GCTCGTTTAAAC. The resulting PCR product was transformed into the BY4743 strain (*MAT***a**/α, *his3-Δ0/his3-Δ0, leu2-Δ0/leu2-Δ0, ura3-Δ0/ura3-Δ0, TRP1/TRP1, LYS2/lys2-Δ0, MET15/met15-Δ0, KAR2/KAR2*) and transformants were selected on yeast extract-peptone-dextrose medium supplemented with nourseothricin. To identify strains in which one copy of the chromosomal *KAR2* gene was replaced with either the *kar2-DamP-NAT* **or** *KAR2-UTR-NAT* cassettes, PCR amplification was performed with the primer pair:- 5' primer: GGCTATGTAATTCTAAAGATTAACGT, and 3' primer: GTATGAAGCTCGAAGTTTGAATTAGCT, **or** 5' primer: GGCTATGTAATTCTAAAGATTAACGT, and 3' primer: GTTATCTTAGGGTCATACTCATCAATT, respectively. The PCR product was observed two bands after agarose gel electrophoresis corresponding to 2.1 kb (endogenous *KAR2*) and either 3.3 kb (*kar2-DamP-NAT*) or 3.9 kb (*KAR2-UTR-NAT*). Next, the desired diploid strains were subjected to sporulation and tetrad analysis, and haploid strains of the genotype *MAT***a**, *his3-Δ1, leu2-Δ0, ura3-Δ0, met15-Δ0*, *kar2-DamP-NAT* or *MAT***a**, *his3-Δ1, leu2-Δ0, ura3-Δ0, met15-Δ0*, *KAR2-UTR-NAT* were selected for further analysis. These *NAT*-marked strains were called *kar2-DamP::NAT* and *KAR2::NAT*, respectively, and are isogenic to BY4741.

To construct the mutant *kar2* strains, a point mutation corresponding to R217A BiP was introduced into the pkar2-DamP-NAT and pKAR2-UTR-NAT vectors using the primer pair:- 5' primer: GCTGGTTTGAACGTTTGGCAATTGTTAATGAACCAACCGC, and 3' primer: GCGGTTGTTCATTAACAATTGCCAAAACGTTCAAACCAGC. The *kar2-R217A::NAT* strain was generated in a similar manner to that described for the wild-type *KAR2* gene. However, several attempts to generate the *kar2-R217A-DamP::NAT* strain were unsuccessful

suggesting that reducing the levels of R217A BiP is lethal, as observed in Chapter 2 (Figure 13E). Next, a point mutation corresponding to P515L BiP was introduced into the pkar2-DamP-NAT and pKAR2-UTR-NAT vectors using the primer pair: 5' primer: CCAGCACCAAGAGGTGTACTTCAAATTGAAGTCACATTTG, and 3' primer: CAAATGTGACTTCAATTTGAAGTACACCTCTTGGTGCTGG, and the *kar2-P515L::NAT* and *kar2-P515L-DamP::NAT* strains were generated in a manner similar to that described for the wild-type *KAR2* gene. Once the strains were generated, the chromosomal integration of the wild-type or mutant *kar2* genes was confirmed by PCR (Figure 32) and DNA sequence analysis.

B.2 CHARACTERIZATION OF TRANSLOCATION AND ERAD IN THE *kar2* STRAINS GENERATED FOR UPR-BASED GENETIC ANALYSIS

Prior to utilizing the *KAR2::NAT, kar2-DamP::NAT, kar2-R217A::NAT, kar2-P515L::NAT* and *kar2-P515L-DamP::NAT* strains in the UPR-based genetic screen, I wanted to examine their growth pattern as well as their translocation and ERAD efficiencies. First, I tested was the ability of the strains to grow at elevated temperatures and in the presence of the reducing agent, DTT. To this end, the strains were serially diluted onto yeast extract-peptone-dextrose medium and the plates were incubated at a range of temperatures (Figure 33A). I found that the *KAR2::NAT* and *kar2-DamP::NAT* strains expressing wild-type BiP grew robustly at all temperatures tested whereas the *kar2-P515L::NAT* and *kar2-P515L-DamP::NAT* mutant strains were sensitive to elevated temperatures. This was not surprising because previous studies had shown that the *in vivo* expression of P515L BiP resulted in a temperature-sensitive growth phenotype. Moreover, in keeping with previous observations, the *kar2-P515L::NAT* and *kar2-*

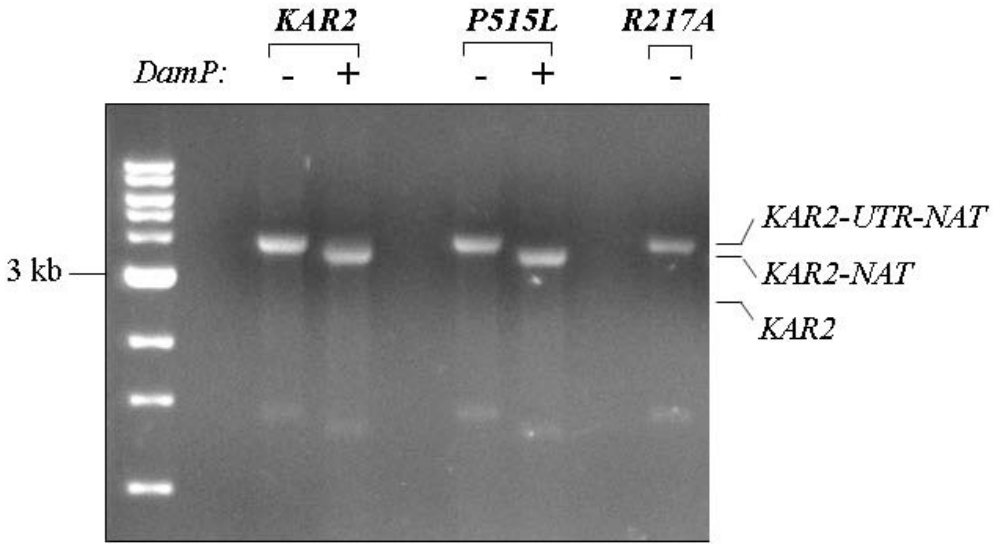

Figure 32: PCR amplification of wild-type and mutant *kar2* alleles from genomic DNA.

Genomic DNA was prepared from the indicated wild-type and mutant *NAT*-marked strains and the corresponding *kar2* alleles were amplified using the primers described in section B.1. The expected sizes of the bands are: *KAR2*=2.1 kb, *KAR2-NAT* corresponding to the *DamP*ed allele=3.3 kb, and *KAR2-UTR-NAT*=3.9 kb.

P515L-DamP::NAT mutant strains were also sensitive to DTT[181] (Figure 33A). In contrast, the behavior of the *kar2-R217A::NAT* strain, which was slow-growing at all temperatures and in the presence of DTT (Figure 33A), was highly unexpected. This was because I had previously observed that the *TEF1-R217A* strain was not sensitive to temperature or DTT, similar to the wild-type *TEF1-KAR2* strain (Figure 14 in Chapter 2). But, given that R217A BiP is expressed from its endogenous promoter at the *KAR2* choromosomal locus in the *kar2-R217A::NAT* strain and from the plasmid-borne P_{TEF1} promoter in the *TEF1-R217A* strain, its transcriptional regulation in these strains is most likely different. This could, in turn, account for the differential growth patterns. Therefore, it became imperative to test the functional defects exhibited by *kar2-R217A::NAT*.

Next, I examined the expression levels of wild-type and mutant BiP proteins in the *KAR2::NAT, kar2-DamP::NAT, kar2-R217A::NAT, kar2-P515L::NAT* and *kar2-P515L-DamP::NAT* strains. I prepared cell extracts from these strains, resolved them using SDS-PAGE and subjected them to immunoblotting with anti-BiP antisera. As shown in Figure 33B, there was a ~30% and ~50% reduction in the levels of BiP expression in the *kar2-DamP::NAT* and *kar2-P515L-DamP::NAT* strains as compared to the *KAR2::NAT* and *kar2-P515L::NAT* strains, respectively. Since the *DamP*ing technique causes a reduction in mRNA stability and consequently a decrease in protein expression[344], this result was anticipated. On the other hand, the *kar2-R217A::NAT* strain showed increased levels of BiP expression (Figure 33B). However, this could be accounted for by the observation that pre-BiP accumulates in this strain (indicated by '6%' where a lower percentage of acrylamide was used for SDS-PAGE), and derives from the ~8 kDa difference in molecular mass between pre-BiP and BiP, which cannot be resolved on a 10% gel.

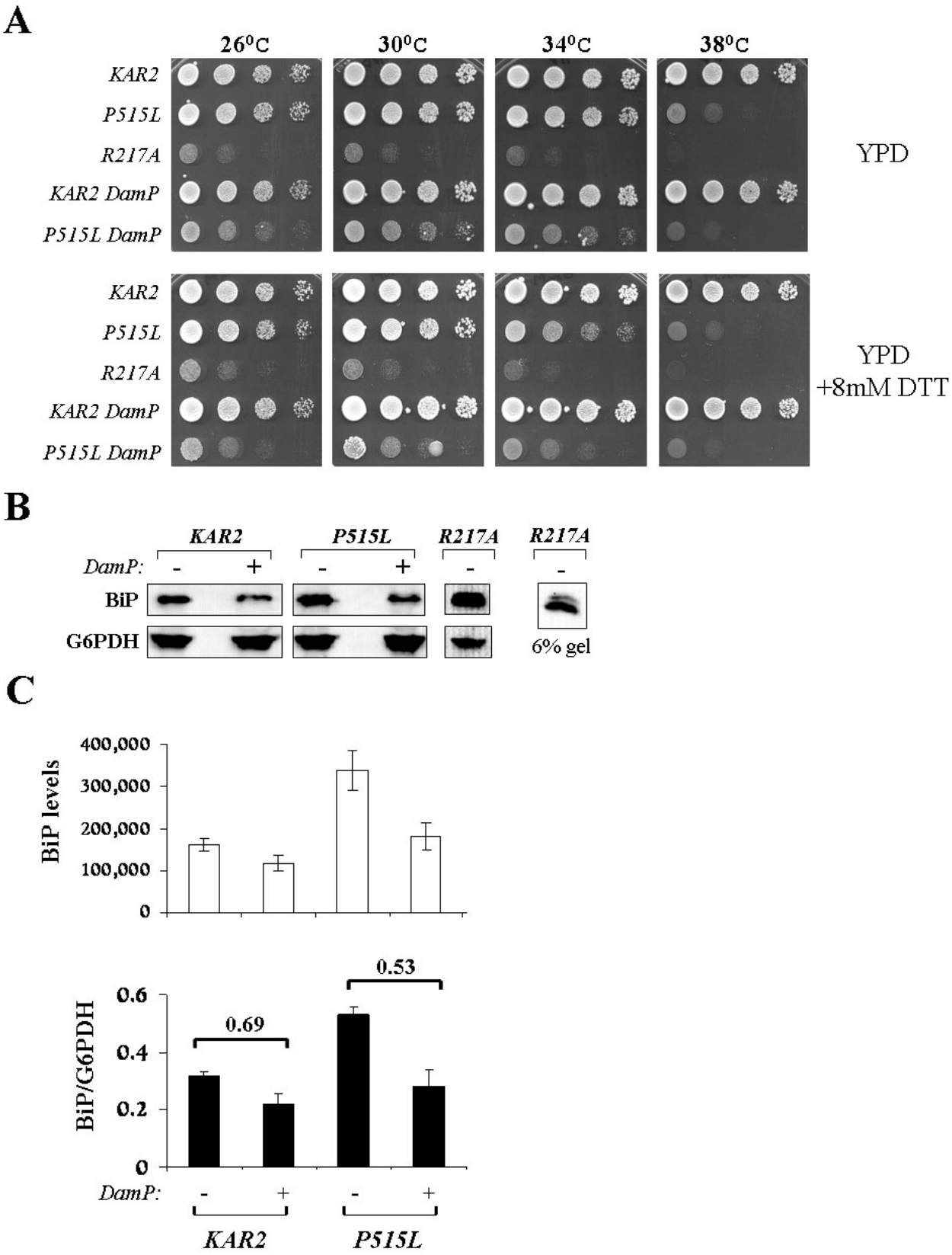
A
26°C
30°C
34°C
38°C
KAR2
P515L
R217A
KAR2 DamP
P515L DamP
YPD
YPD
+8mM DTT
B
KAR2
P515L
R217A
R217A
DamP:
BiP
G6PDH
6% gel
C
BiP levels
400,000
300,000
200,000
100,000
0
BiP/G6PDH
0.6
0.4
0.2
0
0.69
0.53
DamP:
KAR2
P515L

Figure 33: Characterization of the growth patterns and BiP expression levels in the wild-type and mutant *kar2* strains generated for the UPR-based genetic screen.

(A) Ten-fold serial dilutions of the wild-type and mutant *NAT*-marked strains were plated onto yeast extract-peptone-dextrose (YPD) medium either lacking or containing 8 mM DTT. Plates were incubated at 26, 30, 34 and 38°C for 2 d. ***(B)*** Cell extracts prepared from the indicated wild-type or mutant strains grown at 30°C were resolved by SDS-PAGE and immunoblotted with polyclonal anti-BiP antisera. The level of G6PDH in cell extracts served as a loading control. Unless indicated, the cell extracts were resolved on 10% polyacrylamide gels under non-native and reducing conditions. ***(C)*** Top panel: Quantification of BiP levels in the indicated strains using the Kodak ImageStation software. Bottom panel: Normalization of BiP levels in the indicated strains to the levels of G6PDH. The numbers 0.69 and 0.53 indicate the fold change in BiP levels observed in the *kar2-DamP::NAT* and *kar2-P515L-DamP::NAT* strains, respectively, as compared to the corresponding un*DamP*ed strains. Data represent the means of four determinations $\pm$ standard deviation.

Given that the expression of P515L BiP leads to a constitutive induction of the UPR[181] and consequently, a DTT-sensitive growth phenotype, BiP levels in the *kar2-P515L::NAT* and *kar2-P515L-DamP::NAT* strains were used as a direct measure of UPR induction. This is because BiP expressed from its endogenous promoter is upregulated upon UPR induction[204, 205]. Therefore, I quantified the amount of BiP in these strains and compared the levels either directly or after normalizing BiP levels to those of glucose-6-phosphate dehydrogenase (G6PDH), a loading control that is not a UPR target[199] (Figure 33C). As expected, there was a 2-fold increase in the levels of BiP in the *kar2-P515L::NAT* and *kar2-P515L-DamP::NAT* strains as compared to *KAR2::NAT* and *kar2-DamP::NAT*, respectively, indicating that the UPR is induced upon P515L BiP expression. I also confirmed this result using β-galactosidase reporter assays to measure UPR induction (data not shown).

Next, I measured the ERAD efficiencies of the five strains by following the degradation of CPY* using pulse-chase followed by immunoprecipitation assays (as described in Chapter 2). As shown in Figure 34A, CPY* was efficiently degraded in the *KAR2::NAT* and *kar2-DamP::NAT* strains at 30°C. In contrast, there was a stabilization of CPY* in the *kar2-P515L-DamP::NAT* strain at 30°C (Figure 34A) indicating that this strain exhibited an ERAD defect. Unexpectedly, the *kar2-P515L::NAT* strain degraded CPY* to levels similar to the *KAR2::NAT* strain at 30°C. However, when the assay was performed at 37°C (Figure 34B), the mutant strain exhibited an ERAD defect. Therefore, it appears that the *kar2-P515L::NAT* strain has a temperature-dependent ERAD defect. Finally, I examined the CPY* degradation efficiency of the *kar2-R217A::NAT* strain. I observed that this strain had a strong defect for CPY* translocation (data not shown), and hence, I was unable to accurately quantify the amounts of CPY* present at various time points. An alternate *in vitro* approach needs to be taken to measure

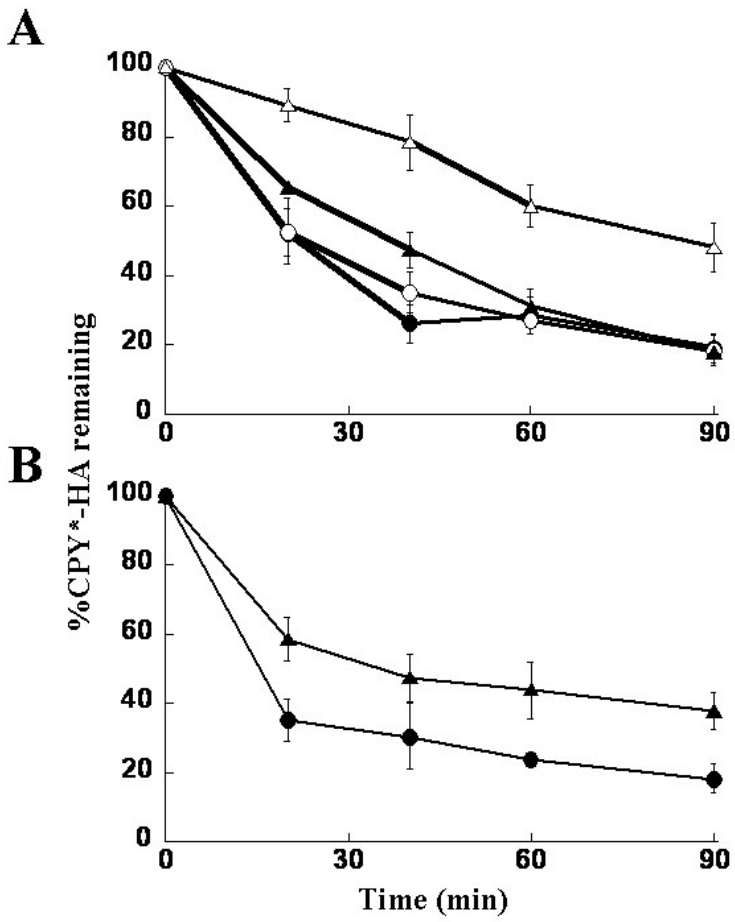

Figure 34: Characterization of the ERAD efficiencies of the wild-type and mutant strains generated for the UPR-based genetic screen.

To analyze the degradation efficiency of an HA-tagged form of CPY*, pulse-chase followed by immunoprecipitation assays using anti-HA antibodies were performed on ***(A)*** *KAR2::NAT* (●), *kar2-DamP::NAT* (○), *kar2-P515L::NAT* (▲) and *kar2-P515L-DamP::NAT* (△) strains grown at 30°C, and ***(B)*** *KAR2::NAT* (●) and *kar2-P515L::NAT* (▲) grown at 37°C.

the ERAD efficiency of this strain, but it is beyond the scope of this study.

Lastly, I analyzed the translocation efficiency of the *KAR2::NAT, kar2-DamP::NAT, kar2-R217A::NAT, kar2-P515L::NAT* and *kar2-P515L-DamP::NAT* strains. To this end, I examined the translocation of ER-lumenal Sls1p, BiP's nucleotide exchange factor (refer to section 1.2.3). I found that as Sls1p translocates into the ER, it is modified by the addition of N-linked glycans, and this is observed as an increase in molecular mass (Figure 35A). The sensitivity of the glycosylated species to endoglycosidase H, an enzyme that cleaves N-linked oligosaccharides (Figure 35A, compare the Endo-H treated and untreated lanes), and the absence of the glycosylated band in the *sec63-1* strain which carries a translocation-deficient mutant allele of *SEC63*, confirms that the N-linked glycosylation of Sls1p occurs upon translocation. Next, I prepared cell extracts from the five strains, resolved the proteins using SDS-PAGE and performed immunoblotting with anti-Sls1p antisera. As shown in Figure 35B, the unglycosylated form of Sls1p accumulated in the *kar2-R217A::NAT* strain, similar to the control strain, *sec63-1*. Therefore, the expression of R217A BiP from the *KAR2* endogenous promoter resulted in a translocation defect, as anticipated. The remaining strains efficiently translocated Sls1p, as evidenced by the formation of the glycosylated species in these strains (Figure 35B), suggesting that they are not deficient for translocation.

Taken together, these data indicate that the *kar2-P515L::NAT* and *kar2-P515L-DamP::NAT* strains exhibit ERAD-specific defects, and this results in a constitutive induction of the UPR. In contrast, the *kar2-R217A::NAT* strain exhibits a translocation defect, although the absence of an ERAD defect cannot be ruled out without performing additional assays. However, the severe growth phenotype of this strain can most likely be attributed to its translocation deficiency.

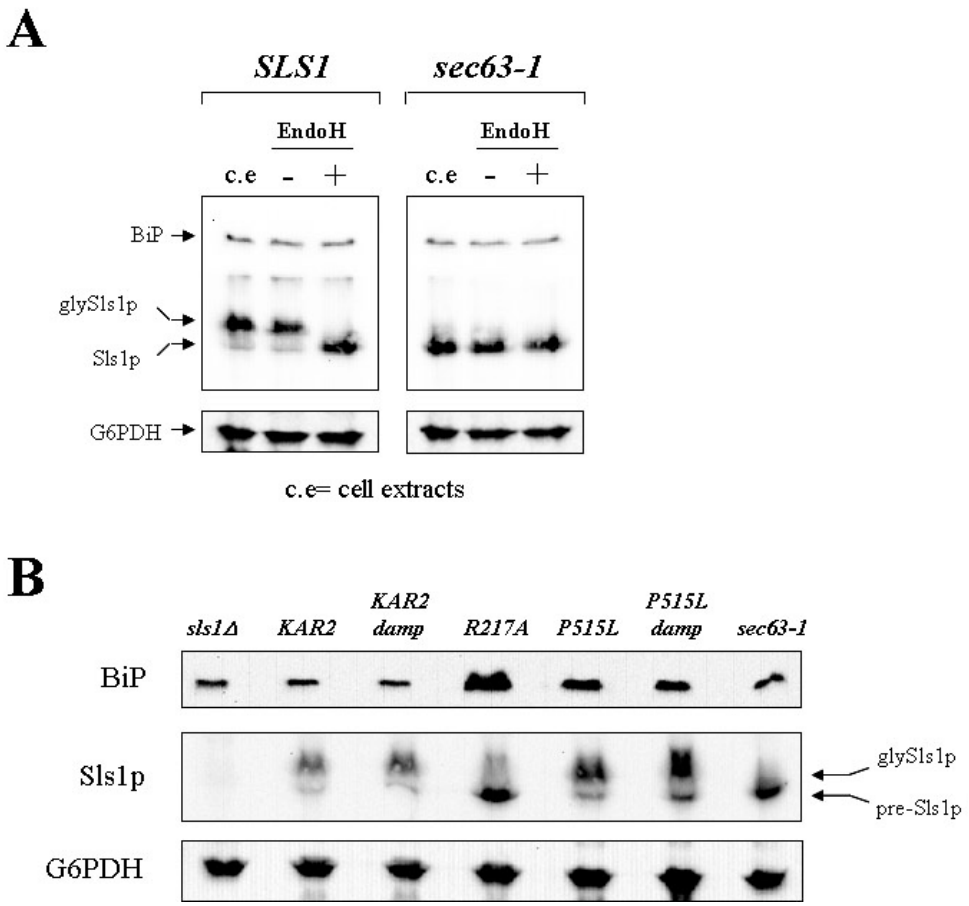

Figure 35: Characterization of the translocation efficiencies of the wild-type and mutant *kar2* strains generated for the UPR-based genetic screen.

(A) Cell extracts prepared from wild-type (*SLS1*) or translocation-deficient (*sec63-1*) strains were subjected to endoglycosidase H (Endo H) treatment as indicated. The resulting samples were resolved using SDS-PAGE and immunoblotted with anti-Sls1p antisera (a kind gift of M. Kabani and C. Gaillardin, INRA, France). The anti-Sls1p antiserum has not been affinity-purified and therefore cross-reacts with a higher molecular mass band that corresponds to BiP. G6PDH served as a loading control. ***(B)*** Cell extracts prepared from the indicated strains were resolved using SDS-PAGE and immunoblotted with anti-BiP or anti-Sls1p antisera. G6PDH served as a loading control.

B.3 ANALYSIS OF GENETIC INTERACTIONS OF THE VARIOUS WILD-TYPE AND MUTANT *kar2* STRAINS

After examining the phenotypes of the *KAR2::NAT, kar2-DamP::NAT, kar2-R217A::NAT, kar2-P515L::NAT* and *kar2-P515L-DamP::NAT* strains, the next step was to cross each strain individually against the ~ 350 individual gene deletions (listed in Table 2), that contain a fluorescent UPR reporter plasmid. Because these deletion strains exhibit a constitutive induction of the UPR, it is assumed that the absence of each of these ~350 genes perturbs the ER folding environment[121]. As described in Chapter 2, SGA analysis was performed to generate double mutant haploid strains with the following genotypes: *KAR2::NAT, yfg::KANMX,* pUPRE-GFP **or** *kar2-R217A::NAT, yfg::KANMX,* pUPRE-GFP, and so on. To measure the levels of UPR induction in the resultant haploid strains, flow cytometry was performed and the results were quantified according to Jonikas *et al*[121]. The GFP-fluorescence data obtained for each of the *kar2* strains are tabulated in Tables 3 through 6. The data obtained for the *KAR2::NAT* and *kar2-R217A::NAT* strains are represented in graphical form in Figure 18 in Chapter 2 while those obtained for the *kar2-DamP::NAT, kar2-P515L::NAT* and *kar2-P515L-DamP::NAT* strains are represented in graphical form in Figure 36.

When perusing these graphs there are certain key features that need to be noted[121]. As indicated in the figure legends of Figures 18 and 36, the horizontal blue line represents the basal level of UPR induction observed in the *kar2* strains in the absence of any gene deletion. Therefore, if a gene deletion does not aggravate or alleviate the basal ER stress of the *kar2* strains, then its datapoint on the graph will lie on the horizontal blue line. This suggests that the presence of wild-type or mutant BiP has an epistatic or 'fully masking' effect on the gene deletion. Next, the diagonal blue line in the graphs represents the expected values of UPR

A

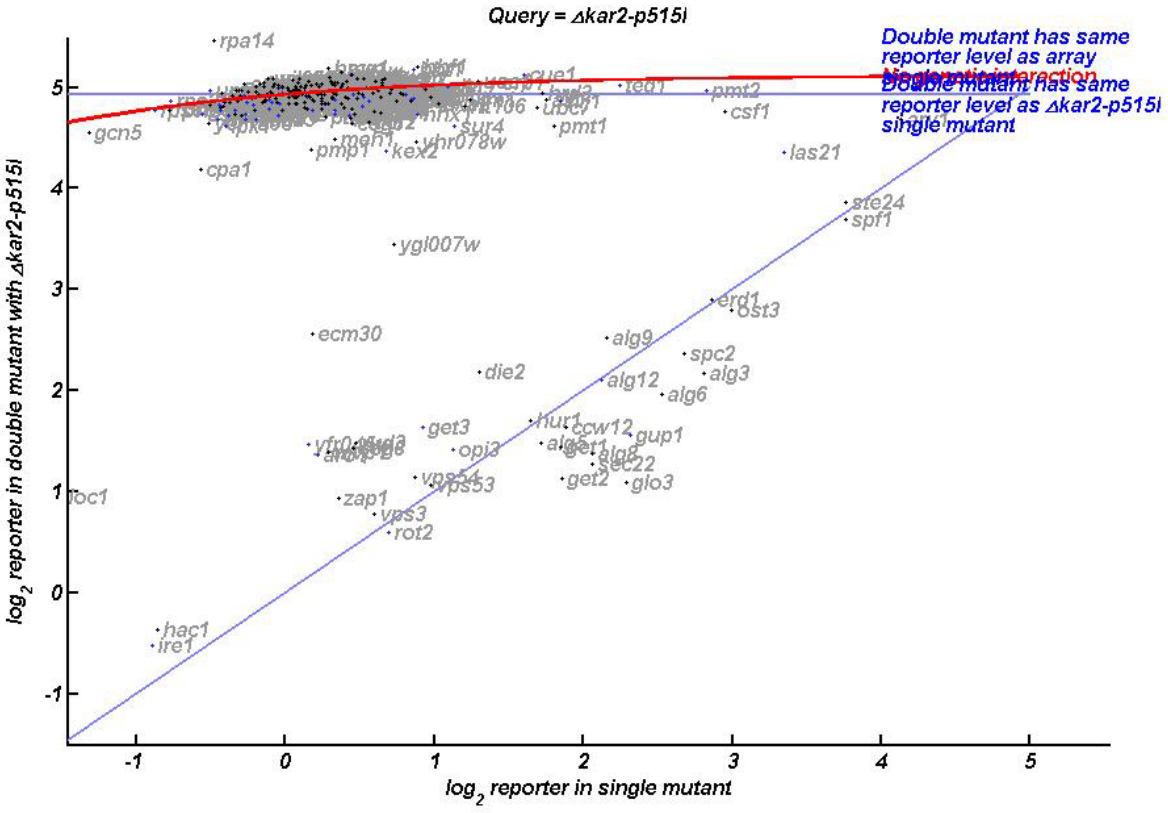
Query = Δkar2-p515i
Double mutant has same reporter level as array
No genetic interaction
Double mutant has same reporter level as Δkar2-p515i single mutant
log2 reporter in double mutant with Δkar2-p515i
log2 reporter in single mutant
rpa14
gcn5
cpa1
pmp1
kex2
yhr078w
sur4
pmt1
pmt2
csf1
las21
ste24
spf1
ygl007w
erd1
ost3
ecm30
alg9
spc2
alg3
die2
alg12
alg6
get3
hur1
ccw12
gup1
opi3
sec22
get2
glo3
vps53
zap1
vps3
rot2
loc1
hac1
ire1

B

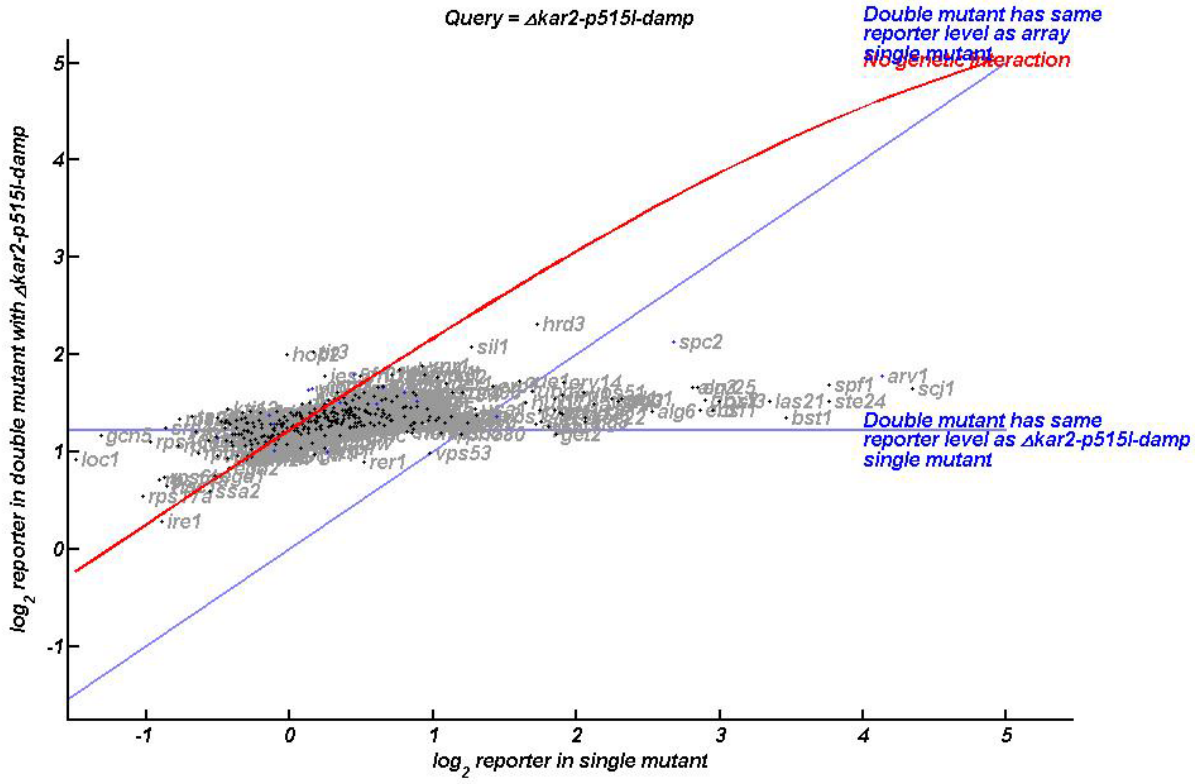
Query = Δkar2-p515i-damp
Double mutant has same reporter level as array single mutant
No genetic interaction
Double mutant has same reporter level as Δkar2-p515i-damp single mutant
log2 reporter in double mutant with Δkar2-p515i-damp
log2 reporter in single mutant
hrd3
sil1
spc2
spf1
arv1
scj1
ste24
las21
bst1
alg6
get2
vps53
rer1
ire1
loc1

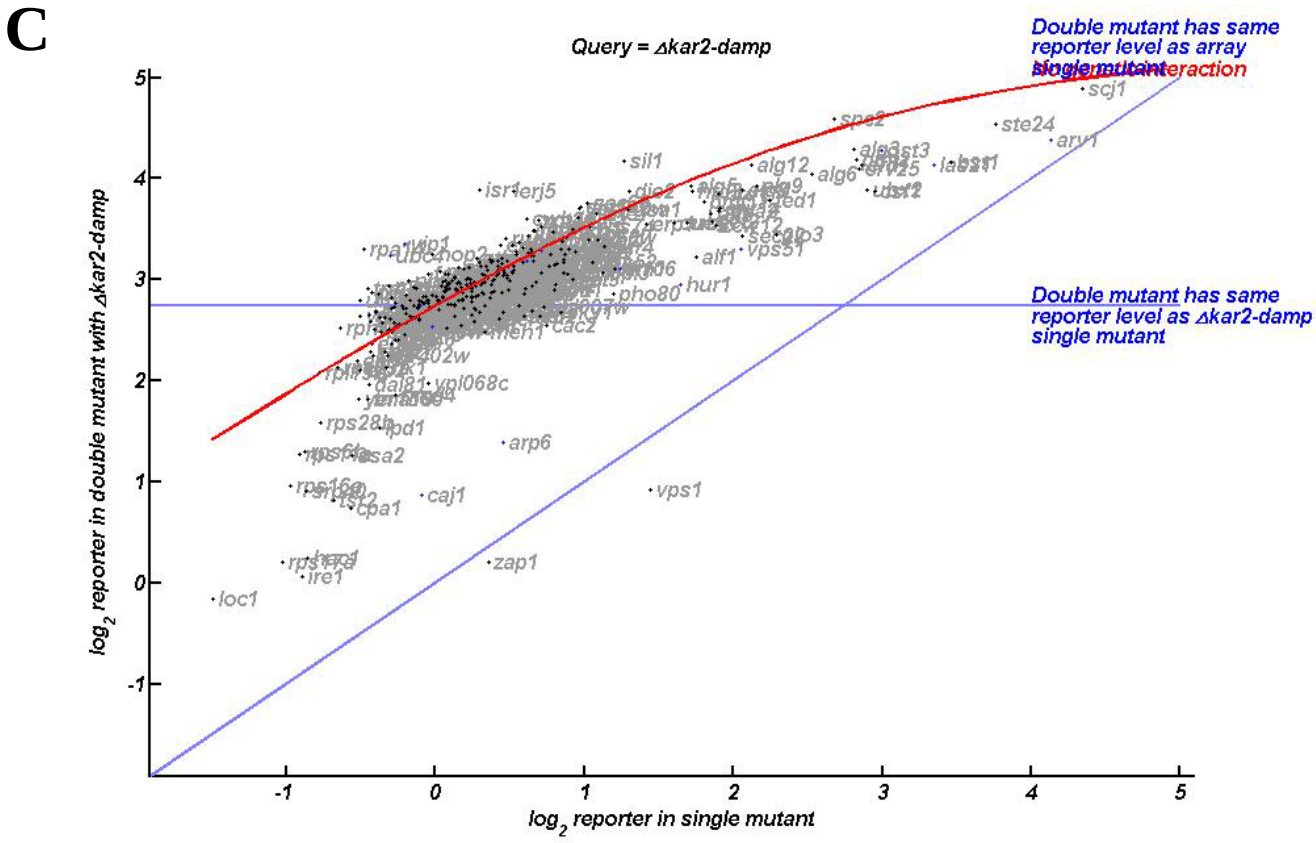

Figure 36: Genetic interaction profiles of the indicated mutant *kar2* strains.

The level of UPR induction in the 350 gene deletion strains was measured using a fluorescent reporter either in the absence (values represented on the x-axis) or presence (values represented on the y-axis) of ***(A)*** *kar2-P515L::NAT*, ***(B)*** *kar2-P515L-DamP::NAT*, or ***(C)*** *kar2-DamP::NAT*, with each datapoint on the graph corresponding to a unique gene deletion. The horizontal blue line represents the basal level of UPR induction observed in the *kar2* mutant strain. The diagonal blue line represents the expected values of UPR induction in each of the individual deletions if the presence of the *kar2* allele does not induce an additional ER stress. The red line represents the 'best fit' curve to the predicted values in the double mutant strains when each gene deletion is combined with *kar2-P515L, kar2-P515L-DamP* or *kar2-DamP*.

induction in each of the individual deletion strains if the presence of wild-type or mutant *kar2* does not induce an additional ER stress or alternately, result in a reduction of ER stress. Therefore, if a datapoint lies on the diagonal blue line, this suggests that the corresponding gene deletion exhibits an epistatic effect on wild-type or mutant BiP. Finally, the red line represents the 'best fit' curve to the predicted values in the double mutant strains when each gene deletion is combined with wild-type or mutant *KAR2*; the predicted values are computationally generated as described in Jonikas *et al*[121]. If the experimental values lie on the red line, it is suggestive of a lack of genetic interaction between the gene deletion and wild-type or mutant *kar2*. Conversely, if the experimental values lie either above or below this line, it is indicative of aggravating or alleviating genetic interactions, respectively. There are several ways in which such datapoints can be interpreted. Aggravating interactions can occur when a given gene deletion and wild-type or mutant BiP affect the function of parallel pathways or protein complexes. Alleviating interactions can occur when a given gene deletion and wild-type or mutant BiP affect the function of the same pathway or protein complex. Therefore, based on the observed UPR induction values, it is possible to generate hypotheses as to whether the gene corresponding to an individual deletion complements BiP function. This becomes especially useful in the case of understanding potential functions of uncharacterized open reading frames.

Another key feature of the graphs which is indicative of the behavior of the wild-type and mutant *kar2* strains in this UPR-based genetic assay is the location of the datapoints corresponding to *hac1Δ* and *ire1Δ*[121]. To recapitulate, Ire1p is the ER transmembrane signal transducer kinase of the UPR, and its downstream target, Hac1p, is the dedicated transcriptional regulator of the UPR (refer to section 1.2.7). Therefore, in the absence of either *hac1* or *ire1,* the UPR cannot be induced, and datapoints corresponding to *hac1Δ* and *ire1Δ* should lie on the

diagonal blue line, very close to the (0,0) value on the graph. Accordingly, in Figure 18, parts A and B, and in Figure 36A, the positions of the *hac1Δ* and *ire1Δ* datapoints are as expected. This indicates that the genetic interaction profiles obtained for the *KAR2::NAT, kar2-R217A::NAT, kar2-P515L::NAT* strains are robust and can be trusted. However, as observed in Figure 36, parts B and C, the positions of the *hac1Δ* and *ire1Δ* datapoints are either on the red line or are skewed from the diagonal blue line. This indicates that the behavior of the *kar2-P515L-DamP::NAT* and *kar2-DamP::*NAT strains in the UPR-based genetic assay cannot be trusted. The reason for this effect is not clear. Overall, I can conclude that this assay has lent us valuable information with regard to the genetic interactions of *kar2-R217A* and *kar2-P515L*, and I begin to address some of these in the subsequent sections.

B.4 PRELIMINARY CHARACTERIZATION OF SELECT GENETIC INTERACTIONS EXHIBITED BY R217A BIP

Since the *kar2-R217A::NAT* strain was the focus of this study, computational analysis was used to generate a correlation coefficient that quantified the similarity of genetic interactions exhibited by *KAR2::NAT* or *kar2-R217A::NAT* and *yfg::KANMX*. Deletion strains that exhibited the highest values of the correlation coefficient were considered most similar to *KAR2::NAT* or *kar2-R217A::NAT* with regard to their genetic interactions with the 349 other deletion strains. Based on this, it was determined that the genetic interaction profiles of *sec71Δ* and *sec72Δ* yeast (Sec71p and Sec72p are components of the Sec63 complex; refer to section 1.2.4) were highly correlated to that of *kar2-R217A::NAT*. Therefore, this novel genetic screen independently

confirmed that the expression of R217A BiP from its endogenous promoter resulted in a translocation-specific phenotype, as predicted (Chapter 2).

A second value was generated which corresponded to the likelihood of genetic interactions between *KAR2::NAT* or *kar2-R217A::NAT* and *yfg::KANMX*. Again, the more positive this value, the higher the probability that *KAR2::NAT* or *kar2-R217A::NAT* and *yfg::KANMX* genetically interact. To identify the most suitable candidates for further analysis, I asked whether a given gene deletion showed a positive genetic interaction value with *kar2-R217A::NAT*, *sec71Δ* and *sec72Δ*. This would increase the possibility that the corresponding gene participates in translocation. The results from this analysis, as summarized in Table 7, led to the identification of *ilm1Δ, sur4Δ* and *erd1Δ* as putative candidates for analysis in translocation assays. In Chapter 2, I showed that *ilm1Δ* yeast exhibit a specific defect for BiP translocation and also established an interaction between Ilm1p and components of the translocation machinery (Figures 18 and 19). Here, I report on the initial characterization of *sur4Δ* and *erd1Δ* yeast.

The first property of the *sur4Δ* and *erd1Δ* strains that I examined was the *in vivo* translocation efficiencies for pre-pro-alpha factor (ppαF) and BiP. I found that ppαF and pre-BiP did not accumulate in these strains (Figure 37A) as compared to the *sec63-1* control, suggesting that Sur4p and Erd1p do not play a role in translocation. In contrast, when I performed *in vitro* assays for ppαF translocation, I found that microsomes derived from *sur4Δ* and *erd1Δ* yeast were deficient for ppαF translocation as compared to microsomes derived from the BY4742 wild-type strain (Figure 37B). This was initially surprising, but given that Sur4p is a fatty acid elongase[318, 319], it is possible that the integrity of the ER is affected in *sur4Δ* yeast. Therefore, the microsomal membranes derived from these cells might be fragile/defective, in turn affecting translocation efficiency. On the other hand, although Erd1p is an uncharacterized protein, the

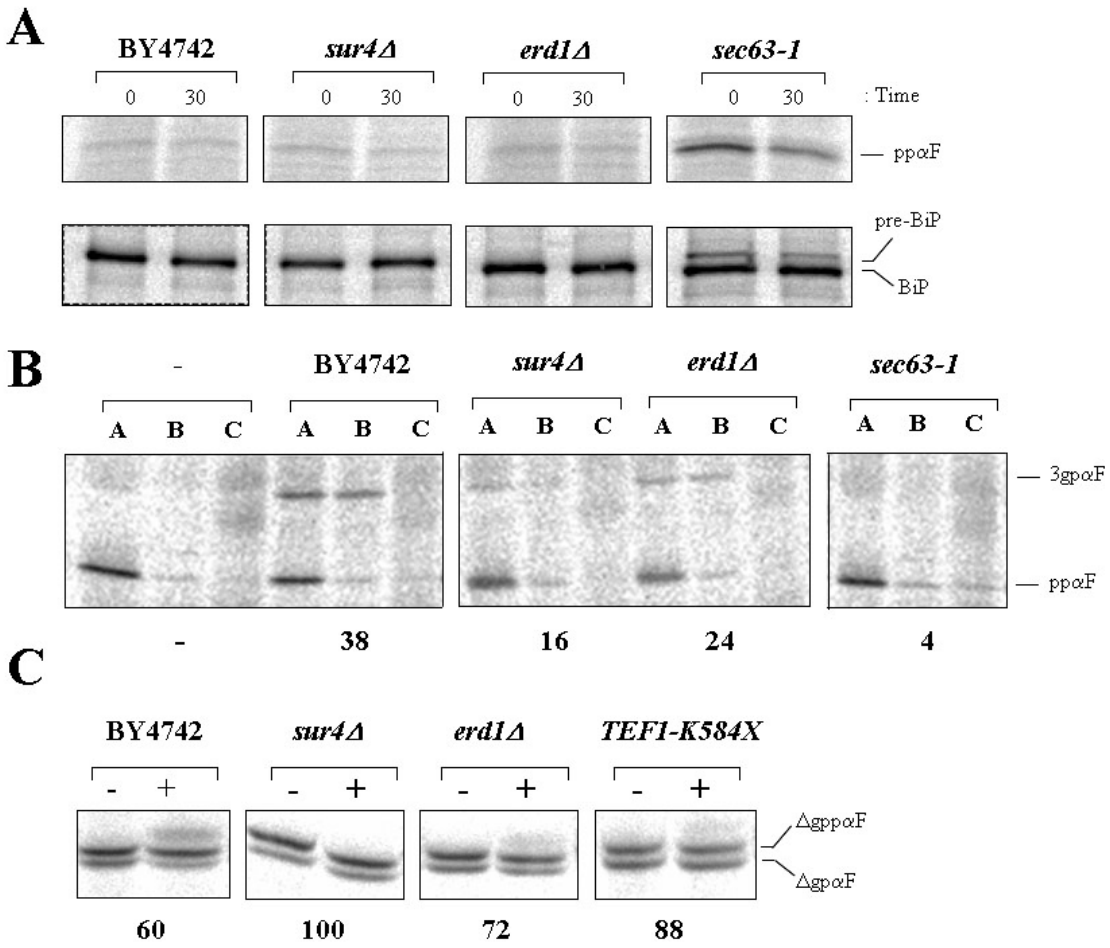
A
BY4742
sur4Δ
erd1Δ
sec63-1
0 30
: Time
ppαF
pre-BiP
BiP
B
-
BY4742
sur4Δ
erd1Δ
sec63-1
A B C
3gpαF
ppαF
- 38 16 24 4
C
BY4742
sur4Δ
erd1Δ
TEF1-K584X
- +
ΔgppαF
ΔgpαF
60 100 72 88
D
%CPY* remaining
100
80
60
40
20
0
0 30 60 90 120
Time (min)

Figure 37: Characterization of the translocation and ERAD efficiencies of *sur4Δ* and *erd1Δ* yeast.

(A) The translocation efficiency of ppαF and BiP was assessed in the indicated wild-type and mutant strains by performing a pulse-chase followed by immunoprecipitation assay at 30°C. The *sec63-1* strain which carries a translocation-defective allele of *SEC63* served as a positive control. ***(B)*** The ability of microsomes derived from the indicated strains to translocate ppαF was measured at 20°C. Each sample was divided and treated in one of three ways: A-buffer alone, B-trypsin, C-trypsin and triton X-100. The percent translocation efficiency is indicated below each panel. Data are representative of a minimum of two independent experiments. ***(C)*** *In vitro* ERAD assays using microsomes derived from the indicated strains were performed either in the absence (-) or presence (+) of an ATP regenerating system and 0.5 mg/ml of yeast cytosol at 30°C. Microsomes derived from the *TEF1-K584X* strain served as a positive control. The percent ERAD efficiency is indicated below each panel. Data are representative of a minimum of two independent experiments. ***(D)*** The CPY* ERAD efficiencies of wild-type (BY4742) (■), *sur4Δ* (△), and *erd1Δ* yeast (◇) were compared using cycloheximide chase assays at 30°C. Data represent the means of a minimum of three independent experiments ± standard errors.

erd1Δ strain exhibits a BiP secretion phenotype[316, 317]. Therefore, the microsomes derived from *erd1Δ* yeast might have reduced amounts of BiP which could indirectly affect translocation.

Next, I tested the ERAD efficiencies of the *sur4Δ* and *erd1Δ* strains. I analyzed the degradation of mutant pαF *in vitro* and found that there was a marked stabilization (~100%) of mutant pαF in microsomes prepared from the *sur4Δ* strain (Figure 37C), and as slight stabilization (~72%) in the microsomes prepared from *erd1Δ* yeast. Again, these ERAD defects may be attributed to the reduced integrity of *sur4Δ* microsomes, and the reduced amounts of BiP present in *erd1Δ* microsomes. Finally, I tested the ability of these strains to degrade CPY* using cycloheximide chase assays *in vivo* (Figure 37D). Intriguingly, while the *sur4Δ* strain (top panel of Figure 37D) did not exhibit a significant defect for CPY* degradation, there was an acceleration of CPY* degradation in the *erd1Δ* strain (bottom panel of Figure 37D). However, since the *erd1Δ* strain secretes BiP[316, 317], it is possible that the accelerated degradation observed in Figure 37D is an indirect effect of CPY* secretion. Alternately, a factor other than BiP that contributes to CPY* folding/stabilization might be secreted in *erd1Δ* yeast, and it will be interesting to determine the identity of this pro-stabilization factor.

Another uncharacterized gene that I analyzed was *YLR104w*. Although *ylr104wΔ* did not exhibit a positive genetic interaction with R217A BiP, it showed positive genetic interactions with *sec71Δ* and *sec72Δ* yeast (Table 7 of Appendix B). Ylr104p is predicted to be an integral membrane protein of the ER, and the study by Jonikas *et al.* grouped Ylr104p with proteins that participate in ERAD[121]. First, I examined the translocation efficiency of *ylr104wΔ* yeast and found that ppαF and pre-BiP did not accumulate in this strain (Figure 38A), indicating that Ylr104p does not contribute to translocation. Next, I examined the ability of *ylr104wΔ* yeast to

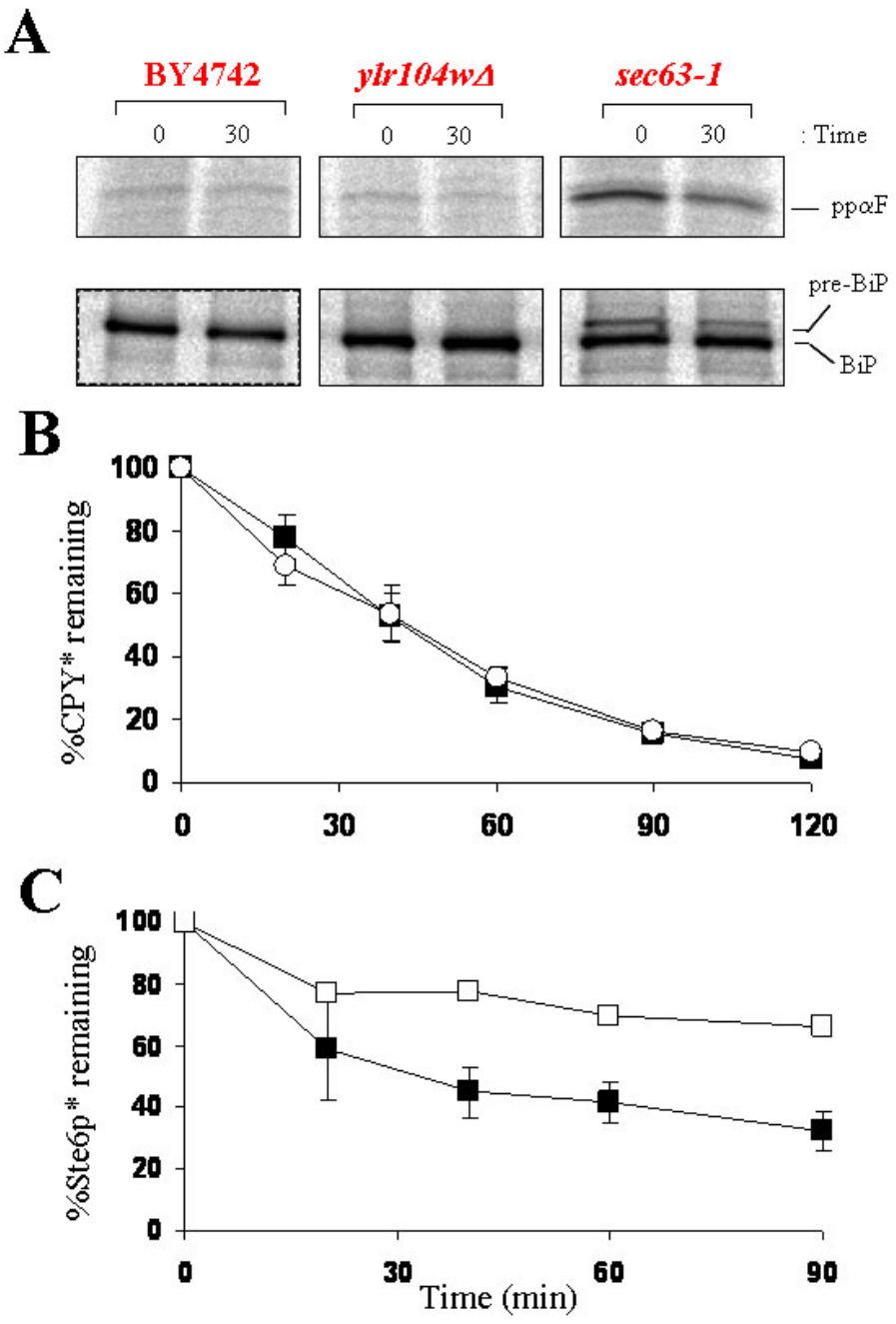
A
BY4742
ylr104wΔ
sec63-1
0
30
0
30
0
30
: Time
ppαF
pre-BiP
BiP
B
%CPY* remaining
100
80
60
40
20
0
0
30
60
90
120
C
%Ste6p* remaining
100
80
60
40
20
0
0
30
60
90
Time (min)

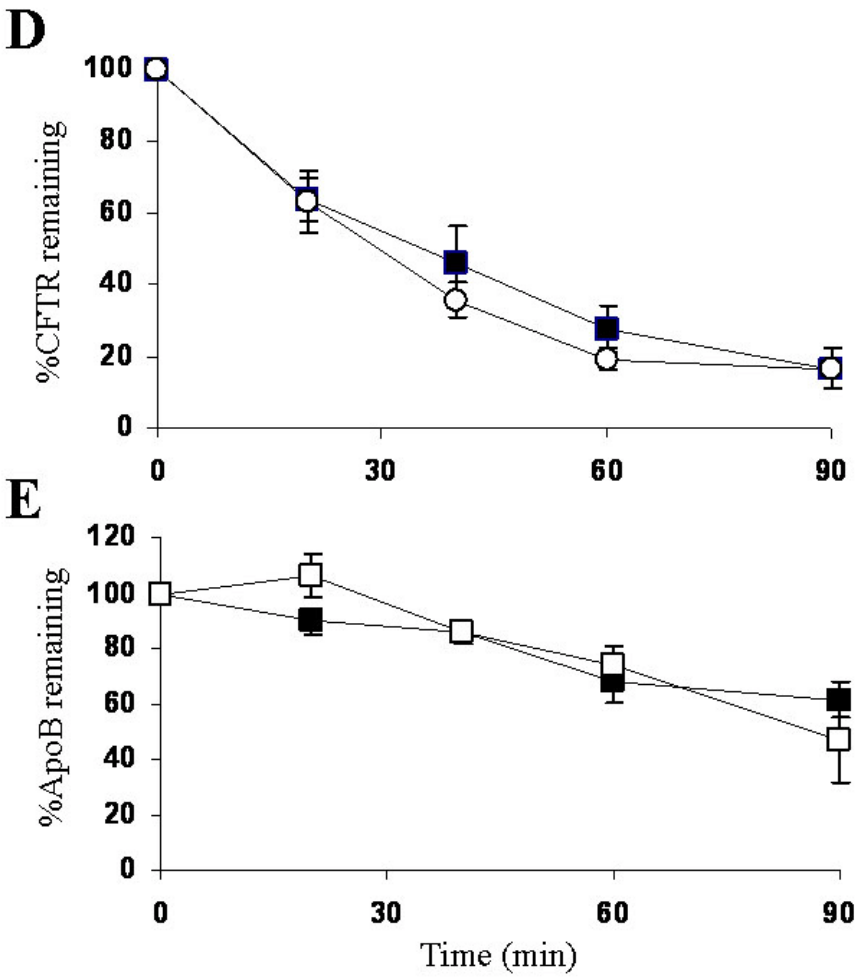

Figure 38: Characterization of the translocation and ERAD efficiencies of *ylr104wΔ* yeast.

(A) The translocation efficiency of ppαF and BiP was assessed in the indicated wild-type and mutant strains by performing a pulse-chase followed by immunoprecipitation assay at 30°C. The *sec63-1* strain which carries a translocation-defective allele of *SEC63* served as a positive control. The ERAD efficiencies of wild-type (BY4742) (■) and *ylr104wΔ* (□) yeast were compared using a cycloheximide chase assay for ***(B)*** CPY* (assayed at 30°C), ***(C)*** Ste6p* (assayed at 37°C), ***(D)*** CFTR (assayed at 40°C), and ***(E)*** ApoB29 (assayed at 30°C). Data represent the means of a minimum of three independent experiments ± standard errors. The data for Ste6p* ERAD in the *ylr104wΔ* strain are preliminary and will be repeated.

degrade different classes of ERAD substrates *in vivo*: (i) substrates with ER lumenal lesions, such as CPY* (Figure 38B); (ii) integral membrane substrates with cytosolic lesions, such as Ste6p* (Figure 38C) and CFTR (Figure 38D); and (iii) co-translocationally degraded substrates such as ApoB29 (Figure 38E). While CPY*, CFTR and ApoB29 were efficiently turned-over in *ylr104wΔ* yeast, I observed that there was a marked stabilization of Ste6p* as compared to the wild-type strain. Therefore, it is possible that Ylr104p contributes to the ERAD of select integral membrane substrates. Two other integral membrane substrates that remain to be tested are Sec61-2p, a mutant form of the translocon subunit Sec61p[395], and HMG-CoA reductase, a key enzyme in the sterol biosynthesis pathway that is regulated by ERAD[396].

Overall, the genetic interactions exhibited by R217A BiP have led to the formulation of several new hypotheses which remain to be tested.

B.5 A BRIEF ANALYSIS OF THE GENETIC INTERACTIONS EXHIBITED BY P515L BIP

It is evident from the position of the horizontal blue line in the genetic interaction profile of *kar-P515L::NAT* (Figure B5-A) that there is a very high basal induction of the UPR upon P515L BiP expression, as expected[181]. Furthermore, the proximity of the red line to the horizontal blue line, and the clustering of several datapoints onto the red line, indicate that a majority of the gene deletions do not exhibit genetic interactions with *kar2-P515L::NAT*. However, a subset of the datapoints localizes to the diagonal blue line, suggesting that the corresponding gene deletions are epistatic to P515L BiP. Strikingly, all the members of the GET complex (*get1Δ*, *get2Δ* and *get3Δ*), which is required for tail-anchored protein insertion[397], and several members of the N-

linked glycosylation pathway that are involved in the assembly of the oligosaccharide moiety[398] (*alg3Δ, alg5Δ, alg6Δ, alg8Δ, alg9Δ, alg12Δ* and *ost3Δ),* belong to this category. While this effect could be an experimental artefact, the presence of several members of a complex or pathway suggests that this is a true genetic interaction.

What is the significance of the epistasis exhibited by members of the GET complex for P515L BiP? It has been observed that deletion of the members of the GET complex leads to BiP secretion[333]. Accordingly, it is feasible that a reduction in the amounts of P515L BiP in the ER of *kar2-P515L::NAT getΔ* strains results in an ER environment that resembles the single *getΔ* strains. This is observed as an epistatic genetic interaction in the UPR-based screen. Alternately, the genetic interaction might be an indirect effect of GET complex function. The GET complex is required for the membrane insertion of tail-anchored (TA) proteins, *i.e.,* proteins that are inserted into lipid bilayers via a single C-terminal transmembrane domain[397]. TA proteins participate in multiple processes including protein translocation into the ER (*i.e.,* Sbh1p), secretory vesicle fusion (*i.e.,* SNAREs), membrane protein degradation, and apoptotic signaling (i.e., Bcl2 in mammalian cells). One such SNARE, Sec22p, plays a key role in the retention of several ER-lumenal proteins, including BiP, in the yeast ER[383, 399, 400]. Therefore, it is formally possible that deletion of members of the GET complex in the *kar2-P515L::NAT* strain results in Sec22p mislocalization, in turn affecting P515L BiP retention in the ER. This possibility is also supported by the epistatic interactions exhibited by *sec22Δ* towards *kar2-P515L::NAT* (figure 36A). Another intriguing scenario is that BiP plays an as yet unidentified role in TA protein insertion, which may be addressed in the future.

Likewise, what are the consequences of the genetic interactions between P515L BiP and members of the N-linked glysocylation pathway? A previous study demonstrated that mutant

alleles of an essential member of the oligosaccharyltransferase complex, *WBP1*, exhibit synthetic interactions with the *kar2-1* allele of BiP (*kar2-1* encodes P515L BiP), establishing the first connection between the N-linked glycosylation pathway and P515L BiP[401]. Since the addition of N-linked glycans is required for the stable folding of several secretory glycoproteins[402], this study suggested that combining an N-glycosylation defect with a mutant *kar2* allele that is defective for folding generates high levels of ER folding stress. This, in turn, affects cell growth. The epistatic effects exhibited by the *alg3Δ, alg5Δ, alg6Δ, alg8Δ, alg9Δ, alg12Δ* and *ost3Δ* strains for *kar2-P515:::NAT* in the screen described here can also be interpreted in light of the folding defects that may arise due to P515L BiP expression. Conversely, it is also well-known that the glycosylation status of mutant proteins, in particular the number and positioning of the N-linked glycans, is an important recognition element for the ERAD machinery[5]. Therefore, in the absence of the correct glycans, it is possible that proteins are inefficiently recognized and/or targeted for degradation. In such a situation, BiP function during ERAD may become unnecessary. However, all of these hypotheses are rudimentary and need to be addressed in the future.

Given the ERAD-specific defect exhibited by P515L BiP[181], the genetic interaction profile of *kar-P515L::NAT* was expected to resemble other ERAD-related genes such as *hrd1Δ* and *yos9Δ*. Surprisingly, this screen resulted in the identification of several novel and unprecedented P515L BiP interactions. Moreover, since the *kar-P515L::NAT* genetic interaction profile does not show a significant correlation to the profile of any other gene deletion in this UPR-based screen, it will be interesting to further test this mutant in a growth/colony size-based assay in which the *kar-P515L::NAT* strain will be crossed against the entire YKO collection.

Table 6: A list of the genes that were analyzed in the UPR-based screen

Gene name	ORF	Cellular localization	Function (either established or predicted)
ADD66/PAC2	*YKL206C*	cytoplasm	Proteasome assembly; also plays a role in ERAD
AGX1	*YFL030W*	mitochondrion	Alanine : glyoxylate aminotransferase, catalyzes the synthesis of glycine from glyoxylate,
AHC2	*YCR082W*	cytoplasm, nucleus	Protein of unknown function, putative transcriptional regulator; proposed to be a Ada Histone acetyltransferase complex component
ALF1	*YNL148C*	ambiguous	Alpha-tubulin folding protein, similar to mammalian cofactor B; apart from folding alpha-tubulin,may play an additional role in microtubule maintenance
ALG12	*YNR030W*	ER	Alpha-1,6-mannosyltransferase involved in the N-linked glycosylation pathway
ALG3	*YBL082C*	cytoplasm, vacuole	Dolichol-P-Man dependent alpha(1-3) mannosyltransferase involved in the N-linked glycosylation pathway
ALG5	*YPL227C*	ER	UDP-glucose:dolichyl-phosphate glucosyltransferase involved in asparagine-linked glycosylation in the endoplasmic reticulum
ALG6	*YOR002W*	ER	Glucosyltransferase, involved in transfer of oligosaccharides from dolichyl pyrophosphate to asparagine residues of proteins during N-linked protein glycosylation
ALG8	*YOR067C*	ER membrane	Glucosyltransferase similar to Alg6p
ALG9	*YNL219C*	ER	Mannosyltransferase, involved in N-linked glycosylation; catalyzes the transfer of mannose from Dol-P-Man to lipid-linked oligosaccharides
APE3	*YBR286W*	ER membrane	Vacuolar aminopeptidase Y, processed to mature form by Prb1p
ARC18	*YLR370C*	actin?	Subunit of the ARP2/3 complex, which is required for the motility and integrity of cortical actin patches
ARL1	*YBR164C*	punctate composite, early Golgi	Soluble GTPase with a role in regulation of membrane traffic; regulates potassium influx; G protein of the Ras superfamily, similar to ADP-ribosylation factor

ARO1	*YDR127W*	cytoplasm	Pentafunctional arom protein, catalyzes steps 2 through 6 in the biosynthesis of chorismate, which is a precursor to aromatic amino acids
ARP6	*YLR085C*	cytoplasm, nucleus	Nuclear actin-related protein involved in chromatin remodeling
ARV1	*YLR242C*	ER/Golgi	Protein required for normal intracellular sterol distribution and for sphingolipid metabolism; similar to Nup120p
ASM4	*YDL088C*	nuclear periphery	Nuclear pore complex subunit, part of a subcomplex also containing Nup53p, Nup170p, and Pse1p
ATG8	*YBL078C*	cytoplasm	Protein involved in autophagy; E2-like enzyme that plays a role in formation of Atg8p-phosphatidylethanolamine conjugates
BNR1	*YIL159W*	bud neck	Formin, nucleates the formation of linear actin filaments during budding and mitotic spindle orientation; functionally redundant with BNI1
BOP2	*YLR267W*	0	Protein of unknown function, overproduction suppresses a pam1 slv3 double null mutation
BRE5	*YNR051C*	cytoplasm	Ubiquitin protease cofactor; forms deubiquitination complex with Ubp3p that coregulates anterograde and retrograde transport between the ER and Golgi compartments
BST1	*YFL025C*	ER	GPI inositol deacylase of the ER that negatively regulates COPII vesicle formation
BTS1	*YPL069C*	mitochondrion	Geranylgeranyl diphosphate synthase; increases the intracellular pool of geranylgeranyl diphosphate,
BUG1	*YDL099W*	punctate composite, early Golgi	Protein of unknown function
CAC2	*YML102W*	Nucleus	Component of the chromatin assembly complex (with Rlf2p and Msi1p) that assembles newly synthesized histones onto recently replicated DNA
CAJ1	*YER048C*	Nucleus, cytoplasm	Nuclear type II Hsp40
CAP1	*YKL007W*	Cortical actin	Beta subunit of the capping protein (CP) heterodimer (Cap1p and Cap2p) which binds to the barbed ends of actin filaments preventing further polymerization
CCW12	*YLR110C*	ER/Cell wall	Cell wall protein, mutants are defective in mating and agglutination

CKA2	*YOR061W*	cytoplasm, nucleus	Alpha' catalytic subunit of casein kinase 2, a Ser/Thr protein kinase with roles in cell growth and proliferation
CNE1	*YAL058W*	ER	Calnexin; integral membrane ER chaperone involved in folding and quality control of glycoproteins;
COG5	*YNL051W*	Golgi, early Golgi	Component of the conserved oligomeric Golgi complex (Cog1p through Cog8p), a cytosolic tethering complex that functions in protein trafficking
COG6	*YNL041C*	Golgi	Component of the conserved oligomeric Golgi complex (Cog1p through Cog8p)
COG8	*YML071C*	punctate composite	Component of the conserved oligomeric Golgi complex (Cog1p through Cog8p)
CPA1	*YOR303W*	cytoplasm	Small subunit of carbamoyl phosphate synthetase, which catalyzes a step in the synthesis of citrulline, an arginine precursor
CPR6	*YLR216C*	cytoplasm	Peptidyl-prolyl cis-trans isomerase (cyclophilin), catalyzes the cis-trans isomerization of peptide bonds N-terminal to proline residues
CRD1	*YDL142C*	mitochondrion	Cardiolipin synthase; produces cardiolipin, an important constituent of mitochondrial membranes that is required for normal mitochondrial membrane potential and function
CSF1	*YLR087C*	0	Protein required for fermentation at low temperature
CSN12	*YJR084W*	cytoplasm, nucleus	Subunit of the Cop9 signalosome, which is required for deneddylation, or removal of the ubiquitin-like protein Rub1p from Cdc53p (cullin)
CUE1	*YMR264W*	ER, cytoplasm	Endoplasmic reticulum membrane protein that recruits the E2 ubiquitin-conjugating enzyme Ubc7p to the ER where it functions in protein degradation
CWH41	*YGL027C*	ER membrane	Processing alpha glucosidase I; ER type II integral membrane N-glycoprotein involved in assembly of cell wall beta 1,6 glucan and asparagine-linked protein glycosylation
CWH43	*YCR017C*	ER	Putative sensor/transporter protein involved in cell wall biogenesis
CYS3	*YAL012W*	cytoplasm	Cystathionine gamma-lyase, catalyzes one of the two reactions involved in the transsulfuration pathway that yields cysteine from homocysteine
DAL81	*YIR023W*	nucleus	Positive regulator of genes in multiple nitrogen degradation pathways

DAS1	*YJL149W*	0	Putative SCF ubiquitin ligase F-box protein of unknown function; interacts physically with both Cdc53p and Skp1 and genetically with CDC34
DER1	*YBR201W*	ER membrane	Involved in ER-associated protein degradation, during retrotranslocation
DFG10	*YIL049W*	0	Protein of unknown function, involved in filamentous growth
DGK1/HSD1	*YOR311C*	ER	Overproduction induces enlargement of ER-like membrane structures and suppresses a temperature-sensitive sly1 mutation
DIE2	*YGR227W*	0	Dolichyl-phosphoglucose-dependent glucosyltransferase of the ER; involved in N-linked glycosylation
DOM34	*YNL001W*	cytoplasm	Probable RNA-binding protein, functions in protein translation to promote G1 progression and differentiation
DRS2	*YAL026C*	early Golgi, late Golgi	Integral membrane Ca(2+)-ATPase involved in aminophospholipid translocation
DUS3	*YLR401C*	cytoplasm, nucleus	Dihydrouridine synthase, member of a widespread family of conserved proteins including Smm1p, Dus1p, and Dus4p
ECM30	*YLR436C*	cytoplasm	Non-essential protein of unknown function
EDE1	*YBL047C*	punctate composite	Key endocytic protein, binds to membranes in a ubiquitin-dependent manner
EGD1	*YPL037C*	cytoplasm	Subunit beta1 of the nascent polypeptide-associated complex (NAC) involved in protein targeting
EGD2	*YHR193C*	cytoplasm	Alpha subunit of the heteromeric nascent polypeptide-associated complex (NAC)
ELF1	*YKL160W*	nucleus	Transcription elongation factor that contains a conserved zinc finger domain
ELP2	*YGR200C*	cytoplasm	Elongator protein, part of the six-subunit RNA polymerase II Elongator histone acetyltransferase complex
EMP47	*YFL048C*	vacuolar membrane	Integral membrane component of ER-derived COPII-coated vesicles, which function in ER to Golgi transport
ENT3	*YJR125C*	0	Protein containing an N-terminal epsin-like domain involved in clathrin recruitment and traffic between the Golgi and endosomes; associates with the clathrin adaptor Gga2p
ERD1	*YDR414C*	ambiguous	Predicted membrane protein required for the retention of lumenal endoplasmic reticulum proteins; mutants secrete the endogenous ER protein, BiP (Kar2p)

ERG2	*YMR202W*	ambiguous	C-8 sterol isomerase, catalyzes the isomerization of the delta-8 double bond to the delta-7 position at an intermediate step in ergosterol biosynthesis
ERJ5	*YFR041C*	ER	DnaJ-like protein; may function as a BiP cofactors
ERP1	*YAR002C-A*	vacuolar membrane	Protein that forms a heterotrimeric complex with Erp2p, Emp24p, and Erv25p; involved in COPII-mediated ER to Golgi transport
ERP2	*YAL007C*	ER	Protein that forms a heterotrimeric complex with Erp1p, Emp24p, and Erv25p
ERV14	*YGL054C*	ER, vacuole	Protein localized to COPII-coated vesicles, involved in vesicle formation and incorporation of specific secretory cargo
ERV25	*YML012W*	ER	Protein that forms a heterotrimeric complex with Erp1, Erp2p, and Emp24
ERV29	*YGR284C*	ER	Protein localized to COPII-coated vesicles, involved in vesicle formation and incorporation of specific secretory cargo
ERV41	*YML067C*	ER	Protein localized to COPII-coated vesicles, forms a complex with Erv46p; involved in the membrane fusion stage of transport
ERV46	*YAL042W*	0	Protein localized to COPII-coated vesicles, forms a complex with Erv41p; involved in the membrane fusion stage of transport
EUG1	*YDR518W*	0	Protein disulfide isomerase of the endoplasmic reticulum lumen; may interact with nascent polypeptides in the ER
FAR8	*YMR029C*	ER, cytoplasm	Protein involved in G1 cell cycle arrest in response to pheromone; interacts with Far3p, Far7p, Far9p, Far10p, and Far11p
FAT1	*YBR041W*	lipid particle	Fatty acid transporter and very long-chain fatty acyl-CoA synthetase
FKH1	*YIL131C*	Nucleus	Transcription factor of the forkhead family that regulates the cell cycle and pseudohyphal growth
FLX1	*YIL134W*	0	Protein required for transport of flavin adenine dinucleotide (FAD) from mitochondria to the cytosol
FRE4	*YNR060W*	0	Ferric reductase, reduces a specific subset of siderophore-bound iron prior to uptake by transporters
FUN30	*YAL019W*	Nucleus	Protein whose overexpression affects chromosome stability, potential Cdc28p substrate; homolog of Snf2p

FYV6	*YNL133C*	Nucleus	Protein of unknown function; proposed to regulate double-strand break repair via non-homologous end-joining
GCN2	*YDR283C*	cytoplasm	Protein kinase, phosphorylates the alpha-subunit of translation initiation factor eIF2 (Sui2p) in response to starvation
GCN20	*YFR009W*	cytoplasm	Positive regulator of the Gcn2p kinase activity, forms a complex with Gcn1p
GCN5	*YGR252W*	Nucleus	Histone acetyltransferase, acetylates N-terminal lysines on histones H2B and H3; catalytic subunit of the ADA and SAGA histone acetyltransferase complexes
GCR2	*YNL199C*	0	Transcriptional activator of genes involved in glycolysis
GCS1	*YDL226C*	cytoplasm	ADP-ribosylation factor GTPase activating protein (ARF GAP), involved in ER-Golgi transport
GDA1	*YEL042W*	ambiguous, Golgi	Guanosine diphosphatase involved in the transport of GDP-mannose into the Golgi lumen
GET1	*YGL020C*	ER	Subunit of the GET complex; required for the retrieval of HDEL proteins from the Golgi to the ER in an ERD2 dependent fashion and for tail-anchored protein insertion
GET2	*YER083C*	ER	Subunit of the GET complex
GET3	*YDL100C*	ER	ATPase subunit of the GET complex
GLO3	*YER122C*	Golgi, early Golgi	ADP-ribosylation factor GTPase activating protein (ARF GAP), involved in ER-Golgi transport
GNP1	*YDR508C*	ER,cell periphery	High-affinity glutamine permease, also transports Leu, Ser, Thr, Cys, Met and Asn
GOS1	*YHL031C*	0	v-SNARE protein involved in Golgi transport, homolog of the mammalian protein GOS-28/GS28
GOT1	*YMR292W*	ER	Evolutionarily conserved non-essential protein found in early Golgi cisternae; may be involved in ER-Golgi transport
GSG1	*YDR108W*	cytoplasm	Subunit of TRAPP (transport protein particle); involved in targeting and/or fusion of ER-to-Golgi transport vesicles with their acceptor compartment
GSH2	*YOL049W*	cytoplasm	Glutathione synthetase, catalyzes the ATP-dependent synthesis of glutathione (GSH) from gamma-glutamylcysteine and glycine

GTB1	*YDR221W*	ER	Glucosidase II beta subunit; forms a complex with alpha subunit Rot2p, involved in removal of two glucose residues from N-linked glycans
GTR1	*YML121W*	vacuolar membrane	Cytoplasmic GTP binding protein and negative regulator, of the Ran/Tc4 GTPase cycle
GUP1	*YGL084C*	ER?	Plasma membrane protein with a possible role in proton symport of glycerol; member of the MBOAT family of putative membrane-bound O-acyltransferases
GYP8	*YFL027C*	mitochondrion	GTPase-activating protein for yeast Rab family members; involved in the regulation of ER to Golgi vesicle transport
HAC1	*YFL031W*	cytoplasm, nucleus	bZIP transcription factor (ATF/CREB1 homolog) that regulates the unfolded protein response
HAM1	*YJR069C*	cytoplasm, nucleus	Protein of unknown function that may be involved in DNA repair
HAT2	*YEL056W*	nucleus	Subunit of the Hat1p-Hat2p histone acetyltransferase complex; has a role in telomeric silencing
HEK2	*YBL032W*	cytoplasm	RNA binding protein with similarity to hnRNP-K that localizes to the cytoplasm and to subtelomeric DNA
HHF1	*YBR009C*	nucleus	One of two identical histone H4 proteins (see also HHF2);
HHT1	*YBR010W*	nucleus	One of two identical histone H3 proteins (see also HHT2)
HHT2	*YNL031C*	ambiguous	One of two identical histone H3 proteins (see also HHT1)
HIR3	*YJR140C*	nucleus	Transcriptional corepressor involved in the cell cycle-regulated transcription of histone genes HTA1, HTB1, HHT1, and HHT2
HLJ1	*YMR161W*	ER	Hsp40 Co-chaperone anchored in the ER membrane; promotes ER-associated protein degradation (ERAD) of integral membrane substrates
HMG1	*YML075C*	nuclear periphery	One of two isozymes of HMG-CoA reductase that catalyzes the conversion of HMG-CoA to mevalonate
HOP2	*YGL033W*	nucleus	Meiosis-specific protein that localizes to chromosomes, preventing synapsis between nonhomologous chromosomes and ensuring synapsis between homologs
HPC2	*YBR215W*	nucleus	Highly charged, basic protein required for normal cell-cycle regulation of histone gene transcription

HRD1	*YOL013C*	ER membrane	Ubiquitin-protein ligase required for endoplasmic reticulum-associated degradation; regulated through association with Hrd3p; contains an H2 ring finger
HRD3	*YLR207W*	ER membrane	Forms the HRD complex with Hrd1p and ERAD determinants; engages in ER lumen to cytosol communication and coordination of ERAD events
HSM3	*YBR272C*	cytoplasm	Protein of unknown function, involved in DNA mismatch repair during slow growth; has weak similarity to Msh1p
HSV2	*YGR223C*	Punctate cytoplasmic	Phosphatidylinositol 3,5-bisphosphate-binding protein, predicted to fold as a seven-bladed beta-propeller
HTB2	*YBL002W*	nucleus	One of two nearly identical (see HTB1) histone H2B subtypes required for chromatin assembly and chromosome function
HTZ1	*YOL012C*	nucleus	Histone variant H2AZ; involved in transcriptional regulation through prevention of the spread of silent heterochromatin
HUR1	*YGL168W*	0	Protein required for hydroxyurea resistance; has possible roles in DNA replication and maintenance of proper telomere length
HXK2	*YGL253W*	cytoplasm	Hexokinase isoenzyme 2 that catalyzes phosphorylation of glucose in the cytosol
HXT8	*YJL214W*	0	Protein of unknown function with similarity to hexose transporter family members
ICE2	*YIL090W*	ER membrane	Mutations cause defects in cortical ER morphology in both the mother and daughter cells
IDH1	*YNL037C*	mitochondrion	Subunit of mitochondrial NAD(+)-dependent isocitrate dehydrogenase, which catalyzes the oxidation of isocitrate to alpha-ketoglutarate in the TCA cycle
IES1	*YFL013C*	nucleus	Subunit of the INO80 chromatin remodeling complex
IES4	*YOR189W*	nucleus	Protein that associates with the INO80 chromatin remodeling complex under low-salt conditions
IES5	*YER092W*	nucleus	Protein that associates with the INO80 chromatin remodeling complex under low-salt conditions
ILM1	*YJR118C*	ER	Protein of unknown function; may be involved in mitochondrial DNA maintenance
INP53	*YOR109W*	punctate composite	Phosphatidylinositol 4,5-bisphosphate 5-phosphatase; plays a role in a TGN (trans Golgi network)-to-early endosome pathway

IPK1	*YDR315C*	nucleus	Inositol 1,3,4,5,6-pentakisphosphate 2-kinase; ipk1 gle1 double mutant is inviable
IRC21	*YMR073C*	cytoplasm	Putative protein of unknown function; shares similarity to a human cytochrome oxidoreductase
IRE1	*YHR079C*	ER membrane	Serine-threonine kinase and endoribonuclease; transmembrane protein that initiates the unfolded protein response signal by regulating synthesis of Hac1p through HAC1 mRNA splicing
ISC1	*YER019W*	0	Inositol phosphosphingolipid phospholipase C
ISR1	*YPR106W*	0	Predicted protein kinase, overexpression causes sensitivity to staurosporine, which is a potent inhibitor of protein kinase C
ISW1	*YBR245C*	nucleus	Member of the imitation-switch (ISWI) class of ATP-dependent chromatin remodeling complexes
ISW2	*YOR304W*	nucleus	Member of the imitation-switch (ISWI) class of ATP-dependent chromatin remodeling complexes
ITR1	*YDR497C*	cell periphery, vacuole	Myo-inositol transporter; member of the sugar transporter superfamily
IXR1	*YKL032C*	nucleus	Contains two HMG (high mobility group box) domains and bends cisplatin-modified DNA by binding to the DNA; mediates aerobic transcriptional repression of COX5b
JEM1	*YJL073W*	ER	DnaJ-like chaperone required for nuclear membrane fusion during mating, BiP cofactor during ERAD
KEL1	*YHR158C*	bud neck, cell periphery, bud	Protein required for proper cell fusion and cell morphology; functions in a complex with Kel2p to negatively regulate mitotic exit
KEX2	*YNL238W*	punctate composite, early Golgi	Subtilisin-like protease (proprotein convertase), a calcium-dependent serine protease involved in the activation of proproteins of the secretory pathway
KIN3	*YAR018C*	0	Nonessential protein kinase with unknown cellular role
KRE1	*YNL322C*	ER	Cell wall glycoprotein involved in beta-glucan assembly
KRE11	*YGR166W*	punctate composite	Protein involved in biosynthesis of cell wall beta-glucans; subunit of the TRAPP (transport protein particle) complex

KRE27	*YIL027C*	ER	Protein of unknown function; null mutant shows K1 killer toxin resistance
KTI12	*YKL110C*	cytoplasm	Protein associated with the RNA polymerase II Elongator complex
LAS21	*YJL062W*	ER, plasma membrane	Integral plasma membrane protein involved in the synthesis of the glycosylphosphatidylinositol (GPI) core structure; mutations affect cell wall integrity
LEM3	*YNL323W*	ER, plasma membrane	Membrane protein of the plasma membrane and ER, involved in translocation of phospholipids and alkylphosphocholine drugs across the plasma membrane
LEU3	*YLR451W*	nucleus	Zinc-finger transcription factor that regulates genes involved in branched chain amino acid biosynthesis and ammonia assimilation
LOC1	*YFR001W*	nucleus	Nuclear protein involved in asymmetric localization of ASH1 mRNA; binds double-stranded RNA in vitro; constituent of 66S pre-ribosomal particles
LPD1	*YFL018C*	mitochondrion	The Dihydrolipoamide dehydrogenase of the pyruvate dehydrogenase and 2-oxoglutarate dehydrogenase multi-enzyme complexes
LRC3	*YKL207W*	0	Hypothetical protein
MAF1	*YDR005C*	cytoplasm,nucleus	Negative regulator of RNA polymerase III by targeting the initiation factor TFIIIB
MDY2	*YOL111C*	cytoplasm	Protein required for efficient mating; involved in shmoo formation and nuclear migration in the pre-zygote; contains a ubiquitin-like (UBL) domain
MEH1	*YKR007W*	vacuolar membrane	Component of the EGO complex (involved in the regulation of microautophagy) and GSE complex (required for proper sorting of amino acid permease Gap1p)
MGA2	*YIR033W*	ER membrane	Along with its homolog Spt23p, regulates OLE1 transcription
MKC7	*YDR144C*	vacuole	GPI-anchored aspartyl protease (yapsin) involved in protein processing; shares functions with Yap3p and Kex2p
MNL1	*YHR204W*	ER	Alpha mannosidase-like protein of the endoplasmic reticulum required for degradation of glycoproteins but not for processing of N-linked oligosaccharides

MNN2	*YBR015C*	Golgi	Alpha-1,2-mannosyltransferase, responsible for addition of the first alpha-1,2-linked mannose to form the branches on the mannan backbone of oligosaccharides
MNN4	*YKL201C*	0	Putative positive regulator of mannosylphosphate transferase (Mnn6p), involved in mannosylphosphorylation of N-linked oligosaccharides
MNN5	*YJL186W*	punctate composite	Alpha-1,2-mannosyltransferase, responsible for addition of the second alpha-1,2-linked mannose of the branches on the mannan backbone of oligosaccharides
MNN9	*YPL050C*	Golgi	Subunit of Golgi mannosyltransferase complex containing Anp1p, Mnn10p, Mnn11p, and Hoc1p that mediates elongation of the polysaccharide mannan backbone
MNS1	*YJR131W*	ER membrane	Alpha-1,2-mannosidase involved in ER quality control; catalyzes the removal of one mannose residue from $Man_9GlcNAc$ to produce a single isomer of $Man_8GlcNAc$
MPD1	*YOR288C*	vacuole	Member of the protein disulfide isomerase (PDI) family
MSC1	*YML128C*	ER	Protein of unknown function; msc1 mutants are defective in directing meiotic recombination events to homologous chromatids
MSI1	*YBR195C*	cytoplasm, nucleus	Subunit of chromatin assembly factor I (CAF-I); homologous to human retinoblastoma binding proteins RbAp48 and RbAp46
MTC1	*YJL123C*	cytoplasm, Golgi, early Golgi	Putative protein of unknown function; mtc1 is synthetically lethal with cdc13-1
MTC5	*YDR128W*	vacuolar membrane	Hypothetical protein
MVP1	*YMR004W*	endosome	Protein required for sorting proteins to the vacuole; Mvp1p and Vps1p act in concert to promote membrane traffic to the vacuole
NEM1	*YHR004C*	punctate composite	Protein of the nuclear envelope required for the spherical shape of the nucleus; required for normal sporulation
NFT1	*YKR103W*	cytoplasm,nucleus	Putative transporter of the multidrug resistance-associated protein (MRP) subfamily.
NHP6A	*YPR052C*	nucleus	High-mobility group non-histone chromatin protein, functionally redundant with Nhp6Bp; acts to recruit transcription factor Rcs1p to certain promoters

NHX1	*YDR456W*	endosome	Endosomal Na+/H+ exchanger, required for intracellular sequestration of Na+
NMD4	*YLR363C*	cytoplasm	Protein interacting with Nam7p, may be involved in the nonsense-mediated mRNA decay pathway
NPL4	*YBR170C*	cytoplasm, nucleus	Forms a complex with Cdc48p and Ufd1p that recognizes ubiquitinated proteins in the endoplasmic reticulum and delivers them to the proteasome for degradation
OLA1	*YBR025C*	cytoplasm	Hypothetical protein
OPI10	*YOL032W*	cytoplasm, nucleus	ORF, Uncharacterized
OPI3	*YJR073C*	ER, vacuole	Phospholipid methyltransferase (methylene-fatty-acyl-phospholipid synthase), catalyzes the last two steps in phosphatidylcholine biosynthesis
OST3	*YOR085W*	ER	Gamma subunit of the oligosaccharyltransferase complex of the ER lumen, which catalyzes N-linked glycosylation of newly synthesized proteins
OST5	*YGL226C-A*	ER	Zeta subunit of the oligosaccharyltransferase complex of the ER lumen, which catalyzes N-linked glycosylation of newly synthesized proteins
OYE2	*YHR179W*	cytoplasm, nucleus	Widely conserved NADPH oxidoreductase containing flavin mononucleotide (FMN)
PBP1	*YGR178C*	cytoplasm, nucleus	Protein interacting with poly(A)-binding protein Pab1p; may be involved in controlling the extent of mRNA polyadenylation
PCT1	*YGR202C*	nuclear periphery	Cholinephosphate cytidylyltransferase, also known as CTP:phosphocholine cytidylyltransferase, rate-determining enzyme of the CDP-choline pathway for phosphatidylcholine synthesis
PEF1	*YGR058W*	cytoplasm, nucleus	Putative protein of unknown function
PEP7	*YDR323C*	endosome	Multivalent adaptor protein that facilitates vesicle-mediated vacuolar protein sorting by ensuring high-fidelity vesicle docking and fusion
PEP8	*YJL053W*	endosome	Vacuolar sorting protein that forms part of the multimeric membrane-associated retromer complex along with Vps35p, Vps29p, Vps17p, and Vps5p; essential for endosome-to-Golgi retrograde protein transport

PET18	*YCR020C*	ambiguous	Protein required for respiratory growth and stability of the mitochondrial genome
PHO80	*YOL001W*	cytoplasm, nucleus	Cyclin, negatively regulates phosphate metabolism; Pho80p-Pho85p (cyclin-CDK complex) phosphorylates Pho4p and Swi5p; truncated form of PHO80 affects vacuole inheritance
PHO86	*YJL117W*	ER	Required for ER exit of the high-affinity phosphate transporter Pho84p, specifically required for packaging of Pho84p into COPII vesicles
PMP1	*YCR024C-A*	cell periphery, vacuole	Small single-membrane span proteolipid that functions as a regulatory subunit of the plasma membrane H(+)-ATPase Pma1p
PMR1	*YGL167C*	ER	High affinity Ca2+/Mn2+ P-type ATPase required for Ca2+ and Mn2+ transport into Golgi; involved in Ca2+ dependent protein sorting and processing
PMT1	*YDL095W*	ER membrane	Protein O-mannosyltransferase, transfers mannose residues from dolichyl phosphate-D-mannose to protein serine/threonine residues; acts in a complex with Pmt2p
PMT2	*YAL023C*	ER	Protein O-mannosyltransferase, transfers mannose residues from dolichyl phosphate-D-mannose to protein serine/threonine residues; acts in a complex with Pmt1p
PPH21	*YDL134C*	cytoplasm, nucleus	Catalytic subunit of protein phosphatase 2A, functionally redundant with Pph22p
PPT1	*YGR123C*	cytoplasm, nucleus	Protein serine/threonine phosphatase with similarity to human phosphatase PP5
PRM2	*YIL037C*	vacuole	Pheromone-regulated protein, predicted to have 4 transmembrane segments and a coiled coil domain; regulated by Ste12p
PSD2	*YGR170W*	Golgi, vacuole	Phosphatidylserine decarboxylase of the Golgi and vacuolar membranes, converts phosphatidylserine to phosphatidylethanolamine
PTC2	*YER089C*	cytoplasm, nucleus	Type 2C protein phosphatase; dephosphorylates Hog1p to limit maximal osmostress induced kinase activity; dephosphorylates Ire1p to downregulate the unfolded protein response
PTK2	*YJR059W*	cytoplasm	Putative serine/threonine protein kinase involved in regulation of ion transport across plasma membrane

PTP1	*YDL230W*	cytoplasm, mitochondria	Phosphotyrosine-specific protein phosphatase that dephosphorylates a broad range of substrates in vivo
PTR2	*YKR093W*	cell periphery, vacuole	Integral membrane peptide transporter, mediates transport of di- and tri-peptides
RAD23	*YEL037C*	cytoplasm, nucleus	Protein with ubiquitin-like N terminus, recognizes and binds damaged DNA (with Rad4p) during nucleotide excision repair
RAV1	*YJR033C*	ambiguous	Subunit of the RAVE complex (Rav1p, Rav2p, Skp1p), which promotes assembly of the V-ATPase holoenzyme
RCO1	*YMR075W*	nucleus	Essential subunit of the histone deacetylase Rpd3S complex; interacts with Eaf3p
RER1	*YCL001W*	punctate composite	Protein involved in retention of membrane proteins, including Sec12p, in the ER
REX4	*YOL080C*	nucleolus, nucleus	Putative RNA exonuclease possibly involved in pre-rRNA processing and ribosome assembly
RGP1	*YDR137W*	early Golgi	Subunit of a Golgi membrane exchange factor (Ric1p-Rgp1p) that catalyzes nucleotide exchange on Ypt6p
RLF2	*YPR018W*	Nucleus	Largest subunit (p90) of the Chromatin Assembly Complex (CAF-I); along with Cac2p and Msi1p, assembles newly synthesized histones onto recently replicated DNA
ROT2	*YBR229C*	ER, mitochondrion	Glucosidase II catalytic subunit required for normal cell wall synthesis
ROX1	*YPR065W*	nucleus	Heme-dependent repressor of hypoxic genes; contains an HMG domain that is responsible for DNA bending activity
RPA14	*YDR156W*	nucleolus	RNA polymerase I subunit A14
RPL19B	*YBL027W*	cytoplasm	Protein component of the large (60S) ribosomal subunit, nearly identical to Rpl19Ap
RPN10	*YHR200W*	cytoplasm, nucleus	Non-ATPase base subunit of the 19S regulatory particle (RP) of the 26S proteasome
RPS11A	*YDR025W*	cytoplasm	Protein component of the small (40S) ribosomal subunit; identical to Rps11Bp
RPS12	*YOR369C*	cytoplasm	Protein component of the small (40S) ribosomal subunit; has similarity to rat ribosomal protein S12

RPS16A	*YMR143W*	cytoplasm	Protein component of the small (40S) ribosomal subunit; identical to Rps16Bp
RPS17A	*YML024W*	cytoplasm	Ribosomal protein 51 (rp51) of the small (40s) subunit; nearly identical to Rps17Bp
RPS23A	*YGR118W*	cytoplasm	Ribosomal protein 28 (rp28) of the small (40S) ribosomal subunit, required for translational accuracy; nearly identical to Rps23Bp
RPS28B	*YLR264W*	cytoplasm	Protein component of the small (40S) ribosomal subunit; nearly identical to Rps28Ap
RPS4B	*YHR203C*	cytoplasm	Protein component of the small (40S) ribosomal subunit; identical to Rps4Ap
RPS6B	*YBR181C*	cytoplasm	Protein component of the small (40S) ribosomal subunit; identical to Rps6Ap
RTN1	*YDR233C*	ER, cell periphery	ER membrane protein that interacts with exocyst subunit Sec6p and with Yip3p
RTT10	*YPL183C*	cytoplasm	Hypothetical protein; Cytoplasmic protein with a role in regulation of Ty1 transposition
RTT106	*YNL206C*	nucleus	Protein with a role in regulation of Ty1 transposition
RUD3	*YOR216C*	punctate composite, Golgi	Golgi matrix protein involved in the structural organization of the cis-Golgi
SAC7	*YDR389W*	cytoplasm	GTPase activating protein (GAP) for Rho1p, involved in signaling to the actin cytoskeleton
SBH2	*YER019C-A*	ER	Ssh1p-Sss1p-Sbh2p complex component, involved in protein translocation into the endoplasmic reticulum; homologous to Sbh1p
SCJ1	*YMR214W*	ER	DnaJ homolog that cooperates with BiP to mediate maturation of proteins as well as during ERAD
SEC22	*YLR268W*	Golgi	R-SNARE protein; assembles into SNARE complex with Bet1p, Bos1p and Sed5p; involved in anterograde and retrograde transport between the ER and Golgi
SEC28	*YIL076W*	Golgi, early Golgi	Epsilon-COP subunit of the coatomer; regulates retrograde Golgi-to-ER protein traffic
SEC66	*YBR171W*	ER membrane	Non-essential subunit of the Sec63 complex; with Sec61 complex and Sec62, performes SRP-dependent and post-translational SRP-independent protein targeting and import into the ER

SEC72	*YLR292C*	cytoplasm, ER-localized	Non-essential subunit of the Sec63 complex; with Sec61 complex and Sec62, performes SRP-dependent and post-translational SRP-independent protein targeting and import into the ER
SED4	*YCR067C*	ER membrane	Functions as a positive regulator of Sar1p probably through inhibition of GTPase activation by Sec23p; participates in vesicle formation, similar to Sec12p
SET3	*YKR029C*	nucleus	Defining member of the SET3 histone deacetylase complex which is a meiosis-specific repressor of sporulation genes
SEY1	*YOR165W*	punctate composite	Protein of unknown function, contains two predicted GTP-binding motifs GXXXXGKS and DXXG near the N-terminus
SFB2	*YNL049C*	ER to Golgi	Probable component of COPII coated vesicles that binds to Sec23p; involved in ER to Golgi transport and in autophagy
SGM1	*YJR134C*	Golgi, early Golgi	Protein of unknown function; localizes to COPI coated vesicles and the Golgi apparatus
SGT2	*YOR007C*	cytoplasm	Glutamine-rich cytoplasmic protein of unknown function, contains tetratricopeptide (TPR) repeats, which often mediate protein-protein interactions
SIF2	*YBR103W*	nucleus	WD40 repeat-containing subunit of the Set3C histone deacetylase complex, which represses early/middle sporulation genes
SIL1	*YOL031C*	ER	Nucleotide exchange factor BiP, required for protein translocation into the ER
SKY1	*YMR216C*	cytoplasm	SR protein kinase (SRPK) involved in regulating proteins involved in mRNA metabolism and cation homeostasis
SLA1	*YBL007C*	cytoplasm, actin	Cytoskeletal protein binding protein required for assembly of the cortical actin cytoskeleton; interacts with proteins regulating actin dynamics and involved in endocytosis
SLP1	*YOR154W*	ambiguous	Hypothetical protein
SMI1	*YGR229C*	punctate composite, late Golgi	Protein involved in the regulation of cell wall synthesis; proposed to be involved in coordinating cell cycle progression with cell wall integrity
SNT1	*YCR033W*	nucleus	Subunit of the Set3C deacetylase complex; putative DNA-binding protein
SOP4	*YJL192C*	ER membrane	Suppressor of pma1-7; deletion of SOP4 slows down the export of wild-type Pma1p and Pma1-7 from the ER

SPC1	*YJR010C-A*	ER	Subunit of the signal peptidase complex (SPC), which cleaves the signal sequence from proteins targeted to the endoplasmic reticulum (ER)
SPC2	*YML055W*	ER	Subunit of signal peptidase complex (Spc1p, Spc2p, Spc3p, Sec11p), which catalyzes cleavage of N-terminal signal sequences of proteins targeted to the secretory pathway
SPE3	*YPR069C*	cytoplasm, nucleus	Spermidine synthase, involved in biosynthesis of spermidine and pantothenic acid; spermidine is required for growth of wild-type cells
SPE4	*YLR146C*	cytoplasm	Spermine synthase, required for the biosynthesis of spermine and pantothenic acid
SPF1	*YEL031W*	ER	P-type ATPase, ion transporter of the ER membrane involved in ER function and Ca2+ homeostasis; required for regulating Hmg2p degradation
SQS1	*YNL224C*	cytoplasm, nucleus	Hypothetical protein
SRP40	*YKR092C*	nucleolus	Serine-rich protein with a role in preribosome assembly or transport; may function as a chaperone of small nucleolar ribonucleoprotein particles (snoRNPs)
SSA2	*YLL024C*	cytoplasm, nucleus	Member of heat shock protein 70 (HSP70) family; associated with the chaperonin-containing T-complex
SSA3	*YBL075C*	cytoplasm	Member of the heat shock protein 70 (HSP70) family; plays a role in SRP-dependent cotranslational protein-membrane targeting and translocation
SSA4	*YER103W*	cytoplasm	Heat shock protein 70 that is highly induced upon stress; plays a role in SRP-dependent cotranslational protein-membrane targeting and translocation
SSM4	*YIL030C*	ER	Ubiquitin-protein ligase of the ER/nuclear envelope, required for degradation of Alpha2p and other proteins containing a Deg1 degradation signal
STE24	*YJR117W*	ER	Highly conserved zinc metalloprotease that functions in two steps of a-factor maturation, C-terminal CAAX proteolysis and the first step of N-terminal proteolytic processing
STP22	*YCL008C*	endosome	Component of the ESCRT-I complex, which is involved in ubiquitin-dependent sorting of proteins into the endosome;
SUM1	*YDR310C*	nucleus	Transcriptional repressor required for mitotic repression of middle sporulation-specific genes; telomere maintenance

SUR4	*YLR372W*	ER	Elongase, involved in fatty acid and sphingolipid biosynthesis; synthesizes very long chain 20-26-carbon fatty acids from C18-CoA primers
SVP26	*YHR181W*	ER	May function to promote retention of proteins in the early Golgi compartment; mutation affects protein N-glycosylation and cell wall integrity
SWC3	*YAL011W*	nucleus	Protein of unknown function, component of the Swr1p complex that incorporates Htz1p into chromatin
SWC5	*YBR231C*	nucleus	Protein of unknown function, component of the Swr1p complex that incorporates Htz1p into chromatin
SWP82	*YFL049W*	nucleus	Member of the SWI/SNF chromatin remodeling complex in which it plays an as yet unidentified role
SYS1	*YJL004C*	early Golgi	Integral membrane protein of the Golgi required for targeting of the Arf-like GTPase Arl3p to the Golgi
TED1	*YIL039W*	ER	Conserved phosphoesterase domain-containing protein that acts together with Emp24p/Erv25p in cargo exit from the ER
THI6	*YPL214C*	cytoplasm, punctate composite	Bifunctional enzyme with thiamine-phosphate pyrophosphorylase and 4-methyl-5-beta-hydroxyethylthiazole kinase activities, required for thiamine biosynthesis
TIR3	*YIL011W*	Cell wall	Cell wall mannoprotein of the Srp1p/Tip1p family of serine-alanine-rich proteins; expressed under anaerobic conditions and required for anaerobic growth
TLG2	*YOL018C*	early endosome, trans-Golgi	Syntaxin-like t-SNARE that forms a complex with Tlg1p and Vti1p and mediates fusion of endosome-derived vesicles with the late Golgi
TMA19	*YKL056C*	cytoplasm	Protein of unknown function that associates with ribosomes
TOF2	*YKR010C*	nucleolus, mitochondrion	Protein required for rDNA silencing and mitotic rDNA condensation; stimulates Cdc14p phosphatase activity and may function to coordinate the release of Cdc14p during anaphase
TRM1	*YDR120C*	nucleus, mitochondrion	tRNA methyltransferase; produces the modified base N2,N2-dimethylguanosine in tRNAs
TRM7	*YBR061C*	cytoplasm	2'-O-ribose methyltransferase, methylates the 2'-O-ribose of nucleotides at positions 32 and 34 of the tRNA anticodon loop
TRP3	*YKL211C*	cytoplasm	Bifunctional enzyme exhibiting both indole-3-glycerol-phosphate synthase and anthranilate synthase activities

TSR2	*YLR435W*	cytoplasm, nucleus	Protein with a potential role in pre-rRNA processing
UBC4	*YBR082C*	cytoplasm, nucleus	Ubiquitin-conjugating enzyme that mediates degradation of short-lived and abnormal proteins; interacts with many SCF ubiquitin protein ligases
UBC7	*YMR022W*	ER	Ubiquitin conjugating enzyme, involved in the ER-associated protein degradation pathway; requires Cue1p for recruitment to the ER membrane
UBR1	*YGR184C*	0	Ubiquitin-protein ligase (E3) that interacts with Rad6p/Ubc2p to ubiquitinate substrates of the N-end rule pathway
UBR2	*YLR024C*	cytoplasm	Cytoplasmic ubiquitin-protein ligase (E3)
UBX2	*YML013W*	ER	UBX (ubiquitin regulatory X) domain-containing protein that interacts with Cdc48p; required for degradation of a ubiquitylated model substrate
UBX4	*YMR067C*	cytoplasm, nucleus	UBX (ubiquitin regulatory X) domain-containing protein that interacts with Cdc48p
UFD2	*YDL190C*	cytoplasm, nucleus	Ubiquitin chain assembly factor (E4) that cooperates with the ubiquitination machinery to conjugate ubiquitin to substrates; also functions as an E3
UME1	*YPL139C*	cytoplasm, nucleus	Negative regulator of meiosis, required for repression of a subset of meiotic genes during vegetative growth
USA1	*YML029W*	ER membrane	Protein involved in ER-associated protein degradation (ERAD); component of the Hrd1p complex; interacts with the U1 snRNP-specific protein, Snp1p
UTH1	*YKR042W*	vacuole	Mitochondrial outer membrane and cell wall localized SUN family member required for mitochondrial autophagy
VPS1	*YKR001C*	cytoplasm, punctate composite, endosome	GTPase required for vacuolar protein sorting; involved in regulating peroxisome biogenesis
VPS28	*YPL065W*	punctate composite	Component of the ESCRT-I complex, which is involved in ubiquitin-dependent sorting of proteins into the endosome
VPS29	*YHR012W*	ambiguous	Endosomal protein that is a subunit of the membrane-associated retromer complex essential for endosome-to-Golgi retrograde transport
VPS3	*YDR495C*	punctate composite	Cytoplasmic protein required for the sorting and processing of soluble vacuolar proteins, acidification of the vacuolar lumen, and assembly of the vacuolar H+-ATPase

VPS30	*YPL120W*	vacuole	Protein that forms a membrane-associated complex with Apg14p that is essential for autophagy; involved in vacuolar protein sorting
VPS38	*YLR360W*	endosome	Part of a Vps34p phosphatidylinositol 3-kinase complex that functions in carboxypeptidase Y (CPY) sorting
VPS51	*YKR020W*	punctate composite	Component of the GARP (Golgi-associated retrograde protein) complex, Vps51p-Vps52p-Vps53p-Vps54p, which is required for the recycling of proteins from endosomes to the late Golgi
VPS52	*YDR484W*	punctate composite	Component of the GARP (Golgi-associated retrograde protein) complex
VPS53	*YJL029C*	punctate composite, early Golgi	Component of the GARP (Golgi-associated retrograde protein) complex
VPS54	*YDR027C*	punctate composite, early Golgi	Component of the GARP (Golgi-associated retrograde protein) complex
VPS71	*YML041C*	nucleus	Protein of unknown function, component of the Swr1p complex that incorporates Htz1p into chromatin; required for vacuolar protein sorting
VPS72	*YDR485C*	nucleus	Protein of unknown function, component of the Swr1p complex that incorporates Htz1p into chromatin; required for vacuolar protein sorting
VPS74	*YDR372C*	cytoplasm, nucleus	may be involved in vacuolar protein sorting; belongs to a family of cytosolic Golgi-associated proteins suggesting that it may play a role in secretion
VPS75	*YNL246W*	nucleus	Protein of unknown function involved in vacuolar protein sorting; detected in the nucleus
VTC1	*YER072W*	ER	Vacuolar transporter chaperon (VTC) involved in distributing V-ATPase and other membrane proteins
VTC4	*YJL012C*	0	Vacuolar membrane protein involved in vacuolar polyphosphate accumulation; functions as a regulator of vacuolar H+-ATPase activity and vacuolar transporter chaperones; involved in non-autophagic vacuolar fusion
WSC4	*YHL028W*	vacuole	ER membrane protein involved in the translocation of soluble secretory proteins and insertion of membrane proteins into the ER membrane
YAP5	*YIR018W*	cytoplasm, nucleus	Basic leucine zipper (bZIP) transcription factor
YBR137W	*YBR137W*	cytoplasm	Protein of unknown function; binds to Replication Protein A (RPA)
YBR226C	*YBR226C*	0	Hypothetical protein

YBR238C	*YBR238C*	cytoplasm, mitochondrion	Putative protein of unknown function
YCK1	*YHR135C*	cytoplasm, nucleus	Palmitoylated, plasma membrane-bound casein kinase I isoform; shares redundant functions with Yck2p in morphogenesis, proper septin assembly, endocytic trafficking
YCK2	*YNL154C*	cytoplasm, nucleus	Palmitoylated, plasma membrane-bound casein kinase I isoform; shares redundant functions with Yck1p
YCL045C	*YCL045C*	ER	Protein of unknown function
YDL133W	*YDL133W*	0	Hypothetical protein
YDL157C	*YDL157C*	mitochondrion	Hypothetical protein
YDL242W	*YDL242W*	0	Hypothetical protein
YDR049W	*YDR049W*	cytoplasm	Hypothetical protein
YDR056C	*YDR056C*	ER	Hypothetical protein
YDR161W	*YDR161W*	cytoplasm, nucleus	interacts with PP2C
YEL014C	*YEL014C*	Cytoplasm	Hypothetical protein
YEL047C	*YEL047C*	cytoplasm, nucleus	Fumurate ReDuctase Soluble
YER064C	*YER064C*	Nucleus	Non-essential nuclear protein; null mutation has global effects on transcription
YER140W	*YER140W*	Ambiguous	Hypothetical protein
YER156C	*YER156C*	cytoplasm, nucleus	Hypothetical protein
YET1	*YKL065C*	ER	Endoplasmic reticulum transmembrane protein, homolog of human BAP31 protein
YFR018C	*YFR018C*	0	Hypothetical protein
YFR045W	*YFR045W*	0	Putative mitochondrial transport protein; null mutant is viable
YGL007W	*YGL007W*	0	Hypothetical protein
YGL231C	*YGL231C*	ER	Putative protein of unknown function
YHR003C	*YHR003C*	Mitochondrion	Protein of unknown function, localized to the mitochondrial outer membrane

YHR078W	*YHR078W*	0	Hypothetical protein
YIL029C	*YIL029C*	0	Hypothetical protein
YIL032C	*YIL032C*	0	Hypothetical protein
YIL055C	*YIL055C*	Ambiguous	Hypothetical protein
YIP3	*YNL044W*	Golgi, early Golgi	Protein localized to COPII vesicles, proposed to be involved in ER to Golgi transport
YJL055W	*YJL055W*	cytoplasm, nucleus	Putative protein of unknown function
YJR088C	*YJR088C*	ER	Putative protein of unknown function
YKR043C	*YKR043C*	cytoplasm, nucleus	Putative protein of unknown function
YLL014W	*YLL014W*	ER	Putative protein of unknown function
YLR104W	*YLR104W*	0	Hypothetical protein
YLR278C	*YLR278C*	Nucleus	Zinc-cluster protein of unknown function
YLR287C	*YLR287C*	Cytoplasm	Putative protein of unknown function
YLR402W	*YLR402W*	0	Hypothetical protein
YML108W	*YML108W*	cytoplasm, nucleus	Putative protein of unknown function whose structure defines a new subfamily of the split beta-alpha-beta sandwiches
YMR209C	*YMR209C*	Ambiguous	Hypothetical protein
YNL205C	*YNL205C*	0	Hypothetical protein
YOL159C	*YOL159C*	0	Hypothetical protein
YOR164C	*YOR164C*	Cytoplasm	Protein of unknown function; interacts with Mdy2p
YOS9	*YDR057W*	ER	Soluble ER lumenal lectin; member of the OS-9 protein family; similar to mannose-6-phosphate receptors (MPRs); serves as a receptor that recognizes misfolded proteins during ERAD
YPL068C	*YPL068C*	Nucleus	Hypothetical protein
YPR063C	*YPR063C*	ER	Hypothetical protein

YPR084W	*YPR084W*	0	Hypothetical protein
YPR130C	*YPR130C*	0	Hypothetical protein
YUR1	*YJL139C*	Golgi	Mannosyltransferase of the KTR1 family, involved in protein N-glycosylation; located in the Golgi apparatus
ZAP1	*YJL056C*	cytoplasm, nucleus	Zinc-regulated transcription factor; contains seven zinc-finger domains
VIP1	*YLR410W*	Cytoplasm	Protein of unknown function probably involved in the function of the cortical actin cytoskeleton
YJR088C	*YJR088C*	ER	Putative protein of unknown function

Table 7: The $\log_2$ (GFP/RFP) reporter values obtained in the double mutant strains when *KAR2::NAT* or *kar2-R217A::NAT* were crossed against the genes listed in table 6

* N/A indicates either that the double mutant strain was inviable or that a value was not obtained due to experimental error

Gene name	*KAR2 (1)*	*KAR2 (2)*	*KAR2 (3)*	*kar2-R217A (1)*	*kar2-R217A (2)*
ADD66	N/A	-0.3026	-0.1376	-0.4876	-0.5018
AGX1	-0.1732	-0.095	-0.1543	-0.1537	0.2545
AHC2	-0.0227	0.0194	N/A	0.1109	0.0936
ALF1	N/A	1.12	2.1491	-0.0737	0.1374
ALG12	1.5689	1.4467	N/A	2.0574	1.9003
ALG3	2.2605	2.3585	2.6165	2.5239	2.5824
ALG5	1.4492	1.5665	1.68	1.6203	1.7557
ALG6	2.0957	2.041	2.1605	1.9784	2.1465
ALG8	1.6379	1.7204	1.9019	1.4186	1.6471
ALG9	1.4766	1.5067	2.0133	1.82	2.0601
APE3	-0.3075	-0.1964	-0.0032	-0.2365	-0.1701
ARC18	0.5786	0.6766	0.8138	0.2962	0.4633
ARL1	0.6144	0.435	0.4247	0.0415	0.0395
ARO1	0.444	N/A	0.0412	N/A	1.2409
ARP6	0.1656	0.1677	0.2997	0.9609	0.7772
ARV1	N/A	4.0563	N/A	3.9095	4.0868
ASM4	-0.476	-0.3149	N/A	-0.3786	-0.3079
ATG8	-0.2395	-0.1303	N/A	-0.2163	-0.1927
BNR1	-0.0254	-0.1099	0.25	0.1393	0.0236
BOP2	-0.0678	0.0262	0.0132	-0.1844	-0.0688
BRE5	N/A	-0.0609	0.0013	-0.3313	0.7041
BST1	3.4961	3.4596	N/A	N/A	N/A
BTS1	N/A	0.5123	0.5163	0.5372	0.7367
BUG1	-0.0477	0.1057	N/A	-0.026	0.0119
CAC2	0.7982	0.8701	0.6998	0.4597	0.4973
CAJ1	-0.1593	-0.146	-0.0958	-0.1968	0.0422
CAP1	N/A	-0.0499	0.1806	0.0908	0.0732
CCW12	1.4203	1.4255	1.6152	1.106	1.169
CKA2	0.8758	0.7563	1.1658	0.873	0.9537
CNE1	1.1871	N/A	1.0195	0.4831	0.6078
COG5	N/A	0.1272	N/A	0.0747	0.12
COG6	0.2687	0.3235	N/A	0.3348	0.2651
COG8	0.281	0.2635	N/A	0.3694	0.3772
CPA1	-0.6105	-0.6124	-0.8076	-0.072	-0.366

CPR6	0.1262	0.1764	0.1472	0.0706	0.0308
CRD1	-0.265	-0.3036	N/A	-0.4933	-0.5364
CSF1	3.1702	3.2738	3.2965	3.1871	N/A
CSN12	-0.6172	-0.524	N/A	-0.2944	-0.2212
CUE1	1.0488	1.0241	1.2673	1.2724	1.2411
CWH41	0.5218	0.5415	0.5079	0.2974	0.5037
CWH43	0.2596	0.1953	N/A	0.2471	0.4399
CYS3	0.7431	1.2647	N/A	1.4175	1.3339
DAL81	N/A	-0.406	N/A	0.27	-0.5153
DAS1	-0.2274	-0.2246	-0.2562	-0.4231	-0.4143
DER1	0.8412	0.8263	1.1548	1.0472	1.2184
DFG10	-0.2762	-0.1662	0.0423	-0.1904	-0.1534
DGK1	0.0309	-0.0801	0.1163	-0.1759	0.0266
DIE2	0.7309	0.747	0.9767	1.0174	1.1332
DOM34	-0.5762	-0.3832	-0.1897	-0.2838	-0.2428
DRS2	0.2218	0.3238	0.3777	0.8509	0.2448
DUS3	0.0404	-0.0945	N/A	0.0086	0.1504
ECM30	0.0089	0.1319	N/A	0.1495	0.1953
EDE1	0.2082	0.118	N/A	0.1742	N/A
EGD1	-0.5359	-0.485	-0.5189	-0.696	-0.6082
EGD2	-0.4217	-0.3985	-0.3263	-0.4963	-0.5187
ELF1	N/A	0.3241	0.3915	0.3261	0.1272
ELP2	N/A	-0.4381	-0.2428	-0.339	-0.1011
EMP47	-0.1593	N/A	N/A	-0.1422	0.291
ENT3	-0.1379	-0.17	0.1291	-0.1583	-0.1574
ERD1	2.7915	2.8649	2.6871	1.2	1.4274
ERG2	0.3868	0.3605	0.4795	0.7894	1.6577
ERJ5	0.3344	0.1339	N/A	0.543	0.5779
ERP1	N/A	0.8865	N/A	1.0173	1.1452
ERP2	0.0939	0.1487	0.3537	0.1355	0.2605
ERV14	1.9212	1.9181	2.0844	1.5479	1.7306
ERV25	2.497	2.4537	2.5138	2.8049	3.0125
ERV29	0.3171	0.4791	0.5387	0.7029	0.8533
ERV41	N/A	-0.2395	-0.3675	-0.3299	-0.2084
ERV46	-0.3368	-0.3478	-0.3832	-0.5196	-0.3205
EUG1	0.3093	0.343	0.4621	0.0887	0.0895
FAR8	-0.1493	-0.1394	-0.0579	0.0008	-0.0352
FAT1	0.9667	0.9204	0.7502	1.1394	1.825
FKH1	0.3118	0.346	0.5493	0.2544	N/A
FLX1	N/A	-0.3259	N/A	-0.4937	-0.5717
FRE4	-0.1671	-0.2638	N/A	-0.3606	-0.3763

FUN30	0.1668	0.1873	0.35	-0.0711	0.0053
FYV6	N/A	N/A	3.7707	0.9685	1.0173
GCN2	-0.1473	-0.1909	N/A	-0.1679	0.0118
GCN20	-0.2321	-0.2038	N/A	-0.1502	-0.0798
GCN5	-0.9911	-1.1073	-1.1178	-0.9159	-0.5784
GCR2	0.6388	0.523	1.0012	0.3368	0.4716
GCS1	0.2911	0.3262	0.2994	0.0912	0.133
GDA1	0.271	0.2536	0.217	0.3804	0.4991
GET1	1.0074	2.1743	N/A	1.9191	N/A
GET1	N/A	2.174	N/A	1.8053	1.4826
GET2	1.6531	2.1291	2.1414	0.2439	2.8273
GET2	N/A	1.9979	2.2189	N/A	1.6552
GET3	1.088	0.7439	0.8375	0.3272	0.4952
GET3	N/A	0.7498	0.8965	0.5615	0.6747
GLO3	N/A	2.1866	2.2768	1.0825	1.0169
GNP1	N/A	0.0259	N/A	1.04	N/A
GOS1	0.3619	0.3907	0.6255	0.0733	0.6558
GOT1	0.0115	0.0354	-0.0765	-0.0645	0.066
GSG1	0.1271	0.2326	N/A	0.2418	0.4019
GSH2	-0.2563	-0.2227	-0.2941	-0.1497	0.0155
GTB1	-0.0084	0.0241	N/A	0.0436	0.0931
GTR1	N/A	N/A	0.2049	1.0502	-0.1575
GUP1	2.8145	2.8369	N/A	1.7755	1.7267
GYP8	-0.1225	-0.206	N/A	-0.2162	-0.0275
HAC1	-0.6855	-0.7625	N/A	-0.816	0.303
HAM1	-0.4729	-0.3843	N/A	-0.3973	-0.3429
HAT2	-0.2885	-0.2775	-0.2965	-0.2645	-0.2518
HEK2	0.5033	0.4717	0.609	0.6581	0.563
HHF1	0.7234	0.8716	N/A	0.7388	0.7461
HHT1	1.0153	0.9416	N/A	0.7024	0.84
HHT2	0.3736	0.4076	0.4018	0.446	0.3579
HIR3	N/A	0.4039	0.1789	-0.1718	-0.1544
HLJ1	1.4252	1.4709	1.5424	0.1801	0.3611
HMG1	-0.1158	0.0493	0.171	-0.1673	-0.135
HOP2	0.3593	-0.0382	0.6456	0.5424	0.6955
HPC2	0.1999	0.2083	0.1395	0.1312	0.2662
HRD1	1.7439	1.7391	1.9685	2.4488	2.4536
HRD3	1.3626	1.4187	1.607	1.7897	1.7966
HSM3	-0.3339	-0.3362	N/A	-0.2623	-0.3894
HSV2	-0.3109	-0.2498	-0.0406	-0.2932	-0.2978
HTB2	0.1298	0.144	N/A	0.086	0.1547

HTZ1	0.2764	0.2698	0.257	0.566	1.2143
HUR1	N/A	1.8088	N/A	1.3924	N/A
HXK2	0.0828	0.2006	0.1962	0.3654	0.1047
HXT8	N/A	-0.0195	0.0632	0.2699	0.3059
ICE2	0.3416	0.2721	N/A	0.2817	0.3756
IDH1	-0.2366	N/A	N/A	-0.501	-0.3749
IES1	0.4161	N/A	0.2072	-0.1153	-0.1279
IES4	0.4649	0.5466	0.5486	0.1704	0.3549
IES5	0.2702	0.2765	0.2859	0.026	-0.0222
ILM1	0.2108	0.3122	N/A	-0.2657	-0.0502
INP53	-0.03	0.0561	N/A	0.1179	0.1255
IPK1	N/A	-0.5209	-0.4467	-0.9641	-0.9679
IRC21	0.0136	0.0856	0.0625	0.1232	0.0515
IRE1	-0.7221	-0.7557	N/A	-1.0045	-0.8061
ISC1	0.1473	0.0055	N/A	0.0409	0.2065
ISR1	0.2265	0.1717	N/A	0.094	0.1752
ISW1	N/A	0.4587	0.4685	0.3464	0.5052
ISW2	0.0596	0.0086	0.1836	-0.2034	-0.1699
ITR1	0.2206	0.1759	0.2569	0.2211	0.1748
IXR1	-0.4814	-0.3697	N/A	-0.3248	-0.2413
JEM1	0.0926	0.1329	0.3924	-0.1534	-0.0173
KEL1	0.3544	0.3648	N/A	0.0383	N/A
KEX2	N/A	N/A	N/A	N/A	N/A
KIN3	0.7964	0.8447	0.9724	N/A	N/A
KRE1	0.4205	0.4233	0.3309	0.3132	0.5162
KRE11	0.1763	0.2615	0.1922	0.0133	0.1022
KRE27	-0.0748	0.0715	0.2655	-0.0805	0.2121
KRE27	1.2348	2.0262	N/A	N/A	1.25
KTI12	-0.3934	-0.4262	N/A	0.8172	-0.1848
LAS21	3.5378	3.4031	3.5912	-0.0934	0.1325
LEM3	N/A	0.5108	0.33	0.2846	1.1182
LEU3	-0.1948	-0.1944	-0.1252	-0.4378	-0.2416
LOC1	-0.2638	-0.409	-0.1821	-0.4263	-0.0198
LPD1	-0.3023	-0.3497	-0.3742	-0.1595	-0.0621
LRC3	0.0041	0.0238	0.0868	0.2484	0.3037
MAF1	N/A	-0.3837	N/A	-0.4498	-0.2919
MDY2	0.1337	0.0862	0.0857	0.0623	0.0617
MDY2	0.1783	0.0393	N/A	0.005	0.0333
MEH1	0.1631	0.2058	N/A	-0.1206	-0.0277
MGA2	1.2413	1.855	N/A	N/A	1.9579
MKC7	-0.0639	-0.0909	N/A	-0.1583	0.0147

MNL1	0.0096	0.0099	0.1955	0.0729	0.2774
MNN2	0.3513	0.6881	0.3409	0.499	0.6841
MNN4	N/A	0.0459	N/A	0.0742	0.1266
MNN5	-0.0905	-0.0526	-0.1528	-0.2587	-0.0497
MNN9	-0.2798	-0.1796	N/A	-0.128	-0.0967
MNS1	-0.1794	-0.0977	N/A	-0.1314	-0.0371
MPD1	0.4312	0.3992	0.7255	0.6005	0.7523
MSC1	N/A	0.5625	N/A	0.5933	0.6133
MSI1	0.6863	0.5688	N/A	0.4273	0.5566
MTC1	0.0223	0.0666	0.0614	-0.1691	-0.1998
MTC5	N/A	-0.0859	0.0661	-0.0218	0.1173
MVP1	N/A	0.1273	0.0625	0.1958	0.1987
NEM1	0.6303	0.6236	0.4901	0.0258	0.0761
NFT1	-0.3019	-0.2045	-0.2793	-0.106	-0.1756
NHP6A	N/A	-0.2897	N/A	-0.4614	-0.4874
NHX1	0.9253	0.9087	0.9669	0.9044	N/A
NMD4	-0.411	-0.3996	N/A	-0.535	-0.0132
NPL4	-0.0547	-0.1038	0.0783	-0.089	N/A
OLA1	-0.3817	-0.2636	N/A	0.7315	-0.2662
OPI10	-0.2182	-0.194	-0.1824	-0.3669	-0.2127
OPI3	1.1738	1.1042	0.9375	-0.1078	0.0547
OST3	2.7665	2.7924	3.032	2.5737	2.6961
OST5	0.3574	0.4436	N/A	0.8451	0.9685
OYE2	-0.3308	-0.354	N/A	-0.297	-0.1042
PBP1	-0.386	-0.3965	-0.383	-0.711	-0.5665
PCT1	0.2794	0.5333	0.3472	0.2782	0.492
PEF1	0.2869	0.2857	0.3	0.6235	0.8662
PEP7	-0.5521	-0.4327	-0.4213	-0.8385	-0.7175
PEP8	N/A	0.2154	0.2205	0.1158	-0.0813
PET18	-0.0978	-0.1114	N/A	-0.1177	0.0981
PHO80	1.0206	1.0998	1.4642	0.936	0.8744
PHO86	0.1507	0.1335	N/A	-0.1547	0.0003
PMP1	-0.2068	-0.0008	N/A	0.3381	0.2259
PMR1	N/A	N/A	N/A	N/A	0.6695
PMT1	1.6268	1.7885	1.9023	1.2376	1.331
PMT2	2.8731	2.8002	2.9393	2.2456	2.4578
PPH21	-0.2545	-0.2571	-0.0514	-0.237	-0.1926
PPT1	0.0788	0.0994	0.129	0.0285	0.1921
PRM2	-0.5108	-0.3813	-0.3011	-0.3609	-0.3631
PSD2	0.1872	0.2804	0.2537	1.7204	1.796
PTC2	-0.1572	-0.0722	-0.1546	-0.245	-0.2654

PTK2	0.1057	0.1609	0.1273	-0.2059	-0.1662
PTP1	-0.3056	-0.2552	N/A	-0.2269	-0.129
PTR2	-0.3999	-0.2411	N/A	-0.1117	-0.0904
RAD23	N/A	-0.1593	N/A	-0.3249	-0.0511
RAV1	N/A	0.3196	N/A	-0.1338	-0.1359
RCO1	0.2493	0.2599	0.5879	0.3516	0.3989
RER1	0.0691	0.1834	0.1244	0.0761	0.1606
REX4	-0.3452	-0.3693	-0.3771	-0.4492	-0.1796
RGP1	0.0552	0.0129	0.1388	-0.0049	0.0837
RLF2	N/A	0.7573	0.7118	0.4716	0.5184
ROT2	0.3608	0.4799	0.3556	0.2779	0.9212
ROX1	-0.3262	-0.2562	N/A	-0.4062	-0.238
RPA14	-0.4042	-0.3279	-0.3745	-0.2453	-0.1017
RPL19B	N/A	-0.7237	N/A	-0.7764	-0.5536
RPN10	-0.4709	-0.4916	-0.4196	1.0811	-0.4969
RPS11A	N/A	-0.5539	N/A	-0.7182	-0.6761
RPS12	0.2615	0.3334	N/A	0.3318	0.3558
RPS16A	N/A	-0.9726	-0.7198	-0.937	0.2938
RPS17A	-1.2305	-1.1744	-0.8818	-0.0176	0.0956
RPS23A	-0.6533	-0.6831	-0.5535	-0.5988	-0.573
RPS28B	-0.7381	-0.7216	-0.6388	-0.6339	-0.5967
RPS4B	-0.1945	-0.2129	-0.1689	-0.3294	-0.1384
RPS6B	-0.7838	-0.7447	-0.7354	-0.8648	-0.698
RTN1	N/A	-0.0583	N/A	0.0908	0.1747
RTT10	-0.4918	-0.4255	-0.4272	-0.1585	-0.1299
RTT106	N/A	1.2206	1.1135	0.8873	0.9736
RUD3	0.2108	0.3105	0.3976	0.5774	0.5627
SAC7	0.5047	0.4314	0.5158	0.1759	0.2177
SBH2	N/A	-0.1002	0.016	-0.1303	-0.1895
SCJ1	4.3649	4.3413	4.1895	3.5932	3.641
SEC22	N/A	0.2104	1.4091	1.0644	1.162
SEC28	-0.4445	-0.4157	-0.2068	-0.6077	N/A
SEC66	0.5823	0.9039	N/A	0.4617	0.6793
SEC72	-0.3077	-0.1593	-0.1711	-0.298	-0.118
SED4	0.2098	0.1935	0.1375	0.0082	0.1349
SET3	0.0413	0.0383	N/A	0.46	0.4766
SEY1	0.2502	0.282	0.6789	0.2016	0.2979
SFB2	0.0108	-0.0072	N/A	-0.087	-0.1069
SGM1	N/A	-0.1728	N/A	-0.0444	-0.1467
SGT2	-0.1256	-0.0435	0.0839	-0.097	-0.0427
SGT2	-0.0765	-0.0216	N/A	-0.0302	-0.0098

SIF2	0.4409	0.3734	0.7118	0.6732	0.7489
SIL1	0.8427	0.7952	0.7596	2.1738	2.2858
SKY1	1.0151	0.8525	0.8692	0.2682	0.8929
SLA1	-0.2451	-0.2056	0.0081	-0.0572	0.0827
SLP1	0.6604	0.6694	N/A	1.0961	1.0042
SMI1	0.7192	0.7371	0.6811	0.2787	0.2534
SNT1	0.3716	0.2889	N/A	0.619	1.0913
SOP4	-0.1696	-0.1335	0.0836	-0.2512	0.0421
SOP4	4.3107	4.1647	N/A	4.0464	4.2255
SPC1	0.2288	0.2772	N/A	-0.1584	-0.0734
SPC2	2.1501	2.1871	2.1595	2.4255	2.4953
SPE3	N/A	-0.2623	N/A	-0.3921	-0.1916
SPE4	-0.241	-0.2159	N/A	-0.1479	-0.1131
SPF1	4.0355	4.1732	3.8854	N/A	3.8116
SQS1	-0.3071	-0.3278	-0.2937	-0.4015	-0.2982
SRP40	-0.7416	-0.5081	-0.7442	-0.6237	-0.5571
SSA2	-0.5445	-0.5422	-0.4248	-0.6427	-0.4835
SSA3	-0.2614	-0.1021	0.0131	-0.269	-0.0007
SSA4	-0.1672	-0.1969	-0.0541	-0.1219	-0.1605
SSM4	0.1148	0.1015	N/A	-0.0253	0.1036
STE24	3.9376	3.6018	3.8783	N/A	0.1414
STP22	0.1079	0.6202	-0.0128	0.4843	0.5861
SUM1	N/A	0.4928	0.7867	0.7798	1.508
SUR4	N/A	1.1244	1.0379	-0.0916	0.1502
SVP26	-0.1751	-0.0725	N/A	-0.1587	0.0089
SWC3	0.0677	0	0.2299	0.2857	0.5833
SWC5	N/A	-0.279	0.3543	0.3558	1.7145
SWP82	-0.2823	-0.2759	N/A	N/A	N/A
SYS1	0.4507	0.431	0.433	-0.1955	-0.057
TED1	N/A	1.5382	2.1462	1.6456	1.7689
THI6	-0.444	-0.3306	-0.2218	-0.3299	-0.0818
TIR3	-0.2403	-0.0796	-0.0087	0.0329	0.051
TLG2	0.5092	0.5614	0.3656	0.4581	0.4941
TMA19	N/A	-0.3673	-0.377	-0.3432	-0.4059
TOF2	N/A	-0.3272	N/A	-0.3709	-0.2987
TRM1	-0.4789	-0.449	-0.3835	-0.3593	-0.2654
TRM7	-0.474	-0.5292	N/A	-0.0954	-0.1453
TRP3	-0.2819	-0.0773	N/A	-0.2883	-0.2353
TSR2	-0.7142	-0.6913	-0.645	-0.4088	0.3838
UBC4	-0.3746	-0.4678	N/A	1.1159	0.3997
UBC7	1.2917	1.3429	1.3783	1.358	1.5773

UBR1	-0.2902	-0.2535	N/A	-0.4382	-0.156
UBR2	-0.2537	-0.2914	-0.305	-0.5643	-0.3329
UBX2	2.2662	2.4889	2.3746	2.458	2.4054
UBX4	0.2618	0.4447	0.5309	0.1884	0.241
UFD2	0.4012	0.528	0.5861	1.1096	0.9859
UME1	-0.4168	-0.4635	-0.5409	-0.1632	-0.1802
USA1	1.0185	1.0454	1.2426	1.1749	1.4187
UTH1	0.5497	0.5791	0.5505	0.4946	0.3289
VPS1	0.2615	1.3673	N/A	0.8884	0.6482
VPS28	N/A	0.8283	0.4264	0.7599	0.8172
VPS29	N/A	0.4075	0.2719	0.2056	0.3904
VPS3	N/A	0.8052	0.6096	0.8975	1.6597
VPS30	0.2661	0.0493	0.2336	0.3586	1.3592
VPS38	0.2221	0.3942	0.3203	0.5317	0.706
VPS51	N/A	2.1661	N/A	1.3343	1.5537
VPS52	N/A	1.2331	0.5436	0.5543	0.3038
VPS53	N/A	0.1693	N/A	-0.2292	-0.1082
VPS54	0.6302	0.5483	N/A	0.337	0.7403
VPS71	-0.0318	-0.0182	N/A	0.1414	0.306
VPS72	-0.0939	0.0442	0.3653	0.7041	0.7383
VPS74	N/A	0.9709	1.1047	0.8605	1.1428
VPS75	-0.4308	-0.4433	-0.4397	-0.6214	-0.4574
VTC1	0.0772	0.0065	N/A	-0.1919	-0.0342
VTC4	0.3828	0.2715	N/A	-0.1161	-0.1791
WSC4	-0.0957	-0.169	0.0905	-0.1852	-0.0453
WT_dhis3::KAN	-0.1836	-0.1906	-0.1037	-0.1763	0.1001
WT_dhis3::KAN	-0.1523	-0.097	N/A	0.1061	0.0495
WT_dhis3::KAN	-0.1307	-0.109	0.0082	-0.0741	0.1277
WT_dhis3::KAN	-0.1233	-0.0407	N/A	-0.0738	0.0594
YAP5	-0.1668	-0.0007	-0.0522	N/A	0.1035
YBR137W	-0.1055	-0.1762	N/A	-0.1323	-0.1364
YBR226C	-0.0984	-0.0587	-0.1332	-0.0587	0.1039
YBR238C	N/A	0.2066	0.2906	0.0929	0.1563
YCK1	-0.005	-0.0189	N/A	-0.122	0.0542
YCK2	0.0358	-0.0969	0.2266	-0.0074	0.1632
YCL045C	0.0717	-0.0305	0.2163	0.1052	0.6969
YDL133W	-0.1234	-0.0421	0.0388	0.064	0.2046
YDL157C	-0.2988	-0.2004	N/A	-0.2868	-0.2408
YDL242W	-0.2379	-0.1205	N/A	-0.1759	-0.1594
YDR049W	N/A	-0.3052	-0.1223	-0.4842	-0.3574
YDR056C	-0.2469	-0.1725	-0.0526	-0.2367	-0.0418

YDR056C	1.3567	N/A	2.1945	0.7662	1.8717
YDR161W	-0.4503	-0.4022	-0.2544	-0.5186	-0.5056
YEL014C	0.0173	-0.0925	0.2138	-0.074	0.1172
YEL047C	-0.2065	-0.1979	N/A	-0.21	-0.065
YER064C	0.2553	0.2963	0.3512	N/A	2.4839
YER140W	0.7416	0.7471	N/A	1.0665	0.969
YER156C	-0.5263	-0.517	-0.4806	-0.5059	-0.3889
YET1	-0.1345	-0.1613	-0.1194	-0.1821	-0.1451
YFR018C	0.1718	0.3126	0.4628	0.0037	0.2754
YFR045W	0.0339	-0.038	0.1938	0.3731	0.4134
YGL007W	N/A	0.5094	0.7305	0.4308	0.4724
YGL231C	0.0115	0.1188	N/A	0.0824	0.1496
YHR003C	0.1275	0.2187	0.4649	-0.0519	-0.0349
YHR078W	0.5428	0.6113	0.648	0.4358	0.4099
YIL029C	-0.0554	-0.0092	0.1888	-0.0902	-0.0856
YIL032C	-0.1071	-0.0326	N/A	-0.1036	-0.0306
YIL055C	-0.0576	0.0158	0.0324	-0.0591	0.0176
YIP3	-0.0173	0.0412	N/A	0.0664	-0.033
YJL055W	-0.3194	-0.2775	N/A	-0.285	-0.131
YJR088C	0.0671	0.0375	N/A	-0.0391	-0.1507
YKR043C	-0.0495	-0.0833	N/A	0.0727	0.015
YLL014W	0.1803	-0.1132	N/A	-0.0378	-0.1071
YLL014W	N/A	0.1607	0.0963	-0.1837	-0.0326
YLR104W	0.5985	0.58	0.6315	0.2215	0.4957
YLR278C	-0.0155	0.0214	0.2383	0.0856	0.6129
YLR287C	-0.2186	-0.2049	-0.008	-0.0991	-0.0138
YLR402W	-0.2761	-0.2491	-0.4318	0.5954	-0.2476
YML108W	-0.4711	-0.4113	-0.3721	-0.2133	-0.186
YMR209C	-0.4081	-0.271	-0.2711	-0.2617	-0.0463
YNL205C	0.3131	0.5516	0.5127	0.0254	0.2043
YOL159C	-0.3676	N/A	N/A	-0.2251	-0.1985
YOR164C	0.1316	0.1569	N/A	0.0244	0.0748
YOR164C	N/A	-0.0558	N/A	0.027	0.0058
YOS9	0.6535	0.6013	0.6826	0.9719	1.0111
YPL068C	-0.455	-0.3522	N/A	-0.1252	0.098
YPR063C	-0.1219	-0.0351	0.1772	-0.2367	-0.0881
YPR063C	-0.0519	-0.0073	0.0014	-0.1651	0.0621
YPR084W	-0.3238	-0.2365	-0.0222	-0.3274	-0.1833
YPR130C	0.2057	0.2216	0.3872	0.3415	0.3893
YUR1	0.6046	0.7038	N/A	-0.2322	-0.1238
ZAP1	N/A	-0.061	N/A	-0.167	-0.1172

VIP1	N/A	N/A	N/A	-0.5155	-0.5359
YJR088C	N/A	N/A	N/A	0.5239	0.4926

Table 8: The $\log_2$ (GFP/RFP) reporter values obtained in the double mutant strains when *KAR2* or *kar2-P515L* were crossed against the genes listed in table 6

* N/A indicates either that the double mutant strain was inviable or that a value was not obtained due to experimental error

Gene name	*KAR2-WT (1)*	*KAR2-WT (2)*	*KAR2-WT (3)*	*kar2-P515L (1)*	*kar2-P515L (2)*	*kar2-P515L (3)*	*kar2-P515L (4)*
ADD66	N/A	-0.3026	-0.1376	4.8475	N/A	N/A	N/A
AGX1	-0.1732	-0.095	-0.1543	4.905	N/A	4.9017	4.9017
AHC2	-0.0227	0.0194	N/A	4.9802	5.1409	5.0149	5.0149
ALF1	N/A	1.12	2.1491	4.8706	4.9816	4.8704	4.8704
ALG12	1.5689	1.4467	N/A	N/A	2.035	N/A	N/A
ALG3	2.2605	2.3585	2.6165	N/A	2.2571	2.1496	2.1496
ALG5	1.4492	1.5665	1.68	1.2547	1.5159	1.4863	1.4863
ALG6	2.0957	2.041	2.1605	N/A	N/A	1.9092	1.9092
ALG8	1.6379	1.7204	1.9019	N/A	1.9946	1.3604	1.3604
ALG9	1.4766	1.5067	2.0133	2.8034	N/A	2.4384	2.4384
APE3	-0.3075	-0.1964	-0.0032	4.9586	5.044	5.0007	5.0007
ARC18	0.5786	0.6766	0.8138	N/A	N/A	N/A	N/A
ARL1	0.6144	0.435	0.4247	N/A	N/A	N/A	N/A
ARO1	0.444	N/A	0.0412	N/A	1.3669	N/A	N/A
ARP6	0.1656	0.1677	0.2997	4.9271	N/A	N/A	N/A
ARV1	N/A	4.0563	N/A	N/A	4.6	4.6823	4.6823
ASM4	-0.476	-0.3149	N/A	4.9356	5.095	5.037	5.037
ATG8	-0.2395	-0.1303	N/A	N/A	N/A	N/A	N/A
BNR1	-0.0254	-0.1099	0.25	N/A	N/A	N/A	N/A
BOP2	-0.0678	0.0262	0.0132	4.8088	5.0131	4.928	4.928
BRE5	N/A	-0.0609	0.0013	N/A	1.3018	0.0688	0.0688
BST1	3.4961	3.4596	N/A	N/A	N/A	N/A	N/A
BTS1	N/A	0.5123	0.5163	4.8386	N/A	4.9379	4.9379
BUG1	-0.0477	0.1057	N/A	4.9805	5.0361	N/A	N/A
CAC2	0.7982	0.8701	0.6998	4.8977	4.8911	4.8273	4.8273
CAJ1	-0.1593	-0.146	-0.0958	4.8542	N/A	N/A	N/A
CAP1	N/A	-0.0499	0.1806	N/A	N/A	N/A	N/A
CCW12	1.4203	1.4255	1.6152	N/A	1.6561	1.6358	1.6358
CKA2	0.8758	0.7563	1.1658	4.8301	5.0097	4.8435	4.8435
CNE1	1.1871	N/A	1.0195	N/A	N/A	N/A	N/A
COG5	N/A	0.1272	N/A	N/A	N/A	N/A	N/A
COG6	0.2687	0.3235	N/A	N/A	N/A	4.6417	4.6417
COG8	0.281	0.2635	N/A	N/A	N/A	1.4328	1.4328

CPA1	-0.6105	-0.6124	-0.8076	3.9528	4.3089	4.1934	4.1934
CPR6	0.1262	0.1764	0.1472	4.8898	4.9829	5.0948	5.0948
CRD1	-0.265	-0.3036	N/A	4.8087	4.9672	4.8971	4.8971
CSF1	3.1702	3.2738	3.2965	4.7932	4.9517	4.7345	4.7345
CSN12	-0.6172	-0.524	N/A	4.7509	N/A	4.9118	4.9118
CUE1	1.0488	1.0241	1.2673	4.9709	N/A	N/A	N/A
CWH41	0.5218	0.5415	0.5079	0.0139	1.8236	0.0657	0.0657
CWH43	0.2596	0.1953	N/A	N/A	N/A	N/A	N/A
CYS3	0.7431	1.2647	N/A	N/A	N/A	N/A	N/A
DAL81	N/A	-0.406	N/A	N/A	N/A	N/A	N/A
DAS1	-0.2274	-0.2246	-0.2562	4.8597	5.0383	4.9589	4.9589
DER1	0.8412	0.8263	1.1548	4.9363	N/A	N/A	N/A
DFG10	-0.2762	-0.1662	0.0423	N/A	N/A	N/A	N/A
DGK1	0.0309	-0.0801	0.1163	5.0142	5.0489	N/A	N/A
DIE2	0.7309	0.747	0.9767	N/A	1.857	2.1451	2.1451
DOM34	-0.5762	-0.3832	-0.1897	N/A	N/A	N/A	N/A
DRS2	0.2218	0.3238	0.3777	N/A	N/A	N/A	N/A
DUS3	0.0404	-0.0945	N/A	4.9419	4.99	4.9113	4.9113
ECM30	0.0089	0.1319	N/A	N/A	N/A	2.5608	2.5608
EDE1	0.2082	0.118	N/A	N/A	N/A	N/A	N/A
EGD1	-0.5359	-0.485	-0.5189	N/A	N/A	N/A	N/A
EGD2	-0.4217	-0.3985	-0.3263	4.8987	4.9343	4.9451	4.9451
ELF1	N/A	0.3241	0.3915	4.6219	4.8121	4.6901	4.6901
ELP2	N/A	-0.4381	-0.2428	N/A	N/A	N/A	N/A
EMP47	-0.1593	N/A	N/A	5.003	5.1176	4.9622	4.9622
ENT3	-0.1379	-0.17	0.1291	N/A	N/A	N/A	N/A
ERD1	2.7915	2.8649	2.6871	2.4024	N/A	2.8696	2.8696
ERG2	0.3868	0.3605	0.4795	N/A	N/A	N/A	N/A
ERJ5	0.3344	0.1339	N/A	N/A	N/A	N/A	N/A
ERP1	N/A	0.8865	N/A	5.0081	N/A	4.9538	4.9538
ERP2	0.0939	0.1487	0.3537	4.8963	N/A	4.8319	4.8319
ERV14	1.9212	1.9181	2.0844	N/A	N/A	N/A	N/A
ERV25	2.497	2.4537	2.5138	N/A	N/A	N/A	N/A
ERV29	0.3171	0.4791	0.5387	5.0374	5.0604	5.0641	5.0641
ERV41	N/A	-0.2395	-0.3675	4.9209	4.9793	N/A	N/A
ERV46	-0.3368	-0.3478	-0.3832	4.7351	N/A	N/A	N/A
EUG1	0.3093	0.343	0.4621	5.0642	5.0033	5.0615	5.0615
FAR8	-0.1493	-0.1394	-0.0579	4.7214	N/A	N/A	N/A
FAT1	0.9667	0.9204	0.7502	4.9533	5.222	N/A	N/A
FKH1	0.3118	0.346	0.5493	5.0494	5.161	4.9853	4.9853
FLX1	N/A	-0.3259	N/A	4.8974	4.9553	4.9713	4.9713

FRE4	-0.1671	-0.2638	N/A	4.8737	5.0043	5.0557	5.0557
FUN30	0.1668	0.1873	0.35	N/A	N/A	N/A	N/A
FYV6	N/A	N/A	3.7707	N/A	N/A	N/A	N/A
GCN2	-0.1473	-0.1909	N/A	4.9728	N/A	5.0071	5.0071
GCN20	-0.2321	-0.2038	N/A	4.8089	4.9757	4.8633	4.8633
GCN5	-0.9911	-1.1073	-1.1178	4.4177	4.5699	4.5461	4.5461
GCR2	0.6388	0.523	1.0012	4.6344	4.7974	4.6531	4.6531
GCS1	0.2911	0.3262	0.2994	N/A	N/A	N/A	N/A
GDA1	0.271	0.2536	0.217	4.8675	4.9016	N/A	N/A
GET1	1.0074	2.1743	N/A	1.4237	1.5037	1.4687	1.4687
GET1	N/A	2.174	N/A	1.2572	1.4764	1.1663	1.1663
GET2	1.6531	2.1291	2.1414	1.3742	1.0155	1.5855	1.5855
GET2	N/A	1.9979	2.2189	0.9009	1.2431	1.0052	1.0052
GET3	1.088	0.7439	0.8375	N/A	N/A	N/A	N/A
GET3	N/A	0.7498	0.8965	N/A	1.6618	N/A	N/A
GLO3	N/A	2.1866	2.2768	N/A	1.484	1.0926	1.0926
GNP1	N/A	0.0259	N/A	N/A	N/A	N/A	N/A
GOS1	0.3619	0.3907	0.6255	N/A	N/A	N/A	N/A
GOT1	0.0115	0.0354	-0.0765	4.7679	N/A	N/A	N/A
GSG1	0.1271	0.2326	N/A	4.7775	N/A	N/A	N/A
GSH2	-0.2563	-0.2227	-0.2941	4.7858	N/A	N/A	N/A
GTB1	-0.0084	0.0241	N/A	N/A	N/A	N/A	N/A
GTR1	N/A	N/A	0.2049	N/A	N/A	N/A	N/A
GUP1	2.8145	2.8369	N/A	N/A	1.564	N/A	N/A
GYP8	-0.1225	-0.206	N/A	5.0308	5.0353	5.0615	5.0615
HAC1	-0.6855	-0.7625	N/A	-0.4921	-0.3815	-0.4008	-0.4008
HAM1	-0.4729	-0.3843	N/A	4.8761	5.0353	5.0037	5.0037
HAT2	-0.2885	-0.2775	-0.2965	4.948	4.9718	4.8339	4.8339
HEK2	0.5033	0.4717	0.609	5.0438	5.0951	4.9242	4.9242
HHF1	0.7234	0.8716	N/A	5.2798	5.2597	5.1748	5.1748
HHT1	1.0153	0.9416	N/A	N/A	5.2259	N/A	N/A
HHT2	0.3736	0.4076	0.4018	5.0319	N/A	5.0838	5.0838
HIR3	N/A	0.4039	0.1789	4.9602	5.0852	5.0716	5.0716
HLJ1	1.4252	1.4709	1.5424	4.7715	N/A	N/A	N/A
HMG1	-0.1158	0.0493	0.171	5.0581	5.1311	5.1103	5.1103
HOP2	0.3593	-0.0382	0.6456	4.9879	5.0827	4.8954	4.8954
HPC2	0.1999	0.2083	0.1395	4.8399	N/A	4.9458	4.9458
HRD1	1.7439	1.7391	1.9685	N/A	N/A	N/A	N/A
HRD3	1.3626	1.4187	1.607	4.8857	4.9661	N/A	N/A
HSM3	-0.3339	-0.3362	N/A	4.84	4.9028	N/A	N/A
HSV2	-0.3109	-0.2498	-0.0406	4.972	5.0522	N/A	N/A

HTB2	0.1298	0.144	N/A	5.1025	5.2308	5.0985	5.0985
HTZ1	0.2764	0.2698	0.257	4.9917	N/A	4.907	4.907
HUR1	N/A	1.8088	N/A	1.6749	1.7251	N/A	N/A
HXK2	0.0828	0.2006	0.1962	5.0751	5.0806	5.0286	5.0286
HXT8	N/A	-0.0195	0.0632	N/A	1.5888	2.6444	2.6444
ICE2	0.3416	0.2721	N/A	N/A	N/A	N/A	N/A
IDH1	-0.2366	N/A	N/A	4.8428	4.9899	N/A	N/A
IES1	0.4161	N/A	0.2072	4.9054	4.9457	4.8693	4.8693
IES4	0.4649	0.5466	0.5486	5.1402	5.1547	5.0405	5.0405
IES5	0.2702	0.2765	0.2859	4.6967	4.8733	4.8389	4.8389
ILM1	0.2108	0.3122	N/A	4.6726	4.8708	4.8858	4.8858
INP53	-0.03	0.0561	N/A	N/A	N/A	N/A	N/A
IPK1	N/A	-0.5209	-0.4467	4.5937	N/A	N/A	N/A
IRC21	0.0136	0.0856	0.0625	4.8417	4.9941	N/A	N/A
IRE1	-0.7221	-0.7557	N/A	N/A	-0.5201	N/A	N/A
ISC1	0.1473	0.0055	N/A	4.7271	4.8558	N/A	N/A
ISR1	0.2265	0.1717	N/A	N/A	N/A	4.9644	4.9644
ISW1	N/A	0.4587	0.4685	N/A	N/A	4.658	4.658
ISW2	0.0596	0.0086	0.1836	4.7884	4.8788	N/A	N/A
ITR1	0.2206	0.1759	0.2569	5.0406	5.1085	5.0552	5.0552
IXR1	-0.4814	-0.3697	N/A	4.7271	4.8979	4.8093	4.8093
JEM1	0.0926	0.1329	0.3924	4.9603	5.0946	5.0282	5.0282
KEL1	0.3544	0.3648	N/A	4.8795	N/A	4.9238	4.9238
KEX2	N/A	N/A	N/A	N/A	4.3747	N/A	N/A
KIN3	0.7964	0.8447	0.9724	4.8769	N/A	N/A	N/A
KRE1	0.4205	0.4233	0.3309	N/A	N/A	N/A	N/A
KRE11	0.1763	0.2615	0.1922	N/A	N/A	N/A	N/A
KRE27	-0.0748	0.0715	0.2655	4.9526	4.9377	4.8536	4.8536
KRE27	1.2348	2.0262	N/A	N/A	N/A	N/A	N/A
KTI12	-0.3934	-0.4262	N/A	4.5282	N/A	4.7962	4.7962
LAS21	3.5378	3.4031	3.5912	N/A	4.3515	N/A	N/A
LEM3	N/A	0.5108	0.33	4.6951	N/A	N/A	N/A
LEU3	-0.1948	-0.1944	-0.1252	N/A	N/A	4.7667	4.7667
LOC1	-0.2638	-0.409	-0.1821	0.8579	0.8958	0.9927	0.9927
LPD1	-0.3023	-0.3497	-0.3742	4.682	N/A	4.8509	4.8509
LRC3	0.0041	0.0238	0.0868	4.7828	4.9824	4.9158	4.9158
MAF1	N/A	-0.3837	N/A	4.8597	4.9494	4.988	4.988
MDY2	0.1337	0.0862	0.0857	4.8511	N/A	N/A	N/A
MDY2	0.1783	0.0393	N/A	4.8032	N/A	N/A	N/A
MEH1	0.1631	0.2058	N/A	4.3977	N/A	4.4841	4.4841
MGA2	1.2413	1.855	N/A	N/A	N/A	N/A	N/A

MKC7	-0.0639	-0.0909	N/A	4.8147	4.9683	N/A	N/A
MNL1	0.0096	0.0099	0.1955	4.8114	4.9512	4.9229	4.9229
MNN2	0.3513	0.6881	0.3409	N/A	N/A	N/A	N/A
MNN4	N/A	0.0459	N/A	4.961	5.1569	5.0768	5.0768
MNN5	-0.0905	-0.0526	-0.1528	4.9084	N/A	N/A	N/A
MNN9	-0.2798	-0.1796	N/A	4.8905	N/A	4.9598	4.9598
MNS1	-0.1794	-0.0977	N/A	4.8817	N/A	4.9288	4.9288
MPD1	0.4312	0.3992	0.7255	4.8904	N/A	4.8805	4.8805
MSC1	N/A	0.5625	N/A	4.9396	N/A	N/A	N/A
MSI1	0.6863	0.5688	N/A	4.7716	N/A	4.7582	4.7582
MTC1	0.0223	0.0666	0.0614	N/A	N/A	N/A	N/A
MTC5	N/A	-0.0859	0.0661	4.8602	N/A	4.8324	4.8324
MVP1	N/A	0.1273	0.0625	N/A	1.6008	1.3831	1.3831
NEM1	0.6303	0.6236	0.4901	N/A	N/A	N/A	N/A
NFT1	-0.3019	-0.2045	-0.2793	4.9085	5.0007	5.0541	5.0541
NHP6A	N/A	-0.2897	N/A	4.9413	5.0527	4.9104	4.9104
NHX1	0.9253	0.9087	0.9669	4.7306	N/A	N/A	N/A
NMD4	-0.411	-0.3996	N/A	4.6773	N/A	N/A	N/A
NPL4	-0.0547	-0.1038	0.0783	4.7343	4.9444	4.8506	4.8506
OLA1	-0.3817	-0.2636	N/A	4.7715	N/A	N/A	N/A
OPI10	-0.2182	-0.194	-0.1824	4.8091	N/A	4.7772	4.7772
OPI3	1.1738	1.1042	0.9375	N/A	1.4184	N/A	N/A
OST3	2.7665	2.7924	3.032	2.4841	N/A	2.7566	2.7566
OST5	0.3574	0.4436	N/A	N/A	N/A	N/A	N/A
OYE2	-0.3308	-0.354	N/A	4.8774	N/A	N/A	N/A
PBP1	-0.386	-0.3965	-0.383	N/A	N/A	N/A	N/A
PCT1	0.2794	0.5333	0.3472	4.9564	5.0012	4.917	4.917
PEF1	0.2869	0.2857	0.3	4.7166	N/A	N/A	N/A
PEP7	-0.5521	-0.4327	-0.4213	N/A	N/A	N/A	N/A
PEP8	N/A	0.2154	0.2205	N/A	N/A	N/A	N/A
PET18	-0.0978	-0.1114	N/A	4.8922	N/A	4.9635	4.9635
PHO80	1.0206	1.0998	1.4642	N/A	N/A	N/A	N/A
PHO86	0.1507	0.1335	N/A	4.5831	N/A	4.8015	4.8015
PMP1	-0.2068	-0.0008	N/A	4.5719	4.724	4.1826	4.1826
PMR1	N/A	N/A	N/A	N/A	N/A	N/A	N/A
PMT1	1.6268	1.7885	1.9023	4.8475	N/A	4.7204	4.7204
PMT2	2.8731	2.8002	2.9393	4.9697	N/A	N/A	N/A
PPH21	-0.2545	-0.2571	-0.0514	4.9636	5.0113	5.0842	5.0842
PPT1	0.0788	0.0994	0.129	4.8278	5.0542	4.937	4.937
PRM2	-0.5108	-0.3813	-0.3011	4.7651	N/A	4.9172	4.9172
PSD2	0.1872	0.2804	0.2537	4.7455	N/A	N/A	N/A

PTC2	-0.1572	-0.0722	-0.1546	4.8724	5.0909	4.8134	4.8134
PTK2	0.1057	0.1609	0.1273	4.6736	4.6726	4.7514	4.7514
PTP1	-0.3056	-0.2552	N/A	4.7791	N/A	N/A	N/A
PTR2	-0.3999	-0.2411	N/A	4.8314	4.9002	4.8568	4.8568
RAD23	N/A	-0.1593	N/A	4.684	N/A	N/A	N/A
RAV1	N/A	0.3196	N/A	N/A	N/A	N/A	N/A
RCO1	0.2493	0.2599	0.5879	4.8797	N/A	4.9871	4.9871
RER1	0.0691	0.1834	0.1244	N/A	N/A	N/A	N/A
REX4	-0.3452	-0.3693	-0.3771	4.818	N/A	N/A	N/A
RGP1	0.0552	0.0129	0.1388	N/A	N/A	N/A	N/A
RLF2	N/A	0.7573	0.7118	4.9558	4.9143	N/A	N/A
ROT2	0.3608	0.4799	0.3556	N/A	0.4715	N/A	N/A
ROX1	-0.3262	-0.2562	N/A	N/A	4.8139	N/A	N/A
RPA14	-0.4042	-0.3279	-0.3745	5.4107	5.503	N/A	N/A
RPL19B	N/A	-0.7237	N/A	4.6689	4.765	4.7895	4.7895
RPN10	-0.4709	-0.4916	-0.4196	4.7383	N/A	4.8414	4.8414
RPS11A	N/A	-0.5539	N/A	N/A	N/A	N/A	N/A
RPS12	0.2615	0.3334	N/A	4.9478	5.0448	4.984	4.984
RPS16A	N/A	-0.9726	-0.7198	N/A	N/A	N/A	N/A
RPS17A	-1.2305	-1.1744	-0.8818	N/A	N/A	N/A	N/A
RPS23A	-0.6533	-0.6831	-0.5535	N/A	N/A	N/A	N/A
RPS28B	-0.7381	-0.7216	-0.6388	4.8616	N/A	N/A	N/A
RPS4B	-0.1945	-0.2129	-0.1689	4.8894	4.8838	4.9081	4.9081
RPS6B	-0.7838	-0.7447	-0.7354	4.789	N/A	N/A	N/A
RTN1	N/A	-0.0583	N/A	N/A	N/A	N/A	N/A
RTT10	-0.4918	-0.4255	-0.4272	4.7068	N/A	N/A	N/A
RTT106	N/A	1.2206	1.1135	4.6798	4.9507	4.7708	4.7708
RUD3	0.2108	0.3105	0.3976	1.3502	1.1519	1.5549	1.5549
SAC7	0.5047	0.4314	0.5158	N/A	N/A	N/A	N/A
SBH2	N/A	-0.1002	0.016	4.9132	4.9896	N/A	N/A
SCJ1	4.3649	4.3413	4.1895	N/A	N/A	N/A	N/A
SEC22	N/A	0.2104	1.4091	N/A	1.9324	1.2763	1.2763
SEC28	-0.4445	-0.4157	-0.2068	4.8435	N/A	4.7341	4.7341
SEC66	0.5823	0.9039	N/A	N/A	N/A	N/A	N/A
SEC72	-0.3077	-0.1593	-0.1711	4.9476	4.9245	4.8347	4.8347
SED4	0.2098	0.1935	0.1375	N/A	5.1198	N/A	N/A
SET3	0.0413	0.0383	N/A	N/A	N/A	4.9314	4.9314
SEY1	0.2502	0.282	0.6789	4.9784	5.0932	4.979	4.979
SFB2	0.0108	-0.0072	N/A	5.0021	5.1779	5.0605	5.0605
SGM1	N/A	-0.1728	N/A	4.8527	5.0487	4.9646	4.9646
SGT2	-0.1256	-0.0435	0.0839	N/A	N/A	4.9093	4.9093

SGT2	-0.0765	-0.0216	N/A	4.9204	N/A	N/A	N/A
SIF2	0.4409	0.3734	0.7118	4.9299	N/A	N/A	N/A
SIL1	0.8427	0.7952	0.7596	N/A	N/A	N/A	N/A
SKY1	1.0151	0.8525	0.8692	4.8474	4.9463	4.7741	4.7741
SLA1	-0.2451	-0.2056	0.0081	4.8129	5.1908	4.9326	4.9326
SLP1	0.6604	0.6694	N/A	4.8377	4.9626	4.8105	4.8105
SMI1	0.7192	0.7371	0.6811	N/A	N/A	N/A	N/A
SNT1	0.3716	0.2889	N/A	N/A	N/A	N/A	N/A
SOP4	-0.1696	-0.1335	0.0836	5.023	N/A	4.902	4.902
SOP4	4.3107	4.1647	N/A	N/A	N/A	N/A	N/A
SPC1	0.2288	0.2772	N/A	N/A	N/A	N/A	N/A
SPC2	2.1501	2.1871	2.1595	1.9617	2.1142	2.3728	2.3728
SPE3	N/A	-0.2623	N/A	4.8302	N/A	N/A	N/A
SPE4	-0.241	-0.2159	N/A	5.0643	5.1149	N/A	N/A
SPF1	4.0355	4.1732	3.8854	3.7708	3.8997	3.7111	3.7111
SQS1	-0.3071	-0.3278	-0.2937	N/A	N/A	N/A	N/A
SRP40	-0.7416	-0.5081	-0.7442	N/A	N/A	N/A	N/A
SSA2	-0.5445	-0.5422	-0.4248	4.7344	N/A	N/A	N/A
SSA3	-0.2614	-0.1021	0.0131	4.9032	N/A	4.974	4.974
SSA4	-0.1672	-0.1969	-0.0541	5.0645	N/A	4.9256	4.9256
SSM4	0.1148	0.1015	N/A	4.8749	5.2087	N/A	N/A
STE24	3.9376	3.6018	3.8783	N/A	4.5955	3.8806	3.8806
STP22	0.1079	0.6202	-0.0128	N/A	N/A	N/A	N/A
SUM1	N/A	0.4928	0.7867	N/A	N/A	N/A	N/A
SUR4	N/A	1.1244	1.0379	4.612	N/A	N/A	N/A
SVP26	-0.1751	-0.0725	N/A	N/A	N/A	N/A	N/A
SWC3	0.0677	0	0.2299	5.0359	5.1268	4.9658	4.9658
SWC5	N/A	-0.279	0.3543	4.9967	5.1128	5.0591	5.0591
SWP82	-0.2823	-0.2759	N/A	4.965	N/A	4.9758	4.9758
SYS1	0.4507	0.431	0.433	N/A	N/A	N/A	N/A
TED1	N/A	1.5382	2.1462	N/A	4.857	N/A	N/A
THI6	-0.444	-0.3306	-0.2218	4.928	4.9764	N/A	N/A
TIR3	-0.2403	-0.0796	-0.0087	4.8293	5.0918	4.9058	4.9058
TLG2	0.5092	0.5614	0.3656	N/A	N/A	N/A	N/A
TMA19	N/A	-0.3673	-0.377	N/A	N/A	N/A	N/A
TOF2	N/A	-0.3272	N/A	4.9101	N/A	N/A	N/A
TRM1	-0.4789	-0.449	-0.3835	4.8815	N/A	4.8473	4.8473
TRM7	-0.474	-0.5292	N/A	4.6852	N/A	N/A	N/A
TRP3	-0.2819	-0.0773	N/A	4.5727	4.7837	4.7171	4.7171
TSR2	-0.7142	-0.6913	-0.645	N/A	N/A	N/A	N/A
UBC4	-0.3746	-0.4678	N/A	N/A	N/A	N/A	N/A

UBC7	1.2917	1.3429	1.3783	4.7704	N/A	4.7828	4.7828
UBR1	-0.2902	-0.2535	N/A	4.8827	4.9669	4.8562	4.8562
UBR2	-0.2537	-0.2914	-0.305	4.8534	N/A	N/A	N/A
UBX2	2.2662	2.4889	2.3746	N/A	N/A	N/A	N/A
UBX4	0.2618	0.4447	0.5309	N/A	4.9412	N/A	N/A
UFD2	0.4012	0.528	0.5861	4.872	4.9804	4.9068	4.9068
UME1	-0.4168	-0.4635	-0.5409	4.9621	N/A	N/A	N/A
USA1	1.0185	1.0454	1.2426	4.9623	N/A	4.9626	4.9626
UTH1	0.5497	0.5791	0.5505	4.9346	5.0852	4.9142	4.9142
VPS1	0.2615	1.3673	N/A	N/A	N/A	N/A	N/A
VPS28	N/A	0.8283	0.4264	N/A	N/A	N/A	N/A
VPS29	N/A	0.4075	0.2719	N/A	N/A	N/A	N/A
VPS3	N/A	0.8052	0.6096	0.7544	1.5432	0.7802	0.7802
VPS30	0.2661	0.0493	0.2336	4.7348	N/A	N/A	N/A
VPS38	0.2221	0.3942	0.3203	4.6567	N/A	4.7274	4.7274
VPS51	N/A	2.1661	N/A	N/A	N/A	N/A	N/A
VPS52	N/A	1.2331	0.5436	N/A	N/A	N/A	N/A
VPS53	N/A	0.1693	N/A	1.0983	1.0152	1.0706	1.0706
VPS54	0.6302	0.5483	N/A	1.1974	N/A	1.1372	1.1372
VPS71	-0.0318	-0.0182	N/A	4.9423	N/A	4.9771	4.9771
VPS72	-0.0939	0.0442	0.3653	5.0342	5.2261	5.0731	5.0731
VPS74	N/A	0.9709	1.1047	N/A	N/A	N/A	N/A
VPS75	-0.4308	-0.4433	-0.4397	4.8047	4.8379	N/A	N/A
VTC1	0.0772	0.0065	N/A	4.835	N/A	N/A	N/A
VTC4	0.3828	0.2715	N/A	5.0979	N/A	5.1222	5.1222
WSC4	-0.0957	-0.169	0.0905	4.8885	N/A	4.9041	4.9041
WT_dhis3::KAN	-0.1836	-0.1906	-0.1037	4.8189	N/A	4.8037	4.8037
WT_dhis3::KAN	-0.1523	-0.097	N/A	4.8551	N/A	5.009	5.009
WT_dhis3::KAN	-0.1307	-0.109	0.0082	4.7755	5.044	N/A	N/A
WT_dhis3::KAN	-0.1233	-0.0407	N/A	4.9636	4.9464	4.8969	4.8969
YAP5	-0.1668	-0.0007	-0.0522	4.9589	5.0585	N/A	N/A
YBR137W	-0.1055	-0.1762	N/A	5.0961	N/A	4.9454	4.9454
YBR226C	-0.0984	-0.0587	-0.1332	N/A	4.9943	N/A	N/A
YBR238C	N/A	0.2066	0.2906	4.9173	4.973	4.9262	4.9262
YCK1	-0.005	-0.0189	N/A	4.7895	N/A	4.8592	4.8592
YCK2	0.0358	-0.0969	0.2266	4.9584	5.0138	4.9083	4.9083
YCL045C	0.0717	-0.0305	0.2163	4.9179	5.0346	4.8829	4.8829
YDL133W	-0.1234	-0.0421	0.0388	4.8683	4.9657	4.9903	4.9903
YDL157C	-0.2988	-0.2004	N/A	4.8773	4.9667	4.9132	4.9132
YDL242W	-0.2379	-0.1205	N/A	4.9408	4.9842	5.011	5.011
YDR049W	N/A	-0.3052	-0.1223	N/A	N/A	N/A	N/A

YDR056C	-0.2469	-0.1725	-0.0526	4.9039	4.9786	4.8769	4.8769
YDR056C	1.3567	N/A	2.1945	4.716	N/A	N/A	N/A
YDR161W	-0.4503	-0.4022	-0.2544	4.7213	N/A	N/A	N/A
YEL014C	0.0173	-0.0925	0.2138	4.7233	4.8364	N/A	N/A
YEL047C	-0.2065	-0.1979	N/A	4.8579	N/A	4.8527	4.8527
YER064C	0.2553	0.2963	0.3512	4.8314	4.9477	4.7721	4.7721
YER140W	0.7416	0.7471	N/A	N/A	N/A	N/A	N/A
YER156C	-0.5263	-0.517	-0.4806	4.5741	4.6056	4.6928	4.6928
YET1	-0.1345	-0.1613	-0.1194	4.882	4.9803	N/A	N/A
YFR018C	0.1718	0.3126	0.4628	4.8222	4.968	4.7512	4.7512
YFR045W	0.0339	-0.038	0.1938	N/A	1.465	N/A	N/A
YGL007W	N/A	0.5094	0.7305	N/A	N/A	3.4512	3.4512
YGL231C	0.0115	0.1188	N/A	4.8734	4.9368	4.8587	4.8587
YHR003C	0.1275	0.2187	0.4649	4.9562	5.0713	4.9411	4.9411
YHR078W	0.5428	0.6113	0.648	N/A	N/A	4.479	4.479
YIL029C	-0.0554	-0.0092	0.1888	4.9549	N/A	N/A	N/A
YIL032C	-0.1071	-0.0326	N/A	4.8917	5.0296	N/A	N/A
YIL055C	-0.0576	0.0158	0.0324	4.8008	5.0357	N/A	N/A
YIP3	-0.0173	0.0412	N/A	4.9537	5.0773	N/A	N/A
YJL055W	-0.3194	-0.2775	N/A	4.8702	N/A	5.0816	5.0816
YJR088C	0.0671	0.0375	N/A	N/A	4.8799	N/A	N/A
YKR043C	-0.0495	-0.0833	N/A	4.8608	5.0382	5.0378	5.0378
YLL014W	0.1803	-0.1132	N/A	N/A	5.0348	N/A	N/A
YLL014W	N/A	0.1607	0.0963	4.8652	N/A	N/A	N/A
YLR104W	0.5985	0.58	0.6315	N/A	N/A	N/A	N/A
YLR278C	-0.0155	0.0214	0.2383	4.8983	5.052	5.0131	5.0131
YLR287C	-0.2186	-0.2049	-0.008	4.8996	N/A	4.9972	4.9972
YLR402W	-0.2761	-0.2491	-0.4318	N/A	N/A	N/A	N/A
YML108W	-0.4711	-0.4113	-0.3721	4.8246	4.9602	4.8951	4.8951
YMR209C	-0.4081	-0.271	-0.2711	5.1044	5.0539	N/A	N/A
YNL205C	0.3131	0.5516	0.5127	4.8877	5.0766	4.9432	4.9432
YOL159C	-0.3676	N/A	N/A	4.7779	4.9752	4.8913	4.8913
YOR164C	0.1316	0.1569	N/A	4.8373	N/A	4.8794	4.8794
YOR164C	N/A	-0.0558	N/A	4.6761	N/A	4.8455	4.8455
YOS9	0.6535	0.6013	0.6826	N/A	N/A	N/A	N/A
YPL068C	-0.455	-0.3522	N/A	5.0066	N/A	5.0229	5.0229
YPR063C	-0.1219	-0.0351	0.1772	4.8921	5.0559	5.0042	5.0042
YPR063C	-0.0519	-0.0073	0.0014	4.8225	5.0008	4.9675	4.9675
YPR084W	-0.3238	-0.2365	-0.0222	4.8502	5.0079	N/A	N/A
YPR130C	0.2057	0.2216	0.3872	4.8456	N/A	4.8912	4.8912
YUR1	0.6046	0.7038	N/A	N/A	5.007	N/A	N/A

ZAP1	N/A	-0.061	N/A	N/A	1.3806	0.9357	0.9357
VIP1	N/A	N/A	N/A	N/A	N/A	N/A	N/A
YJR088C	N/A	N/A	N/A	N/A	N/A	N/A	N/A

Table 9: The $\log_2$ (GFP/RFP) reporter values obtained in the double mutant strains when *KAR2::NAT* or *kar2-P515L-DamP::NAT* were crossed against the genes listed in table 6

* N/A indicates either that the double mutant strain was inviable or that a value was not obtained due to experimental error

Array name	KAR2-WT (1)	KAR2-WT (2)	KAR2-WT (3)	kar2-P515L-DamP (1)	kar2-P515L-DamP (2)	kar2-P515L-DamP (3)
ADD66	N/A	-0.3026	-0.1376	1.2085	1.3261	1.3036
AGX1	-0.1732	-0.095	-0.1543	1.3184	1.4848	N/A
AHC2	-0.0227	0.0194	N/A	1.1874	1.334	1.4429
ALF1	N/A	1.12	2.1491	1.344	1.2716	N/A
ALG12	1.5689	1.4467	N/A	1.6915	1.4232	1.3722
ALG3	2.2605	2.3585	2.6165	1.6522	1.4654	1.9978
ALG5	1.4492	1.5665	1.68	1.1646	1.2825	1.3523
ALG6	2.0957	2.041	2.1605	1.2927	1.4438	N/A
ALG8	1.6379	1.7204	1.9019	1.0997	1.2918	1.3923
ALG9	1.4766	1.5067	2.0133	N/A	N/A	N/A
APE3	-0.3075	-0.1964	-0.0032	1.133	1.3161	0.8998
ARC18	0.5786	0.6766	0.8138	1.3672	1.3607	1.4121
ARL1	0.6144	0.435	0.4247	1.2193	1.4985	1.2915
ARO1	0.444	N/A	0.0412	1.2788	1.2712	1.3964
ARP6	0.1656	0.1677	0.2997	1.2688	1.4044	1.351
ARV1	N/A	4.0563	N/A	N/A	N/A	1.7804
ASM4	-0.476	-0.3149	N/A	1.3517	1.4696	N/A
ATG8	-0.2395	-0.1303	N/A	1.3919	1.3725	1.0304
BNR1	-0.0254	-0.1099	0.25	1.5128	N/A	1.2935
BOP2	-0.0678	0.0262	0.0132	1.4773	1.6924	1.3978
BRE5	N/A	-0.0609	0.0013	1.4151	1.6425	1.3542
BST1	3.4961	3.4596	N/A	N/A	1.3815	1.2512
BTS1	N/A	0.5123	0.5163	1.8871	2.2546	1.2025
BUG1	-0.0477	0.1057	N/A	1.3772	1.5591	1.1671
CAC2	0.7982	0.8701	0.6998	1.5713	1.6411	1.5231
CAJ1	-0.1593	-0.146	-0.0958	1.3602	1.421	1.4738
CAP1	N/A	-0.0499	0.1806	1.3169	1.3613	1.2333
CCW12	1.4203	1.4255	1.6152	1.3702	1.5081	1.4044
CKA2	0.8758	0.7563	1.1658	1.3843	1.7614	1.8113
CNE1	1.1871	N/A	1.0195	1.3048	1.2239	1.292
COG5	N/A	0.1272	N/A	1.2195	1.2176	1.3197

COG6	0.2687	0.3235	N/A	1.3728	1.5027	1.3182
COG8	0.281	0.2635	N/A	1.45	1.5356	1.2231
CPA1	-0.6105	-0.6124	-0.8076	1.01	1.118	1.225
CPR6	0.1262	0.1764	0.1472	1.3859	1.5037	1.4232
CRD1	-0.265	-0.3036	N/A	1.3638	1.1944	1.2403
CSF1	3.1702	3.2738	3.2965	1.4231	1.4478	1.4199
CSN12	-0.6172	-0.524	N/A	1.1814	1.1932	1.0864
CUE1	1.0488	1.0241	1.2673	1.5819	1.8063	1.4657
CWH41	0.5218	0.5415	0.5079	1.6628	1.9109	1.242
CWH43	0.2596	0.1953	N/A	1.4282	1.3978	1.2821
CYS3	0.7431	1.2647	N/A	1.3414	N/A	1.3688
DAL81	N/A	-0.406	N/A	1.1538	1.1183	1.1124
DAS1	-0.2274	-0.2246	-0.2562	0.7985	1.0798	1.2254
DER1	0.8412	0.8263	1.1548	1.6344	2.0282	1.5346
DFG10	-0.2762	-0.1662	0.0423	1.2798	1.2799	1.116
DGK1	0.0309	-0.0801	0.1163	1.3575	1.3247	1.4716
DIE2	0.7309	0.747	0.9767	1.2285	1.3323	1.5417
DOM34	-0.5762	-0.3832	-0.1897	1.1267	1.2258	1.0474
DRS2	0.2218	0.3238	0.3777	1.2452	1.3204	1.35
DUS3	0.0404	-0.0945	N/A	1.343	1.5386	1.2808
ECM30	0.0089	0.1319	N/A	1.3736	1.3881	1.0424
EDE1	0.2082	0.118	N/A	1.1855	1.2883	1.2417
EGD1	-0.5359	-0.485	-0.5189	0.7362	0.6065	1.2035
EGD2	-0.4217	-0.3985	-0.3263	0.6712	0.8267	1.0712
ELF1	N/A	0.3241	0.3915	1.3764	1.376	N/A
ELP2	N/A	-0.4381	-0.2428	1.3201	1.1906	1.3696
EMP47	-0.1593	N/A	N/A	1.4585	1.4009	1.4058
ENT3	-0.1379	-0.17	0.1291	1.1239	1.3909	1.2647
ERD1	2.7915	2.8649	2.6871	1.1923	1.4203	1.4007
ERG2	0.3868	0.3605	0.4795	0.9431	1.3308	1.3032
ERJ5	0.3344	0.1339	N/A	1.6101	1.3683	1.4167
ERP1	N/A	0.8865	N/A	1.9039	1.5768	1.3411
ERP2	0.0939	0.1487	0.3537	1.4133	1.3711	1.2611
ERV14	1.9212	1.9181	2.0844	1.7614	2.0047	1.5675
ERV25	2.497	2.4537	2.5138	1.5177	1.4715	1.634
ERV29	0.3171	0.4791	0.5387	1.7034	1.736	1.4974
ERV41	N/A	-0.2395	-0.3675	1.1535	1.1688	1.074
ERV46	-0.3368	-0.3478	-0.3832	0.7421	0.9939	0.9487
EUG1	0.3093	0.343	0.4621	1.4904	N/A	N/A
FAR8	-0.1493	-0.1394	-0.0579	1.1623	1.2928	1.3615
FAT1	0.9667	0.9204	0.7502	1.3661	1.5601	1.5512

FKH1	0.3118	0.346	0.5493	N/A	N/A	1.6651
FLX1	N/A	-0.3259	N/A	1.4329	1.3416	1.4058
FRE4	-0.1671	-0.2638	N/A	1.3029	1.0992	0.7137
FUN30	0.1668	0.1873	0.35	1.4583	1.4928	1.517
FYV6	N/A	N/A	3.7707	1.1166	1.1468	1.2354
GCN2	-0.1473	-0.1909	N/A	1.0331	1.12	N/A
GCN20	-0.2321	-0.2038	N/A	1.2835	1.429	1.2285
GCN5	-0.9911	-1.1073	-1.1178	1.1615	1.1642	1.3648
GCR2	0.6388	0.523	1.0012	1.3922	1.384	1.2907
GCS1	0.2911	0.3262	0.2994	1.2876	1.4013	1.3111
GDA1	0.271	0.2536	0.217	1.2463	1.3983	1.416
GET1	1.0074	2.1743	N/A	1.251	1.5964	1.424
GET1	N/A	2.174	N/A	1.4287	1.5456	1.2639
GET2	1.6531	2.1291	2.1414	1.1161	1.303	1.1641
GET2	N/A	1.9979	2.2189	1.1887	1.204	1.1559
GET3	1.088	0.7439	0.8375	1.3095	1.4931	1.4989
GET3	N/A	0.7498	0.8965	N/A	1.1577	1.3213
GLO3	N/A	2.1866	2.2768	1.4833	1.6502	1.5158
GNP1	N/A	0.0259	N/A	0.9554	1.1085	N/A
GOS1	0.3619	0.3907	0.6255	1.2517	1.3514	1.2728
GOT1	0.0115	0.0354	-0.0765	1.2998	1.3359	1.2961
GSG1	0.1271	0.2326	N/A	1.2592	1.6761	1.3042
GSH2	-0.2563	-0.2227	-0.2941	1.1592	1.2904	1.2214
GTB1	-0.0084	0.0241	N/A	1.4393	1.491	1.5725
GTR1	N/A	N/A	0.2049	0.9645	0.9785	1.3166
GUP1	2.8145	2.8369	N/A	1.5706	1.5491	1.1434
GYP8	-0.1225	-0.206	N/A	1.3388	1.2733	1.3813
HAC1	-0.6855	-0.7625	N/A	0.6111	0.6941	0.537
HAM1	-0.4729	-0.3843	N/A	-0.0336	-0.2384	1.1161
HAT2	-0.2885	-0.2775	-0.2965	1.0907	1.2806	1.0342
HEK2	0.5033	0.4717	0.609	1.7912	1.688	1.8775
HHF1	0.7234	0.8716	N/A	N/A	N/A	1.5359
HHT1	1.0153	0.9416	N/A	N/A	1.4757	1.2255
HHT2	0.3736	0.4076	0.4018	1.4472	1.6219	1.3177
HIR3	N/A	0.4039	0.1789	1.5803	1.4809	1.4345
HLJ1	1.4252	1.4709	1.5424	1.3038	1.5259	1.4562
HMG1	-0.1158	0.0493	0.171	1.3338	1.2805	1.5527
HOP2	0.3593	-0.0382	0.6456	1.9731	2.0025	2.1094
HPC2	0.1999	0.2083	0.1395	1.1804	1.2984	1.3113
HRD1	1.7439	1.7391	1.9685	1.4955	1.6066	1.7561
HRD3	1.3626	1.4187	1.607	1.8509	2.2958	2.5182

HSM3	-0.3339	-0.3362	N/A	1.3436	1.3689	1.3456
HSV2	-0.3109	-0.2498	-0.0406	0.9543	1.106	1.1079
HTB2	0.1298	0.144	N/A	1.2897	1.5062	1.3139
HTZ1	0.2764	0.2698	0.257	1.3119	1.5172	1.4319
HUR1	N/A	1.8088	N/A	1.4252	1.5811	N/A
HXK2	0.0828	0.2006	0.1962	N/A	N/A	1.5114
HXT8	N/A	-0.0195	0.0632	N/A	1.1646	1.116
ICE2	0.3416	0.2721	N/A	1.5249	1.8163	1.4205
IDH1	-0.2366	N/A	N/A	1.2402	1.4247	1.0758
IES1	0.4161	N/A	0.2072	1.4961	1.5706	1.4908
IES4	0.4649	0.5466	0.5486	1.6234	1.4294	1.3954
IES5	0.2702	0.2765	0.2859	1.7733	2.0119	1.4092
ILM1	0.2108	0.3122	N/A	1.2081	1.4293	1.3005
INP53	-0.03	0.0561	N/A	1.3394	1.3619	1.4145
IPK1	N/A	-0.5209	-0.4467	1.1663	1.2189	0.9864
IRC21	0.0136	0.0856	0.0625	1.3971	1.6048	N/A
IRE1	-0.7221	-0.7557	N/A	0.2803	0.5253	0.2888
ISC1	0.1473	0.0055	N/A	1.291	1.4106	1.3857
ISR1	0.2265	0.1717	N/A	N/A	1.4325	1.3985
ISW1	N/A	0.4587	0.4685	1.3335	1.4628	1.4419
ISW2	0.0596	0.0086	0.1836	N/A	N/A	N/A
ITR1	0.2206	0.1759	0.2569	1.4597	1.4928	1.1999
IXR1	-0.4814	-0.3697	N/A	1.2839	N/A	1.2919
JEM1	0.0926	0.1329	0.3924	1.2527	1.4349	1.5575
KEL1	0.3544	0.3648	N/A	1.2086	1.266	1.372
KEX2	N/A	N/A	N/A	N/A	N/A	N/A
KIN3	0.7964	0.8447	0.9724	1.1237	1.2663	1.3754
KRE1	0.4205	0.4233	0.3309	1.1988	1.304	1.2926
KRE11	0.1763	0.2615	0.1922	1.1715	1.3599	1.166
KRE27	-0.0748	0.0715	0.2655	1.4773	N/A	1.3378
KRE27	1.2348	2.0262	N/A	1.208	N/A	1.3081
KTI12	-0.3934	-0.4262	N/A	1.3165	1.4653	1.4437
LAS21	3.5378	3.4031	3.5912	1.527	1.5235	1.3899
LEM3	N/A	0.5108	0.33	1.4935	1.5046	1.7544
LEU3	-0.1948	-0.1944	-0.1252	1.3918	1.1941	1.2512
LOC1	-0.2638	-0.409	-0.1821	0.8067	1.0657	0.9176
LPD1	-0.3023	-0.3497	-0.3742	1.3208	1.4176	1.272
LRC3	0.0041	0.0238	0.0868	1.3747	N/A	1.5393
MAF1	N/A	-0.3837	N/A	1.0667	1.382	0.9576
MDY2	0.1337	0.0862	0.0857	1.2459	1.5308	1.2809
MDY2	0.1783	0.0393	N/A	N/A	N/A	1.1502

MEH1	0.1631	0.2058	N/A	1.2977	N/A	1.2994
MGA2	1.2413	1.855	N/A	1.3952	1.5407	1.2119
MKC7	-0.0639	-0.0909	N/A	1.2357	1.2909	1.3012
MNL1	0.0096	0.0099	0.1955	1.2897	1.3456	1.4916
MNN2	0.3513	0.6881	0.3409	1.3408	1.5266	1.3917
MNN4	N/A	0.0459	N/A	1.175	1.3069	N/A
MNN5	-0.0905	-0.0526	-0.1528	1.2361	1.4207	1.3058
MNN9	-0.2798	-0.1796	N/A	1.035	1.2891	1.2224
MNS1	-0.1794	-0.0977	N/A	1.2638	N/A	1.2137
MPD1	0.4312	0.3992	0.7255	1.5134	1.7032	1.6953
MSC1	N/A	0.5625	N/A	1.4253	1.2648	1.2741
MSI1	0.6863	0.5688	N/A	1.3928	1.4599	1.3423
MTC1	0.0223	0.0666	0.0614	1.373	1.433	1.1041
MTC5	N/A	-0.0859	0.0661	1.1699	1.1847	1.3581
MVP1	N/A	0.1273	0.0625	1.3085	1.3468	1.1516
NEM1	0.6303	0.6236	0.4901	1.1252	1.1959	1.2322
NFT1	-0.3019	-0.2045	-0.2793	1.2408	1.3591	1.3241
NHP6A	N/A	-0.2897	N/A	1.1691	1.282	0.8856
NHX1	0.9253	0.9087	0.9669	1.3524	1.5373	1.4686
NMD4	-0.411	-0.3996	N/A	1.1848	N/A	0.862
NPL4	-0.0547	-0.1038	0.0783	1.3152	N/A	N/A
OLA1	-0.3817	-0.2636	N/A	1.202	1.4063	1.3359
OPI10	-0.2182	-0.194	-0.1824	1.3003	1.482	1.4013
OPI3	1.1738	1.1042	0.9375	1.3647	1.4385	1.3341
OST3	2.7665	2.7924	3.032	1.3312	1.4938	1.4736
OST5	0.3574	0.4436	N/A	1.3811	1.3714	2.1107
OYE2	-0.3308	-0.354	N/A	N/A	N/A	1.2821
PBP1	-0.386	-0.3965	-0.383	0.6763	0.957	1.2827
PCT1	0.2794	0.5333	0.3472	1.1717	1.7385	1.5698
PEF1	0.2869	0.2857	0.3	1.4102	1.5384	1.3055
PEP7	-0.5521	-0.4327	-0.4213	1.255	1.4311	1.3183
PEP8	N/A	0.2154	0.2205	N/A	1.4587	1.3428
PET18	-0.0978	-0.1114	N/A	1.2347	1.2398	N/A
PHO80	1.0206	1.0998	1.4642	1.0284	1.181	1.2134
PHO86	0.1507	0.1335	N/A	1.0908	1.2473	1.3851
PMP1	-0.2068	-0.0008	N/A	1.3189	1.4367	1.0666
PMR1	N/A	N/A	N/A	1.4306	1.5947	1.256
PMT1	1.6268	1.7885	1.9023	1.3667	1.6166	0.8062
PMT2	2.8731	2.8002	2.9393	N/A	N/A	N/A
PPH21	-0.2545	-0.2571	-0.0514	1.3773	N/A	N/A
PPT1	0.0788	0.0994	0.129	1.4085	1.4911	1.3733

PRM2	-0.5108	-0.3813	-0.3011	N/A	0.9595	0.8702
PSD2	0.1872	0.2804	0.2537	1.5748	1.8388	1.3987
PTC2	-0.1572	-0.0722	-0.1546	1.2749	1.4181	0.9693
PTK2	0.1057	0.1609	0.1273	1.1338	1.3596	1.2573
PTP1	-0.3056	-0.2552	N/A	N/A	1.0062	N/A
PTR2	-0.3999	-0.2411	N/A	1.1609	1.4355	1.1161
RAD23	N/A	-0.1593	N/A	1.1837	1.4606	1.284
RAV1	N/A	0.3196	N/A	1.1947	1.2663	1.3983
RCO1	0.2493	0.2599	0.5879	1.4564	1.4695	1.2276
RER1	0.0691	0.1834	0.1244	0.5543	0.7864	1.2147
REX4	-0.3452	-0.3693	-0.3771	1.1144	1.3307	1.5057
RGP1	0.0552	0.0129	0.1388	1.3136	1.427	1.3147
RLF2	N/A	0.7573	0.7118	1.3581	N/A	1.2942
ROT2	0.3608	0.4799	0.3556	1.2546	1.2631	1.2334
ROX1	-0.3262	-0.2562	N/A	N/A	1.3723	1.2899
RPA14	-0.4042	-0.3279	-0.3745	1.3145	1.2998	1.3547
RPL19B	N/A	-0.7237	N/A	1.0705	1.3145	0.8418
RPN10	-0.4709	-0.4916	-0.4196	0.8291	1.1272	0.9901
RPS11A	N/A	-0.5539	N/A	0.5651	0.7442	0.7185
RPS12	0.2615	0.3334	N/A	1.3134	1.3382	1.266
RPS16A	N/A	-0.9726	-0.7198	1.0976	1.1275	0.5827
RPS17A	-1.2305	-1.1744	-0.8818	0.5455	0.7648	0.5229
RPS23A	-0.6533	-0.6831	-0.5535	1.1653	1.1708	N/A
RPS28B	-0.7381	-0.7216	-0.6388	1.3337	1.3962	1.2337
RPS4B	-0.1945	-0.2129	-0.1689	1.2514	1.3098	1.2183
RPS6B	-0.7838	-0.7447	-0.7354	0.6354	0.9658	0.7481
RTN1	N/A	-0.0583	N/A	N/A	N/A	1.0288
RTT10	-0.4918	-0.4255	-0.4272	1.2274	1.1721	1.0792
RTT106	N/A	1.2206	1.1135	1.4465	1.566	1.9725
RUD3	0.2108	0.3105	0.3976	1.2728	1.4141	1.1596
SAC7	0.5047	0.4314	0.5158	1.3438	1.4465	1.4548
SBH2	N/A	-0.1002	0.016	1.0674	1.1948	1.5431
SCJ1	4.3649	4.3413	4.1895	1.4231	1.5774	1.6153
SEC22	N/A	0.2104	1.4091	1.2745	1.3561	1.3528
SEC28	-0.4445	-0.4157	-0.2068	1.1839	1.2679	1.0218
SEC66	0.5823	0.9039	N/A	N/A	1.6404	1.0147
SEC72	-0.3077	-0.1593	-0.1711	1.0151	1.1716	1.1387
SED4	0.2098	0.1935	0.1375	1.6305	1.5332	1.4254
SET3	0.0413	0.0383	N/A	1.3158	1.5088	1.2223
SEY1	0.2502	0.282	0.6789	1.3614	1.4814	1.5156
SFB2	0.0108	-0.0072	N/A	N/A	1.4124	1.3549

SGM1	N/A	-0.1728	N/A	1.2342	1.2171	1.0964
SGT2	-0.1256	-0.0435	0.0839	1.7652	1.7638	0.9859
SGT2	-0.0765	-0.0216	N/A	1.2975	1.2572	1.2638
SIF2	0.4409	0.3734	0.7118	1.4601	1.4704	1.4899
SIL1	0.8427	0.7952	0.7596	2.1508	2.0302	1.3515
SKY1	1.0151	0.8525	0.8692	1.3125	1.3964	1.4169
SLA1	-0.2451	-0.2056	0.0081	1.1669	1.2259	1.0008
SLP1	0.6604	0.6694	N/A	1.2748	1.2411	2.0419
SMI1	0.7192	0.7371	0.6811	1.1648	1.3114	1.2073
SNT1	0.3716	0.2889	N/A	N/A	N/A	1.6083
SOP4	-0.1696	-0.1335	0.0836	1.2314	1.2421	1.3799
SOP4	4.3107	4.1647	N/A	1.8681	1.8673	N/A
SPC1	0.2288	0.2772	N/A	1.4882	1.5582	1.515
SPC2	2.1501	2.1871	2.1595	N/A	N/A	2.0062
SPE3	N/A	-0.2623	N/A	1.2779	1.4497	1.3306
SPE4	-0.241	-0.2159	N/A	1.3411	1.5517	1.23
SPF1	4.0355	4.1732	3.8854	1.7391	1.827	1.6193
SQS1	-0.3071	-0.3278	-0.2937	1.0435	1.3113	1.0628
SRP40	-0.7416	-0.5081	-0.7442	1.1306	1.2113	1.1925
SSA2	-0.5445	-0.5422	-0.4248	N/A	0.5627	0.6317
SSA3	-0.2614	-0.1021	0.0131	1.1775	1.3789	1.2748
SSA4	-0.1672	-0.1969	-0.0541	1.3195	1.3719	1.5504
SSM4	0.1148	0.1015	N/A	1.1614	1.2996	1.4552
STE24	3.9376	3.6018	3.8783	1.545	1.6058	1.4167
STP22	0.1079	0.6202	-0.0128	1.4053	1.428	1.4299
SUM1	N/A	0.4928	0.7867	1.3473	1.5455	1.329
SUR4	N/A	1.1244	1.0379	1.6287	1.606	1.4034
SVP26	-0.1751	-0.0725	N/A	1.1946	1.297	1.1311
SWC3	0.0677	0	0.2299	1.2296	1.3869	1.3419
SWC5	N/A	-0.279	0.3543	1.269	1.4145	1.3435
SWP82	-0.2823	-0.2759	N/A	1.2516	1.2585	1.3513
SYS1	0.4507	0.431	0.433	1.4686	1.3535	1.4038
TED1	N/A	1.5382	2.1462	N/A	1.2814	1.4875
THI6	-0.444	-0.3306	-0.2218	N/A	1.2275	1.2805
TIR3	-0.2403	-0.0796	-0.0087	2.0435	2.0162	N/A
TLG2	0.5092	0.5614	0.3656	1.3162	1.43	1.3724
TMA19	N/A	-0.3673	-0.377	1.0432	1.2841	1.25
TOF2	N/A	-0.3272	N/A	1.0176	1.1208	1.1468
TRM1	-0.4789	-0.449	-0.3835	N/A	1.1247	1.0752
TRM7	-0.474	-0.5292	N/A	1.3014	1.4943	1.1727
TRP3	-0.2819	-0.0773	N/A	1.057	1.2335	1.2193

TSR2	-0.7142	-0.6913	-0.645	1.0766	1.486	1.3685
UBC4	-0.3746	-0.4678	N/A	1.1952	1.5088	1.2774
UBC7	1.2917	1.3429	1.3783	1.6042	1.6115	1.7886
UBR1	-0.2902	-0.2535	N/A	1.1165	1.1473	1.1367
UBR2	-0.2537	-0.2914	-0.305	1.0406	1.2484	1.2786
UBX2	2.2662	2.4889	2.3746	1.5324	1.6453	1.1544
UBX4	0.2618	0.4447	0.5309	1.6651	1.3666	1.3796
UFD2	0.4012	0.528	0.5861	1.3641	1.2966	1.405
UME1	-0.4168	-0.4635	-0.5409	N/A	N/A	1.1389
USA1	1.0185	1.0454	1.2426	1.2826	1.3429	1.9966
UTH1	0.5497	0.5791	0.5505	1.4341	1.5415	1.4521
VPS1	0.2615	1.3673	N/A	N/A	N/A	1.3602
VPS28	N/A	0.8283	0.4264	1.3465	1.3262	1.138
VPS29	N/A	0.4075	0.2719	1.4069	1.4506	1.4385
VPS3	N/A	0.8052	0.6096	1.1195	1.39	1.4858
VPS30	0.2661	0.0493	0.2336	1.3152	1.335	1.3384
VPS38	0.2221	0.3942	0.3203	1.2594	1.2821	1.1267
VPS51	N/A	2.1661	N/A	1.6906	1.6099	1.5593
VPS52	N/A	1.2331	0.5436	1.2403	1.1907	0.9941
VPS53	N/A	0.1693	N/A	0.9574	1.3321	0.9876
VPS54	0.6302	0.5483	N/A	1.2935	1.4449	1.2212
VPS71	-0.0318	-0.0182	N/A	1.1151	1.4836	1.3071
VPS72	-0.0939	0.0442	0.3653	1.2739	1.4339	1.4797
VPS74	N/A	0.9709	1.1047	1.2554	1.3554	1.3866
VPS75	-0.4308	-0.4433	-0.4397	1.0391	0.8712	N/A
VTC1	0.0772	0.0065	N/A	1.387	1.3688	1.2579
VTC4	0.3828	0.2715	N/A	1.2573	1.0931	1.3416
WSC4	-0.0957	-0.169	0.0905	1.2109	1.3528	1.2051
WT_dhis3::KAN	-0.1836	-0.1906	-0.1037	1.1828	1.3547	1.362
WT_dhis3::KAN	-0.1523	-0.097	N/A	1.3866	1.4266	1.2943
WT_dhis3::KAN	-0.1307	-0.109	0.0082	1.4181	1.5422	1.1536
WT_dhis3::KAN	-0.1233	-0.0407	N/A	1.0803	1.3806	1.3996
YAP5	-0.1668	-0.0007	-0.0522	1.3449	1.3965	1.4791
YBR137W	-0.1055	-0.1762	N/A	0.8448	1.2813	1.3909
YBR226C	-0.0984	-0.0587	-0.1332	1.3191	1.4964	1.3058
YBR238C	N/A	0.2066	0.2906	1.4843	1.5536	1.5507
YCK1	-0.005	-0.0189	N/A	1.2878	1.4766	1.3152
YCK2	0.0358	-0.0969	0.2266	1.341	1.367	1.3693
YCL045C	0.0717	-0.0305	0.2163	1.5941	1.6003	1.5495
YDL133W	-0.1234	-0.0421	0.0388	1.362	1.4191	1.2095
YDL157C	-0.2988	-0.2004	N/A	1.1208	N/A	1.0219

YDL242W	-0.2379	-0.1205	N/A	1.2086	1.2495	1.0765
YDR049W	N/A	-0.3052	-0.1223	1.1069	1.0795	1.3349
YDR056C	-0.2469	-0.1725	-0.0526	1.2334	1.2098	1.2863
YDR056C	1.3567	N/A	2.1945	1.1759	1.2431	1.3075
YDR161W	-0.4503	-0.4022	-0.2544	0.8104	0.9824	0.8856
YEL014C	0.0173	-0.0925	0.2138	1.3312	1.3709	1.6713
YEL047C	-0.2065	-0.1979	N/A	1.2013	1.2855	1.2537
YER064C	0.2553	0.2963	0.3512	1.4698	1.5901	1.4876
YER140W	0.7416	0.7471	N/A	1.2755	1.4658	1.161
YER156C	-0.5263	-0.517	-0.4806	1.0079	1.1611	1.2494
YET1	-0.1345	-0.1613	-0.1194	1.371	1.4433	N/A
YFR018C	0.1718	0.3126	0.4628	N/A	N/A	1.7982
YFR045W	0.0339	-0.038	0.1938	1.0881	1.142	1.089
YGL007W	N/A	0.5094	0.7305	N/A	N/A	N/A
YGL231C	0.0115	0.1188	N/A	1.3657	1.5072	1.8734
YHR003C	0.1275	0.2187	0.4649	1.3698	1.6072	N/A
YHR078W	0.5428	0.6113	0.648	1.5723	1.5933	1.9016
YIL029C	-0.0554	-0.0092	0.1888	1.4044	1.505	1.2702
YIL032C	-0.1071	-0.0326	N/A	N/A	N/A	1.6423
YIL055C	-0.0576	0.0158	0.0324	N/A	1.6474	N/A
YIP3	-0.0173	0.0412	N/A	1.4422	1.6121	1.3722
YJL055W	-0.3194	-0.2775	N/A	1.0943	N/A	1.2663
YJR088C	0.0671	0.0375	N/A	1.5648	1.5113	1.413
YKR043C	-0.0495	-0.0833	N/A	1.1545	1.5397	1.2877
YLL014W	0.1803	-0.1132	N/A	1.1763	1.311	1.4977
YLL014W	N/A	0.1607	0.0963	1.4255	1.2536	1.5711
YLR104W	0.5985	0.58	0.6315	1.7867	1.8268	2.0021
YLR278C	-0.0155	0.0214	0.2383	1.4494	1.5661	1.4338
YLR287C	-0.2186	-0.2049	-0.008	1.2097	1.3232	1.2614
YLR402W	-0.2761	-0.2491	-0.4318	1.2214	1.2906	1.2172
YML108W	-0.4711	-0.4113	-0.3721	N/A	0.9704	1.4419
YMR209C	-0.4081	-0.271	-0.2711	1.2776	1.1654	1.1672
YNL205C	0.3131	0.5516	0.5127	1.7752	1.9589	1.4742
YOL159C	-0.3676	N/A	N/A	0.9597	0.9966	0.5792
YOR164C	0.1316	0.1569	N/A	1.1363	1.4046	1.0235
YOR164C	N/A	-0.0558	N/A	1.2163	1.1282	1.1693
YOS9	0.6535	0.6013	0.6826	1.6682	2.0266	1.25
YPL068C	-0.455	-0.3522	N/A	1.2823	1.3717	1.2345
YPR063C	-0.1219	-0.0351	0.1772	1.2808	1.3464	1.2715
YPR063C	-0.0519	-0.0073	0.0014	1.5655	1.4855	1.2752
YPR084W	-0.3238	-0.2365	-0.0222	1.2869	1.2331	1.1877

YPR130C	0.2057	0.2216	0.3872	1.5138	1.5537	1.5685
YUR1	0.6046	0.7038	N/A	1.8835	1.8934	1.1988
ZAP1	N/A	-0.061	N/A	1.3266	1.2887	1.2528
VIP1	N/A	N/A	N/A	1.4133	1.4638	1.3198
YJR088C	N/A	N/A	N/A	1.3236	1.3598	1.3772

Table 10: The $\log_2$ (GFP/RFP) reporter values obtained in the double mutant strains when *KAR2::NAT* or *kar2-DamP::NAT* were crossed against the genes listed in table 6

* N/A indicates either that the double mutant strain was inviable or that a value was not obtained due to experimental error

Array name	*KAR2-WT (1)*	*KAR2-WT (2)*	*KAR2-WT (3)*	*kar2-DamP (1)*	*kar2-DamP (2)*	*kar2-DamP (3)*
ADD66	N/A	-0.3026	-0.1376	2.5465	2.4373	2.6834
AGX1	-0.1732	-0.095	-0.1543	2.8911	2.7169	3.1566
AHC2	-0.0227	0.0194	N/A	2.9825	2.8081	3.1582
ALF1	N/A	1.12	2.1491	3.1292	3.2188	3.4635
ALG12	1.5689	1.4467	N/A	4.065	3.9737	4.1249
ALG3	2.2605	2.3585	2.6165	4.2769	4.1799	4.458
ALG5	1.4492	1.5665	1.68	3.9246	3.8527	4.0534
ALG6	2.0957	2.041	2.1605	3.988	3.8859	4.094
ALG8	1.6379	1.7204	1.9019	3.8557	3.8763	3.9603
ALG9	1.4766	1.5067	2.0133	3.8455	3.7143	4.1095
APE3	-0.3075	-0.1964	-0.0032	2.8132	2.5373	2.7676
ARC18	0.5786	0.6766	0.8138	3.2375	3.0596	N/A
ARL1	0.6144	0.435	0.4247	3.2318	3.0029	3.1179
ARO1	0.444	N/A	0.0412	3.0749	N/A	2.7678
ARP6	0.1656	0.1677	0.2997	N/A	N/A	1.3841
ARV1	N/A	4.0563	N/A	N/A	4.3813	N/A
ASM4	-0.476	-0.3149	N/A	2.7297	2.4785	2.8706
ATG8	-0.2395	-0.1303	N/A	2.7951	2.8023	2.9815
BNR1	-0.0254	-0.1099	0.25	2.9367	2.7232	2.9099
BOP2	-0.0678	0.0262	0.0132	2.9143	2.826	3.1534
BRE5	N/A	-0.0609	0.0013	3.1659	2.9928	3.4063
BST1	3.4961	3.4596	N/A	N/A	4.0688	4.1959
BTS1	N/A	0.5123	0.5163	3.2477	3.1468	3.479
BUG1	-0.0477	0.1057	N/A	3.0298	2.8981	3.0287
CAC2	0.7982	0.8701	0.6998	2.4896	N/A	2.6174
CAJ1	-0.1593	-0.146	-0.0958	N/A	N/A	0.8649
CAP1	N/A	-0.0499	0.1806	2.7368	2.7007	2.9446
CCW12	1.4203	1.4255	1.6152	3.5601	3.5229	N/A
CKA2	0.8758	0.7563	1.1658	3.3463	3.3891	3.5639
CNE1	1.1871	N/A	1.0195	3.7495	3.6487	3.6209
COG5	N/A	0.1272	N/A	3.0597	2.8972	3.1394
COG6	0.2687	0.3235	N/A	3.1571	3.0191	3.1701
COG8	0.281	0.2635	N/A	3.1594	2.939	3.0471

CPA1	-0.6105	-0.6124	-0.8076	N/A	0.7245	0.7495
CPR6	0.1262	0.1764	0.1472	2.8794	2.7975	2.8961
CRD1	-0.265	-0.3036	N/A	2.6619	2.5602	2.74
CSF1	3.1702	3.2738	3.2965	3.8797	3.8107	3.8819
CSN12	-0.6172	-0.524	N/A	2.5755	2.1655	2.6344
CUE1	1.0488	1.0241	1.2673	3.3636	3.4115	3.6266
CWH41	0.5218	0.5415	0.5079	3.6007	3.5231	3.6546
CWH43	0.2596	0.1953	N/A	3.0602	3.0004	3.2231
CYS3	0.7431	1.2647	N/A	2.7749	0.7769	0.594
DAL81	N/A	-0.406	N/A	1.8445	N/A	2.0848
DAS1	-0.2274	-0.2246	-0.2562	2.746	N/A	N/A
DER1	0.8412	0.8263	1.1548	3.3119	3.3254	3.6256
DFG10	-0.2762	-0.1662	0.0423	2.7896	2.607	2.8758
DGK1	0.0309	-0.0801	0.1163	2.7984	2.8383	2.9692
DIE2	0.7309	0.747	0.9767	3.6338	N/A	4.0154
DOM34	-0.5762	-0.3832	-0.1897	2.5631	2.217	2.8243
DRS2	0.2218	0.3238	0.3777	2.8358	2.7873	3.0148
DUS3	0.0404	-0.0945	N/A	2.9885	2.7648	3.1584
ECM30	0.0089	0.1319	N/A	2.8082	2.6597	2.9784
EDE1	0.2082	0.118	N/A	3.0617	2.8891	3.2135
EGD1	-0.5359	-0.485	-0.5189	2.1864	2.0266	2.2946
EGD2	-0.4217	-0.3985	-0.3263	2.4522	2.2991	2.3553
ELF1	N/A	0.3241	0.3915	3.3535	3.3188	N/A
ELP2	N/A	-0.4381	-0.2428	2.1496	2.0744	1.6163
EMP47	-0.1593	N/A	N/A	3.1133	2.8127	3.0563
ENT3	-0.1379	-0.17	0.1291	3.0287	2.78	3.0036
ERD1	2.7915	2.8649	2.6871	N/A	4.0922	4.1165
ERG2	0.3868	0.3605	0.4795	2.6141	N/A	2.74
ERJ5	0.3344	0.1339	N/A	3.8756	3.7731	3.9357
ERP1	N/A	0.8865	N/A	3.4511	3.3027	3.581
ERP2	0.0939	0.1487	0.3537	2.9572	2.9197	3.3003
ERV14	1.9212	1.9181	2.0844	3.7492	3.6891	3.878
ERV25	2.497	2.4537	2.5138	3.9585	3.9073	4.0946
ERV29	0.3171	0.4791	0.5387	3.2628	3.206	3.5264
ERV41	N/A	-0.2395	-0.3675	2.5686	2.3715	2.7124
ERV46	-0.3368	-0.3478	-0.3832	2.263	2.4016	2.6447
EUG1	0.3093	0.343	0.4621	2.9165	2.7959	2.9438
FAR8	-0.1493	-0.1394	-0.0579	3.0565	2.8663	3.2273
FAT1	0.9667	0.9204	0.7502	3.4794	3.4849	3.1712
FKH1	0.3118	0.346	0.5493	3.2749	3.065	3.3213
FLX1	N/A	-0.3259	N/A	2.2277	2.0448	N/A

FRE4	-0.1671	-0.2638	N/A	2.7928	2.6258	2.8527
FUN30	0.1668	0.1873	0.35	3.1766	3.1091	3.2636
FYV6	N/A	N/A	3.7707	N/A	N/A	N/A
GCN2	-0.1473	-0.1909	N/A	2.8612	N/A	2.8283
GCN20	-0.2321	-0.2038	N/A	2.6275	2.4935	2.7376
GCN5	-0.9911	-1.1073	-1.1178	0.2752	1.3052	1.1574
GCR2	0.6388	0.523	1.0012	2.7389	2.4653	2.9423
GCS1	0.2911	0.3262	0.2994	3.1776	2.8061	2.9281
GDA1	0.271	0.2536	0.217	3.1889	3.1869	3.3276
GET1	1.0074	2.1743	N/A	3.7403	N/A	3.69
GET1	N/A	2.174	N/A	0.6968	N/A	N/A
GET2	1.6531	2.1291	2.1414	3.5438	3.5312	3.6069
GET2	N/A	1.9979	2.2189	N/A	N/A	3.6282
GET3	1.088	0.7439	0.8375	3.0495	3.0315	3.201
GET3	N/A	0.7498	0.8965	2.8429	2.6966	3.0059
GLO3	N/A	2.1866	2.2768	3.2772	N/A	3.6136
GNP1	N/A	0.0259	N/A	2.6539	2.3769	2.9122
GOS1	0.3619	0.3907	0.6255	3.1786	2.9582	3.3504
GOT1	0.0115	0.0354	-0.0765	2.8663	2.7866	3.0223
GSG1	0.1271	0.2326	N/A	2.9718	2.9325	3.2026
GSH2	-0.2563	-0.2227	-0.2941	2.7218	N/A	2.8758
GTB1	-0.0084	0.0241	N/A	3.2048	2.9705	3.3221
GTR1	N/A	N/A	0.2049	N/A	2.5203	2.5749
GUP1	2.8145	2.8369	N/A	N/A	N/A	N/A
GYP8	-0.1225	-0.206	N/A	2.9422	N/A	2.997
HAC1	-0.6855	-0.7625	N/A	0.2194	0.2538	0.0556
HAM1	-0.4729	-0.3843	N/A	2.7226	2.584	2.7865
HAT2	-0.2885	-0.2775	-0.2965	2.7424	2.6747	2.8807
HEK2	0.5033	0.4717	0.609	3.0631	3.0304	3.2032
HHF1	0.7234	0.8716	N/A	3.065	N/A	3.0687
HHT1	1.0153	0.9416	N/A	3.1306	2.9705	3.1238
HHT2	0.3736	0.4076	0.4018	3.0903	N/A	2.9383
HIR3	N/A	0.4039	0.1789	3.0878	2.9818	3.1983
HLJ1	1.4252	1.4709	1.5424	3.534	3.5602	3.6727
HMG1	-0.1158	0.0493	0.171	2.9064	2.8927	3.0003
HOP2	0.3593	-0.0382	0.6456	3.2908	3.2556	3.2139
HPC2	0.1999	0.2083	0.1395	2.6725	2.8546	3.0477
HRD1	1.7439	1.7391	1.9685	3.8746	3.8638	4.0252
HRD3	1.3626	1.4187	1.607	3.8574	3.8234	4.0247
HSM3	-0.3339	-0.3362	N/A	2.5105	2.4283	2.6904
HSV2	-0.3109	-0.2498	-0.0406	2.7412	2.5043	2.9103

HTB2	0.1298	0.144	N/A	2.6711	2.5248	2.9081
HTZ1	0.2764	0.2698	0.257	0.7159	2.2788	2.6363
HUR1	N/A	1.8088	N/A	2.9534	N/A	N/A
HXK2	0.0828	0.2006	0.1962	3.0196	2.7899	3.1457
HXT8	N/A	-0.0195	0.0632	2.6217	2.4447	2.8173
ICE2	0.3416	0.2721	N/A	0.9514	2.5682	N/A
IDH1	-0.2366	N/A	N/A	2.6664	2.5984	3.0893
IES1	0.4161	N/A	0.2072	2.5145	2.832	2.9241
IES4	0.4649	0.5466	0.5486	3.0713	3.1358	3.37
IES5	0.2702	0.2765	0.2859	2.8985	2.6584	2.8234
ILM1	0.2108	0.3122	N/A	3.1048	N/A	N/A
INP53	-0.03	0.0561	N/A	3.1301	3.0524	3.2428
IPK1	N/A	-0.5209	-0.4467	2.6782	2.5167	2.7568
IRC21	0.0136	0.0856	0.0625	2.9122	2.5898	2.9599
IRE1	-0.7221	-0.7557	N/A	0.0145	0.1204	N/A
ISC1	0.1473	0.0055	N/A	2.8153	2.7094	3.0367
ISR1	0.2265	0.1717	N/A	3.9926	3.6432	3.8853
ISW1	N/A	0.4587	0.4685	3.2237	3.1486	3.3355
ISW2	0.0596	0.0086	0.1836	2.8313	2.9232	3.0102
ITR1	0.2206	0.1759	0.2569	2.9568	2.7884	2.9854
IXR1	-0.4814	-0.3697	N/A	2.3203	1.9981	2.2462
JEM1	0.0926	0.1329	0.3924	2.9921	2.9242	3.1801
KEL1	0.3544	0.3648	N/A	3.0195	3.0719	3.2556
KEX2	N/A	N/A	N/A	N/A	N/A	N/A
KIN3	0.7964	0.8447	0.9724	3.2633	3.296	3.5473
KRE1	0.4205	0.4233	0.3309	3.4334	3.3613	3.4477
KRE11	0.1763	0.2615	0.1922	3.0944	2.9066	3.196
KRE27	-0.0748	0.0715	0.2655	2.8602	2.6789	3.0919
KRE27	1.2348	2.0262	N/A	3.0246	2.8901	2.7729
KTI12	-0.3934	-0.4262	N/A	2.3927	2.262	2.2906
LAS21	3.5378	3.4031	3.5912	4.1402	N/A	N/A
LEM3	N/A	0.5108	0.33	2.8922	2.9669	3.0478
LEU3	-0.1948	-0.1944	-0.1252	2.7296	2.7123	2.9304
LOC1	-0.2638	-0.409	-0.1821	0.004	-0.3145	N/A
LPD1	-0.3023	-0.3497	-0.3742	1.4837	1.5295	1.8212
LRC3	0.0041	0.0238	0.0868	N/A	2.6247	3.1179
MAF1	N/A	-0.3837	N/A	3.0948	2.8557	2.9406
MDY2	0.1337	0.0862	0.0857	2.8443	2.8365	2.909
MDY2	0.1783	0.0393	N/A	2.7037	2.6129	2.8261
MEH1	0.1631	0.2058	N/A	2.3406	N/A	2.6145
MGA2	1.2413	1.855	N/A	3.6848	3.473	3.9056

MKC7	-0.0639	-0.0909	N/A	2.7526	2.8378	2.9364
MNL1	0.0096	0.0099	0.1955	2.9223	2.8778	3.1582
MNN2	0.3513	0.6881	0.3409	3.5477	3.3866	3.4778
MNN4	N/A	0.0459	N/A	2.9762	2.8418	2.9954
MNN5	-0.0905	-0.0526	-0.1528	N/A	2.8157	3.1151
MNN9	-0.2798	-0.1796	N/A	3.109	N/A	3.0434
MNS1	-0.1794	-0.0977	N/A	3.0205	2.8068	3.1103
MPD1	0.4312	0.3992	0.7255	3.173	3.0925	3.485
MSC1	N/A	0.5625	N/A	3.3638	3.006	3.2515
MSI1	0.6863	0.5688	N/A	2.6413	2.584	2.8259
MTC1	0.0223	0.0666	0.0614	3.0975	2.9287	3.2276
MTC5	N/A	-0.0859	0.0661	2.9682	2.9428	2.8893
MVP1	N/A	0.1273	0.0625	2.8482	2.6354	2.8746
NEM1	0.6303	0.6236	0.4901	3.3705	3.3794	3.5123
NFT1	-0.3019	-0.2045	-0.2793	2.772	2.6218	2.9645
NHP6A	N/A	-0.2897	N/A	2.9881	2.7324	3.0752
NHX1	0.9253	0.9087	0.9669	3.4638	3.1182	3.2983
NMD4	-0.411	-0.3996	N/A	1.2725	1.8642	2.1158
NPL4	-0.0547	-0.1038	0.0783	2.645	2.626	2.7379
OLA1	-0.3817	-0.2636	N/A	2.2866	2.0933	2.3149
OPI10	-0.2182	-0.194	-0.1824	2.3101	2.4523	2.499
OPI3	1.1738	1.1042	0.9375	N/A	2.9526	3.1901
OST3	2.7665	2.7924	3.032	N/A	4.232	N/A
OST5	0.3574	0.4436	N/A	3.5245	N/A	3.5891
OYE2	-0.3308	-0.354	N/A	2.606	2.5539	2.761
PBP1	-0.386	-0.3965	-0.383	2.4829	2.4234	2.6335
PCT1	0.2794	0.5333	0.3472	3.322	2.9788	3.3089
PEF1	0.2869	0.2857	0.3	2.6662	2.5107	2.5976
PEP7	-0.5521	-0.4327	-0.4213	2.8939	2.7317	2.9853
PEP8	N/A	0.2154	0.2205	2.9984	2.893	3.0943
PET18	-0.0978	-0.1114	N/A	2.9683	2.8198	3.1702
PHO80	1.0206	1.0998	1.4642	2.5382	N/A	3.1939
PHO86	0.1507	0.1335	N/A	2.6379	2.4922	3.074
PMP1	-0.2068	-0.0008	N/A	2.8842	2.7168	3.0581
PMR1	N/A	N/A	N/A	N/A	N/A	N/A
PMT1	1.6268	1.7885	1.9023	3.8769	3.7149	3.9298
PMT2	2.8731	2.8002	2.9393	4.2059	4.0725	4.188
PPH21	-0.2545	-0.2571	-0.0514	2.9366	2.9231	2.831
PPT1	0.0788	0.0994	0.129	3.0069	2.9469	3.131
PRM2	-0.5108	-0.3813	-0.3011	2.6102	2.4737	2.7358
PSD2	0.1872	0.2804	0.2537	2.7043	2.6188	2.9686

PTC2	-0.1572	-0.0722	-0.1546	2.7997	2.5252	2.7871
PTK2	0.1057	0.1609	0.1273	2.7016	2.3755	2.7284
PTP1	-0.3056	-0.2552	N/A	2.76	2.6616	3.0096
PTR2	-0.3999	-0.2411	N/A	2.623	2.5558	2.7258
RAD23	N/A	-0.1593	N/A	2.8456	2.6912	2.9642
RAV1	N/A	0.3196	N/A	2.9881	2.9164	3.0474
RCO1	0.2493	0.2599	0.5879	3.1567	N/A	3.0973
RER1	0.0691	0.1834	0.1244	3.2369	3.1283	3.3479
REX4	-0.3452	-0.3693	-0.3771	2.6546	2.6458	2.853
RGP1	0.0552	0.0129	0.1388	3.1472	2.8321	3.0638
RLF2	N/A	0.7573	0.7118	2.7614	2.6434	2.6264
ROT2	0.3608	0.4799	0.3556	3.462	3.3515	3.5004
ROX1	-0.3262	-0.2562	N/A	2.7084	2.5016	2.8336
RPA14	-0.4042	-0.3279	-0.3745	N/A	3.2361	3.3746
RPL19B	N/A	-0.7237	N/A	2.0774	1.9401	2.212
RPN10	-0.4709	-0.4916	-0.4196	2.0841	2.5159	2.6369
RPS11A	N/A	-0.5539	N/A	1.468	1.0653	N/A
RPS12	0.2615	0.3334	N/A	3.2767	N/A	3.2744
RPS16A	N/A	-0.9726	-0.7198	0.9374	0.9633	1.1238
RPS17A	-1.2305	-1.1744	-0.8818	0.2816	0.1368	0.2106
RPS23A	-0.6533	-0.6831	-0.5535	1.9199	N/A	2.2467
RPS28B	-0.7381	-0.7216	-0.6388	1.6051	1.3	1.5796
RPS4B	-0.1945	-0.2129	-0.1689	2.6024	2.4834	2.8117
RPS6B	-0.7838	-0.7447	-0.7354	1.3172	1.1735	1.4549
RTN1	N/A	-0.0583	N/A	2.6248	2.5622	3.1061
RTT10	-0.4918	-0.4255	-0.4272	2.8499	2.5663	2.8621
RTT106	N/A	1.2206	1.1135	3.0048	N/A	3.1166
RUD3	0.2108	0.3105	0.3976	3.3791	3.2006	3.4653
SAC7	0.5047	0.4314	0.5158	3.1824	N/A	N/A
SBH2	N/A	-0.1002	0.016	2.7162	2.6472	2.9145
SCJ1	4.3649	4.3413	4.1895	4.7751	4.9275	4.8058
SEC22	N/A	0.2104	1.4091	3.4796	3.3956	3.4277
SEC28	-0.4445	-0.4157	-0.2068	2.6313	2.5664	2.9394
SEC66	0.5823	0.9039	N/A	3.8299	3.7579	3.5583
SEC72	-0.3077	-0.1593	-0.1711	2.6316	2.5705	2.8723
SED4	0.2098	0.1935	0.1375	3.138	2.9358	3.1128
SET3	0.0413	0.0383	N/A	2.6104	2.4798	3.0672
SEY1	0.2502	0.282	0.6789	3.2642	3.1521	3.4138
SFB2	0.0108	-0.0072	N/A	3.1322	2.8112	3.1244
SGM1	N/A	-0.1728	N/A	2.7363	N/A	2.9101
SGT2	-0.1256	-0.0435	0.0839	2.7442	N/A	2.7529

SGT2	-0.0765	-0.0216	N/A	2.7761	2.7286	3.0444
SIF2	0.4409	0.3734	0.7118	2.9558	2.7769	3.1048
SIL1	0.8427	0.7952	0.7596	4.1279	4.0968	4.2479
SKY1	1.0151	0.8525	0.8692	2.6191	2.7431	2.626
SLA1	-0.2451	-0.2056	0.0081	2.7031	2.9154	3.0219
SLP1	0.6604	0.6694	N/A	3.6367	3.5457	3.6958
SMI1	0.7192	0.7371	0.6811	3.2659	3.0535	N/A
SNT1	0.3716	0.2889	N/A	2.9019	2.7798	3.1685
SOP4	-0.1696	-0.1335	0.0836	2.8041	2.6672	2.9562
SOP4	4.3107	4.1647	N/A	N/A	4.4091	N/A
SPC1	0.2288	0.2772	N/A	3.5198	3.4022	3.7074
SPC2	2.1501	2.1871	2.1595	N/A	4.4818	4.4578
SPE3	N/A	-0.2623	N/A	2.7156	2.5734	2.8932
SPE4	-0.241	-0.2159	N/A	2.9366	N/A	2.8974
SPF1	4.0355	4.1732	3.8854	N/A	N/A	N/A
SQS1	-0.3071	-0.3278	-0.2937	2.9326	2.4152	2.6733
SRP40	-0.7416	-0.5081	-0.7442	0.854	0.7463	1.0875
SSA2	-0.5445	-0.5422	-0.4248	1.1362	1.2638	1.519
SSA3	-0.2614	-0.1021	0.0131	2.8105	2.5929	N/A
SSA4	-0.1672	-0.1969	-0.0541	3.0795	2.6967	2.9376
SSM4	0.1148	0.1015	N/A	3.0409	2.7941	3.0654
STE24	3.9376	3.6018	3.8783	4.5561	4.5266	4.71
STP22	0.1079	0.6202	-0.0128	3.2683	N/A	3.1268
SUM1	N/A	0.4928	0.7867	3.2263	3.2521	3.4499
SUR4	N/A	1.1244	1.0379	3.4442	N/A	3.2132
SVP26	-0.1751	-0.0725	N/A	3.0174	2.8297	3.1419
SWC3	0.0677	0	0.2299	2.8763	2.7758	2.9982
SWC5	N/A	-0.279	0.3543	0.9132	1.8942	N/A
SWP82	-0.2823	-0.2759	N/A	2.8378	2.6982	2.8603
SYS1	0.4507	0.431	0.433	3.339	N/A	3.1705
TED1	N/A	1.5382	2.1462	3.6137	3.4538	3.8598
THI6	-0.444	-0.3306	-0.2218	2.3984	2.3741	2.6304
TIR3	-0.2403	-0.0796	-0.0087	2.9643	2.7827	3.1547
TLG2	0.5092	0.5614	0.3656	3.2882	3.1991	3.2059
TMA19	N/A	-0.3673	-0.377	1.8164	1.6427	2.0072
TOF2	N/A	-0.3272	N/A	2.5296	N/A	2.6112
TRM1	-0.4789	-0.449	-0.3835	2.4714	2.5132	2.7583
TRM7	-0.474	-0.5292	N/A	2.9097	2.6074	3.0938
TRP3	-0.2819	-0.0773	N/A	2.3632	2.1605	2.3783
TSR2	-0.7142	-0.6913	-0.645	1.6298	0.815	0.7744
UBC4	-0.3746	-0.4678	N/A	3.2077	N/A	N/A

UBC7	1.2917	1.3429	1.3783	3.2812	3.5457	3.9213
UBR1	-0.2902	-0.2535	N/A	2.4926	2.3375	2.5815
UBR2	-0.2537	-0.2914	-0.305	2.5418	2.6623	2.6207
UBX2	2.2662	2.4889	2.3746	4.1043	N/A	3.6718
UBX4	0.2618	0.4447	0.5309	3.4238	N/A	3.4711
UFD2	0.4012	0.528	0.5861	3.2315	3.0315	3.3212
UME1	-0.4168	-0.4635	-0.5409	2.7891	2.6684	2.999
USA1	1.0185	1.0454	1.2426	3.5164	N/A	3.6818
UTH1	0.5497	0.5791	0.5505	3.5934	3.3705	3.465
VPS1	0.2615	1.3673	N/A	N/A	0.9219	0.9268
VPS28	N/A	0.8283	0.4264	3.2947	N/A	N/A
VPS29	N/A	0.4075	0.2719	3.0525	3.0165	3.1224
VPS3	N/A	0.8052	0.6096	2.9092	N/A	2.8017
VPS30	0.2661	0.0493	0.2336	3.04	2.9275	3.052
VPS38	0.2221	0.3942	0.3203	3.0688	2.9769	3.1425
VPS51	N/A	2.1661	N/A	3.3009	N/A	N/A
VPS52	N/A	1.2331	0.5436	3.199	N/A	3.1438
VPS53	N/A	0.1693	N/A	N/A	N/A	N/A
VPS54	0.6302	0.5483	N/A	3.3282	N/A	3.1722
VPS71	-0.0318	-0.0182	N/A	N/A	2.5521	3.0799
VPS72	-0.0939	0.0442	0.3653	2.9319	2.8832	3.1025
VPS74	N/A	0.9709	1.1047	3.5251	3.438	3.5782
VPS75	-0.4308	-0.4433	-0.4397	2.6352	2.433	2.7126
VTC1	0.0772	0.0065	N/A	2.7134	2.6735	2.9317
VTC4	0.3828	0.2715	N/A	2.8766	2.7609	2.9074
WSC4	-0.0957	-0.169	0.0905	2.8811	2.7297	2.8914
WT_dhis3::KAN	-0.1836	-0.1906	-0.1037	2.6099	2.5797	2.8337
WT_dhis3::KAN	-0.1523	-0.097	N/A	2.8722	2.7211	2.9742
WT_dhis3::KAN	-0.1307	-0.109	0.0082	2.7491	2.6386	2.9858
WT_dhis3::KAN	-0.1233	-0.0407	N/A	2.9647	2.5932	2.9928
YAP5	-0.1668	-0.0007	-0.0522	2.9958	2.8162	3.0039
YBR137W	-0.1055	-0.1762	N/A	2.7868	2.5566	2.8057
YBR226C	-0.0984	-0.0587	-0.1332	N/A	2.5409	N/A
YBR238C	N/A	0.2066	0.2906	3.1121	3.1279	3.232
YCK1	-0.005	-0.0189	N/A	2.7122	2.5065	2.9442
YCK2	0.0358	-0.0969	0.2266	2.9744	2.6823	3.1728
YCL045C	0.0717	-0.0305	0.2163	3.006	2.8568	3.1365
YDL133W	-0.1234	-0.0421	0.0388	2.9	2.7258	3.0115
YDL157C	-0.2988	-0.2004	N/A	2.6387	2.5476	2.6918
YDL242W	-0.2379	-0.1205	N/A	2.8562	2.4892	2.7678
YDR049W	N/A	-0.3052	-0.1223	2.6189	2.5266	N/A

YDR056C	-0.2469	-0.1725	-0.0526	2.7715	2.6433	N/A
YDR056C	1.3567	N/A	2.1945	N/A	2.8184	3.4509
YDR161W	-0.4503	-0.4022	-0.2544	2.6419	2.3207	2.5315
YEL014C	0.0173	-0.0925	0.2138	2.8714	2.9043	3.2099
YEL047C	-0.2065	-0.1979	N/A	2.7943	2.799	2.9254
YER064C	0.2553	0.2963	0.3512	2.8813	2.8125	3.039
YER140W	0.7416	0.7471	N/A	3.6608	3.4553	3.6717
YER156C	-0.5263	-0.517	-0.4806	1.9875	1.6668	N/A
YET1	-0.1345	-0.1613	-0.1194	2.8357	2.8351	3.0001
YFR018C	0.1718	0.3126	0.4628	3.1931	N/A	3.2364
YFR045W	0.0339	-0.038	0.1938	2.6447	N/A	2.9486
YGL007W	N/A	0.5094	0.7305	2.5107	N/A	2.9468
YGL231C	0.0115	0.1188	N/A	2.9281	2.8855	3.1128
YHR003C	0.1275	0.2187	0.4649	3.058	3.0393	3.1417
YHR078W	0.5428	0.6113	0.648	3.3316	3.4334	3.4925
YIL029C	-0.0554	-0.0092	0.1888	2.769	2.9657	3.1493
YIL032C	-0.1071	-0.0326	N/A	3.0066	N/A	3.0545
YIL055C	-0.0576	0.0158	0.0324	2.9755	2.6341	3.0795
YIP3	-0.0173	0.0412	N/A	2.9284	2.7978	3.0609
YJL055W	-0.3194	-0.2775	N/A	2.659	N/A	3.0149
YJR088C	0.0671	0.0375	N/A	2.7397	N/A	2.9611
YKR043C	-0.0495	-0.0833	N/A	2.764	2.7849	2.9805
YLL014W	0.1803	-0.1132	N/A	3.0683	2.8969	2.9985
YLL014W	N/A	0.1607	0.0963	2.7313	2.6235	3.0018
YLR104W	0.5985	0.58	0.6315	3.0919	3.1183	3.5239
YLR278C	-0.0155	0.0214	0.2383	3.1216	2.8648	3.114
YLR287C	-0.2186	-0.2049	-0.008	2.8009	2.562	2.9834
YLR402W	-0.2761	-0.2491	-0.4318	2.2528	2.0721	2.2696
YML108W	-0.4711	-0.4113	-0.3721	2.7038	2.2523	N/A
YMR209C	-0.4081	-0.271	-0.2711	2.7183	2.6305	2.7969
YNL205C	0.3131	0.5516	0.5127	2.8976	2.6854	3.0763
YOL159C	-0.3676	N/A	N/A	2.827	2.5746	3.0011
YOR164C	0.1316	0.1569	N/A	2.7957	2.5802	3.0102
YOR164C	N/A	-0.0558	N/A	2.7324	2.5636	2.9671
YOS9	0.6535	0.6013	0.6826	3.2603	3.1857	N/A
YPL068C	-0.455	-0.3522	N/A	1.9766	1.6325	2.3994
YPR063C	-0.1219	-0.0351	0.1772	2.8197	2.7892	2.8922
YPR063C	-0.0519	-0.0073	0.0014	2.9047	2.8168	3.1021
YPR084W	-0.3238	-0.2365	-0.0222	2.7326	2.5418	2.8408
YPR130C	0.2057	0.2216	0.3872	3.0359	3.0021	3.0793
YUR1	0.6046	0.7038	N/A	3.634	3.3977	3.4959

ZAP1	N/A	-0.061	N/A	0.4101	N/A	-0.0107
VIP1	N/A	N/A	N/A	3.3562	N/A	N/A
YJR088C	N/A	N/A	N/A	4.0615	N/A	N/A

Table 11: A list of the gene deletions that exhibited the highest correlation coefficients for (A) *kar2-R217A::NAT*, (B) *sec71Δ*, and (C) *sec72Δ*, and their corresponding genetic interaction values.

* A positive genetic interaction value which is statistically significant is highlighted in yellow and a negative value in blue.

** A positive genetic interaction value means that the double mutant strain had a lower level of UPR induction than what was predicted

*** N/A indicates either that the double mutant strain was inviable or that a value was not obtained due to experimental error

(A) *kar2-R217A::NAT*

Mutant	*SEC72*	*VPS52*	*SEC71*	*GTR1*	*GNP1*	*NPL4*	*SPT4*	*ILM1*	*STP22*	*MEH1*	*PMR1*	*VTC4*	*PMP1*	*MVP1*	*SMI1*	*GCR2*	*RAV1*	*ERG2*	*VPS53*
Correlation coefficient	0.4514	0.4054	0.3969	0.3958	0.3706	0.3695	0.3385	0.3299	0.3204	0.3161	0.3101	0.3017	0.2959	0.2922	0.2912	0.2871	0.2754	0.27	0.2639
kar2-R217A	-0.0826	0.478	0.2962	N/A	-0.9504	0.06	N/A	1.2534	-0.3178	0.2567	0.9296	0.4451	-0.2634	-0.0643	0.399	0.0052	0.4813	N/A	0.993
sec71Δ	-0.2528	N/A	N/A	-0.0566	N/A	0.2683	0.7198	-0.1357	N/A	0.3284	N/A	0.0184	-0.1995	-0.0316	-0.418	0.1127	0.39	-0.0686	N/A
sec72Δ	N/A	N/A	-0.2528	N/A	N/A	N/A	-0.1563	0.778	N/A	N/A	0.4156	N/A	N/A	N/A	N/A	N/A	N/A	N/A	N/A

(B) *sec71Δ*

Mutant	*CCW12*	*SEC72*	*YGL007W*	*ARC18*	*PMT2*	*ERD1*	*KIN3*	*PMP1*	*STP22*	*ILM1*	*SUR4*	*EUG1*	*ERV14*	*LAS21*	*PER1*	*VTC4*	*LHS1*	*ERG2*	*ERV25*
Correlation coefficient	0.6328	0.6128	0.5676	0.5645	0.5465	0.5417	0.5341	0.524	0.5099	0.5091	0.5014	0.4834	0.4796	0.4792	0.4755	0.4713	0.4701	0.4623	0.4603
kar2-R217A	0.6068	-0.0826	0.1297	0.2665	0.3465	1.3922	N/A	-0.2634	-0.3178	1.2534	0.9569	0.3607	0.1744	3.2132	N/A	0.4451	N/A	N/A	-0.3317
sec71Δ	N/A	-0.2528	N/A	N/A	N/A	1.4758	0.1551	-0.1995	N/A	-0.1357	0.3603	0.2961	0.7577	N/A	2.879	0.0184	N/A	-0.0686	0.6962
sec72Δ	0.4514	N/A	N/A	N/A	-0.1295	0.3587	N/A	N/A	N/A	0.778	0.4122	N/A	0.4913	0.1916	0.5395	N/A	0.3387	N/A	0.0842

(C) *sec72Δ*

Mutant	*SEC66*	*kar2-R217A*	*IRC21*	*SPT4*	*ILM1*	*YLR104W*	*SKY1*	*VTC4*	*ERV41*	*RPS4B*	*VTC1*	*PEF1*	*NPL4*	*PTK2*	*MKC7*	*YPL068C*	*GTR1*	*PHO80*	*PSD2*
Correlation coefficient	0.6128	0.4514	0.3885	0.3719	0.3471	0.338	0.3336	0.3272	0.3245	0.3195	0.3059	0.3047	0.3025	0.2975	0.2958	0.2843	0.2819	0.2709	0.2708
kar2-R217A	0.2962	N/A	-0.1058	N/A	1.2534	0.2392	0.0598	0.4451	-0.081	-0.0326	0.2215	-0.4772	0.06	0.3016	-0.1455	-0.1854	N/A	0.1383	-1.6155
sec71Δ	N/A	0.2962	0.4533	0.7198	-0.1357	-0.8337	0.7792	0.0184	-0.3313	0.1517	0.2916	0.498	0.2683	0.195	-0.0131	0.0107	-0.0566	0.9376	-0.0806
sec72Δ	-0.2528	-0.0826	N/A	-0.1563	0.778	-0.3427	0.6003	N/A	N/A	N/A	N/A	0.2264	N/A	N/A	N/A	N/A	N/A	0.4689	-0.0871

APPENDIX C

STRUCTURAL DETERMINATION OF A TRUNCATION MUTANT OF BIP THAT IS CONFINED TO AN ADP-BOUND CONFORMATION DUE TO THE G247D MUTATION IN THE ATPASE DOMAIN

This work was performed with an undergraduate researcher, Brigid K. Jensen, in the Brodsky laboratory, and in collaboration with the laboratory of Andrew VanDemark at the University of Pittsburgh, Department of Biological Sciences.

As described in section 2.2.1, after nearly 2 decades of research, the field of x-ray crystallography still faces the challenge of obtaining the crystal structure of a full-length Hsp70. The closest rejoinder to this challenge has been the resolution of the crystal structure of Hsp70 truncation mutants that lack the flexible lid domain[7, 12]. The first such structure to be solved was of truncated bovine Hsc70 in the nucleotide-free state, and it revealed a conformation in which the substrate binding domain wrapped around the ATPase domain by establishing contacts with the inter-domain linker as well as subdomain Ia of the ATPase domain[7] (Figure 4A). However, these observations were contradictory to NMR and directed mutagenesis studies with full-length bacterial Hsp70. Specifically, it had been shown that indicated that the ATPase and substrate binding domains are disjointed in the nucleotide-free and ADP-bound states, whereas they are closely packed in the ATP-bound state[78-81]. Given that the crystal structure of truncated bovine

Hsc70 was stabilized by mutating charged surface residues and by adding osmolytes[7], it is possible that certain aspects of this structure are experimental artefacts. To resolve these contradictions, a crystal structure of truncated rat Hsc70 in the ADP-bound state was solved[12] and showed that the ATPase and substrate binding domains are indeed disjointed in the presence of ADP (Figure 4B), as suggested by NMR and directed mutagenesis studies. Free movement between these domains in the presence of ADP is further supported by the protease susceptibility patterns of several Hsp70s in the presence of different nucleotides[403-406]. Alternately, it is plausible that different Hsp70s adopt different conformations, and therefore, the three-dimensional structures of bovine and rat Hsc70 truncations varied. This implies that the crystal structure of every prokaryotic or eukaryotic Hsp70 may need to be solved in order to understand the function of that specific Hsp70.

The crystal structures of neither full-length BiP nor individual BiP domains have been solved. Since human BiP is correlated to several diseases (refer to section 1.2.9), knowledge of its three-dimensional structure, in the absence and presence of specific cofactors, can be utilized for targeted drug design. Because yeast and human BiP share 70% overall sequence identity, the immediate goal of this study is to obtain the three-dimensional crystal structure of yeast BiP by combining previous successful approaches with a novel approach. To this end, two truncation mutants of yeast BiP, D559X and K584X, were generated by site-directed mutagenesis in the plasmid pMR2623[151] that drives IPTG-inducible hexahistidine-tagged BiP expression in *E. coli*; this was in accordance with successful attempts to crystallize Hsp70 truncations[7, 12]. Additionally, a point mutation, G247D, was introduced into BiP's ATPase domain, which causes the protein to be trapped in an ADP-bound conformation[151]; this approach is novel and is predicted to surmount the contradictions observed in previous NMR and crystallographic studies.

The first step involved the optimization of BiP purification in a heterologous bacterial expression system for improved protein purity and yield. Next, the biochemical properties of the G247D-D559X and G247D-K584X BiP truncation mutants were compared to wild-type and G247D BiP. Finally, prior to crystallization, the multimeric status of each preparation was examined using size-exclusion chromatography and native gel electrophoresis. Based on these results, conditions are being optimized to obtain a homogeneous protein preparation of G247D-K584X BiP that contains a single oligomeric state.

C.1 OPTIMIZATION OF PROTEIN PURIFICATION

In this section, I outline an optimized protein purification protocol which yields around 60-100 mg of protein at concentrations of 6-10 mg/ml. To arrive at this protocol, several modifications were made to a purification method that was described by McClellan *et al.,* 1998[151].

C.1.1 Protein induction using the ZYP-5052 autoinduction medium

(Note that the autoinduction medium can be used for IPTG-inducible proteins expressed from the T7 promoter only.)

1. Grow overnight cultures (2*50mls) of the desired strain in LB-Amp (Ampicillin at a conc. of 50ug/ml) at 37°C (~16-18hrs).

2. The next day, spin down cells at 5000 rpm for 5 min. Resuspend in 2*20ml ZY media.

3. Add this to 2*2L of ZYP-5052+Amp in 4 L Fermbach flasks (refer to section C.1.3 for information with regards to ZY and ZYP-5052 media preparation).

4. Split each 2L volume into 4*500ml quantities in 1L flasks. Grow at 37°C until OD_{600} is close to 2. This could take anywhere from 4-6 h based on the *E. coli* strain.

5. Once the desired OD_{600} is reached, grow at room temperature (23°C) for 24hrs.

[Principle behind autoinduction: When the OD_{600} is 2 or higher, the cells enter stationary phase. During this stage of growth, they switch from utilizing glucose as a carbon source to utilizing lactose, which is when the protein of interest is induced.]

6. Harvest cells at 5000 rpm for 5 min (2*2L total).

7. Wash pellets with 2*200ml sterile double-distilled water

8. Wash pellets with 2*50ml sonication buffer (50mM HEPES, pH 7.4, 300mM NaCl, 10mM imidazole, 5mM β-mercaptaoethanol, 10%glycerol) and store pellets at -20°C.

C.1.2 Protein purification

Column 1-

1. Thaw cells on ice. Resuspend in 30 ml of sonication buffer. Add protease inhibitors (PMSF, pepstatin, leupeptin) to a final concentration 1mM.

2. Sonicate cells at a medium setting for 6 x 30 seconds with 2 minutes on ice in-between. The setting depends on the sonicator brand.

3. Centrifuge at 10,000 rpm for 10 minutes in a Sorvall SS-34 rotor. This is to spin out cell debris and unbroken cells.

4. Load the cleared cell lysate onto a 10 ml Ni^{2+}-NTA column equilibrated in sonication buffer. Collect flow through.

5. Wash the column with the following solutions and save each wash for analysis by SDS-PAGE:

Wash 0	50ml sonication buffer
Wash 1	55ml sonication buffer + 1% Triton X-100
Wash 2	55ml sonication buffer + 1M NaCl
Wash 3	55ml sonication buffer + 5mM ATP
Wash 4	55ml sonication buffer + 0.5M Tris, pH 7.4
Wash 5	55ml sonication buffer + 25mM imidazole

*Note that the column may turn grayish in color during the loading step and remain so during the first couple of washes. This isn't anything to panic about!

6. Elution**:** Add 40m L elution b uffer (sonication b uffer + 250m M i midazole). C ollect 2m l fractions. Analyze b y S DS-PAGE and Coomassie B rilliant B lue s taining to determine pe ak fractions.

Column 2-

1. Pool the peak fractions from the first column and dilute 1:3 (to a maximum volume of 50ml) in buffer QA (20mM HEPES, pH 7.4, 150mM KCl, 5mM $MgCl_2$, 10% Glycerol).

2. Load slowly onto a 15ml Q-Sepharose C olumn e quilibrated i n b uffer Q A; collect f low through.

3. Wash and elute with the following solutions:

Wash 1	80ml buffer QA
Wash 2	40ml buffer QB (20mM HEPES, pH 7.4, 350mM KCl, 5mM $MgCl_2$, 10% Glycerol)
Wash 3	20mL buffer QC (20mM HEPES, pH 7.4, 2.15M KCl, 5mM $MgCl_2$, 10% Glycerol)

(BiP truncation mutants bind poorly to the column. Any protein that does bind elutes in washes 1 and 2)

4. Analyze by SDS-PAGE and Coomassie Brilliant Blue staining to determine peak fractions; pool.

Column 3-

1. Slowly load the pooled fractions onto a 4ml Ni^{2+}-NTA column equilibrated in buffer X' (20mM HEPES, pH 7.4, 150mM KCl, 5mM $MgCl_2$, 10 mM Imidazole, 10% Glycerol); collect flow through.

2. Elute with 24 ml of elution buffer (20mM HEPES, pH 7.4, 150mM KCl, 5mM $MgCl_2$, 250 mM Imidazole,10% Glycerol); collect 2 ml fractions.

3. Analyze by SDS-PAGE and Coomassie Brilliant Blue staining to determine peak fractions.

4. Alternatively, measure the concentration of each fraction using a Bradford Assay. This is important if the protein of interest has a tendency to crash out of solution at high concentrations.

Dialysis-

1. Pool the peak fractions and dialyze overnight in the cold room (~16 h) in dialysis buffer (50 mM Tris pH 7.4, 125 mM NaCl, 25 mM KCl, 10% Glycerol) at a ratio of 1 ml protein to1000 ml dialysis buffer.

2. The next day, pool protein and determine concentration using a Bradford assay. Also, resolve the protein using SDS-PAGE and determine its concentration by comparison to BSA standards.

3. The protein can be stored at 4°C for long periods of time.

C.1.3 ZYP-5052 Autoinduction Media

This is to be made directly before use; add in the following order

ZY Media	1856ml
1M $MgSO_4$	2ml
1000x Trace Metals Mix	2ml

50x5052	40ml
20xNPS	100ml

Antibiotics as needed.

- ZY Media

Tryptone	20g
Yeast Extract	10g
DDW	1860ml

Autoclave

- 1000x Trace Metals Mix (see next page)

- 50x5052

Glycerol by weight	125g
DDW	365ml
Glucose (dextrose)	12.5g
Alpha-lactose	50g

Autoclave

- 20xNPS

Final conc. (200mM PO_4, 25mM SO_4, 50mM NH_4, 100mM Na, 50mM K) ph ~6.75

DDW	800ml	
$(NH_4)_2SO_4$	66g	Ammonium Sulfate
KH_2PO_4	136g	(Monobasic) Potassium Phosphate
Na_2HPO_4	142g	Disodium Phosphate

Autoclave

Trace Metals

Lack of trace metals becomes limiting for growth in P-0.5G without added metals. Iron, manganese and cobalt were the most effective in relieving this limitation. A concentration of 0.1x trace metals mixture is sufficient to support maximal growth in P-0.5G. Growth in ZYP medium is not limited by lack of trace metals.

The 1x trace metals mixture is an attempt to saturate almost any metal-containing target protein, even at high levels of expression. The 1x concentrations are below toxic levels, as tested by growth in different concentrations of the metals individually. Target proteins produced at 100 mg/liter would have a concentration of 2 □M for a protein of 50,000 Da or 10 □M for a protein of 10,000 Da. If the metal content of an expressed protein is known, a saturating amount of that metal can be added rather than 1x metals mix.

1000x trace metals mixture (100 ml in ~50 mM HCl)

Add to 36 ml sterile water:

(dissolved in 0.14 M HCl = 100-fold dil of conc HCl) use: of	stock solutions	MW	1x conc (final)	to make stocks: g/x ml dil HCl
50 ml	0.1 M $FeCl_3$-$6H_2O$	270.30	50 M Fe	13.52g / 500ml
2 ml	1 M $CaCl_2$	110.99	20 M Ca	11.10 g/ 100ml
1 ml	1 M $MnCl_2$-$4H_2O$	197.91	10 M Mn	9.90 g/ 50 ml
1 ml	1 M $ZnSO_4$-$7H_2O$	287.56	10 M Zn	14.38 g/ 50 ml
1 ml	0.2 M $CoCl_2$-$6H_2O$	237.95	2 M Co	2.38 g/ 50 ml
2 ml	0.1 M $CuCl_2$-$2H_2O$	170.486	2 M Cu	1.70 g/ 100 ml
1 ml	0.2 M $NiCl_2$-$6H_2O$	237.72	2 M Ni	2.38 g/ 50 ml
2 ml	0.1 M Na_2MoO_4-$5H_2O$	241.98	2 M Mo	2.42 g/ 100 ml
2 ml	0.1 M Na_2SeO_3-$5H_2O$	263.03	2 M Se	2.63 g 100 ml
2 ml	0.1 M H_3BO_3	61.83	2 M H_3BO_3	0.618 g/ 100 ml

Autoclave the stock solutions of the individual metals, except 0.1 M $FeCl_3$ in 1/100 volume conc HCl.

A brief precipitate appeared upon addition of Na_2SeO_3, which redissolved rapidly

C.1.4 An example of the stepwise purification of G247D-K584X BiP

Parts A to C of Figure 39 show Coomassie Brilliant Blue-stained denaturing polyacrylamide gels that were used to analyze the fractions obtained from each column of a sample G247D-K584X BiP preparation.

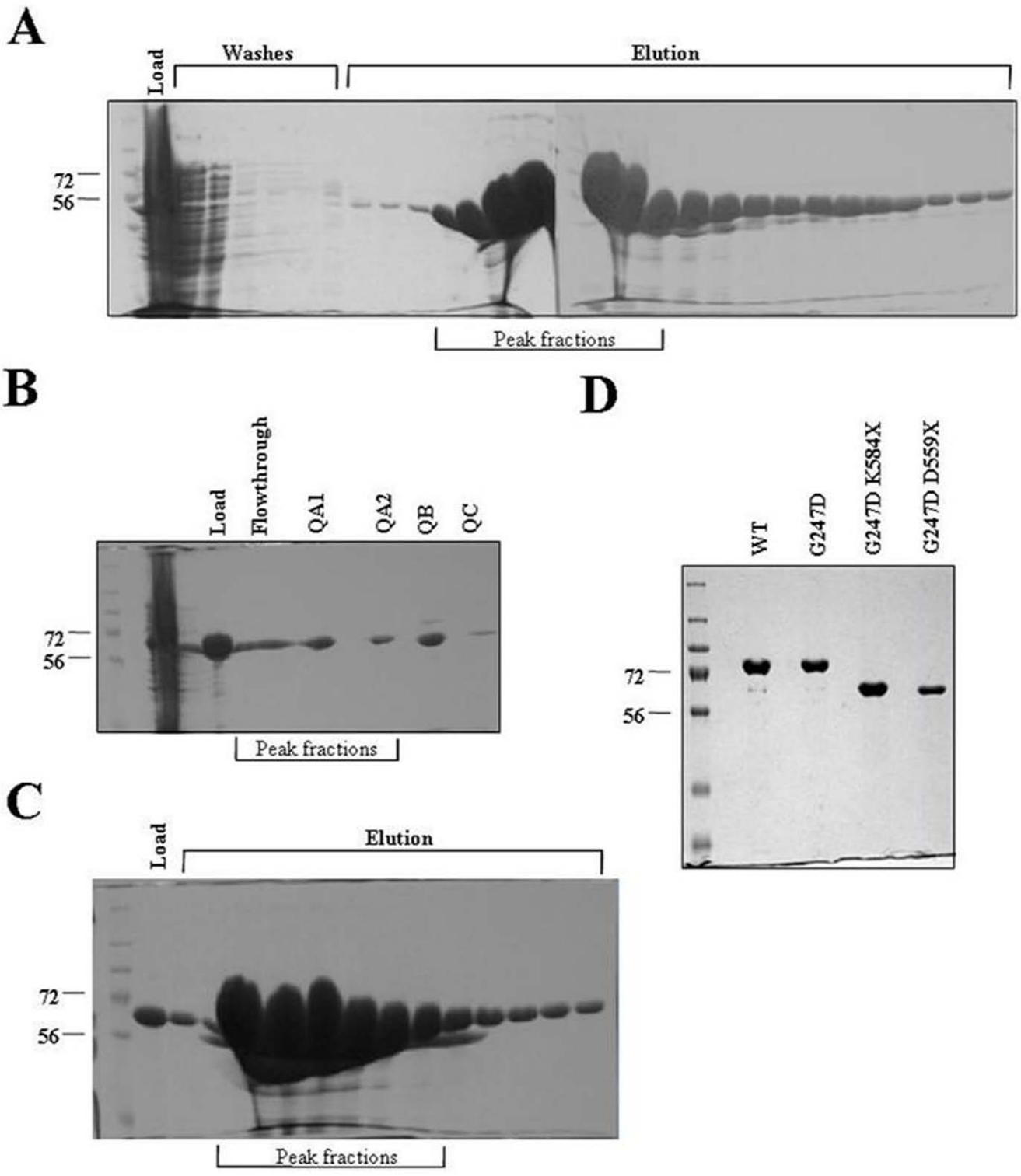
A
Load
Washes
Elution
72
56
Peak fractions
B
Load
Flowthrough
QA1
QA2
QB
QC
72
56
Peak fractions
C
Load
Elution
72
56
Peak fractions
D
WT
G247D
G247D K584X
G247D D559X
72
56

Figure 39: An example of the step-wise purification of G247D-K584X BiP.

The Coomassie Brilliant Blue staining patterns of SDS-PAGE resolved fractions obtained for G247D-K584X BiP from ***(A)*** Column 1= Ni^{2+}-NTA agarose affinity chromatography, ***(B)*** Column 2= Q-sepharose ion exchange chromatography, and ***(C)*** Column 3= Ni^{2+}-NTA agarose affinity chromatography, are shown. The truncated protein migrates at the expected molecular mass of 60 kDa as indicated by its proximity to the 56 kDa band of the molecular mass marker. ***(D)*** A comparison of the indicated wild-type (WT) and mutant BiP proteins purified according to the protocol described in section C.1. 3 μg of wild-type, G247D and G247D-K584X BiP and 1 μg of G247D-D559X BiP were resolved by SDS-PAGE and visualized by Coomassie Brilliant Blue staining.

Using this optimized protocol, wild-type, G247D, G247D-K584X, and G247D-D559X BiP proteins were purified at concentrations of 3.0, 5.5, 8.7 and 5.8 mg/ml, respectively, in volumes greater than 8 ml. Figure 39D depicts a Coomassie Brilliant Blue-stained SDS-PAGE gel that was utilized to compare the wild-type and mutant BiP proteins.

C.2 COMPARING THE BIOCHEMICAL PROPERTIES OF WILD-TYPE AND MUTANT BIP PROTEINS

The first property that was analyzed was the ability of the wild-type and mutant BiP proteins to hydrolyze ATP (as described in chapter 2). It had previously been demonstrated that the 'frozen' conformation adopted by G247D BiP leads to a decrease in its ATP hydrolysis rate[151]. Accordingly, the endogenous ATPase activity of G247D BiP was found to be 0.75 nmol of ATP hydrolyzed/mg/min, nearly 4-fold lower than the endogenous ATPase activity of wild-type BiP (Figure 40). Similarly, the G247D-K584X, and G247D-D559X BiP truncation mutants exhibited greatly reduced ATPase activities.

Next, the protease susceptibility patterns of the wild-type and mutant BiP proteins were examined in the presence of Proteinase K (as described in chapter 2). Preliminary observations indicate that while the wild-type protein undergoes a nucleotide-dependent conformational change which is observed as a change in its protease susceptibility pattern, the three BiP mutants are confined to an ADP-bound conformation, as anticipated[151] (data not shown).

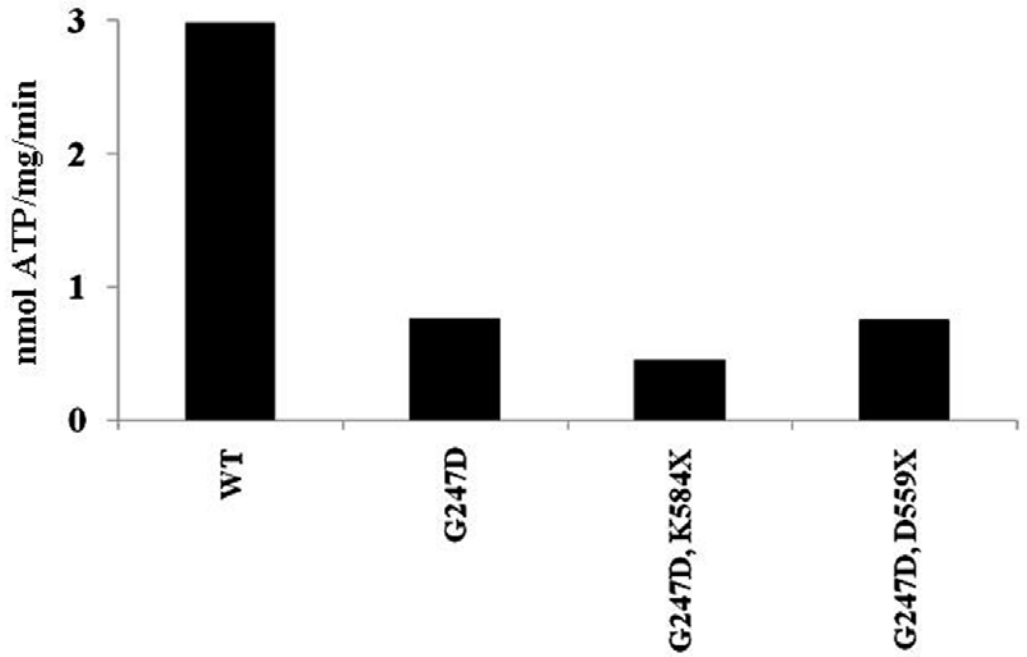

Figure 40: A comparison of the endogenous ATPase activities of wild-type and mutant BiP proteins.

The endogenous ATPase activities of 3 μg of wild-type and mutant BiP isolates was measured at 30°C. ATPase activity is expressed as nmoles of ATP hydrolyzed per milligram of protein per minute. Data represent the means of a minimum of two independent experiments.

C.3 CHARACTERIZATION OF THE MULTIMERIC STATE OF THE G247D-K584X AND G247D-D559X BIP MUTANTS

Several studies with unique Hsp70s, including human BiP, have demonstrated that these proteins form higher order oligomers, predominantly dimers, in solution[407-417]. Therefore, the next step involved the determination of the multimeric state of G247D-K584X and G247D-D559X BiP. This information becomes especially important prior to crystallization because the presence of multiple oligomeric forms can affect crystal formation[418].

First, ~20 mg of G247D-D559X BiP was subjected to size exclusion chromatography using a sephacryl S-300 resin in a GE Healthcare fast protein liquid chromatography (FPLC) setup using the buffer: 50 mM Tris, pH 7.4, 125 mM NaCl, 25 mM KCl, 10% glycerol. As fractions were being collected, the UV absorbance of each fraction was measured at 280 nm, thus generating a column protein profile (Figure 41A, top panel). Intriguingly, G247D-D559X BiP separated as two distinct peaks suggesting that the protein preparation contained at least two different oligomeric states. When the fractions were subsequently resolved by native gel electrophoresis followed by Coomassie Brilliant Blue staining (Figure 41A, bottom panel), I found that the first peak contained two distinct oligomeric species while the second peak contained a third oligomeric form. Furthermore, it appeared that the oligomers comprising the first peak could spontaneously convert into the third oligomeric form if maintained in solution for extended periods of time (data not shown). This observation was not encouraging because crystal formation takes several weeks, and the equilibrium behavior of the oligomeric states of G247D-D559X BiP could abrogate the seeding of a crystal.

Next, ~20 mg of G247D-K584X BiP was subjected to size exclusion chromatography using a sephacryl S-300 resin in a similar FPLC setup with the buffer: 50 mM

A

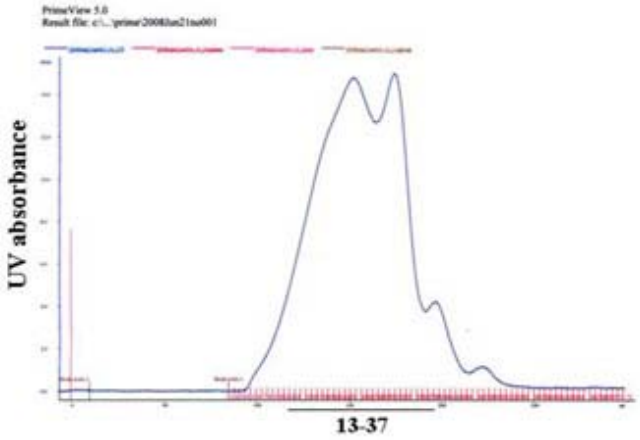

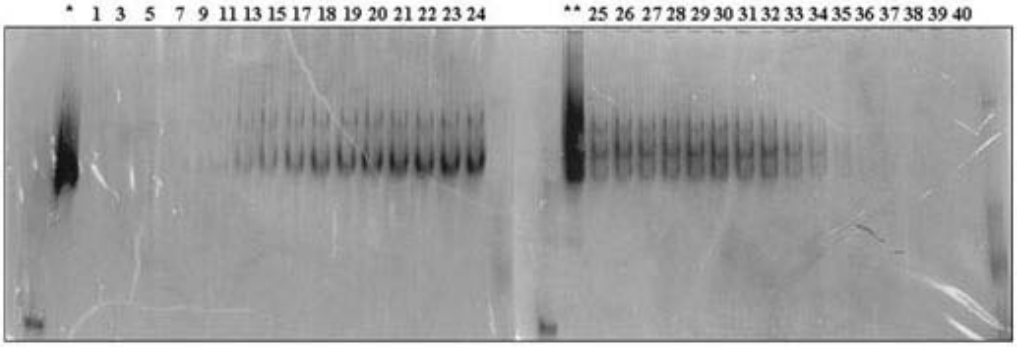

* = Column load in denaturing sample buffer; ** = Column load in native sample buffer

B

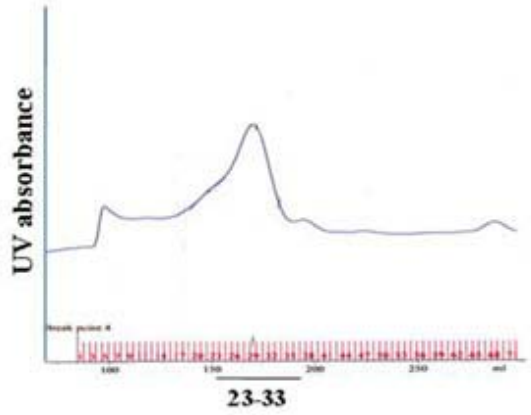

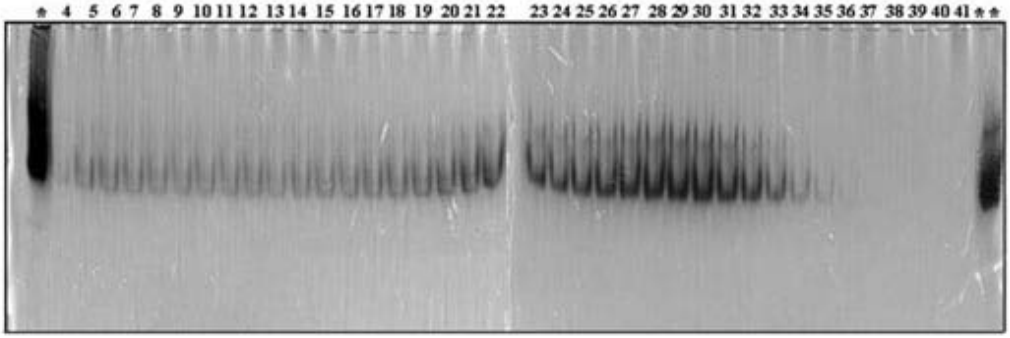

* = Column load in denaturing sample buffer; ** = Column load in native sample buffer

Figure 41: Characterization of the multimeric states of G247D-D559X and G247D-K584X BiP.

Size exclusion chromatography and native gel electrophoresis (followed by Coomassie Brilliant Blue staining) were performed on ***(A)*** G247D-D559X BiP, and ***(B)*** G247D-K584X BiP. The UV absorbance spectra obtained for each protein preparation are shown and the corresponding peak fractions indicated. The lane denoted by a '*' acted as a marker for the position of the monomeric species on the native gel.

Tris, pH 7.4, 125 m M NaCl, 25 m M KCl, 10% glycerol. The resulting column profile (Figure 41B, top panel) contained a single peak that corresponded to a predominant lower order oligomer, with seemingly insignificant amounts of a higher order oligomer (Figure 41B, bottom panel). However, when this preparation of G247D-K584X BiP was utilized in preliminary crystallization attempts, the protein precipitated out of solution, suggesting that the higher order oligomer negatively affected crystal formation. Therefore, different conditions were tested to abolish the contaminating higher order oligomer.

To this end, ~5 mg of G247D-K584X BiP was incubated on ice with the detergent, Triton X-100, at a final concentration of 0.05% and the reducing agent, DTT, at a final concentration of 5 mM for 30 min, and subjected to size exclusion chromatography in the buffer: 50 mM Tris pH 7.4, 125 m M NaCl, 25 m M KCl, 0.05% Triton X-100, 5 m M DTT, 10% glycerol. However, native gel electrophoresis of the resulting fractions showed that this treatment did not eliminate the higher order oligomer (Figure 42A). Next, the pH of the solutions used for columns 2 and 3 during purification was altered from 7.4 to 8.2, in keeping with the crystallization attempts of rat Hsc70[12]. When the resulting protein, which remained soluble over extended periods of time, was analyzed using size exclusion chromatography in the buffer: 50 mM Tris, pH 8.2, 125 mM NaCl, 25 mM KCl, 10% glycerol, followed by native gel electrophoresis, there was a reduction in the higher order oligomeric species (Figure 42B). Finally, size exclusion chromatography was performed with the buffer: 50 mM Tris, pH 8.2, 475 mM NaCl, 25 mM KCl, 10% glycerol, and subsequent native gel electrophoresis determined that the higher order oligomer was abolished (Figure 42C). Taken together, these experiments indicate that G247D-K584X BiP purified at a pH of 8.2 can be resolved into a single oligomeric state when treated with high concentrations of salt (*i.e.,* 500 mM).

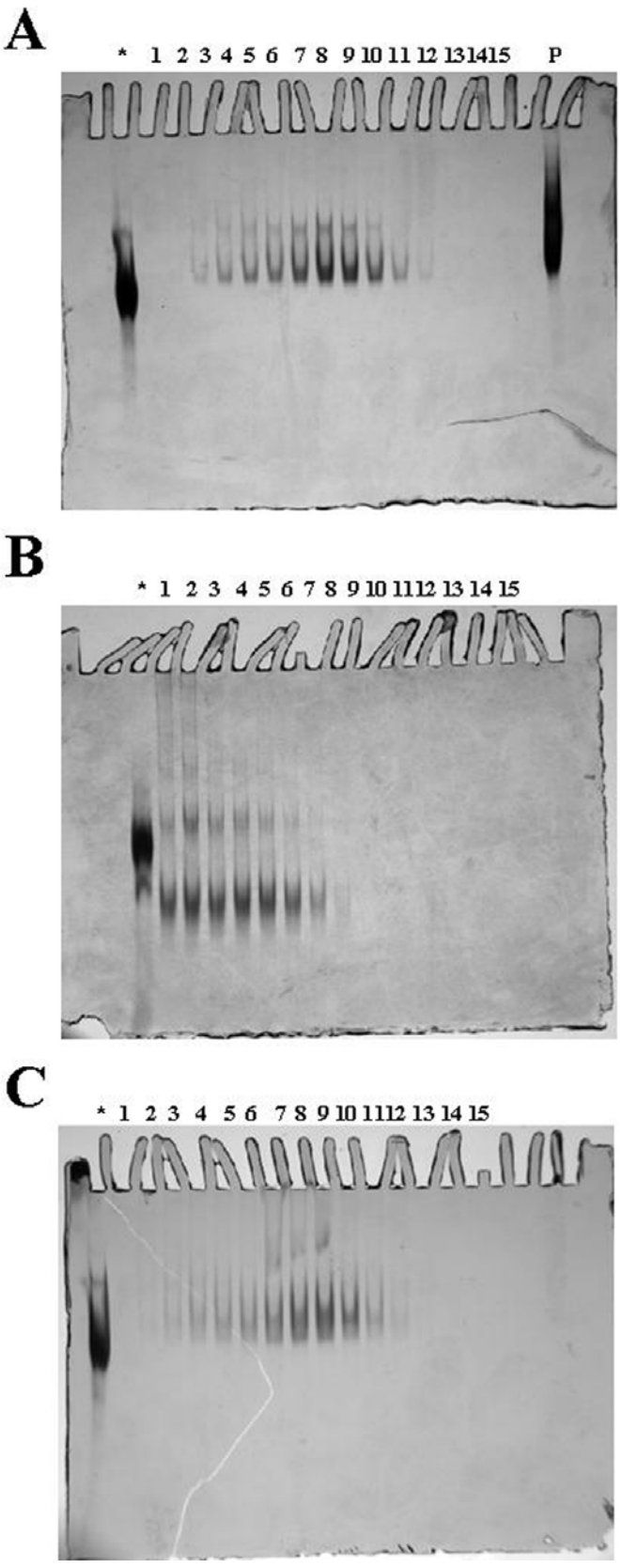
A
* 1 2 3 4 5 6 7 8 9 10 11 12 13 14 15 P
B
* 1 2 3 4 5 6 7 8 9 10 11 12 13 14 15
C
* 1 2 3 4 5 6 7 8 9 10 11 12 13 14 15

Figure 42: Optimization of the conditions under which G247D-K584X BiP separates as a single oligomeric species.

Size exclusion chromatography followed by native gel electrophoresis (visualized using Coomassie Brilliant Blue staining) was performed on G247D-K584X BiP under the following conditions: ***(A)*** 50 mM Tris, pH 7.4, 125 mM NaCl, 25 mM KCl, 0.05% Triton X-100, 5 mM DTT, 10% glycerol, ***(B)*** 50 mM Tris, pH 8.2, 125 mM NaCl, 25 mM KCl, 10% glycerol, and ***(C)*** 50 mM Tris, pH 8.2, 475 mM NaCl, 25 mM KCl, 10% glycerol. * indicates the column load in denaturing sample buffer, while the numbers 1-15 indicate the fractions obtained from size exclusion chromatography.

C.4 CONCLUSIONS AND FUTURE DIRECTIONS

As summarized in the previous sections, a purification protocol has been optimized to yield highly enriched BiP proteins at concentrations that are sufficient for crystallization purposes. Moreover, improved conditions to obtain a single oligomeric state of G247D-K584X BiP have been determined. Therefore, the immediate goal is to obtain large amounts of this protein and crystallize it. In the future, the G247D mutant in the context of full-length BiP will be analyzed in a similar manner, and hopefully, crystallized. Importantly, data obtained from crystallographic studies will be corroborated using NMR analyses, following which mutagenesis studies will be performed to establish a structure-function correlation *in vivo*.

BIBLIOGRAPHY

1. Flaherty, K.M., DeLuca-Flaherty, C. & McKay, D.B. Three-dimensional structure of the ATPase fragment of a 70K heat-shock cognate protein. *Nature* **346**, 623-8 (1990).
2. Li, J., Qian, X. & Sha, B. The crystal structure of the yeast Hsp40 Ydj1 complexed with its peptide substrate. *Structure* **11**, 1475-83 (2003).
3. Denic, V., Quan, E.M. & Weissman, J.S. A luminal surveillance complex that selects misfolded glycoproteins for ER-associated degradation. *Cell* **126**, 349-59 (2006).
4. Corpet, F. Multiple sequence alignment with hierarchical clustering. *Nucleic Acids Res* **16**, 10881-90 (1988).
5. Vembar, S.S. & Brodsky, J.L. One step at a time: endoplasmic reticulum-associated degradation. *Nat Rev Mol Cell Biol* **9**, 944-57 (2008).
6. Thrower, J.S., Hoffman, L., Rechsteiner, M. & Pickart, C.M. Recognition of the polyubiquitin proteolytic signal. *EMBO J* **19**, 94-102 (2000).
7. Jiang, J., Prasad, K., Lafer, E.M. & Sousa, R. Structural basis of interdomain communication in the Hsc70 chaperone. *Mol Cell* **20**, 513-24 (2005).
8. Jahn, T.R. & Radford, S.E. The Yin and Yang of protein folding. *FEBS Journal* **272**, 5962-5970 (2005).
9. Zhu, X. et al. Structural analysis of substrate binding by the molecular chaperone DnaK. *Science* **272**, 1606-14 (1996).
10. Labarga, A., Valentin, F., Anderson, M. & Lopez, R. Web services at the European bioinformatics institute. *Nucleic Acids Res* **35**, W6-11 (2007).
11. Sayle, R.A. & Milner-White, E.J. RASMOL: biomolecular graphics for all. *Trends Biochem Sci* **20**, 374 (1995).
12. Chang, Y.W., Sun, Y.J., Wang, C. & Hsiao, C.D. Crystal structures of the 70-kDa heat shock proteins in domain disjoining conformation. *J Biol Chem* **283**, 15502-11 (2008).
13. Varshavsky, A. Discovery of cellular regulation by protein degradation. *J Biol Chem* **283**, 34469-89 (2008).
14. Liu, Q. & Hendrickson, W.A. Insights into Hsp70 chaperone activity from a crystal structure of the yeast Hsp110 Sse1. *Cell* **131**, 106-20 (2007).
15. Jiang, J. et al. Structural basis of J cochaperone binding and regulation of Hsp70. *Mol Cell* **28**, 422-33 (2007).
16. Ellis, R.J. Macromolecular crowding: obvious but underappreciated. *Trends Biochem Sci.* **26**, 597-604 (2001).
17. Despa, F., Orgill, D.P. & Lee, R.C. Molecular Crowding Effects on Protein Stability. *Annals of the New York Academy of Sciences* **1066**, 54-66 (2005).
18. Jahn, T.R. & Radford, S.E. Folding versus aggregation: polypeptide conformations on competing pathways. *Arch Biochem Biophys* **469**, 100-17 (2008).

19. Bukau, B., Weissman, J.S. & Horwich, A. Molecular Chaperones and Protein Quality Control. *Cell* **125**, 443-451 (2006).
20. Balch, W.E., Morimoto, R.I., Dillin, A. & Kelly, J.W. Adapting Proteostasis for Disease Intervention. *Science* **319**, 916-919 (2008).
21. Gaestel, M. Molecular chaperones in signal transduction. *Handb Exp Pharmacol*, 93-109 (2006).
22. Calderwood, S.K., Mambula, S.S. & Gray, P.J., Jr. Extracellular heat shock proteins in cell signaling and immunity. *Ann N Y Acad Sci* **1113**, 28-39 (2007).
23. Saibil, H. Molecular chaperones: containers and surfaces for folding, stabilising or unfolding proteins. *Curr Opin Struct Biol* **10**, 251-8 (2000).
24. Mayer, M.P. & Bukau, B. Hsp70 chaperones: cellular functions and molecular mechanism. *Cell Mol Life Sci* **62**, 670-84 (2005).
25. Young, J.C., Barral, J.M. & Ulrich Hartl, F. More than folding: localized functions of cytosolic chaperones. *Trends Biochem Sci* **28**, 541-7 (2003).
26. Liberek, K., Lewandowska, A. & Zietkiewicz, S. Chaperones in control of protein disaggregation. *EMBO J* **27**, 328-35 (2008).
27. Rapoport, T.A. Protein translocation across the eukaryotic endoplasmic reticulum and bacterial plasma membranes. *Nature* **450**, 663-9 (2007).
28. Macario, A.J. & Conway de Macario, E. Molecular chaperones: multiple functions, pathologies, and potential applications. *Front Biosci* **12**, 2588-600 (2007).
29. Eisenberg, E. & Greene, L.E. Multiple roles of auxilin and hsc70 in clathrin-mediated endocytosis. *Traffic* **8**, 640-6 (2007).
30. Takayama, S., Reed, J.C. & Homma, S. Heat-shock proteins as regulators of apoptosis. *Oncogene* **22**, 9041-7 (2003).
31. Daugaard, M., Rohde, M. & Jaattela, M. The heat shock protein 70 family: Highly homologous proteins with overlapping and distinct functions. *FEBS Lett* **581**, 3702-10 (2007).
32. Nishikawa, S., Brodsky, J.L. & Nakatsukasa, K. Roles of molecular chaperones in endoplasmic reticulum (ER) quality control and ER-associated degradation (ERAD). *J Biochem* **137**, 551-5 (2005).
33. Buck, T.M., Wright, C.M. & Brodsky, J.L. The activities and function of molecular chaperones in the endoplasmic reticulum. *Semin Cell Dev Biol* **18**, 751-61 (2007).
34. Haas, I.G. & Wabl, M. Immunoglobulin heavy chain binding protein. *Nature* **306**, 387-9 (1983).
35. Munro, S. & Pelham, H.R. An Hsp70-like protein in the ER: identity with the 78 kd glucose-regulated protein and immunoglobulin heavy chain binding protein. *Cell* **46**, 291-300 (1986).
36. Polaina, J. & Conde, J. Genes involved in the control of nuclear fusion during the sexual cycle of Saccharomyces cerevisiae. *Mol Gen Genet* **186**, 253-8 (1982).
37. Rose, M.D., Misra, L.M. & Vogel, J.P. KAR2, a karyogamy gene, is the yeast homolog of the mammalian BiP/GRP78 gene. *Cell* **57**, 1211-21 (1989).
38. Normington, K., Kohno, K., Kozutsumi, Y., Gething, M.J. & Sambrook, J. S. cerevisiae encodes an essential protein homologous in sequence and function to mammalian BiP. *Cell* **57**, 1223-36 (1989).

39. Shiu, R.P., Pouyssegur, J. & Pastan, I. Glucose depletion accounts for the induction of two transformation-sensitive membrane proteinsin Rous sarcoma virus-transformed chick embryo fibroblasts. *Proc Natl Acad Sci U S A* **74**, 3840-4 (1977).
40. Pouyssegur, J., Shiu, R.P. & Pastan, I. Induction of two transformation-sensitive membrane polypeptides in normal fibroblasts by a block in glycoprotein synthesis or glucose deprivation. *Cell* **11**, 941-7 (1977).
41. Carla Fama, M. et al. The Saccharomyces cerevisiae YFR041C/ERJ5 gene encoding a type I membrane protein with a J domain is required to preserve the folding capacity of the endoplasmic reticulum. *Biochim Biophys Acta* **1773**, 232-42 (2007).
42. Brightman, S.E., Blatch, G.L. & Zetter, B.R. Isolation of a mouse cDNA encoding MTJ1, a new murine member of the DnaJ family of proteins. *Gene* **153**, 249-54 (1995).
43. Skowronek, M.H., Rotter, M. & Haas, I.G. Molecular characterization of a novel mammalian DnaJ-like Sec63p homolog. *Biol Chem* **380**, 1133-8 (1999).
44. Tyedmers, J. et al. Homologs of the yeast Sec complex subunits Sec62p and Sec63p are abundant proteins in dog pancreas microsomes. *Proc Natl Acad Sci U S A* **97**, 7214-9 (2000).
45. Bies, C. et al. A Scj1p homolog and folding catalysts present in dog pancreas microsomes. *Biol Chem* **380**, 1175-82 (1999).
46. Yu, M., Haslam, R.H. & Haslam, D.B. HEDJ, an Hsp40 co-chaperone localized to the endoplasmic reticulum of human cells. *J Biol Chem* **275**, 24984-92 (2000).
47. Lau, P.P. et al. A DnaJ protein, apobec-1-binding protein-2, modulates apolipoprotein B mRNA editing. *J Biol Chem* **276**, 46445-52 (2001).
48. Prols, F. et al. Upregulation of the cochaperone Mdg1 in endothelial cells is induced by stress and during in vitro angiogenesis. *Exp Cell Res* **269**, 42-53 (2001).
49. Shen, Y., Meunier, L. & Hendershot, L.M. Identification and characterization of a novel endoplasmic reticulum (ER) DnaJ homologue, which stimulates ATPase activity of BiP in vitro and is induced by ER stress. *J Biol Chem* **277**, 15947-56 (2002).
50. Cunnea, P.M. et al. ERdj5, an endoplasmic reticulum (ER)-resident protein containing DnaJ and thioredoxin domains, is expressed in secretory cells or following ER stress. *J Biol Chem* **278**, 1059-66 (2003).
51. Hosoda, A., Kimata, Y., Tsuru, A. & Kohno, K. JPDI, a novel endoplasmic reticulum-resident protein containing both a BiP-interacting J-domain and thioredoxin-like motifs. *J Biol Chem* **278**, 2669-76 (2003).
52. Lee, T.G., Tang, N., Thompson, S., Miller, J. & Katze, M.G. The 58,000-dalton cellular inhibitor of the interferon-induced double-stranded RNA-activated protein kinase (PKR) is a member of the tetratricopeptide repeat family of proteins. *Mol Cell Biol* **14**, 2331-42 (1994).
53. Barber, G.N. et al. The 58-kilodalton inhibitor of the interferon-induced double-stranded RNA-activated protein kinase is a tetratricopeptide repeat protein with oncogenic properties. *Proc Natl Acad Sci U S A* **91**, 4278-82 (1994).
54. Tang, N.M., Ho, C.Y. & Katze, M.G. The 58-kDa cellular inhibitor of the double stranded RNA-dependent protein kinase requires the tetratricopeptide repeat 6 and DnaJ motifs to stimulate protein synthesis in vivo. *J Biol Chem* **271**, 28660-6 (1996).
55. Saito, H. & Uchida, H. Initiation of the DNA replication of bacteriophage lambda in Escherichia coli K12. *J Mol Biol* **113**, 1-25 (1977).

56. Yochem, J. et al. Genetic analysis of two genes, dnaJ and dnaK, necessary for Escherichia coli and bacteriophage lambda DNA replication. *Mol Gen Genet* **164**, 9-14 (1978).
57. Saito, H. & Uchida, H. Organization and expression of the dnaJ and dnaK genes of Escherichia coli K12. *Mol Gen Genet* **164**, 1-8 (1978).
58. Tilly, K., McKittrick, N., Zylicz, M. & Georgopoulos, C. The dnaK protein modulates the heat-shock response of Escherichia coli. *Cell* **34**, 641-6 (1983).
59. Sousa, R. & Lafer, E.M. Keep the traffic moving: mechanism of the Hsp70 motor. *Traffic* **7**, 1596-603 (2006).
60. Genevaux, P., Georgopoulos, C. & Kelley, W.L. The Hsp70 chaperone machines of Escherichia coli: a paradigm for the repartition of chaperone functions. *Mol Microbiol* **66**, 840-57 (2007).
61. Saibil, H.R. Chaperone machines in action. *Curr Opin Struct Biol* **18**, 35-42 (2008).
62. Meimaridou, E., Gooljar, S.B. & Chapple, J.P. From hatching to dispatching: the multiple cellular roles of the Hsp70 molecular chaperone machinery. *J Mol Endocrinol* **42**, 1-9 (2009).
63. Zylicz, M., LeBowitz, J.H., McMacken, R. & Georgopoulos, C. The dnaK protein of Escherichia coli possesses an ATPase and autophosphorylating activity and is essential in an in vitro DNA replication system. *Proc Natl Acad Sci U S A* **80**, 6431-5 (1983).
64. Macejak, D., Rayfield, M. & Luftig, R. Isolation and characterization of human HSP70 expressed in Escherichia coli. *Arch Biochem Biophys* **280**, 53-60 (1990).
65. Barany, M. ATPase activity of myosin correlated with speed of muscle shortening. *J Gen Physiol* **50**, Suppl:197-218 (1967).
66. Hennessy, F., Nicoll, W.S., Zimmermann, R., Cheetham, M.E. & Blatch, G.L. Not all J domains are created equal: implications for the specificity of Hsp40-Hsp70 interactions. *Protein Sci* **14**, 1697-709 (2005).
67. Rudiger, S., Schneider-Mergener, J. & Bukau, B. Its substrate specificity characterizes the DnaJ co-chaperone as a scanning factor for the DnaK chaperone. *EMBO J* **20**, 1042-50 (2001).
68. Craig, E.A., Huang, P., Aron, R. & Andrew, A. The diverse roles of J-proteins, the obligate Hsp70 co-chaperone. *Rev Physiol Biochem Pharmacol* **156**, 1-21 (2006).
69. Ziegelhoffer, T., Lopez-Buesa, P. & Craig, E.A. The dissociation of ATP from hsp70 of Saccharomyces cerevisiae is stimulated by both Ydj1p and peptide substrates. *J Biol Chem* **270**, 10412-9 (1995).
70. Mayer, M., Reinstein, J. & Buchner, J. Modulation of the ATPase cycle of BiP by peptides and proteins. *J Mol Biol* **330**, 137-44 (2003).
71. Buchberger, A., Valencia, A., McMacken, R., Sander, C. & Bukau, B. The chaperone function of DnaK requires the coupling of ATPase activity with substrate binding through residue E171. *EMBO J* **13**, 1687-95 (1994).
72. Burkholder, W.F. et al. Isolation and characterization of an Escherichia coli DnaK mutant with impaired ATPase activity. *J Mol Biol* **242**, 364-77 (1994).
73. Hendershot, L.M. et al. In vivo expression of mammalian BiP ATPase mutants causes disruption of the endoplasmic reticulum. *Mol Biol Cell* **6**, 283-96 (1995).
74. Hendershot, L. et al. Inhibition of immunoglobulin folding and secretion by dominant negative BiP ATPase mutants. *Proc Natl Acad Sci U S A* **93**, 5269-74 (1996).

75. O'Brien, M.C., Flaherty, K.M. & McKay, D.B. Lysine 71 of the chaperone protein Hsc70 Is essential for ATP hydrolysis. *J Biol Chem* **271**, 15874-8 (1996).
76. Hurley, J.H. The sugar kinase/heat shock protein 70/actin superfamily: implications of conserved structure for mechanism. *Annu Rev Biophys Biomol Struct* **25**, 137-62 (1996).
77. Kassenbrock, C.K. & Kelly, R.B. Interaction of heavy chain binding protein (BiP/GRP78) with adenine nucleotides. *EMBO J* **8**, 1461-7 (1989).
78. Revington, M., Zhang, Y., Yip, G.N., Kurochkin, A.V. & Zuiderweg, E.R. NMR investigations of allosteric processes in a two-domain Thermus thermophilus Hsp70 molecular chaperone. *J Mol Biol* **349**, 163-83 (2005).
79. Swain, J.F. et al. Hsp70 chaperone ligands control domain association via an allosteric mechanism mediated by the interdomain linker. *Mol Cell* **26**, 27-39 (2007).
80. Vogel, M., Mayer, M.P. & Bukau, B. Allosteric regulation of Hsp70 chaperones involves a conserved interdomain linker. *J Biol Chem* **281**, 38705-11 (2006).
81. Vogel, M., Bukau, B. & Mayer, M.P. Allosteric regulation of Hsp70 chaperones by a proline switch. *Mol Cell* **21**, 359-67 (2006).
82. Moro, F., Fernandez-Saiz, V. & Muga, A. The lid subdomain of DnaK is required for the stabilization of the substrate-binding site. *J Biol Chem* **279**, 19600-6 (2004).
83. Fernandez-Saiz, V., Moro, F., Arizmendi, J.M., Acebron, S.P. & Muga, A. Ionic contacts at DnaK substrate binding domain involved in the allosteric regulation of lid dynamics. *J Biol Chem* **281**, 7479-88 (2006).
84. Raviol, H., Sadlish, H., Rodriguez, F., Mayer, M.P. & Bukau, B. Chaperone network in the yeast cytosol: Hsp110 is revealed as an Hsp70 nucleotide exchange factor. *EMBO J* **25**, 2510-8 (2006).
85. Andreasson, C., Fiaux, J., Rampelt, H., Mayer, M.P. & Bukau, B. Hsp110 is a nucleotide-activated exchange factor for Hsp70. *J Biol Chem* **283**, 8877-84 (2008).
86. Harrison, C.J., Hayer-Hartl, M., Di Liberto, M., Hartl, F. & Kuriyan, J. Crystal structure of the nucleotide exchange factor GrpE bound to the ATPase domain of the molecular chaperone DnaK. *Science* **276**, 431-5 (1997).
87. Sondermann, H. et al. Structure of a Bag/Hsc70 complex: convergent functional evolution of Hsp70 nucleotide exchange factors. *Science* **291**, 1553-7 (2001).
88. Polier, S., Dragovic, Z., Hartl, F.U. & Bracher, A. Structural basis for the cooperation of Hsp70 and Hsp110 chaperones in protein folding. *Cell* **133**, 1068-79 (2008).
89. Schuermann, J.P. et al. Structure of the Hsp110:Hsc70 nucleotide exchange machine. *Mol Cell* **31**, 232-43 (2008).
90. Shomura, Y. et al. Regulation of Hsp70 function by HspBP1: structural analysis reveals an alternate mechanism for Hsp70 nucleotide exchange. *Mol Cell* **17**, 367-79 (2005).
91. Suh, W.C. et al. Interaction of the Hsp70 molecular chaperone, DnaK, with its cochaperone DnaJ. *Proc Natl Acad Sci U S A* **95**, 15223-8 (1998).
92. Suh, W.C., Lu, C.Z. & Gross, C.A. Structural features required for the interaction of the Hsp70 molecular chaperone DnaK with its cochaperone DnaJ. *J Biol Chem* **274**, 30534-9 (1999).
93. Rothblatt, J.A., Deshaies, R.J., Sanders, S.L., Daum, G. & Schekman, R. Multiple genes are required for proper insertion of secretory proteins into the endoplasmic reticulum in yeast. *J Cell Biol* **109**, 2641-52 (1989).

94. Sadler, I. et al. A yeast gene important for protein assembly into the endoplasmic reticulum and the nucleus has homology to DnaJ, an Escherichia coli heat shock protein. *J Cell Biol* **109**, 2665-75 (1989).
95. Feldheim, D., Rothblatt, J. & Schekman, R. Topology and functional domains of Sec63p, an endoplasmic reticulum membrane protein required for secretory protein translocation. *Mol Cell Biol* **12**, 3288-96 (1992).
96. Deshaies, R.J., Sanders, S.L., Feldheim, D.A. & Schekman, R. Assembly of yeast Sec proteins involved in translocation into the endoplasmic reticulum into a membrane-bound multisubunit complex. *Nature* **349**, 806-8 (1991).
97. Jermy, A.J., Willer, M., Davis, E., Wilkinson, B.M. & Stirling, C.J. The Brl domain in Sec63p is required for assembly of functional endoplasmic reticulum translocons. *J Biol Chem* **281**, 7899-906 (2006).
98. Brodsky, J.L. & Schekman, R. A Sec63p-BiP complex from yeast is required for protein translocation in a reconstituted proteoliposome. *J Cell Biol* **123**, 1355-63 (1993).
99. Matlack, K.E., Plath, K., Misselwitz, B. & Rapoport, T.A. Protein transport by purified yeast Sec complex and Kar2p without membranes. *Science* **277**, 938-41 (1997).
100. Panzner, S., Dreier, L., Hartmann, E., Kostka, S. & Rapoport, T.A. Posttranslational protein transport in yeast reconstituted with a purified complex of Sec proteins and Kar2p. *Cell* **81**, 561-70 (1995).
101. Green, N., Fang, H. & Walter, P. Mutants in three novel complementation groups inhibit membrane protein insertion into and soluble protein translocation across the endoplasmic reticulum membrane of Saccharomyces cerevisiae. *J Cell Biol* **116**, 597-604 (1992).
102. Feldheim, D., Yoshimura, K., Admon, A. & Schekman, R. Structural and functional characterization of Sec66p, a new subunit of the polypeptide translocation apparatus in the yeast endoplasmic reticulum. *Mol Biol Cell* **4**, 931-9 (1993).
103. Feldheim, D. & Schekman, R. Sec72p contributes to the selective recognition of signal peptides by the secretory polypeptide translocation complex. *J Cell Biol* **126**, 935-43 (1994).
104. Kurihara, T. & Silver, P. Suppression of a sec63 mutation identifies a novel component of the yeast endoplasmic reticulum translocation apparatus. *Mol Biol Cell* **4**, 919-30 (1993).
105. Lyman, S.K. & Schekman, R. Binding of secretory precursor polypeptides to a translocon subcomplex is regulated by BiP. *Cell* **88**, 85-96 (1997).
106. Fang, H. & Green, N. Nonlethal sec71-1 and sec72-1 mutations eliminate proteins associated with the Sec63p-BiP complex from S. cerevisiae. *Mol Biol Cell* **5**, 933-42 (1994).
107. Brodsky, J.L., Hamamoto, S., Feldheim, D. & Schekman, R. Reconstitution of protein translocation from solubilized yeast membranes reveals topologically distinct roles for BiP and cytosolic Hsc70. *J Cell Biol* **120**, 95-102 (1993).
108. Scidmore, M.A., Okamura, H.H. & Rose, M.D. Genetic interactions between KAR2 and SEC63, encoding eukaryotic homologues of DnaK and DnaJ in the endoplasmic reticulum. *Mol Biol Cell* **4**, 1145-59 (1993).
109. Brodsky, J.L., Goeckeler, J. & Schekman, R. BiP and Sec63p are required for both co- and posttranslational protein translocation into the yeast endoplasmic reticulum. *Proc Natl Acad Sci U S A* **92**, 9643-6 (1995).

110. Lyman, S.K. & Schekman, R. Interaction between BiP and Sec63p is required for the completion of protein translocation into the ER of Saccharomyces cerevisiae. *J Cell Biol* **131**, 1163-71 (1995).
111. Corsi, A.K. & Schekman, R. The lumenal domain of Sec63p stimulates the ATPase activity of BiP and mediates BiP recruitment to the translocon in Saccharomyces cerevisiae. *J Cell Biol* **137**, 1483-93 (1997).
112. Misselwitz, B., Staeck, O., Matlack, K.E. & Rapoport, T.A. Interaction of BiP with the J-domain of the Sec63p component of the endoplasmic reticulum protein translocation complex. *J Biol Chem* **274**, 20110-5 (1999).
113. Matlack, K.E., Misselwitz, B., Plath, K. & Rapoport, T.A. BiP acts as a molecular ratchet during posttranslational transport of prepro-alpha factor across the ER membrane. *Cell* **97**, 553-64 (1999).
114. Young, B.P., Craven, R.A., Reid, P.J., Willer, M. & Stirling, C.J. Sec63p and Kar2p are required for the translocation of SRP-dependent precursors into the yeast endoplasmic reticulum in vivo. *EMBO J* **20**, 262-71 (2001).
115. Hamman, B.D., Hendershot, L.M. & Johnson, A.E. BiP maintains the permeability barrier of the ER membrane by sealing the lumenal end of the translocon pore before and early in translocation. *Cell* **92**, 747-58 (1998).
116. Alder, N.N., Shen, Y., Brodsky, J.L., Hendershot, L.M. & Johnson, A.E. The molecular mechanisms underlying BiP-mediated gating of the Sec61 translocon of the endoplasmic reticulum. *J Cell Biol* **168**, 389-99 (2005).
117. Blumberg, H. & Silver, P.A. A homologue of the bacterial heat-shock gene DnaJ that alters protein sorting in yeast. *Nature* **349**, 627-30 (1991).
118. Schlenstedt, G., Harris, S., Risse, B., Lill, R. & Silver, P.A. A yeast DnaJ homologue, Scj1p, can function in the endoplasmic reticulum with BiP/Kar2p via a conserved domain that specifies interactions with Hsp70s. *J Cell Biol* **129**, 979-88 (1995).
119. Silberstein, S., Schlenstedt, G., Silver, P.A. & Gilmore, R. A role for the DnaJ homologue Scj1p in protein folding in the yeast endoplasmic reticulum. *J Cell Biol* **143**, 921-33 (1998).
120. Nishikawa, S.I., Fewell, S.W., Kato, Y., Brodsky, J.L. & Endo, T. Molecular chaperones in the yeast endoplasmic reticulum maintain the solubility of proteins for retrotranslocation and degradation. *J Cell Biol* **153**, 1061-70 (2001).
121. Jonikas, M.C. et al. Comprehensive characterization of genes required for protein folding in the endoplasmic reticulum. *Science* **323**, 1693-7 (2009).
122. Nishikawa, S. & Endo, T. The yeast JEM1p is a DnaJ-like protein of the endoplasmic reticulum membrane required for nuclear fusion. *J Biol Chem* **272**, 12889-92 (1997).
123. Nishikawa, S. & Endo, T. Reinvestigation of the functions of the hydrophobic segment of Jem1p, a yeast endoplasmic reticulum membrane protein mediating nuclear fusion. *Biochem Biophys Res Commun* **244**, 785-9 (1998).
124. Marcus, N.Y., Marcus, R.A., Schmidt, B.Z. & Haslam, D.B. Contribution of the HEDJ/ERdj3 cysteine-rich domain to substrate interactions. *Arch Biochem Biophys* **468**, 147-58 (2007).
125. Jin, Y., Zhuang, M. & Hendershot, L.M. ERdj3, a luminal ER DnaJ homologue, binds directly to unfolded proteins in the mammalian ER: identification of critical residues. *Biochemistry* **48**, 41-9 (2009).

126. Caplan, A.J. & Douglas, M.G. Characterization of YDJ1: a yeast homologue of the bacterial dnaJ protein. *J Cell Biol* **114**, 609-21 (1991).
127. Cyr, D.M., Lu, X. & Douglas, M.G. Regulation of Hsp70 function by a eukaryotic DnaJ homolog. *J Biol Chem* **267**, 20927-31 (1992).
128. Meunier, L., Usherwood, Y.K., Chung, K.T. & Hendershot, L.M. A subset of chaperones and folding enzymes form multiprotein complexes in endoplasmic reticulum to bind nascent proteins. *Mol Biol Cell* **13**, 4456-69 (2002).
129. Shen, Y. & Hendershot, L.M. ERdj3, a stress-inducible endoplasmic reticulum DnaJ homologue, serves as a cofactor for BiP's interactions with unfolded substrates. *Mol Biol Cell* **16**, 40-50 (2005).
130. Jin, Y., Awad, W., Petrova, K. & Hendershot, L.M. Regulated release of ERdj3 from unfolded proteins by BiP. *EMBO J* **27**, 2873-82 (2008).
131. Petrova, K., Oyadomari, S., Hendershot, L.M. & Ron, D. Regulated association of misfolded endoplasmic reticulum lumenal proteins with P58/DNAJc3. *EMBO J* **27**, 2862-72 (2008).
132. Boisrame, A., Beckerich, J.M. & Gaillardin, C. Sls1p, an endoplasmic reticulum component, is involved in the protein translocation process in the yeast Yarrowia lipolytica. *J Biol Chem* **271**, 11668-75 (1996).
133. Boisrame, A., Kabani, M., Beckerich, J.M., Hartmann, E. & Gaillardin, C. Interaction of Kar2p and Sls1p is required for efficient co-translational translocation of secreted proteins in the yeast Yarrowia lipolytica. *J Biol Chem* **273**, 30903-8 (1998).
134. Kabani, M., Beckerich, J.M. & Gaillardin, C. Sls1p stimulates Sec63p-mediated activation of Kar2p in a conformation-dependent manner in the yeast endoplasmic reticulum. *Mol Cell Biol* **20**, 6923-34 (2000).
135. Tyson, J.R. & Stirling, C.J. LHS1 and SIL1 provide a lumenal function that is essential for protein translocation into the endoplasmic reticulum. *EMBO J* **19**, 6440-52 (2000).
136. Craven, R.A., Egerton, M. & Stirling, C.J. A novel Hsp70 of the yeast ER lumen is required for the efficient translocation of a number of protein precursors. *EMBO J* **15**, 2640-50 (1996).
137. Baxter, B.K., James, P., Evans, T. & Craig, E.A. SSI1 encodes a novel Hsp70 of the Saccharomyces cerevisiae endoplasmic reticulum. *Mol Cell Biol* **16**, 6444-56 (1996).
138. Saris, N., Holkeri, H., Craven, R.A., Stirling, C.J. & Makarow, M. The Hsp70 homologue Lhs1p is involved in a novel function of the yeast endoplasmic reticulum, refolding and stabilization of heat-denatured protein aggregates. *J Cell Biol* **137**, 813-24 (1997).
139. Steel, G.J., Fullerton, D.M., Tyson, J.R. & Stirling, C.J. Coordinated activation of Hsp70 chaperones. *Science* **303**, 98-101 (2004).
140. Weitzmann, A., Volkmer, J. & Zimmermann, R. The nucleotide exchange factor activity of Grp170 may explain the non-lethal phenotype of loss of Sil1 function in man and mouse. *FEBS Lett* **580**, 5237-40 (2006).
141. Goeckeler, J.L., Stephens, A., Lee, P., Caplan, A.J. & Brodsky, J.L. Overexpression of yeast Hsp110 homolog Sse1p suppresses ydj1-151 thermosensitivity and restores Hsp90-dependent activity. *Mol Biol Cell* **13**, 2760-70 (2002).
142. Kimura, T. et al. Interactions among yeast protein-disulfide isomerase proteins and endoplasmic reticulum chaperone proteins influence their activities. *J Biol Chem* **280**, 31438-41 (2005).

143. Gillece, P., Luz, J.M., Lennarz, W.J., de La Cruz, F.J. & Romisch, K. Export of a cysteine-free misfolded secretory protein from the endoplasmic reticulum for degradation requires interaction with protein disulfide isomerase. *J Cell Biol* **147**, 1443-56 (1999).
144. Takeuchi, M., Kimata, Y., Hirata, A., Oka, M. & Kohno, K. Saccharomyces cerevisiae Rot1p is an ER-localized membrane protein that may function with BiP/Kar2p in protein folding. *J Biochem* **139**, 597-605 (2006).
145. Takeuchi, M., Kimata, Y. & Kohno, K. Saccharomyces cerevisiae Rot1 is an essential molecular chaperone in the endoplasmic reticulum. *Mol Biol Cell* **19**, 3514-25 (2008).
146. Deshaies, R.J. & Schekman, R. A yeast mutant defective at an early stage in import of secretory protein precursors into the endoplasmic reticulum. *J Cell Biol* **105**, 633-45 (1987).
147. Esnault, Y., Blondel, M.O., Deshaies, R.J., Scheckman, R. & Kepes, F. The yeast SSS1 gene is essential for secretory protein translocation and encodes a conserved protein of the endoplasmic reticulum. *EMBO J* **12**, 4083-93 (1993).
148. Esnault, Y., Feldheim, D., Blondel, M.O., Schekman, R. & Kepes, F. SSS1 encodes a stabilizing component of the Sec61 subcomplex of the yeast protein translocation apparatus. *J Biol Chem* **269**, 27478-85 (1994).
149. Toikkanen, J. et al. Yeast protein translocation complex: isolation of two genes SEB1 and SEB2 encoding proteins homologous to the Sec61 beta subunit. *Yeast* **12**, 425-38 (1996).
150. Sanders, S.L., Whitfield, K.M., Vogel, J.P., Rose, M.D. & Schekman, R.W. Sec61p and BiP directly facilitate polypeptide translocation into the ER. *Cell* **69**, 353-65 (1992).
151. McClellan, A.J. et al. Specific molecular chaperone interactions and an ATP-dependent conformational change are required during posttranslational protein translocation into the yeast ER. *Mol Biol Cell* **9**, 3533-45 (1998).
152. Deshaies, R.J. & Schekman, R. SEC62 encodes a putative membrane protein required for protein translocation into the yeast endoplasmic reticulum. *J Cell Biol* **109**, 2653-64 (1989).
153. Deshaies, R.J. & Schekman, R. Structural and functional dissection of Sec62p, a membrane-bound component of the yeast endoplasmic reticulum protein import machinery. *Mol Cell Biol* **10**, 6024-35 (1990).
154. Meyer, H.A. et al. Mammalian Sec61 is associated with Sec62 and Sec63. *J Biol Chem* **275**, 14550-7 (2000).
155. Gorlich, D., Hartmann, E., Prehn, S. & Rapoport, T.A. A protein of the endoplasmic reticulum involved early in polypeptide translocation. *Nature* **357**, 47-52 (1992).
156. Osborne, A.R., Rapoport, T.A. & van den Berg, B. Protein translocation by the Sec61/SecY channel. *Annu Rev Cell Dev Biol* **21**, 529-50 (2005).
157. McCormick, P.J., Miao, Y., Shao, Y., Lin, J. & Johnson, A.E. Cotranslational protein integration into the ER membrane is mediated by the binding of nascent chains to translocon proteins. *Mol Cell* **12**, 329-41 (2003).
158. Wiedmann, M., Goerlich, D., Hartmann, E., Kurzchalia, T.V. & Rapoport, T.A. Photocrosslinking demonstrates proximity of a 34 kDa membrane protein to different portions of preprolactin during translocation through the endoplasmic reticulum. *FEBS Lett* **257**, 263-8 (1989).
159. Bohni, P.C., Deshaies, R.J. & Schekman, R.W. SEC11 is required for signal peptide processing and yeast cell growth. *J Cell Biol* **106**, 1035-42 (1988).

160. Fang, H., Panzner, S., Mullins, C., Hartmann, E. & Green, N. The homologue of mammalian SPC12 is important for efficient signal peptidase activity in Saccharomyces cerevisiae. *J Biol Chem* **271**, 16460-5 (1996).
161. Mullins, C., Meyer, H.A., Hartmann, E., Green, N. & Fang, H. Structurally related Spc1p and Spc2p of yeast signal peptidase complex are functionally distinct. *J Biol Chem* **271**, 29094-9 (1996).
162. Fang, H., Mullins, C. & Green, N. In addition to SEC11, a newly identified gene, SPC3, is essential for signal peptidase activity in the yeast endoplasmic reticulum. *J Biol Chem* **272**, 13152-8 (1997).
163. Meyer, H.A. & Hartmann, E. The yeast SPC22/23 homolog Spc3p is essential for signal peptidase activity. *J Biol Chem* **272**, 13159-64 (1997).
164. Helenius, A. & Aebi, M. Roles of N-linked glycans in the endoplasmic reticulum. *Annu Rev Biochem* **73**, 1019-49 (2004).
165. Hebert, D.N., Garman, S.C. & Molinari, M. The glycan code of the endoplasmic reticulum: asparagine-linked carbohydrates as protein maturation and quality-control tags. *Trends Cell Biol* **15**, 364-70 (2005).
166. Simons, J.F., Ferro-Novick, S., Rose, M.D. & Helenius, A. BiP/Kar2p serves as a molecular chaperone during carboxypeptidase Y folding in yeast. *J Cell Biol* **130**, 41-9 (1995).
167. Swanton, E. & Bulleid, N.J. Protein folding and translocation across the endoplasmic reticulum membrane. *Mol Membr Biol* **20**, 99-104 (2003).
168. Skach, W.R. The expanding role of the ER translocon in membrane protein folding. *J Cell Biol* **179**, 1333-5 (2007).
169. Gething, M.J. Role and regulation of the ER chaperone BiP. *Semin Cell Dev Biol* **10**, 465-72 (1999).
170. Hendershot, L.M. The ER function BiP is a master regulator of ER function. *Mt Sinai J Med* **71**, 289-97 (2004).
171. Blond-Elguindi, S. et al. Affinity panning of a library of peptides displayed on bacteriophages reveals the binding specificity of BiP. *Cell* **75**, 717-28 (1993).
172. Flynn, G.C., Pohl, J., Flocco, M.T. & Rothman, J.E. Peptide-binding specificity of the molecular chaperone BiP. *Nature* **353**, 726-30 (1991).
173. Ghaemmaghami, S. et al. Global analysis of protein expression in yeast. *Nature* **425**, 737-41 (2003).
174. Kanapin, A. et al. Mouse proteome analysis. *Genome Res* **13**, 1335-44 (2003).
175. Ellgaard, L. & Helenius, A. Quality control in the endoplasmic reticulum. *Nat Rev Mol Cell Biol* **4**, 181-91 (2003).
176. McCracken, A.A. & Brodsky, J.L. Assembly of ER-associated protein degradation in vitro: dependence on cytosol, calnexin, and ATP. *J Cell Biol* **132**, 291-8 (1996).
177. Nair, U. & Klionsky, D.J. Molecular mechanisms and regulation of specific and nonspecific autophagy pathways in yeast. *J Biol Chem* **280**, 41785-8 (2005).
178. Kassenbrock, C.K., Garcia, P.D., Walter, P. & Kelly, R.B. Heavy-chain binding protein recognizes aberrant polypeptides translocated in vitro. *Nature* **333**, 90-3 (1988).
179. Knittler, M.R., Dirks, S. & Haas, I.G. Molecular chaperones involved in protein degradation in the endoplasmic reticulum: quantitative interaction of the heat shock cognate protein BiP with partially folded immunoglobulin light chains that are degraded in the endoplasmic reticulum. *Proc Natl Acad Sci U S A* **92**, 1764-8 (1995).

180. Dong, M., Bridges, J.P., Apsley, K., Xu, Y. & Weaver, T.E. ERdj4 and ERdj5 Are Required for Endoplasmic Reticulum-associated Protein Degradation of Misfolded Surfactant Protein C. *Mol Biol Cell* **19**, 2620-30 (2008).
181. Kabani, M. et al. Dependence of endoplasmic reticulum-associated degradation on the peptide binding domain and concentration of BiP. *Mol Biol Cell* **14**, 3437-48 (2003).
182. Hammond, C. & Helenius, A. Folding of VSV G protein: sequential interaction with BiP and calnexin. *Science* **266**, 456-8 (1994).
183. Stronge, V.S., Saito, Y., Ihara, Y. & Williams, D.B. Relationship between calnexin and BiP in suppressing aggregation and promoting refolding of protein and glycoprotein substrates. *J Biol Chem* **276**, 39779-87 (2001).
184. Zhang, J.X., Braakman, I., Matlack, K.E. & Helenius, A. Quality control in the secretory pathway: the role of calreticulin, calnexin and BiP in the retention of glycoproteins with C-terminal truncations. *Mol Biol Cell* **8**, 1943-54 (1997).
185. Molinari, M., Galli, C., Piccaluga, V., Pieren, M. & Paganetti, P. Sequential assistance of molecular chaperones and transient formation of covalent complexes during protein degradation from the ER. *J Cell Biol* **158**, 247-57 (2002).
186. Molinari, M., Galli, C., Vanoni, O., Arnold, S.M. & Kaufman, R.J. Persistent glycoprotein misfolding activates the glucosidase II/UGT1-driven calnexin cycle to delay aggregation and loss of folding competence. *Mol Cell* **20**, 503-12 (2005).
187. Svedine, S., Wang, T., Halaban, R. & Hebert, D.N. Carbohydrates act as sorting determinants in ER-associated degradation of tyrosinase. *J Cell Sci* **117**, 2937-49 (2004).
188. Le Fourn, V., Siffroi-Fernandez, S., Ferrand, M. & Franc, J.L. Competition between calnexin and BiP in the endoplasmic reticulum can lead to the folding or degradation of human thyroperoxidase. *Biochemistry* **45**, 7380-8 (2006).
189. Ushioda, R. et al. ERdj5 is required as a disulfide reductase for degradation of misfolded proteins in the ER. *Science* **321**, 569-72 (2008).
190. Plemper, R.K., Bohmler, S., Bordallo, J., Sommer, T. & Wolf, D.H. Mutant analysis links the translocon and BiP to retrograde protein transport for ER degradation. *Nature* **388**, 891-5 (1997).
191. Pilon, M., Schekman, R. & Romisch, K. Sec61p mediates export of a misfolded secretory protein from the endoplasmic reticulum to the cytosol for degradation. *EMBO J* **16**, 4540-8 (1997).
192. Kalies, K.U., Allan, S., Sergeyenko, T., Kroger, H. & Romisch, K. The protein translocation channel binds proteasomes to the endoplasmic reticulum membrane. *EMBO J* **24**, 2284-93 (2005).
193. Kostova, Z., Tsai, Y.C. & Weissman, A.M. Ubiquitin ligases, critical mediators of endoplasmic reticulum-associated degradation. *Semin Cell Dev Biol* **18**, 770-9 (2007).
194. Okuda-Shimizu, Y. & Hendershot, L.M. Characterization of an ERAD pathway for nonglycosylated BiP substrates, which require Herp. *Mol Cell* **28**, 544-54 (2007).
195. Schulze, A. et al. The ubiquitin-domain protein HERP forms a complex with components of the endoplasmic reticulum associated degradation pathway. *J Mol Biol* **354**, 1021-7 (2005).
196. Lilley, B.N. & Ploegh, H.L. A membrane protein required for dislocation of misfolded proteins from the ER. *Nature* **429**, 834-40 (2004).

197. Ye, Y., Shibata, Y., Yun, C., Ron, D. & Rapoport, T.A. A membrane protein complex mediates retro-translocation from the ER lumen into the cytosol. *Nature* **429**, 841-7 (2004).
198. Carvalho, P., Goder, V. & Rapoport, T.A. Distinct ubiquitin-ligase complexes define convergent pathways for the degradation of ER proteins. *Cell* **126**, 361-73 (2006).
199. Travers, K.J. et al. Functional and genomic analyses reveal an essential coordination between the unfolded protein response and ER-associated degradation. *Cell* **101**, 249-58 (2000).
200. Casagrande, R. et al. Degradation of proteins from the ER of S. cerevisiae requires an intact unfolded protein response pathway. *Mol Cell* **5**, 729-35 (2000).
201. Ng, D.T., Spear, E.D. & Walter, P. The unfolded protein response regulates multiple aspects of secretory and membrane protein biogenesis and endoplasmic reticulum quality control. *J Cell Biol* **150**, 77-88 (2000).
202. Friedlander, R., Jarosch, E., Urban, J., Volkwein, C. & Sommer, T. A regulatory link between ER-associated protein degradation and the unfolded-protein response. *Nat Cell Biol* **2**, 379-84 (2000).
203. Hollien, J. & Weissman, J.S. Decay of endoplasmic reticulum-localized mRNAs during the unfolded protein response. *Science* **313**, 104-7 (2006).
204. Mori, K. et al. A 22 bp cis-acting element is necessary and sufficient for the induction of the yeast KAR2 (BiP) gene by unfolded proteins. *EMBO J* **11**, 2583-93 (1992).
205. Kohno, K., Normington, K., Sambrook, J., Gething, M.J. & Mori, K. The promoter region of the yeast KAR2 (BiP) gene contains a regulatory domain that responds to the presence of unfolded proteins in the endoplasmic reticulum. *Mol Cell Biol* **13**, 877-90 (1993).
206. Cox, J.S., Shamu, C.E. & Walter, P. Transcriptional induction of genes encoding endoplasmic reticulum resident proteins requires a transmembrane protein kinase. *Cell* **73**, 1197-206 (1993).
207. Mori, K., Ma, W., Gething, M.J. & Sambrook, J. A transmembrane protein with a cdc2+/CDC28-related kinase activity is required for signaling from the ER to the nucleus. *Cell* **74**, 743-56 (1993).
208. Cox, J.S. & Walter, P. A novel mechanism for regulating activity of a transcription factor that controls the unfolded protein response. *Cell* **87**, 391-404 (1996).
209. Nikawa, J., Akiyoshi, M., Hirata, S. & Fukuda, T. Saccharomyces cerevisiae IRE2/HAC1 is involved in IRE1-mediated KAR2 expression. *Nucleic Acids Res* **24**, 4222-6 (1996).
210. Okamura, K., Kimata, Y., Higashio, H., Tsuru, A. & Kohno, K. Dissociation of Kar2p/BiP from an ER sensory molecule, Ire1p, triggers the unfolded protein response in yeast. *Biochem Biophys Res Commun* **279**, 445-50 (2000).
211. Shamu, C.E. & Walter, P. Oligomerization and phosphorylation of the Ire1p kinase during intracellular signaling from the endoplasmic reticulum to the nucleus. *EMBO J* **15**, 3028-39 (1996).
212. Welihinda, A.A. & Kaufman, R.J. The unfolded protein response pathway in Saccharomyces cerevisiae. Oligomerization and trans-phosphorylation of Ire1p (Ern1p) are required for kinase activation. *J Biol Chem* **271**, 18181-7 (1996).
213. Zhou, J. et al. The crystal structure of human IRE1 luminal domain reveals a conserved dimerization interface required for activation of the unfolded protein response. *Proc Natl Acad Sci U S A* **103**, 14343-8 (2006).

214. Kimata, Y. et al. Genetic evidence for a role of BiP/Kar2 that regulates Ire1 in response to accumulation of unfolded proteins. *Mol Biol Cell* **14**, 2559-69 (2003).
215. Kimata, Y., Oikawa, D., Shimizu, Y., Ishiwata-Kimata, Y. & Kohno, K. A role for BiP as an adjustor for the endoplasmic reticulum stress-sensing protein Ire1. *J Cell Biol* **167**, 445-56 (2004).
216. Credle, J.J., Finer-Moore, J.S., Papa, F.R., Stroud, R.M. & Walter, P. On the mechanism of sensing unfolded protein in the endoplasmic reticulum. *Proc Natl Acad Sci U S A* **102**, 18773-84 (2005).
217. Oikawa, D., Kimata, Y. & Kohno, K. Self-association and BiP dissociation are not sufficient for activation of the ER stress sensor Ire1. *J Cell Sci* **120**, 1681-8 (2007).
218. Kimata, Y. et al. Two regulatory steps of ER-stress sensor Ire1 involving its cluster formation and interaction with unfolded proteins. *J Cell Biol* **179**, 75-86 (2007).
219. Sidrauski, C., Cox, J.S. & Walter, P. tRNA ligase is required for regulated mRNA splicing in the unfolded protein response. *Cell* **87**, 405-13 (1996).
220. Patil, C.K., Li, H. & Walter, P. Gcn4p and novel upstream activating sequences regulate targets of the unfolded protein response. *PLoS Biol* **2**, E246 (2004).
221. Aragon, T. et al. Messenger RNA targeting to endoplasmic reticulum stress signalling sites. *Nature* **457**, 736-40 (2009).
222. Korennykh, A.V. et al. The unfolded protein response signals through high-order assembly of Ire1. *Nature* **457**, 687-93 (2009).
223. Liu, C.Y. & Kaufman, R.J. The unfolded protein response. *J Cell Sci* **116**, 1861-2 (2003).
224. Wu, J. & Kaufman, R.J. From acute ER stress to physiological roles of the Unfolded Protein Response. *Cell Death Differ* **13**, 374-84 (2006).
225. Ron, D. & Walter, P. Signal integration in the endoplasmic reticulum unfolded protein response. *Nat Rev Mol Cell Biol* **8**, 519-29 (2007).
226. Burdakov, D., Petersen, O.H. & Verkhratsky, A. Intraluminal calcium as a primary regulator of endoplasmic reticulum function. *Cell Calcium* **38**, 303-10 (2005).
227. Michalak, M., Robert Parker, J.M. & Opas, M. Ca2+ signaling and calcium binding chaperones of the endoplasmic reticulum. *Cell Calcium* **32**, 269-78 (2002).
228. Macer, D.R. & Koch, G.L. Identification of a set of calcium-binding proteins in reticuloplasm, the luminal content of the endoplasmic reticulum. *J Cell Sci* **91 (Pt 1)**, 61-70 (1988).
229. Lievremont, J.P., Rizzuto, R., Hendershot, L. & Meldolesi, J. BiP, a major chaperone protein of the endoplasmic reticulum lumen, plays a direct and important role in the storage of the rapidly exchanging pool of Ca2+. *J Biol Chem* **272**, 30873-9 (1997).
230. Lytton, J., Westlin, M. & Hanley, M.R. Thapsigargin inhibits the sarcoplasmic or endoplasmic reticulum Ca-ATPase family of calcium pumps. *J Biol Chem* **266**, 17067-71 (1991).
231. Brostrom, M.A. & Brostrom, C.O. Calcium dynamics and endoplasmic reticular function in the regulation of protein synthesis: implications for cell growth and adaptability. *Cell Calcium* **34**, 345-63 (2003).
232. Cai, J.W., Henderson, B.W., Shen, J.W. & Subjeck, J.R. Induction of glucose regulated proteins during growth of a murine tumor. *J Cell Physiol* **154**, 229-37 (1993).
233. Gazit, G., Kane, S.E., Nichols, P. & Lee, A.S. Use of the stress-inducible grp78/BiP promoter in targeting high level gene expression in fibrosarcoma in vivo. *Cancer Res* **55**, 1660-3 (1995).

234. Rose, M.D. Nuclear fusion in the yeast Saccharomyces cerevisiae. *Annu Rev Cell Dev Biol* **12**, 663-95 (1996).
235. Conde, J. & Fink, G.R. A mutant of Saccharomyces cerevisiae defective for nuclear fusion. *Proc Natl Acad Sci U S A* **73**, 3651-5 (1976).
236. Rose, M.D. & Fink, G.R. KAR1, a gene required for function of both intranuclear and extranuclear microtubules in yeast. *Cell* **48**, 1047-60 (1987).
237. Ng, D.T. & Walter, P. ER membrane protein complex required for nuclear fusion. *J Cell Biol* **132**, 499-509 (1996).
238. Brizzio, V. et al. Genetic interactions between KAR7/SEC71, KAR8/JEM1, KAR5, and KAR2 during nuclear fusion in Saccharomyces cerevisiae. *Mol Biol Cell* **10**, 609-26 (1999).
239. Quinones, Q.J., de Ridder, G.G. & Pizzo, S.V. GRP78: a chaperone with diverse roles beyond the endoplasmic reticulum. *Histol Histopathol* **23**, 1409-16 (2008).
240. Dudek, J. et al. Functions and pathologies of BiP and its interaction partners. *Cell Mol Life Sci* (2009).
241. Paton, A.W. et al. AB5 subtilase cytotoxin inactivates the endoplasmic reticulum chaperone BiP. *Nature* **443**, 548-52 (2006).
242. Falguieres, T. & Johannes, L. Shiga toxin B-subunit binds to the chaperone BiP and the nucleolar protein B23. *Biol Cell* **98**, 125-34 (2006).
243. Triantafilou, K., Fradelizi, D., Wilson, K. & Triantafilou, M. GRP78, a coreceptor for coxsackievirus A9, interacts with major histocompatibility complex class I molecules which mediate virus internalization. *J Virol* **76**, 633-43 (2002).
244. Jindadamrongwech, S., Thepparit, C. & Smith, D.R. Identification of GRP 78 (BiP) as a liver cell expressed receptor element for dengue virus serotype 2. *Arch Virol* **149**, 915-27 (2004).
245. Davila, S. et al. Mutations in SEC63 cause autosomal dominant polycystic liver disease. *Nat Genet* **36**, 575-7 (2004).
246. Schulmann, K. et al. HNPCC-associated small bowel cancer: clinical and molecular characteristics. *Gastroenterology* **128**, 590-9 (2005).
247. Mori, Y. et al. Instabilotyping reveals unique mutational spectra in microsatellite-unstable gastric cancers. *Cancer Res* **62**, 3641-5 (2002).
248. Annesi, G. et al. SIL1 and SARA2 mutations in Marinesco-Sjogren and chylomicron retention diseases. *Clin Genet* **71**, 288-9 (2007).
249. Jung, V. et al. Genomic and expression analysis of the 3q25-q26 amplification unit reveals TLOC1/SEC62 as a probable target gene in prostate cancer. *Mol Cancer Res* **4**, 169-76 (2006).
250. Nogalska, A. et al. Homocysteine-induced endoplasmic reticulum protein (Herp) is up-regulated in sporadic inclusion-body myositis and in endoplasmic reticulum stress-induced cultured human muscle fibers. *J Neurochem* **96**, 1491-9 (2006).
251. Sai, X. et al. Endoplasmic reticulum stress-inducible protein, Herp, enhances presenilin-mediated generation of amyloid beta-protein. *J Biol Chem* **277**, 12915-20 (2002).
252. Lee, A.S. GRP78 induction in cancer: therapeutic and prognostic implications. *Cancer Res* **67**, 3496-9 (2007).
253. Wang, M., Wey, S., Zhang, Y., Ye, R. & Lee, A.S. Role of the Unfolded Protein Response Regulator GRP78/BiP in Development, Cancer and Neurological Disorders. *Antioxid Redox Signal* (2009).

254. Scheuner, D. & Kaufman, R.J. The unfolded protein response: a pathway that links insulin demand with beta-cell failure and diabetes. *Endocr Rev* **29**, 317-33 (2008).
255. Chung, K.T., Shen, Y. & Hendershot, L.M. BAP, a mammalian BiP-associated protein, is a nucleotide exchange factor that regulates the ATPase activity of BiP. *J Biol Chem* **277**, 47557-63 (2002).
256. Zhang, L., Lai, E., Teodoro, T. & Volchuk, A. GRP78, but Not Protein-disulfide Isomerase, Partially Reverses Hyperglycemia-induced Inhibition of Insulin Synthesis and Secretion in Pancreatic {beta}-Cells. *J Biol Chem* **284**, 5289-98 (2009).
257. Paschen, W. & Mengesdorf, T. Endoplasmic reticulum stress response and neurodegeneration. *Cell Calcium* **38**, 409-15 (2005).
258. Matus, S. et al. The stress rheostat: an interplay between the unfolded protein response (UPR) and autophagy in neurodegeneration. *Curr Mol Med* **8**, 157-72 (2008).
259. Walsh, P., Bursac, D., Law, Y.C., Cyr, D. & Lithgow, T. The J-protein family: modulating protein assembly, disassembly and translocation. *EMBO Rep* **5**, 567-71 (2004).
260. Werner-Washburne, M., Stone, D.E. & Craig, E.A. Complex interactions among members of an essential subfamily of hsp70 genes in Saccharomyces cerevisiae. *Mol Cell Biol* **7**, 2568-77 (1987).
261. Sahi, C. & Craig, E.A. Network of general and specialty J protein chaperones of the yeast cytosol. *Proc Natl Acad Sci U S A* **104**, 7163-8 (2007).
262. Sayeed, A. & Ng, D.T. Search and destroy: ER quality control and ER-associated protein degradation. *Crit Rev Biochem Mol Biol* **40**, 75-91 (2005).
263. Hebert, D.N. & Molinari, M. In and out of the ER: protein folding, quality control, degradation, and related human diseases. *Physiol Rev* **87**, 1377-408 (2007).
264. Anelli, T. & Sitia, R. Protein quality control in the early secretory pathway. *EMBO J* **27**, 315-27 (2008).
265. Brodsky, J.L. The protective and destructive roles played by molecular chaperones during ERAD (endoplasmic-reticulum-associated degradation). *Biochem J* **404**, 353-63 (2007).
266. Bole, D.G., Hendershot, L.M. & Kearney, J.F. Posttranslational association of immunoglobulin heavy chain binding protein with nascent heavy chains in nonsecreting and secreting hybridomas. *J Cell Biol* **102**, 1558-66 (1986).
267. Gething, M.J., McCammon, K. & Sambrook, J. Expression of wild-type and mutant forms of influenza hemagglutinin: the role of folding in intracellular transport. *Cell* **46**, 939-50 (1986).
268. Vogel, J.P., Misra, L.M. & Rose, M.D. Loss of BiP/GRP78 function blocks translocation of secretory proteins in yeast. *J Cell Biol* **110**, 1885-95 (1990).
269. Nguyen, T.H., Law, D.T. & Williams, D.B. Binding protein BiP is required for translocation of secretory proteins into the endoplasmic reticulum in Saccharomyces cerevisiae. *Proc Natl Acad Sci U S A* **88**, 1565-9 (1991).
270. Holkeri, H., Paunola, E., Jamsa, E. & Makarow, M. Dissection of the translocation and chaperoning functions of yeast BiP/Kar2p in vivo. *J Cell Sci* **111 (Pt 6)**, 749-57 (1998).
271. Flynn, G.C., Chappell, T.G. & Rothman, J.E. Peptide binding and release by proteins implicated as catalysts of protein assembly. *Science* **245**, 385-90 (1989).
272. Melnick, J., Aviel, S. & Argon, Y. The endoplasmic reticulum stress protein GRP94, in addition to BiP, associates with unassembled immunoglobulin chains. *J Biol Chem* **267**, 21303-6 (1992).

273. Kuznetsov, G., Chen, L.B. & Nigam, S.K. Multiple molecular chaperones complex with misfolded large oligomeric glycoproteins in the endoplasmic reticulum. *J Biol Chem* **272**, 3057-63 (1997).
274. Skowronek, M.H., Hendershot, L.M. & Haas, I.G. The variable domain of nonassembled Ig light chains determines both their half-life and binding to the chaperone BiP. *Proc Natl Acad Sci U S A* **95**, 1574-8 (1998).
275. Lee, Y.K., Brewer, J.W., Hellman, R. & Hendershot, L.M. BiP and immunoglobulin light chain cooperate to control the folding of heavy chain and ensure the fidelity of immunoglobulin assembly. *Mol Biol Cell* **10**, 2209-19 (1999).
276. Hellman, R., Vanhove, M., Lejeune, A., Stevens, F.J. & Hendershot, L.M. The in vivo association of BiP with newly synthesized proteins is dependent on the rate and stability of folding and not simply on the presence of sequences that can bind to BiP. *J Cell Biol* **144**, 21-30 (1999).
277. Mayer, M., Kies, U., Kammermeier, R. & Buchner, J. BiP and PDI cooperate in the oxidative folding of antibodies in vitro. *J Biol Chem* **275**, 29421-5 (2000).
278. Brodsky, J.L. et al. The requirement for molecular chaperones during endoplasmic reticulum-associated protein degradation demonstrates that protein export and import are mechanistically distinct. *J Biol Chem* **274**, 3453-60 (1999).
279. Lee, R.J. et al. Uncoupling retro-translocation and degradation in the ER-associated degradation of a soluble protein. *EMBO J* **23**, 2206-15 (2004).
280. Morris, J.A., Dorner, A.J., Edwards, C.A., Hendershot, L.M. & Kaufman, R.J. Immunoglobulin binding protein (BiP) function is required to protect cells from endoplasmic reticulum stress but is not required for the secretion of selective proteins. *J Biol Chem* **272**, 4327-34 (1997).
281. Cox, J.S., Chapman, R.E. & Walter, P. The unfolded protein response coordinates the production of endoplasmic reticulum protein and endoplasmic reticulum membrane. *Mol Biol Cell* **8**, 1805-14 (1997).
282. Umebayashi, K., Hirata, A., Horiuchi, H., Ohta, A. & Takagi, M. Unfolded protein response-induced BiP/Kar2p production protects cell growth against accumulation of misfolded protein aggregates in the yeast endoplasmic reticulum. *Eur J Cell Biol* **78**, 726-38 (1999).
283. Bertolotti, A., Zhang, Y., Hendershot, L.M., Harding, H.P. & Ron, D. Dynamic interaction of BiP and ER stress transducers in the unfolded-protein response. *Nat Cell Biol* **2**, 326-32 (2000).
284. Liu, C.Y., Wong, H.N., Schauerte, J.A. & Kaufman, R.J. The protein kinase/endoribonuclease IRE1alpha that signals the unfolded protein response has a luminal N-terminal ligand-independent dimerization domain. *J Biol Chem* **277**, 18346-56 (2002).
285. Latterich, M. & Schekman, R. The karyogamy gene KAR2 and novel proteins are required for ER-membrane fusion. *Cell* **78**, 87-98 (1994).
286. Fourie, A.M., Sambrook, J.F. & Gething, M.J. Common and divergent peptide binding specificities of hsp70 molecular chaperones. *J Biol Chem* **269**, 30470-8 (1994).
287. Todd-Corlett, A., Jones, E., Seghers, C. & Gething, M.J. Lobe IB of the ATPase domain of Kar2p/BiP interacts with Ire1p to negatively regulate the unfolded protein response in Saccharomyces cerevisiae. *J Mol Biol* **367**, 770-87 (2007).

288. Kaiser, C., Michaelis, S., Mitchell, A. & Cold Spring Harbor Laboratory. Methods in yeast genetics : a Cold Spring Harbor Laboratory course manual (Cold Spring Harbor Laboratory Press, Cold Spring Harbor, NY, 1994).
289. Mumberg, D., Muller, R. & Funk, M. Yeast vectors for the controlled expression of heterologous proteins in different genetic backgrounds. *Gene* **156**, 119-22 (1995).
290. Van Driessche, B., Tafforeau, L., Hentges, P., Carr, A.M. & Vandenhaute, J. Additional vectors for PCR-based gene tagging in Saccharomyces cerevisiae and Schizosaccharomyces pombe using nourseothricin resistance. *Yeast* **22**, 1061-8 (2005).
291. Wang, W. & Malcolm, B.A. Two-stage PCR protocol allowing introduction of multiple mutations, deletions and insertions using QuikChange Site-Directed Mutagenesis. *Biotechniques* **26**, 680-2 (1999).
292. Pierpaoli, E.V., Gisler, S.M. & Christen, P. Sequence-specific rates of interaction of target peptides with the molecular chaperones DnaK and DnaJ. *Biochemistry* **37**, 16741-8 (1998).
293. Zhang, Y., Michaelis, S. & Brodsky, J.L. CFTR expression and ER-associated degradation in yeast. *Methods Mol Med* **70**, 257-65 (2002).
294. Stirling, C.J., Rothblatt, J., Hosobuchi, M., Deshaies, R. & Schekman, R. Protein translocation mutants defective in the insertion of integral membrane proteins into the endoplasmic reticulum. *Mol Biol Cell* **3**, 129-42 (1992).
295. Morrow, M.W. & Brodsky, J.L. Yeast ribosomes bind to highly purified reconstituted Sec61p complex and to mammalian p180. *Traffic* **2**, 705-16 (2001).
296. Kim, W., Spear, E.D. & Ng, D.T. Yos9p detects and targets misfolded glycoproteins for ER-associated degradation. *Mol Cell* **19**, 753-64 (2005).
297. Rose, M. & Botstein, D. Construction and use of gene fusions to lacZ (beta-galactosidase) that are expressed in yeast. *Methods Enzymol* **101**, 167-80 (1983).
298. Hansen, W., Garcia, P.D. & Walter, P. In vitro protein translocation across the yeast endoplasmic reticulum: ATP-dependent posttranslational translocation of the prepro-alpha-factor. *Cell* **45**, 397-406 (1986).
299. Nakatsukasa, K., Huyer, G., Michaelis, S. & Brodsky, J.L. Dissecting the ER-associated degradation of a misfolded polytopic membrane protein. *Cell* **132**, 101-12 (2008).
300. Bhamidipati, A., Denic, V., Quan, E.M. & Weissman, J.S. Exploration of the topological requirements of ERAD identifies Yos9p as a lectin sensor of misfolded glycoproteins in the ER lumen. *Mol Cell* **19**, 741-51 (2005).
301. Hrizo, S.L. et al. The Hsp110 molecular chaperone stabilizes apolipoprotein B from endoplasmic reticulum-associated degradation (ERAD). *J Biol Chem* **282**, 32665-75 (2007).
302. Awad, W., Estrada, I., Shen, Y. & Hendershot, L.M. BiP mutants that are unable to interact with endoplasmic reticulum DnaJ proteins provide insights into interdomain interactions in BiP. *Proc Natl Acad Sci U S A* **105**, 1164-9 (2008).
303. Misselwitz, B., Staeck, O. & Rapoport, T.A. J proteins catalytically activate Hsp70 molecules to trap a wide range of peptide sequences. *Mol Cell* **2**, 593-603 (1998).
304. West, R.W., Jr., Yocum, R.R. & Ptashne, M. Saccharomyces cerevisiae GAL1-GAL10 divergent promoter region: location and function of the upstream activating sequence UASG. *Mol Cell Biol* **4**, 2467-78 (1984).
305. Julius, D., Schekman, R. & Thorner, J. Glycosylation and processing of prepro-alpha-factor through the yeast secretory pathway. *Cell* **36**, 309-18 (1984).

306. Waters, M.G. & Blobel, G. Secretory protein translocation in a yeast cell-free system can occur posttranslationally and requires ATP hydrolysis. *J Cell Biol* **102**, 1543-50 (1986).
307. Rothblatt, J.A. & Meyer, D.I. Secretion in yeast: translocation and glycosylation of prepro-alpha-factor in vitro can occur via an ATP-dependent post-translational mechanism. *EMBO J* **5**, 1031-6 (1986).
308. Rothblatt, J.A. & Meyer, D.I. Secretion in yeast: reconstitution of the translocation and glycosylation of alpha-factor and invertase in a homologous cell-free system. *Cell* **44**, 619-28 (1986).
309. Waters, M.G., Evans, E.A. & Blobel, G. Prepro-alpha-factor has a cleavable signal sequence. *J Biol Chem* **263**, 6209-14 (1988).
310. Caplan, S., Green, R., Rocco, J. & Kurjan, J. Glycosylation and structure of the yeast MF alpha 1 alpha-factor precursor is important for efficient transport through the secretory pathway. *J Bacteriol* **173**, 627-35 (1991).
311. Hasilik, A. & Tanner, W. Biosynthesis of the vacuolar yeast glycoprotein carboxypeptidase Y. Conversion of precursor into the enzyme. *Eur J Biochem* **85**, 599-608 (1978).
312. Hemmings, B.A., Zubenko, G.S., Hasilik, A. & Jones, E.W. Mutant defective in processing of an enzyme located in the lysosome-like vacuole of Saccharomyces cerevisiae. *Proc Natl Acad Sci U S A* **78**, 435-9 (1981).
313. Stevens, T., Esmon, B. & Schekman, R. Early stages in the yeast secretory pathway are required for transport of carboxypeptidase Y to the vacuole. *Cell* **30**, 439-48 (1982).
314. Cyr, D.M., Langer, T. & Douglas, M.G. DnaJ-like proteins: molecular chaperones and specific regulators of Hsp70. *Trends Biochem Sci* **19**, 176-81 (1994).
315. Johnson, J.L. & Craig, E.A. An essential role for the substrate-binding region of Hsp40s in Saccharomyces cerevisiae. *J Cell Biol* **152**, 851-6 (2001).
316. Pelham, H.R., Hardwick, K.G. & Lewis, M.J. Sorting of soluble ER proteins in yeast. *EMBO J* **7**, 1757-62 (1988).
317. Hardwick, K.G., Lewis, M.J., Semenza, J., Dean, N. & Pelham, H.R. ERD1, a yeast gene required for the retention of luminal endoplasmic reticulum proteins, affects glycoprotein processing in the Golgi apparatus. *EMBO J* **9**, 623-30 (1990).
318. Oh, C.S., Toke, D.A., Mandala, S. & Martin, C.E. ELO2 and ELO3, homologues of the Saccharomyces cerevisiae ELO1 gene, function in fatty acid elongation and are required for sphingolipid formation. *J Biol Chem* **272**, 17376-84 (1997).
319. Kobayashi, S.D. & Nagiec, M.M. Ceramide/long-chain base phosphate rheostat in Saccharomyces cerevisiae: regulation of ceramide synthesis by Elo3p and Cka2p. *Eukaryot Cell* **2**, 284-94 (2003).
320. Roberts, C.J., Pohlig, G., Rothman, J.H. & Stevens, T.H. Structure, biosynthesis, and localization of dipeptidyl aminopeptidase B, an integral membrane glycoprotein of the yeast vacuole. *J Cell Biol* **108**, 1363-73 (1989).
321. Klionsky, D.J. & Emr, S.D. Membrane protein sorting: biosynthesis, transport and processing of yeast vacuolar alkaline phosphatase. *EMBO J* **8**, 2241-50 (1989).
322. Hann, B.C., Stirling, C.J. & Walter, P. SEC65 gene product is a subunit of the yeast signal recognition particle required for its integrity. *Nature* **356**, 532-3 (1992).
323. Finke, K. et al. A second trimeric complex containing homologs of the Sec61p complex functions in protein transport across the ER membrane of S. cerevisiae. *EMBO J* **15**, 1482-94 (1996).

324. Huyer, G. et al. Distinct machinery is required in Saccharomyces cerevisiae for the endoplasmic reticulum-associated degradation of a multispanning membrane protein and a soluble luminal protein. *J Biol Chem* **279**, 38369-78 (2004).
325. Zhang, Y. et al. Hsp70 molecular chaperone facilitates endoplasmic reticulum-associated protein degradation of cystic fibrosis transmembrane conductance regulator in yeast. *Mol Biol Cell* **12**, 1303-14 (2001).
326. Fewell, S.W., Pipas, J.M. & Brodsky, J.L. Mutagenesis of a functional chimeric gene in yeast identifies mutations in the simian virus 40 large T antigen J domain. *Proc Natl Acad Sci U S A* **99**, 2002-7 (2002).
327. Youker, R.T., Walsh, P., Beilharz, T., Lithgow, T. & Brodsky, J.L. Distinct roles for the Hsp40 and Hsp90 molecular chaperones during cystic fibrosis transmembrane conductance regulator degradation in yeast. *Mol Biol Cell* **15**, 4787-97 (2004).
328. Kang, C.M. & Jiang, Y.W. Genome-wide survey of non-essential genes required for slowed DNA synthesis-induced filamentous growth in yeast. *Yeast* **22**, 79-90 (2005).
329. Huh, W.K. et al. Global analysis of protein localization in budding yeast. *Nature* **425**, 686-91 (2003).
330. Ng, D.T., Brown, J.D. & Walter, P. Signal sequences specify the targeting route to the endoplasmic reticulum membrane. *J Cell Biol* **134**, 269-78 (1996).
331. Hegde, R.S. & Bernstein, H.D. The surprising complexity of signal sequences. *Trends Biochem Sci* **31**, 563-71 (2006).
332. Haeuptle, M.T., Flint, N., Gough, N.M. & Dobberstein, B. A tripartite structure of the signals that determine protein insertion into the endoplasmic reticulum membrane. *J Cell Biol* **108**, 1227-36 (1989).
333. Schuldiner, M. et al. Exploration of the function and organization of the yeast early secretory pathway through an epistatic miniarray profile. *Cell* **123**, 507-19 (2005).
334. Schuldiner, M., Collins, S.R., Weissman, J.S. & Krogan, N.J. Quantitative genetic analysis in Saccharomyces cerevisiae using epistatic miniarray profiles (E-MAPs) and its application to chromatin functions. *Methods* **40**, 344-52 (2006).
335. Collins, S.R., Schuldiner, M., Krogan, N.J. & Weissman, J.S. A strategy for extracting and analyzing large-scale quantitative epistatic interaction data. *Genome Biol* **7**, R63 (2006).
336. Krogan, N.J. et al. Global landscape of protein complexes in the yeast Saccharomyces cerevisiae. *Nature* **440**, 637-43 (2006).
337. Roguev, A., Wiren, M., Weissman, J.S. & Krogan, N.J. High-throughput genetic interaction mapping in the fission yeast Schizosaccharomyces pombe. *Nat Methods* **4**, 861-6 (2007).
338. Collins, S.R. et al. Functional dissection of protein complexes involved in yeast chromosome biology using a genetic interaction map. *Nature* **446**, 806-10 (2007).
339. Collins, S.R. et al. Toward a comprehensive atlas of the physical interactome of Saccharomyces cerevisiae. *Mol Cell Proteomics* **6**, 439-50 (2007).
340. Typas, A. et al. High-throughput, quantitative analyses of genetic interactions in E. coli. *Nat Methods* **5**, 781-7 (2008).
341. Wilmes, G.M. et al. A genetic interaction map of RNA-processing factors reveals links between Sem1/Dss1-containing complexes and mRNA export and splicing. *Mol Cell* **32**, 735-46 (2008).

342. Roguev, A. et al. Conservation and rewiring of functional modules revealed by an epistasis map in fission yeast. *Science* **322**, 405-10 (2008).
343. Typas, A. et al. High-throughput, quantitative analyses of genetic interactions in E. coli. *Nat Methods* **5**, 781-787 (2008).
344. Breslow, D.K. et al. A comprehensive strategy enabling high-resolution functional analysis of the yeast genome. *Nat Methods* **5**, 711-8 (2008).
345. Fiedler, D. et al. Functional organization of the S. cerevisiae phosphorylation network. *Cell* **136**, 952-63 (2009).
346. Young, J.C., Agashe, V.R., Siegers, K. & Hartl, F.U. Pathways of chaperone-mediated protein folding in the cytosol. *Nat Rev Mol Cell Biol* **5**, 781-91 (2004).
347. Liberek, K., Marszalek, J., Ang, D., Georgopoulos, C. & Zylicz, M. Escherichia coli DnaJ and GrpE heat shock proteins jointly stimulate ATPase activity of DnaK. *Proc Natl Acad Sci U S A* **88**, 2874-8 (1991).
348. Gassler, C.S. et al. Mutations in the DnaK chaperone affecting interaction with the DnaJ cochaperone. *Proc Natl Acad Sci U S A* **95**, 15229-34 (1998).
349. Gall, W.E. et al. The auxilin-like phosphoprotein Swa2p is required for clathrin function in yeast. *Curr Biol* **10**, 1349-58 (2000).
350. Cheetham, M.E. & Caplan, A.J. Structure, function and evolution of DnaJ: conservation and adaptation of chaperone function. *Cell Stress Chaperones* **3**, 28-36 (1998).
351. Caplan, A.J., Cyr, D.M. & Douglas, M.G. YDJ1p facilitates polypeptide translocation across different intracellular membranes by a conserved mechanism. *Cell* **71**, 1143-55 (1992).
352. Lu, Z. & Cyr, D.M. The conserved carboxyl terminus and zinc finger-like domain of the co-chaperone Ydj1 assist Hsp70 in protein folding. *J Biol Chem* **273**, 5970-8 (1998).
353. Caplan, A.J., Tsai, J., Casey, P.J. & Douglas, M.G. Farnesylation of YDJ1p is required for function at elevated growth temperatures in Saccharomyces cerevisiae. *J Biol Chem* **267**, 18890-5 (1992).
354. Wei, J. & Hendershot, L.M. Characterization of the nucleotide binding properties and ATPase activity of recombinant hamster BiP purified from bacteria. *J Biol Chem* **270**, 26670-6 (1995).
355. Wright, C.M. et al. The Hsp40 molecular chaperone Ydj1p, along with the protein kinase C pathway, affects cell-wall integrity in the yeast Saccharomyces cerevisiae. *Genetics* **175**, 1649-64 (2007).
356. Ito, H., Fukuda, Y., Murata, K. & Kimura, A. Transformation of intact yeast cells treated with alkali cations. *J Bacteriol* **153**, 163-8 (1983).
357. Coughlan, C.M., Walker, J.L., Cochran, J.C., Wittrup, K.D. & Brodsky, J.L. Degradation of mutated bovine pancreatic trypsin inhibitor in the yeast vacuole suggests post-endoplasmic reticulum protein quality control. *J Biol Chem* **279**, 15289-97 (2004).
358. Christianson, T.W., Sikorski, R.S., Dante, M., Shero, J.H. & Hieter, P. Multifunctional yeast high-copy-number shuttle vectors. *Gene* **110**, 119-22 (1992).
359. Lorenz, M.C. et al. Gene disruption with PCR products in Saccharomyces cerevisiae. *Gene* **158**, 113-7 (1995).
360. Becker, J., Walter, W., Yan, W. & Craig, E.A. Functional interaction of cytosolic hsp70 and a DnaJ-related protein, Ydj1p, in protein translocation in vivo. *Mol Cell Biol* **16**, 4378-86 (1996).

361. Oka, M. et al. Loss of Hsp70-Hsp40 chaperone activity causes abnormal nuclear distribution and aberrant microtubule formation in M-phase of Saccharomyces cerevisiae. *J Biol Chem* **273**, 29727-37 (1998).
362. Kushnirov, V.V., Kryndushkin, D.S., Boguta, M., Smirnov, V.N. & Ter-Avanesyan, M.D. Chaperones that cure yeast artificial [PSI+] and their prion-specific effects. *Curr Biol* **10**, 1443-6 (2000).
363. Park, S.H. et al. The cytoplasmic Hsp70 chaperone machinery subjects misfolded and endoplasmic reticulum import-incompetent proteins to degradation via the ubiquitin-proteasome system. *Mol Biol Cell* **18**, 153-65 (2007).
364. Metzger, M.B., Maurer, M.J., Dancy, B.M. & Michaelis, S. Degradation of a cytosolic protein requires endoplasmic reticulum-associated degradation machinery. *J Biol Chem* **283**, 32302-16 (2008).
365. Lu, Z. & Cyr, D.M. Protein folding activity of Hsp70 is modified differentially by the hsp40 co-chaperones Sis1 and Ydj1. *J Biol Chem* **273**, 27824-30 (1998).
366. Tsai, J. & Douglas, M.G. A conserved HPD sequence of the J-domain is necessary for YDJ1 stimulation of Hsp70 ATPase activity at a site distinct from substrate binding. *J Biol Chem* **271**, 9347-54 (1996).
367. Lesage, G. & Bussey, H. Cell wall assembly in Saccharomyces cerevisiae. *Microbiol Mol Biol Rev* **70**, 317-43 (2006).
368. Fliss, A.E., Rao, J., Melville, M.W., Cheetham, M.E. & Caplan, A.J. Domain requirements of DnaJ-like (Hsp40) molecular chaperones in the activation of a steroid hormone receptor. *J Biol Chem* **274**, 34045-52 (1999).
369. Nelson, R.J., Ziegelhoffer, T., Nicolet, C., Werner-Washburne, M. & Craig, E.A. The translation machinery and 70 kd heat shock protein cooperate in protein synthesis. *Cell* **71**, 97-105 (1992).
370. Shaner, L., Gibney, P.A. & Morano, K.A. The Hsp110 protein chaperone Sse1 is required for yeast cell wall integrity and morphogenesis. *Curr Genet* **54**, 1-11 (2008).
371. Yang, X.X. et al. The molecular chaperone Hsp90 is required for high osmotic stress response in Saccharomyces cerevisiae. *FEMS Yeast Res* **6**, 195-204 (2006).
372. Cintron, N.S. & Toft, D. Defining the requirements for Hsp40 and Hsp70 in the Hsp90 chaperone pathway. *J Biol Chem* **281**, 26235-44 (2006).
373. Caplan, A.J., Langley, E., Wilson, E.M. & Vidal, J. Hormone-dependent transactivation by the human androgen receptor is regulated by a dnaJ protein. *J Biol Chem* **270**, 5251-7 (1995).
374. Luke, M.M., Sutton, A. & Arndt, K.T. Characterization of SIS1, a Saccharomyces cerevisiae homologue of bacterial dnaJ proteins. *J Cell Biol* **114**, 623-38 (1991).
375. Pesce, E.R. et al. The Plasmodium falciparum heat shock protein 40, Pfj4, associates with heat shock protein 70 and shows similar heat induction and localisation patterns. *Int J Biochem Cell Biol* **40**, 2914-26 (2008).
376. Nicoll, W.S. et al. Cytosolic and ER J-domains of mammalian and parasitic origin can functionally interact with DnaK. *Int J Biochem Cell Biol* **39**, 736-51 (2007).
377. Botha, M., Pesce, E.R. & Blatch, G.L. The Hsp40 proteins of Plasmodium falciparum and other apicomplexa: regulating chaperone power in the parasite and the host. *Int J Biochem Cell Biol* **39**, 1781-803 (2007).
378. Burkholder, W.F. et al. Mutations in the C-terminal fragment of DnaK affecting peptide binding. *Proc Natl Acad Sci U S A* **93**, 10632-7 (1996).

379. Gragerov, A., Zeng, L., Zhao, X., Burkholder, W. & Gottesman, M.E. Specificity of DnaK-peptide binding. *J Mol Biol* **235**, 848-54 (1994).
380. Yan, Z. et al. Yeast Barcoders: a chemogenomic application of a universal donor-strain collection carrying bar-code identifiers. *Nat Methods* **5**, 719-25 (2008).
381. Winzeler, E.A. et al. Functional characterization of the S. cerevisiae genome by gene deletion and parallel analysis. *Science* **285**, 901-6 (1999).
382. Giaever, G. et al. Functional profiling of the Saccharomyces cerevisiae genome. *Nature* **418**, 387-91 (2002).
383. Semenza, J.C., Hardwick, K.G., Dean, N. & Pelham, H.R. ERD2, a yeast gene required for the receptor-mediated retrieval of luminal ER proteins from the secretory pathway. *Cell* **61**, 1349-57 (1990).
384. Kalies, K.U., Rapoport, T.A. & Hartmann, E. The beta subunit of the Sec61 complex facilitates cotranslational protein transport and interacts with the signal peptidase during translocation. *J Cell Biol* **141**, 887-94 (1998).
385. Chavan, M., Yan, A. & Lennarz, W.J. Subunits of the translocon interact with components of the oligosaccharyl transferase complex. *J Biol Chem* **280**, 22917-24 (2005).
386. Helmers, J., Schmidt, D., Glavy, J.S., Blobel, G. & Schwartz, T. The beta-subunit of the protein-conducting channel of the endoplasmic reticulum functions as the guanine nucleotide exchange factor for the beta-subunit of the signal recognition particle receptor. *J Biol Chem* **278**, 23686-90 (2003).
387. Toikkanen, J.H., Miller, K.J., Soderlund, H., Jantti, J. & Keranen, S. The beta subunit of the Sec61p endoplasmic reticulum translocon interacts with the exocyst complex in Saccharomyces cerevisiae. *J Biol Chem* **278**, 20946-53 (2003).
388. Lipschutz, J.H., Lingappa, V.R. & Mostov, K.E. The exocyst affects protein synthesis by acting on the translocation machinery of the endoplasmic reticulum. *J Biol Chem* **278**, 20954-60 (2003).
389. Lipschutz, J.H. & Mostov, K.E. Exocytosis: the many masters of the exocyst. *Curr Biol* **12**, R212-4 (2002).
390. Leroux, A. & Rokeach, L.A. Inter-species complementation of the translocon beta subunit requires only its transmembrane domain. *PLoS ONE* **3**, e3880 (2008).
391. De Craene, J.O. et al. Rtn1p is involved in structuring the cortical endoplasmic reticulum. *Mol Biol Cell* **17**, 3009-20 (2006).
392. Gavin, A.C. et al. Functional organization of the yeast proteome by systematic analysis of protein complexes. *Nature* **415**, 141-7 (2002).
393. Gavin, A.C. et al. Proteome survey reveals modularity of the yeast cell machinery. *Nature* **440**, 631-6 (2006).
394. Newman, J.R. et al. Single-cell proteomic analysis of S. cerevisiae reveals the architecture of biological noise. *Nature* **441**, 840-6 (2006).
395. Biederer, T., Volkwein, C. & Sommer, T. Degradation of subunits of the Sec61p complex, an integral component of the ER membrane, by the ubiquitin-proteasome pathway. *EMBO Journal* **15**, 2069–2076 (1996).
396. Hampton, R.Y., Gardner, R.G. & Rine, J. Role of 26S proteasome and HRD genes in the degradation of 3-hydroxy-3- methylglutaryl-CoA reductase, an integral endoplasmic reticulum membrane protein *Molecular Biology of the Cell* **7**, 2029-2044 (1996).

397. Schuldiner, M. et al. The GET complex mediates insertion of tail-anchored proteins into the ER membrane. *Cell* **134**, 634-45 (2008).
398. Weerapana, E. & Imperiali, B. Asparagine-linked protein glycosylation: from eukaryotic to prokaryotic systems. *Glycobiology* **16**, 91R-101R (2006).
399. Lewis, M.J. & Pelham, H.R. SNARE-mediated retrograde traffic from the Golgi complex to the endoplasmic reticulum. *Cell* **85**, 205-15 (1996).
400. Lewis, M.J., Rayner, J.C. & Pelham, H.R. A novel SNARE complex implicated in vesicle fusion with the endoplasmic reticulum. *EMBO J* **16**, 3017-24 (1997).
401. te Heesen, S. & Aebi, M. The genetic interaction of kar2 and wbp1 mutations. Distinct functions of binding protein BiP and N-linked glycosylation in the processing pathway of secreted proteins in Saccharomyces cerevisiae. *Eur J Biochem* **222**, 631-7 (1994).
402. Mitra, N., Sinha, S., Ramya, T.N. & Surolia, A. N-linked oligosaccharides as outfitters for glycoprotein folding, form and function. *Trends Biochem Sci* **31**, 156-63 (2006).
403. Liberek, K., Skowyra, D., Zylicz, M., Johnson, C. & Georgopoulos, C. The Escherichia coli DnaK chaperone, the 70-kDa heat shock protein eukaryotic equivalent, changes conformation upon ATP hydrolysis, thus triggering its dissociation from a bound target protein. *J Biol Chem* **266**, 14491-6 (1991).
404. Banecki, B., Zylicz, M., Bertoli, E. & Tanfani, F. Structural and functional relationships in DnaK and DnaK756 heat-shock proteins from Escherichia coli. *J Biol Chem* **267**, 25051-8 (1992).
405. Buchberger, A. et al. Nucleotide-induced conformational changes in the ATPase and substrate binding domains of the DnaK chaperone provide evidence for interdomain communication. *J Biol Chem* **270**, 16903-10 (1995).
406. Fung, K.L., Hilgenberg, L., Wang, N.M. & Chirico, W.J. Conformations of the nucleotide and polypeptide binding domains of a cytosolic Hsp70 molecular chaperone are coupled. *J Biol Chem* **271**, 21559-65 (1996).
407. Kim, D., Lee, Y.J. & Corry, P.M. Constitutive HSP70: oligomerization and its dependence on ATP binding. *J Cell Physiol* **153**, 353-61 (1992).
408. Heuser, J. & Steer, C.J. Trimeric binding of the 70-kD uncoating ATPase to the vertices of clathrin triskelia: a candidate intermediate in the vesicle uncoating reaction. *J Cell Biol* **109**, 1457-66 (1989).
409. Freiden, P.J., Gaut, J.R. & Hendershot, L.M. Interconversion of three differentially modified and assembled forms of BiP. *EMBO J* **11**, 63-70 (1992).
410. Palleros, D.R., Reid, K.L., Shi, L. & Fink, A.L. DnaK ATPase activity revisited. *FEBS Lett* **336**, 124-8 (1993).
411. Carlino, A. et al. Interactions of liver Grp78 and Escherichia coli recombinant Grp78 with ATP: multiple species and disaggregation. *Proc Natl Acad Sci U S A* **89**, 2081-5 (1992).
412. Blond-Elguindi, S., Fourie, A.M., Sambrook, J.F. & Gething, M.J. Peptide-dependent stimulation of the ATPase activity of the molecular chaperone BiP is the result of conversion of oligomers to active monomers. *J Biol Chem* **268**, 12730-5 (1993).
413. Brown, C.R., Martin, R.L., Hansen, W.J., Beckmann, R.P. & Welch, W.J. The constitutive and stress inducible forms of hsp 70 exhibit functional similarities and interact with one another in an ATP-dependent fashion. *J Cell Biol* **120**, 1101-12 (1993).
414. Anderson, J.V., Haskell, D.W. & Guy, C.L. Differential influence of ATP on native spinach 70-kilodalton heat-shock cognates. *Plant Physiol* **104**, 1371-80 (1994).

415. Schonfeld, H.J., Schmidt, D., Schroder, H. & Bukau, B. The DnaK chaperone system of Escherichia coli: quaternary structures and interactions of the DnaK and GrpE components. *J Biol Chem* **270**, 2183-9 (1995).
416. Bhattacharyya, T. et al. Cloning and subcellular localization of human mitochondrial hsp70. *J Biol Chem* **270**, 1705-10 (1995).
417. Benaroudj, N., Batelier, G., Triniolles, F. & Ladjimi, M.M. Self-association of the molecular chaperone HSC70. *Biochemistry* **34**, 15282-90 (1995).
418. Geerlof, A. et al. The impact of protein characterization in structural proteomics. *Acta Crystallogr D Biol Crystallogr* **62**, 1125-36 (2006).